Decellularised Veins as a Scaffold for *in situ* Vascular Tissue Engineering

Nadiah Binti Sulaiman

A dissertation submitted to the University of Bristol in accordance with the requirements for award of the degree of Doctor of Philosophy (Translational Health Sciences) in the Faculty of Health Sciences, Bristol Medical School

October 2018

Word count: 36 707

ABSTRACT

Development of new arterial-like vascular conduits for coronary and peripheral bypass grafting surgery is desirable to overcome the limitations of currently available biological and/or synthetic grafts; to reduce the incidence of early thrombosis, late intimal thickening and infection. One alternative is to use arterialised decellularised venous scaffolds. The aim of this PhD project was to assess the feasibility and suitability of human saphenous vein (hSV) decellularisation as a way to obtain effective biological acellular scaffold for vascular grafting.

We identified the optimal sodium dodecyl sulphate (SDS) concentration needed to decellularise short segments of hSVs (~0.5 cm). Low concentration (0.01%) (w/v) SDS removed most of the nuclei, but this approach was not effective in removing nuclei when using ~4 cm long hSVs. Hence, a modified flow technique of decellularisation was established with successful decellularisation of longer hSV segments.

Biocompatibility and integrity of decellularised hSVs were then evaluated. Methylene blue assay detected only trivial residual concentrations of SDS after decellularisation. This was biocompatible as this residual amount of SDS did not affect the viability of porcine carotid artery endothelial cells (pCA ECs) to populate the acellular hSV (AlamarBlue) and to proliferate (EdU proliferation assays). Next, the ECM integrity of acellular hSVs was assessed by quantifying major ECM proteins (collagen, elastin and glycosaminoglycan). Results revealed that decellularisation with ≤0.01% (w/v) SDS did not have a significant impact on ECM content. We then tested the feasibility, safety and capacity of acellular hSVs to arterialise following surgical implant with end-to-end anastomoses in pig without immunosuppression. This pilot study showed that porcine carotid artery xenograft of decellularised hSV was feasible and safe, with 50% graft patency rate at 4 weeks and signs of in situ vascular tissue engineering by host cells.

In conclusion, effective decellularisation of hSV is feasible, safe and reproducible as potential acellular vascular scaffolds. Acellular hSVs may be used as vascular acellular scaffolds either for *in situ* vascular engineering by host cells or following *ex vivo* manipulation before implantation. However, this approach warrants further investigations.

ACKNOWLEDGEMENTS

بِسْمِ اللهِ الرَّحْمٰنِ الرَّحِيْمِ

"In the name of God, the Most Gracious, the Most Merciful"

Praise be to Allah (ٱلْحَمْدُ للهِ), here at last writing an acknowledgement that could go on longer than the thesis. I have a lot to be grateful and thankful for whilst working on this thesis project. First and foremost, I am blessed to be granted a mixed of amazing supervisors with very different background that nurture me personally and academically. Thank you to Professor Raimondo Ascione, for all medical knowledge in addition to the chance to be exposed to close-up surgical technique and in theatre experience. In addition to all the visionary approaches in addressing the project and constant guidance, encouragement and endless support. A special thank you to Professor Sarah George, with her extensive knowledge and experience, she helped me a lot through my study years, and always available to overcome any difficulties in addition to making my PhD journey enjoyable by including me in her research group. Thank you to Professor Saadeh Suleiman, for his contribution and encouragement too, keeping me going when times were tough, asking insightful questions, and offering invaluable advice.

I extended my gratitude to all diverse group I am included in. To RA research team past and present; Caroline, Nick, Sandro, and Daniel for their helping hands in addition to their willingness to work, share and get things done together. Thank you especially to Dr. Andy Bond who always has the time to listen, explain and addressing my crazy queries. To SG research group, it was always fun to go to the weekly meeting and share what everyone has thus in part help lessen my anxiety for public speaking. There are too many to mention, each and every single one, past and present, but a fun and helpful group of scientists everyone are. To all friends and lab mates on RFL7 past and present especially those who taken me in personally (Anto, Eva and Elisa), everyone helps making life easier, livelier and bearable as being so far away from home having people who cheer you up close-by is an advantage.

I also wish to express appreciation to all my sponsors, Government of Malaysia via the People's Trust Council (Majlis Amanah Rakyat, MARA) and National University of Malaysia (Universiti Kebangsaan Malaysia, UKM) for the chance to undertake this PhD opportunity and the financial support.

Last but definitely not least, to my family, thank you for believing in me. Thank you for understanding, the support and love. Thank you for being there always, regardless of time difference and all enormous sacrifices done both financially and emotionally because of me over these years. To Mak and Abah thank you for just being the best parents ever. To Akak and Ijal, thank you for taking care of the family whilst I am away (which is most of the time) but I'll take over after this. Best siblings I could ever wish for!

Thank you to those who directly and indirectly contributed in this research and are not mentioned here, you know who you are and your contribution means a lot to me. From the bottom of my heart, thank you very much.

Author's Declaration

I declare that the work in this dissertation was carried out in accordance with the requirements of the University's Regulation and Code of Practice for Research Degree Programmes and that it has not been submitted for any other academic award. Except where indicated by specific reference in the text, work is the candidate's own work. Work done in collaboration with, or with assistance of, others, is indicated as such. Any views expressed in the dissertation are those of the author.

Signed: 

Date: 22nd October 2018

Published Abstract

Sulaiman N, George SJ, Suleiman MS and Ascione R. Effect of decellularisation protocol of human saphenous veins on cytotoxicity and matrix component. *Atherosclerosis*. 2016; 244:e11-e12.

Poster presentation

1. Poster presented at Advances in Cardiovascular Research: from the bench to the patient's bed. International symposium on September 2 – 5th, 2015; Smolenice Castle - Congress Center of the Slovak Academy of Sciences, Bratislava, Slovakia.
2. Poster presented at British Atherosclerosis Society Autumn Meeting 2015. Atherosclerosis: Crossroads of Metabolism and Inflammation on 10th – 11th September 2015; Murray Edwards College, New Hall, University of Cambridge, Cambridge, UK.
3. Poster presented at Translational Biomedical Research Centre Conference & Showcase Event on 7th September 2015; Langford Campus, University of Bristol, UK.
4. Poster presented at Advances in Regenerative Medicine: the road to translation. 3rd South West Regional Regenerative Medicine Meeting on 22nd & 23rd September 2015; DoubleTree by Hilton Cadbury House, Congresbury, Bristol, UK.
5. Poster presented at Population Health Early Career Researchers' Event and Annual Symposium 2016 on 1st December 2016 at Engineer's House, Clifton Down, Bristol, UK.
6. Poster presented at Vascular Biology: Past, Present and Future on 2nd December 2016 at Wills Hall, University of Bristol,UK.
7. Poster presented at 2017 TERMIS-EU Conference on 26 – 30th June, 2017 at Davos Conference Center, Davos, Switzerland.
8. Poster presented at Official Opening of the Specialist Research Institute: Bristol Heart Institute on 30th November 2017 at Life Sciences Building, University of Bristol, UK.
9. Poster presented at 2018 TERMIS World Congress on September 4-7, 2018 at Kyoto International Conference Center, Kyoto, Japan.
10. Poster presented at the Bristol Heart Institute Specialist Research Institute - 2nd Annual Meeting on 20th September 2018 at Life Sciences Building, University of Bristol, UK.

Contents

LIST OF FIGURES

LIST OF TABLES

LIST OF ABBREVIATION

ABI	Ankle brachial index
Abs	Absorbance
ACC/AHA	American College of Cardiology/American Heart Association
ACS	Acute coronary syndrome
ACT	Activated clotting time
ACT	Activated clotting time
AFs	Adventitial fibroblasts
AngII	Angiotensin II
ANOVA	One-way analysis of variance
BA	Balloon angioplasty
bFGF	Basic fibroblast growth factors
BIMA	Bilateral IMA
BM	Basement membrane
BMP	Bone morphogenetic protein
BOEC	Blood outgrowth endothelial cells
bp	base pair
BrdU	Bromodeoxyuridine
BVS	Bio-resorbable vascular scaffolds
CA	Carotid artery
CABG	Coronary artery bypass grafting
CAD	Coronary artery disease
CD31	Cluster of differentiation
CEC	Circulating endothelial cells
CHD	Coronary heart disease
CLI	Critical limb ischemia
Col	Collagen
CVD	Cardiovascular Disease
DAPT	Dual antiplatelet therapy
DBA	Biotinylated Dolichos Biflorus Agglutinin
DES	Drug eluting stents
DMAB	Dimethylamino benzaldehyde
DMEM	Dulbecco’s modified Eagle's medium
DNA	Deoxyribonucleic acid
DPBS	Dulbecco’s Phosphate Buffer Saline
dsDNA	Double-stranded DNA
EC	Endothelial cell
ECG	Electrocardiogram
ECM	Extracellular matrixes
EEL	External elastic lamina
EGF	Epidermal growth factors
EHT	Endothelial-to-hematopoietic cell transition
EMA	European Medical Agency
EMT	Epithelial to mesenchymal transition
eNOS	Endothelial nitric oxide synthesis
EPDC	Epicardial derived cells
ESC	European Society of Cardiology
EVG	Elastin Van Gieson
FCS	Fetal Calf Serum
FDA	Food and Drug Administration

FN	Fibronectin
FU	Follow up
GAGs	Glycosaminoglycan
GLP MA	Good laboratory practice monitoring authority
H&E	Hematoxylin and Eosin
H_2O_2	Hydrogen peroxide
HCl	Hydrochloric acid
HIF	hypoxia induce factor
hIMA	Human internal mammary artery
hMSC	human mesenchymal stem cell
HSPG-2	Heparan sulfate proteoglycan 2
hSV	Human saphenous vein
IEL	Internal elastic lamina
IGF	Insulin growth factors
IH	Intimal hyperplasia
IHD	Ischemic heart disease
IMS	Industrial Methylated Sprits
iPSCs	Induced pluripotent cells
ISR	In-stent restenosis
IV	Intravenous
IVUS	Intravascular ultrasound
LAD	Left anterior descending
LDL	Low-density lipoproteins
LMS	Left main stem
LN	Laminin
MB	Methylene blue
MI	Myocardial infarction
MMPs	Matrix metalloproteinase
mTOR	mammalian TOR receptor
MVD	Multi-vessel disease
NACC	North American Consensus Criteria
NBF	Neutral buffered formalin
NC	Necrotic core
Nc	Notochord
NHS	The National Health Service
NICE	National Institute for Health and Care Excellence
NIH	Neointima hyperplasia
NSTEMI	Non-ST elevated myocardial infarction
NT	Neural tube
OP-1	Osteogenic Protein 1
PAD	Peripheral artery disease
PBMA	poly n-butyl methacrylate

PBS	Phosphate Buffer Saline
pCA	Porcine Carotid Artery
PCI	Percutaneous coronary intervention
PDGF	Platelet-derived growth factors
PECAM	Platelet endothelial cell adhesion molecule
PEG	Polyethylene glycol
PET	Polyethylene terephthalate
PEVA	polyethylene-co-vinyl acetate
PGA	Polyglycolic acid
PHA	Polyhydroxyalkanoate
PLA/PCL	Poly (lactic acid)/polycaprolactone
PLCL	Poly (L-lactide-co-ε-caprolactone)
PLLA	Polyglycolic acid
PP	Polypropylene
PSV	Peak systolic velocity
PTFE	Polytetrafluoroethylene
PWB	Peripheral Whole Blood
RA	Radial artery
ROS	Reactive oxygen species
RTKs	Receptor tyrosine kinases
SDS	Sodium Dodecyl Sulphate
Shh	Sonic hedgehog
SM MHC	Smooth muscle myosin heavy chain
SMC	Smooth muscle cells
SMCGM2	Smooth Muscle Cell Growth Medium 2
ST	Stent thrombosis
STEMI	ST-elevated myocardial infarction
TA	Tunica adventitia
TE	Tissue Engineering
TEVG	Tissue engineered vascular graft
TGF-β	Transforming growth factor β
TI	Tunica intima
TIMPs	Tissue inhibitors of MMPs
TM	Tunica media
UK	United Kingdom
VE-Cad	Vascular endothelial cadherin
VEGFR2	Vascular endothelial growth factor receptor 2
VSMC	Vascular SMCs
vWF	von Willebrand factor
WHO	World Health Organisation
αSMA	Alpha smooth muscle cells

1 INTRODUCTION

1.1 Cardiovascular Disease

According to World Health Organization (WHO) reports, 31% of all global deaths are due to cardiovascular diseases (CVD) (Mendis, Puska, and Norrving 2011). The treatment of CVD has an enormous impact on healthcare systems cost. The National Health Service (NHS) in the United Kingdom (UK) spent more than £6.8 billion treating CVD in the year 2012/2013 (Porth, Matfin, and Porth 2009; Nichols et al. 2014). Although CVD is no longer the biggest killer in the UK (Bhatnagar et al. 2015), there is still a need to reduce CVD to improve the population health and decrease the economic burden of CVD on the NHS. It is important to highlight that CVD covers a range of heart and blood vessel related diseases including but not limited to coronary artery disease (CAD), valvular heart disease, cardiomyopathy and congenital heart disease and peripheral artery disease (PAD). Generally, CAD and PAD affect the heart (cardio) and/or peripheral blood vessels (brain, kidney, liver, gut, limbs, etc), respectively due to the narrowing and blocking of arteries.

1.2 Coronary Artery Disease

In the UK, more than 2.3 million people are living with some form of CAD (Nichols et al. 2014), making CAD the most common type of heart disease. CAD occurs when coronary arteries are restricted or blocked by a build-up of fatty substances. The process of fatty deposits build-up is called atherosclerosis, and the initiating fatty deposits called atheroma that eventually will form atherosclerotic plaques. Atherosclerosis leads to narrowing of coronary arteries leading to reduced blood supply to the myocardium causing insufficient delivery of oxygen in which, if not

resolved can lead to ischemia and death of cardiomyocytes. In a clinical setting this condition is called myocardial infarction, or commonly known as a heart attack. Relating the terminology that medical professionals use in explaining CVD (as shown in **Figure 1.1**) helps in the understanding of the diagnosis of CV and the atherosclerotic plaque condition that substantiates the diagnosis.

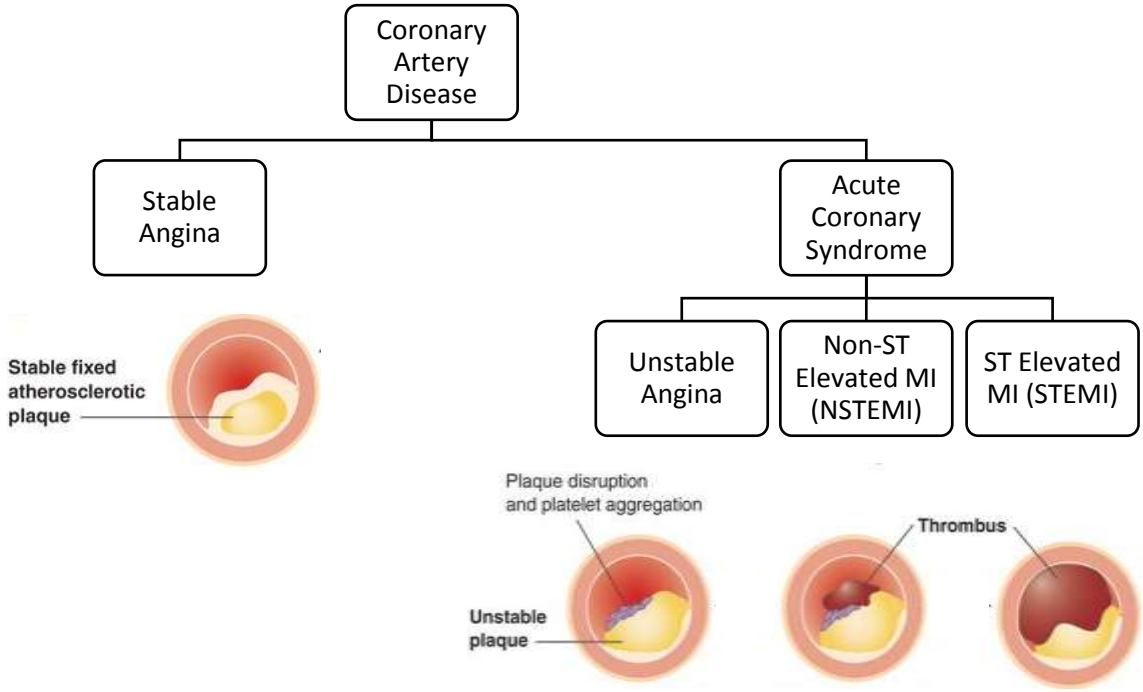

Figure 1.1 <u>Pathophysiology of CAD</u>. A schematic representation of the different terminology and its disease condition (Porth, Matfin, and Porth 2009).

1.2.1 Cellular and Molecular Mechanisms of Atherosclerosis, Pathophysiology and Clinical Diagnosis of CAD

Atherosclerosis which starts with an early atheroma derives its name from Greek; for gruel (athere) and lumps (oma) (Grech 2003). These 'gruel lumps' consist of fat, cholesterol, calcium, connective tissue and inflammatory cells. The build-up of atheroma from an early age is predominantly due to genetic risk factors and several

lifestyle risk factors; the latter being modifiable. Smoking, high cholesterol, diabetes, obesity lack of exercise is among the risk factors that could be controlled via lifestyle changes (Sclavo 2001; Gensini, Comeglio, and Colella 1998; El-Menyar et al. 2011).

Atheroma forms from a deposition of fatty built up in the luminal surface of an artery called a 'fatty streak' seen from an early age (Hong 2010; Misra 2000; Kannel 1976). Although termed fatty deposits they are not composed of just fat cells but as mentioned earlier are a mixture of fat, cholesterol, calcium, connective tissue and inflammatory cells. The accumulation of debris in established atheromas do not appear to be reversible via medications and life style change, but early intervention e.g. healthy lifestyle transformation and prescribed medications, can stabilised their composition and progression (Ahmed et al. 2012; Shai et al. 2010; Bedi et al. 2011; Han et al. 2012; Takayama et al. 2009).

In Greek, the word 'sclerosis' means hardening (Singh et al. 2002). For that reason, atherosclerosis means the hardening of the gruel (fatty) lumps. Atherosclerosis also involves an inflammatory disease component (Ross 1999) and has been defined as "a focal, inflammatory fibro-proliferative response to multiple forms of endothelial injury" (George and Johnson 2010). A normal artery has a lining of single endothelial cells (ECs) on the luminal surface which forms the intima. The ECs are arranged in the direction of the flow on the internal elastic lamina. Beneath the intimal layer is the medial layer that consists of a few layers of concentrically arranged smooth muscle cells (SMCs) and extracellular matrix (ECM) proteins that is bordered by the external elastic lamina (**Figure 1.2 A**). Atheroma is initiated by one; the disruption of the

endothelial lining due to various factors including the risk factors mentioned previously and two; another factor include the physical forces imposed on the ECs due to the location in the circulatory system. This damage of the ECs leads to the accumulation of reactive oxygen species (ROS), upregulation of several adhesion molecules, increased permeability of the arterial wall and activation of circulating platelets. These cumulative events cause the recruitment of low-density lipoproteins (LDL) and leukocytes within the arterial wall (**Figure 1.2 B**). Once inflammatory cells migrate within the arterial wall, monocytes will differentiate into macrophages and subsequently may become foam cell macrophages following uptake of LDL, which has been oxidised within the artery. At this stage, atheroma or 'fatty streaks' are formed these are asymptomatic but have the capacity to progress into atherosclerotic lesions with continued exposure to risk factors (**Figure 1.2 C**).

The further accumulation of foam cell macrophages in the artery wall results in foam cell death and the cells break down, they excrete their cytoplasmic contents that are full of lipids. This leads to the formation of necrotic core within atherosclerotic plaque. The formation of the necrotic core in turn induces further inflammation and proliferation of SMCs that deposit ECM proteins which together result in the formation of a fibrous cap that overlies the necrotic core and can protrude into the lumen of the vessel and partially decrease the lumen size. A thick and intact fibrous cap provides strength to the atherosclerotic plaque and therefore such plaques are classified as stable atherosclerotic plaques (**Figure 1.2 D**). A thin fibrous cap has enhanced propensity to rupture and consequently plaques with a thin cap are categorised as unstable atherosclerotic plaques (**Figure 1.2 E**). Rupture of the fibrous cap exposes the contents of the plaque including necrotic core, cell debris and ECM, to the circulating

blood and leads to the activation of circulating platelets and formation of thrombus that potentially can occlude the lumen and prevents blood flow (**Figure 1.2 F**).

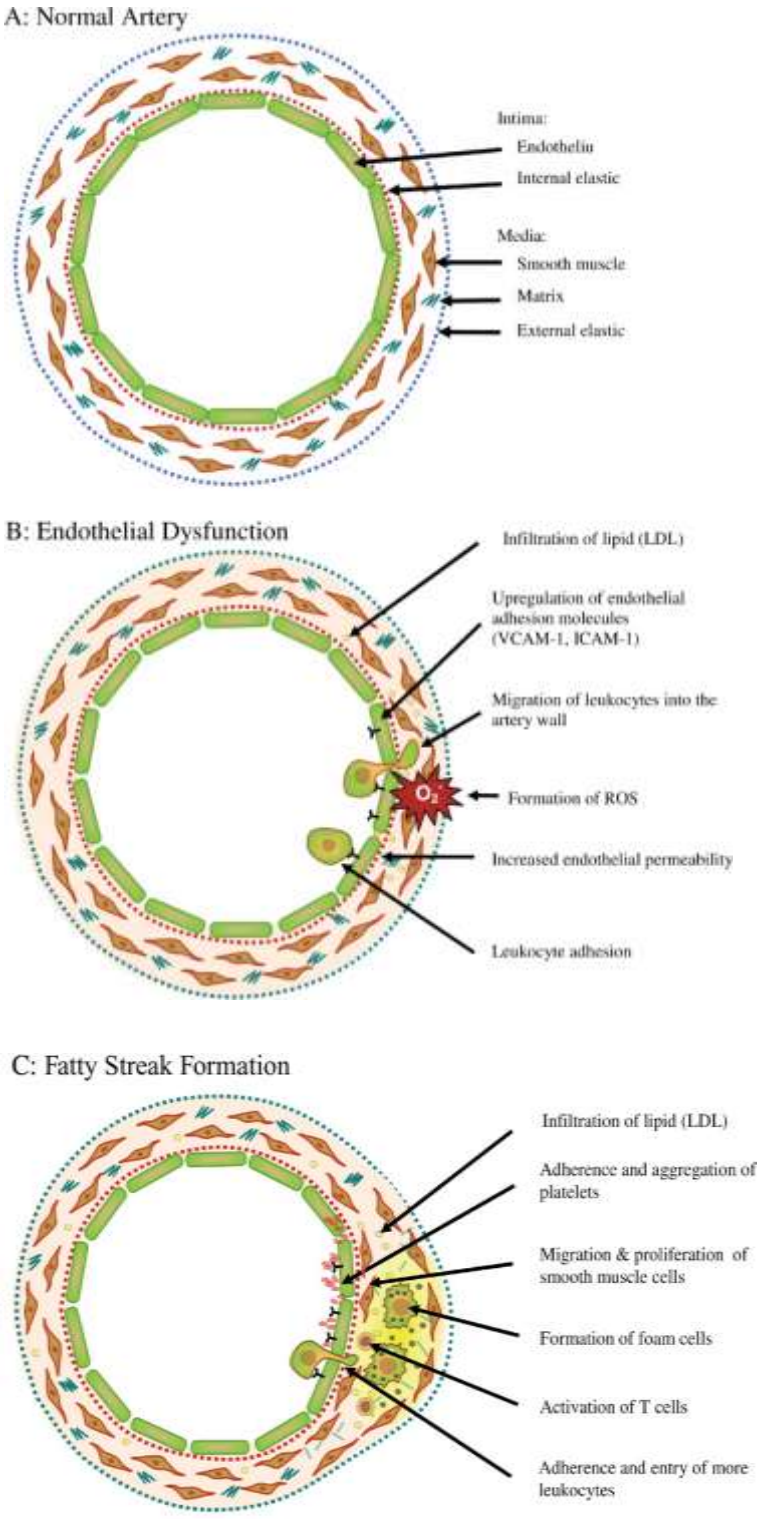

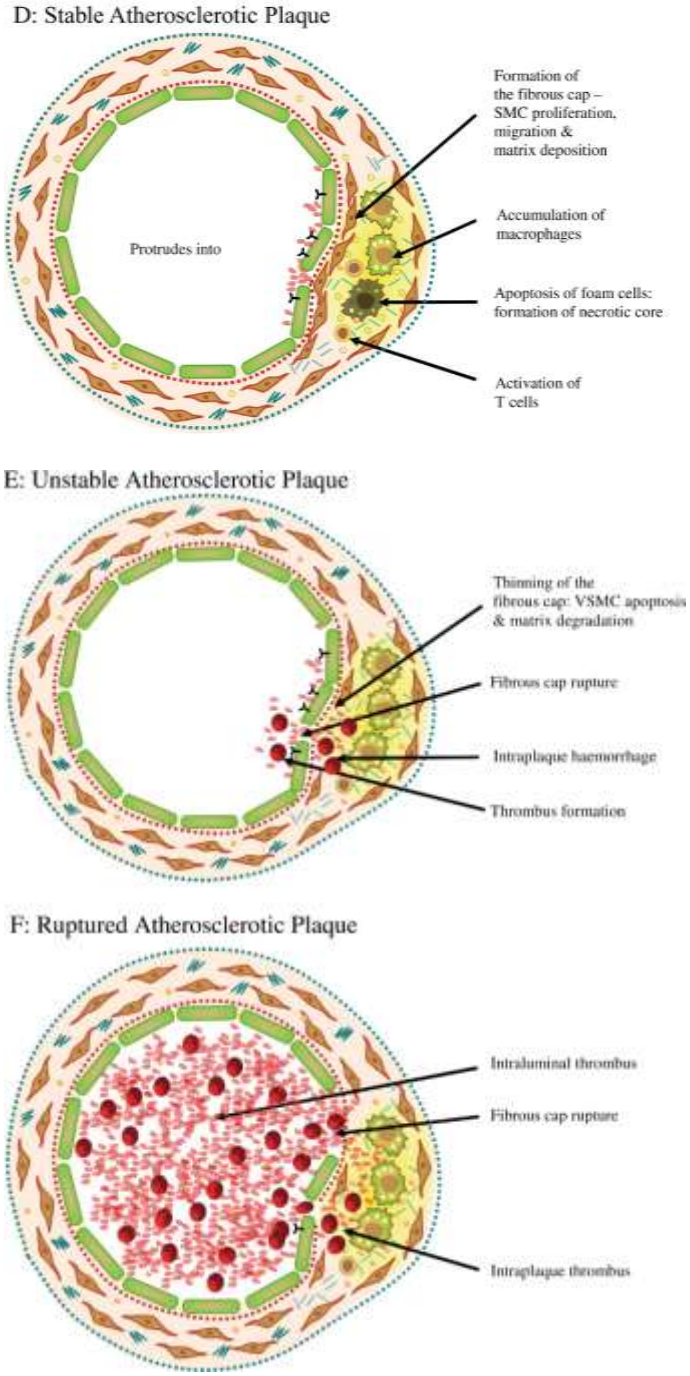

Figure 1.2 <u>Atherosclerotic plaque formation.</u> A simplified schematic representation of atherosclerotic plaque formation of the cellular and molecular level from a normal coronary artery **(A)**, endothelial dysfunction **(B)**, fatty streak formation **(C)**, stable atherosclerotic plaque **(D)**, unstable atherosclerotic plaque **(E)**, to a ruptured atherosclerotic plaque **(F)** (George and Johnson 2010).

Patients with stable atherosclerotic plaques, may not present with any symptoms at rest but may experience symptoms while doing exertive activity due to increased myocardial demand for blood supply and oxygen, that subsides shortly after ceasing the activity. Patients may experience symptoms such as chest discomfort and shortness of breath. These symptoms prompt diagnostic tests to be undertaken and stable angina is diagnosed when certain criteria as ruled out in the ESC guidelines are present (Montalescot et al. 2013, 2014; Roffi et al. 2016). As atherosclerotic plaques progress and fibrous caps are formed, the lumen diameter becomes smaller thus making it harder to pump blood through the diseased coronary artery. Patients will experience the same symptoms as with stable angina but these are more frequent and severe i.e. under mild activity or even at rest. These symptoms may last for several minutes and will subside with rest or with the prescription of anti-angina agents or drugs e.g. diuretics, nitrates, statins, Angiotensin-converting enzyme (ACE) inhibitors, calcium channel blockers and a few others are among the most common drugs in treating CVD as they can reduce workload of the heart. At this stage, the diagnosis is classified as unstable angina (Thygesen et al. 2012; Ambrose and Dangas 2000).

Further progression of atherosclerotic disease triggers more serious clinical effects; either non-ST elevated myocardial infarction (NSTEMI) or ST elevated myocardial infarction (STEMI). STEMI and NSTEMI could be distinguished via electrocardiogram (ECG) patterns; with elevated ST segments in STEMI case due to sudden total blockage of artery/ies. Whereas NSTEMI is often clinically indistinguishable from unstable angina during initial presentation at the hospital. Therefore, the guidelines in management of patients presented with ACS are used as a reference in making a diagnosis (Roffi et al. 2016).

In general, patients admitted to hospital with chest pain/angina undergo an electrocardiogram (ECG) test as well as blood tests to assess the circulating levels of troponins which act as markers of cardiomyocyte death. In the case of confirmed MI with elevated blood troponin, the ECG will help to distinguish between STEMI and NSTEMI. Persistent ST elevation on the ECG is diagnosed as STEMI, which generally reflects a major MI event with substantial myocardial injury in one of the coronary artery territories. If there are abnormalities or undetermined ECG results, further biochemistry testing will be done. Further diagnosis being dependent on the troponin level in the blood: normal troponin level indicates unstable angina; increased or decreased of troponin diagnoses NSTEMI. Simplified diagnosis guidelines are shown in **Figure 1.3**.

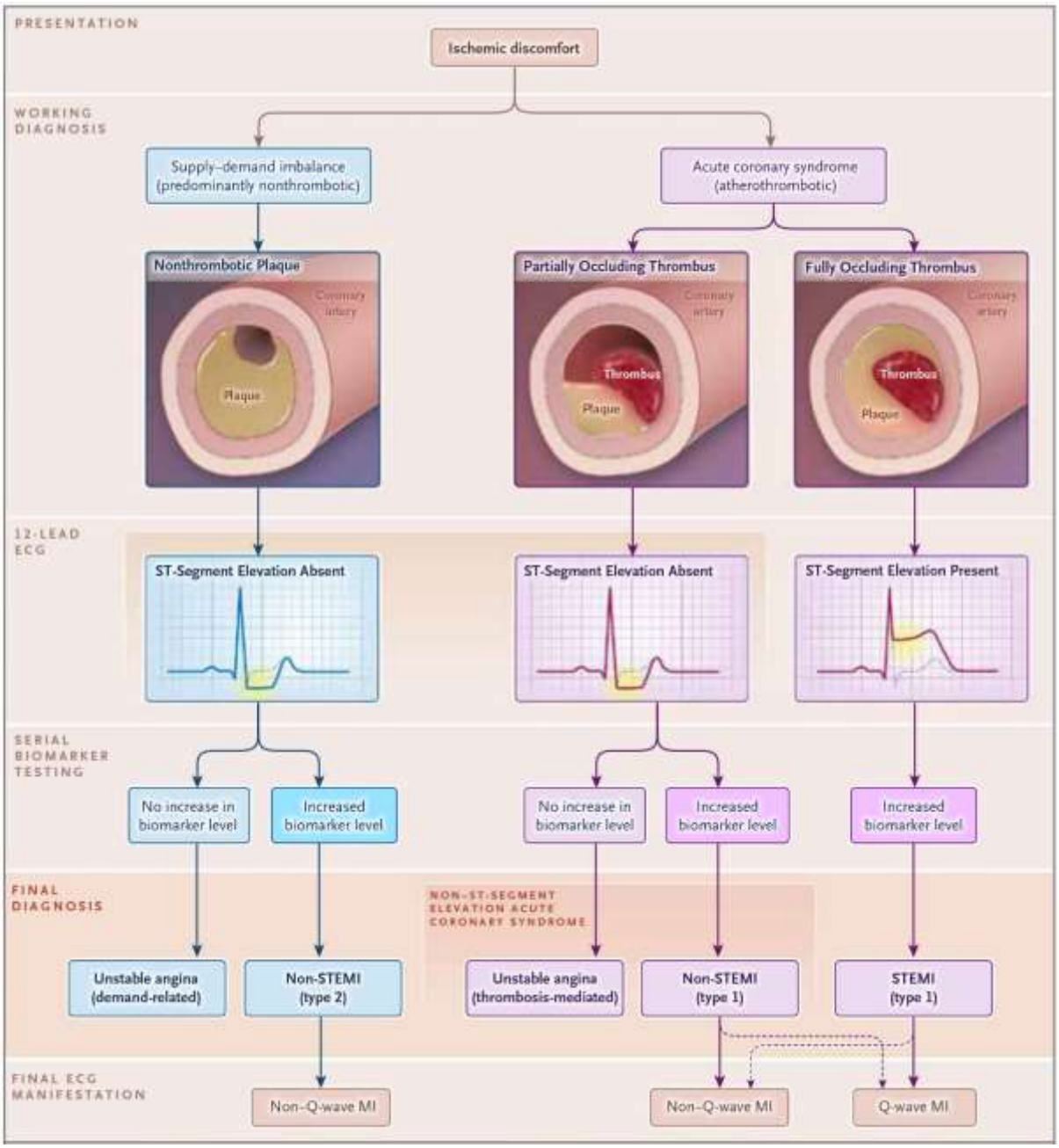

Figure 1.3 <u>Guidelines in diagnosis management of ACS.</u> A simplified flow diagram in diagnosis management of ACS patients published by the European Society of Cardiology (ESC) that is referred to by the majority of medical professionals (Mann et al. 2015; Anderson and Morrow 2017)

The rupture of atherosclerotic plaques with resulting thrombi can lead to total occlusion of the coronary artery, preventing blood flow to the related myocardial territory, hence depriving the heart muscle of oxygen, a condition termed as ischemia and leading to MI. Within 20 minutes to two hours after the on-set of ischemia, the changes to the heart cells are irreversible (Kumar et al. 2010), and without immediate revascularisation and blood reperfusion of the ischemic territory, the cardiomyocytes will undergo necrosis **Figure 1.4**). This in turn will affect the mechanical ability of the heart to pump blood to the entire body (Flachskampf et al. 2011). Therefore, management of the disease before it progresses further is critical.

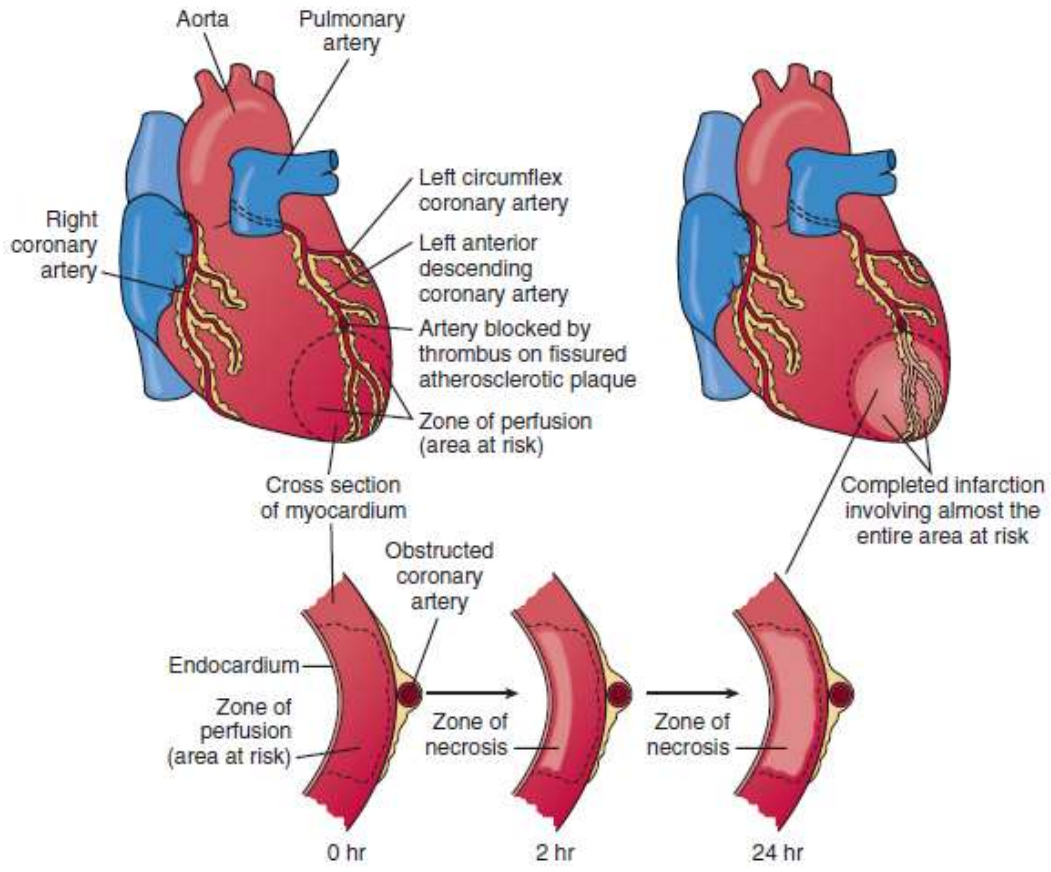

Figure 1.4 **<u>Consequences of atherosclerosis progression.</u>** A schematic representation of atherosclerotic disease progression after total coronary artery occlusion as a result of a ruptured atherosclerotic plaque (Mann et al. 2015).

1.2.2 Currently Applied Treatments and Prevention of CAD Progression

The current treatment options for severe CAD include drug prescription, coronary angioplasty (**Figure 1.5**), surgery (**Figure 1.7**) or heart transplantation (Montalescot et al. 2013, 2014; Roffi et al. 2016). There are a variety of pharmaceutical approaches that can be used for patients with CAD. Anti-platelets, statins, beta-blockers and nitrates are among the most common drugs prescribed for patients with CAD as they can reduce thrombus formation, normalise the cholesterol levels, reduce the oxygen demand of the heart and increase the coronary blood flow. In the case of patients with history of MI, at time diuretics are also used to reduce the workload of the heart. These pharmacological approaches do not treat or reverse the disease but help in preventing progression and curbing the symptoms in the early stages of disease.

Coronary angioplasty is a procedure done to widen the narrowed or blocked arteries with balloon catheter and is also known as percutaneous transluminal coronary angioplasty; PTCA. Angioplasty is also done with the incorporation of a stent where the combinatory use of both angioplasty and stent is called percutaneous coronary intervention; PCI. PCI procedures utilise a variety of commercially available stents. Stents are metal mesh tubes delivered percutaneously into the diseased artery through a needle in a wire catheter and deployed with a balloon. They are used to resolve the narrowing induced by the atherosclerotic blockage to normalise blood supply and relieve symptoms (**Figure 1.5**).

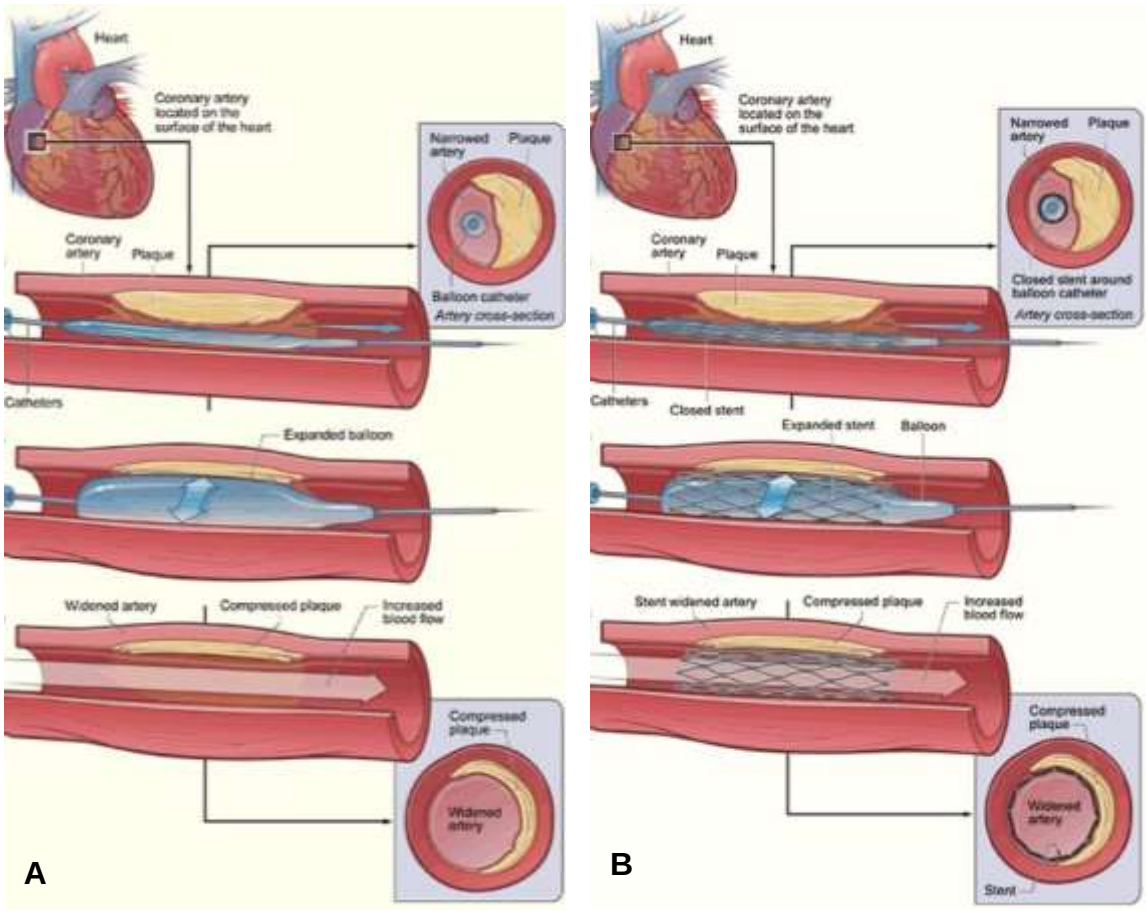

Figure 1.5 <u>Balloon Angioplasty and Stent Implantation Procedure</u>. A special balloon tipped catheter is inserted into the coronary artery. The balloon is inflated which widens the lumen **(A)**. In most cases a stent is implanted within the artery **(B)** (Torpy, Lynm, and Glass 2004).

Bare metal stents (BMS) were the first type of stent device developed to treat CAD. BMS were proven to show better outcome than balloon angioplasty as it lowers the restenosis occurrence to 17 to 41 % (with BMS) from 32 to 55 % (with balloon angioplasty)(Buccheri et al. 2016). Unfortunately, BMS caused high rates of in-stent re-blockage (restenosis) as the permanently deployed metal device triggered chronic SMC proliferation and inflammation within the vascular wall due to EC denudation. Consequently, the intervention that was undertaken to slow down the disease progression failed as the disease progressed in an accelerated fashion (Bhatia,

Bhatia, and Dhindsa 2004).Complications after PCI are usually in-stent restenosis (ISR) were observed within 6 months after the intervention procedure as shown in Figure 1.6 (Mohr et al. 2013; Torrado et al. 2018). ISR is defined by >50% blockage or stenosis at the stent segment or 5 mm adjacent to the stents (Mehran et al. 1999; Kuntz and Baim 1993). Often patients are readmitted to hospital for very expensive repeat revascularisation with additional stents or for CABG surgery.

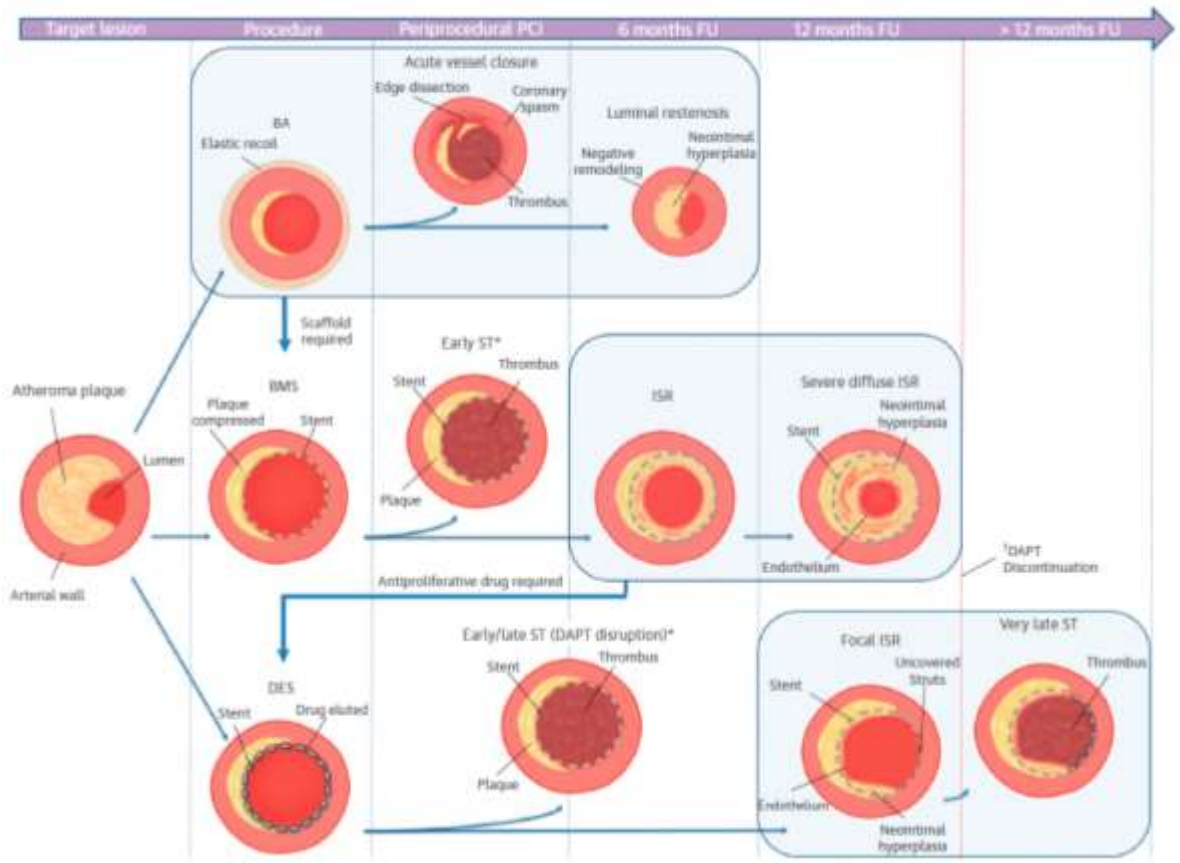

Figure 1.6 <u>Complications of PCI procedures.</u> PCI approaches and the consequent limitations that arise after the procedures due to thrombus formation early-on between periprocedural and up to 6 months follow-up (FU), neointima hyperplasia (NIH) at in the 6 months follow-up, and ISR thereafter (Torrado et al. 2018). (BA: Balloon angioplasty, ST: Stent thrombosis, DAPT: Dual antiplatelet therapy).

Therefore, drug eluting stents (DES) were developed. The first generation of DES includes the use of BMS with the incorporation of anti-proliferative drug to hinder the SMC invasion and proliferation. The main anti-proliferative drugs used in DES are rapamycins and taxanes which has different mode of actions. Rapamycins are called limus-drugs and its analogues (e.g. sirolimus, everolimus, zotarolimus, biolimus etc.) act to inhibit SMC proliferation by acting on the mammalian TOR receptor (mTOR) thus blocking the cell cycle at G1 and S phase (Wessely and Andres 2012; Ielasi, Latib, and Colombo 2014; Yin, Yang, and Wu 2014). Whereas, tanaxes (e.g. paclitaxel) disrupt the cell cycle at G0/1 and G2/M phases by inhibiting the microtubule depolymerisation (Kellogg et al. 2017; Abal, Andreu, and Barasoain 2003). Initial results showed that DES does in fact reduce early ISR to less than 10% occurrence and the need for repeat revascularisation (Chen and Lin 2009; Buccheri et al. 2016; Kastrati et al. 2005). Despite the early positive outcome, the first generation DES causes elevated rates of late and very late stage stent thrombosis (ST) due to inhibition of EC proliferation and repair as the drugs acts non-selectively to different cell types (Lüscher et al. 2007; McFadden et al. ; Iakovou et al. 2005).

The second generation DES include a combination of anti-proliferative drugs and improvement of materials used in the development of stent using polymers instead of metal for their biocompatibility properties e.g. polystyrene-b-isobutylene-b-styrene, polyethylene-co-vinyl acetate (PEVA) and poly n-butyl methacrylate (PBMA). More recently advances are the bioabsorbable and biodegradable stents (commercially known as bioresorbable vascular scaffolds (BVS)) have been developed which aim to limit the occurrence of intimal hyperplasia due to their degradable nature. The feasibility, safety and efficacy of BVS is still being evaluated following the first human

implants undertaken by a Japanese group in 2000 (Iqbal, Gunn, and Serruys 2013). The European Medical Agency (EMA) approved the use of BVS in 2011, initiating the fourth evolution in interventional cardiology (Iqbal, Gunn, and Serruys 2013; Bowen et al. 2016). Unfortunately, the outcome of the first generation of BVS has not met expectations and evidence suggest that they may be associated with higher rate of adverse cardiovascular events compared to DES (Serruys et al. 2016; Ali et al. 2018). Hence, the manufacturer has taken the BVS out of the market voluntarily to improve their technology and they are working with the regulatory bodies, e.g. EMA and Food and Drug Administration (FDA) to address these issues (Henriques and Elias 2017).

Until early 2000, CABG surgery was the gold standard route of revascularization for CAD patients. This remains the case for complex CAD cases with left main stem (LMS) disease, multi-vessel disease (MVD), and impaired LV function, as supported by the landmark SYNTAX trial(Mohr et al. 2013; Serruys et al. 2009). Recent years have shown a shift to PCI procedures for patients with no LMS or MVD disease due to the cost effectiveness of PCI versus CABG even when long-term results of CABG remain superior (Habib et al. 2015; Locker et al. 2016; Ariyaratne et al. 2014; Raja et al. 2015).

Unfortunately, all of the available treatments for CAD have limitations. The pharmacological treatments cause life–long dependencies to administered drugs and are not always effective for reducing symptoms. In addition, in-stent restenosis and thrombosis are common problems with PCI-stent. Transplantation related to CAD is only be considered for end-stage heart failure in CAD patients either suffering several

heart attacks leading to extensive myocardial scarring or afflicted by diffuse coronary disease not amenable to conventional PCI-stent or CABG.

CABG is the most effective treatment in terms of relief of symptoms and long-term benefits (Ariyaratne et al. 2014; Habib et al. 2015; Locker et al. 2016; Raja et al. 2015). CABG consists of harvesting autologous arterial and/or venous conduits from the patient and using the conduit to construct grafts that bypass the blocked segment of the artery to improve/normalise blood supply. The most commonly used conduits for CABG are internal mammary artery (IMA) and saphenous vein (SV). Less often radial artery (RA) or other conduits were used. On average patients undergoing CABG surgery have three bypass grafts using autologous vessels, as mention earlier IMA from the chest and SV from the legs (Otsuka et al. 2013). The autologous SV is the most common conduit used for CABG surgery covering approximately 70-75% of all bypass grafts (Chlupac, Filova, and Bacakova 2009). The remaining 25-30% of all grafts are performed using IMA (Harskamp et al. 2013).

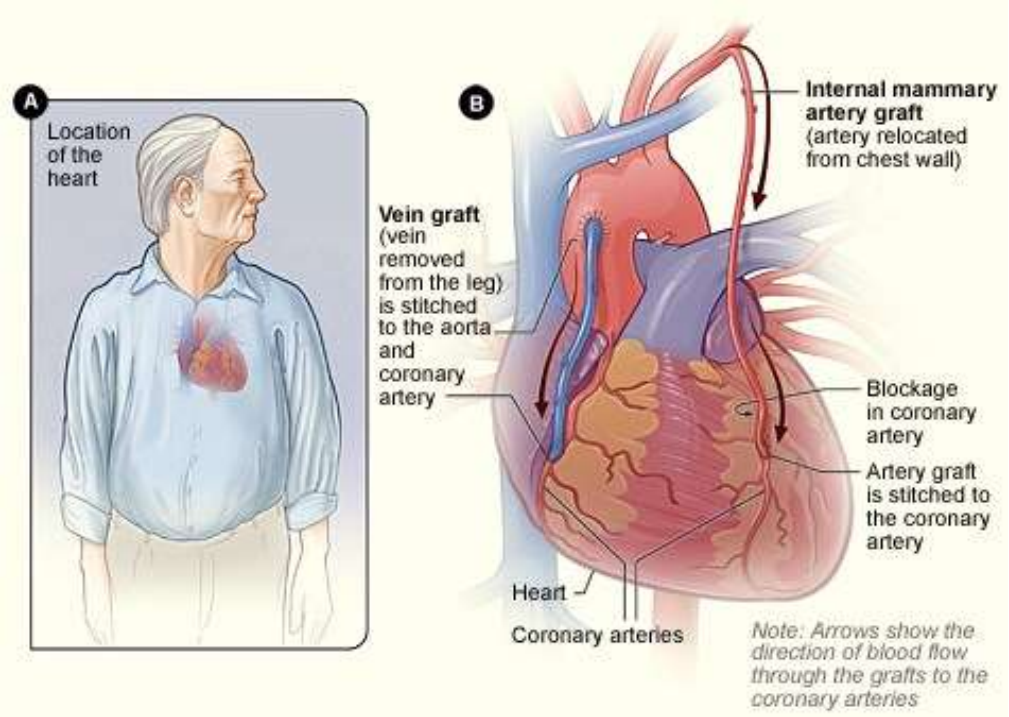

Figure 1.7 Coronary artery bypass graft (CABG). The procedure involves identifying the location of the blockage in the coronary artery and grafting a vascular conduit to bypass the blockage. The conduit is usually a portion of the saphenous vein of the leg (SV) or the internal mammary artery (IMA). The conduit is grafted with the use of very fine sutures (Mann et al. 2015).

Evidence suggests that an IMA graft to the left anterior descending (LAD) coronary artery is associated with improved life expectancy benefits and very high patency rates (92-95 %) at 15-20 years (Cosgrove et al. 1986; Loop et al. 1986). Confirmatory studies demonstrate improved 10-year survival rates associated with the use the IMA conduit as opposed to only SV grafts (Cosgrove et al. 1986; Loop et al. 1986). In keeping with these findings, another confirmatory study suggests that not using an IMA graft is associated with increased risk of late MI, recurrence of angina, and need for repeat revascularisation (Cosgrove et al. 1986; Loop et al. 1986). Unfortunately

10-15% of SV grafts become occluded at 1-year after surgery due to early vein graft thrombosis and up to 50% are occluded at 10 years due to intimal hyperplasia and superimposed atherosclerosis (**Figure 1.9**)(de Vries and Quax 2018; de Vries et al. 2016).

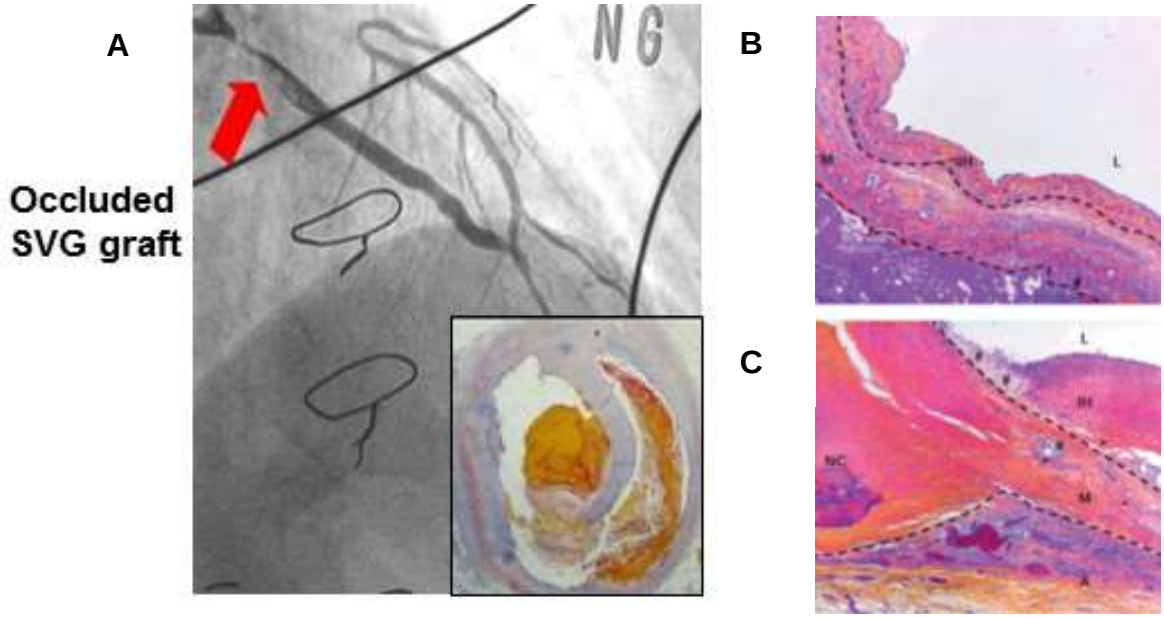

Figure 1.8 <u>Long-term failure of SVG.</u> (A) Angiogram of an occluded SV graft (red arrow indicates the location of the occlusion) due to atherosclerosis (insert). **(B & C)** Further histological analysis of the failed SVG identifies the presence of intimal hyperplasia (IH), necrotic core (NC), foam cells (#) and neo-vessels (*). Adventitia layers, medial layers and lumen are indicated by A, M and L, respectively (de Vries et al. 2016).

The development of vein graft failure is a major concern in vein grafting. SVGs are more prone to atherosclerosis than RA grafts, and IMA grafts display overall resistance to atherosclerosis (Pashneh-Tala, MacNeil, and Claeyssens 2015). The vein grafting procedures causes endothelial damage on the vein graft because of the differences of arterial hemodynamic forces that the vein graft was subjected to within hours of the

procedures (de Vries et al. 2016; Harskamp et al. 2013). Within days after vein graft procedures, endothelial dysfunction results in platelets and leukocytes adhesion that releases a range of growth factors and cytokines which leads to the initiation of the coagulation cascade with fibrin deposition (de Vries et al. 2016). These factors in turn will lead the way to thrombus formation within the first month after CABG.

When monocytes infiltrate in the vessel wall and differentiate into macrophages, this will cause SMC death and release of cytoplasmic contents and factors that causes the remaining of SMC to undergo phenotypic switch from contractile to synthetic phenotype (de Vries and Quax 2018). Synthetic SMC has higher proliferation and migration rate thus causes the development of neointimal hyperplasia within a month to a year after vein grafting. Further development intimal hyperplasia is due to the migration of adventitial fibroblast and SMC secreting ECM within vessel wall and increase thickening of the vessels wall and decreasing lumen size. Atherosclerosis occurs after more than 2 years after CABG (de Vries et al. 2016; Hess et al. 2014).

Therapeutic approaches currently applied to combat vein-graft disease include the practise of “no-touch technique” and “endoscopic vein-graft harvesting” of SVG to help minimise trauma during harvesting and preserving endothelial layer of SVG (Parang and Arora 2009). Prescription of antiplatelet agents such as aspirin and clopidogrel and longer dual antiplatelet therapy post-operative were one other approach undertaken to hinder platelet adhesion on vessel wall that leads to the activation of various factors that marks the beginning of atherosclerosis as mention in figure 1.9 (de Vries and Quax 2018; Becker et al. 2008; Mangano 2002). Glyceryl trinitrate and

verapamil solution which are vasolidator were also use to increase the vessel lumen thus improve the long term patency of vein graft (Roubos et al. 1995).

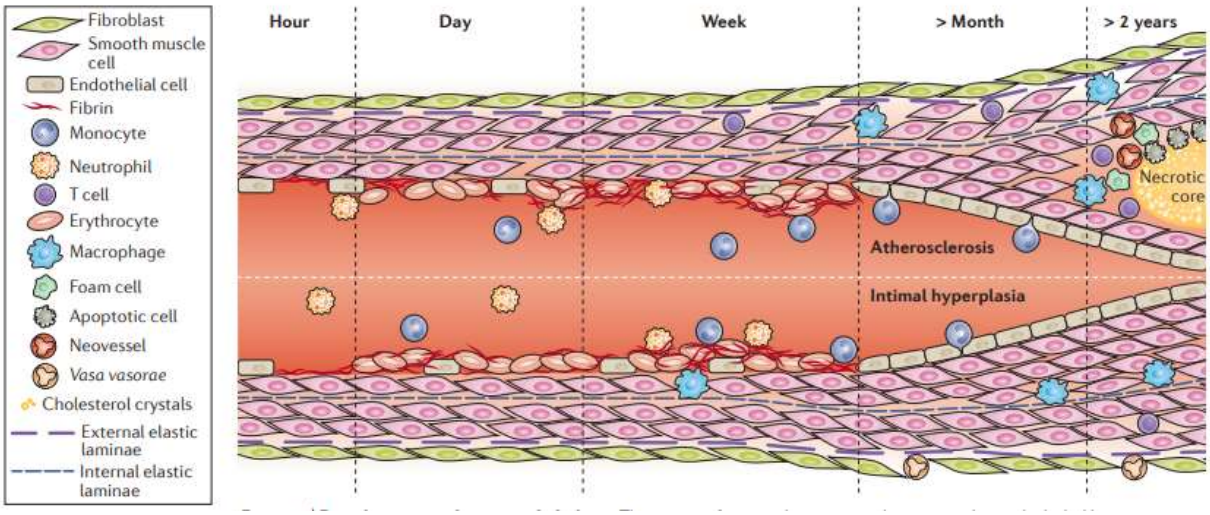

Figure 1.9 Vein graft failure timeline. Sequential events that leads to vein graft failure started as early as a few hours after procedures with endothelial layer dysfunction that causes the recruitment and infiltration of platelets and leukocytes and would further enhanced acceleration of atherosclerosis formation (de Vries and Quax 2018).

The interdisciplinary collaboration between basic science and clinical research help in understanding the mechanism of vein graft failure and the translational application of any possible treatment in a clinical setting. One other hypothesis is that the development of atherosclerosis in grafts maybe due to the anatomic and physiological properties of the conduit (**Table 1.1**). Anatomically, IMA has a smaller diameter (IMA: 1.9 – 2.6 mm and SV: 3.1 – 8.5 mm) and more compact wall thickness about 180 – 430 µm than SV which varies from 180 – 650 µm (Barner 2013; Barner and Farkas 2012). IMA has a thick endothelial layer with very few endothelial fenestrations which

are the contrary of SV. A well define internal elastic lamella (IEL) with high heparin sulphate content were also observed in IMA but not in SV (de Vries and Quax 2018). The SMCs in the medial layer are arranged circumferentially in between IEL of IMA but SMCs has a dual conformational alignment with longitudinally arranged inner layer and circumferentially aligned outer layer (Sur, Sugimoto, and Agrawal 2014). Unlike SV, IMA has minimal dependence on vasa vasorum and has no valves along the length of the vessel. In addition to that, SV has eight times more basic fibroblast growth factors (bFGF) receptors than IMA. In terms of the physiological properties of IMA and SV, their flow reserve, shear stress and production of vasodilators (e.g. nitric oxide and prostacyclin) are the same. The differences are in their contrary vasomotor response to thrombin, vasoconstrictor and vasodilator sensitivity. The lipid lysis, synthesis and uptake were also on the opposing spectrum which heighten the atherosclerosis progression in SV than IMA (Sur, Sugimoto, and Agrawal 2014; Motwani and Topol 1998).

Table 1.1 Comparison of anatomic and physiological properties of IMA and SV (Motwani and Topol 1998; Otsuka et al. 2013).

Properties	IMA	SV
Anatomic properties		
Diameter	1.9 – 2.6 mm	3.1 – 8.5 mm
Wall thickness	180 – 430 microns	180 – 650 microns
Endothelial fenestrations	Few	Many
Intercellular (IC) processes	Many	Few
IC junction permeability	Low	High
Internal elastic lamina (IEL)	Well defined	Poorly defined
Heparan sulphate in IEL/media	High	Low
Dependence on vasa vasorum	Minimal	High
Valves	Absent	Present
Size match with grafted native vessel	Good	Poor
Resistance to trauma of harvesting	High	Low
Physiological properties		
Flow reserve	High	Low
Shear stress	High	Low
Nitric oxide/prostacyclin production	High	Low
Vasomotor response to thrombin	Relaxation	Constriction
Vasoconstrictor sensitivity	Low	High
Vasodilator sensitivity	High	Low
Basic fibroblast growth factor receptors	Few	Many (8 times more than IMA)
Lipolysis	Rapid	Slow
Lipid synthesis	Less active	More active
Lipid uptake	Slow	Rapid

Arterial grafts are therefore considered desirable for CABG. Despite being the graft of choice, surgeons are still not inclined to practice bilateral IMA (BIMA) grafts. Evidence shows there are basically no differences in short-, mid- and long-term patency rates between single or bilateral IMA in CABG (Vallely, Edelman, and Wilson 2013), yet surgeons do not opt for BIMA. This may be due to the fact that total arterial grafting is more time consuming, technically more difficult, and at times may not be advisable due to comorbidities and increased risk of sternal wound poor healing.

In order to treat severe CAD, IMA are a better graft than SV but multiple IMA grafts are not preferred due to several clinical and surgical reasons and due to the lack of sufficient IMA for all the required grafts. The next best conduit is SV, but they do have lower graft patency affecting long-term outcome. The questions remain how can SV graft patency be improved and would arterialisation of veins *in vitro* before implantation be an alternative?

1.3 Peripheral Arterial Disease

Three- to six-fold increase in the risk of CV death is associated with PAD (Davies et al. 2017). PAD covers various diseases that affect non-cardiac and non-intracranial arteries. The main cause of PAD is atherosclerosis. Atherosclerosis can cause a stroke when it occurs in neck and brain arteries, and can cause PAD when it is located in the arms, legs and aorta. PAD prevalence in the Western World population is 13% in those older than 50 years (Crawford et al. 2016). Based on a systemic review by Fowkes *et al.*, it is estimated that the number of people living with PAD increased 23.5% between 2000 to 2010. By the end of 2010 more than 202 million people are reported to be affected by PAD globally (Fowkes et al. 2013). The prevalence of PAD is therefore higher than that of HIV with 34 million people living with HIV, which is classified as a pandemic disease (Hirsch and Duval 2013).

1.3.1 Pathophysiology and Clinical Diagnosis of PAD

PAD is usually asymptomatic with almost 65-75% of patients not realising they suffers from the disease (Morley et al. 2018; Abdulhannan, Russell, and Homer-Vanniasinkam 2012). The classical presenting symptom is usually intermittent

claudication (IC) which occurs the same way as angina occurs but with pain in the leg with PAD, when insufficient blood supply to the leg occurs. The term claudication is derived from the Latin word claudicatio, meaning “to limp” (Mann et al. 2015). Claudication is a condition where pain is experience in the lower extremities during exercise which resolved when at rest. The differential diagnosis of claudication into arterial, neurogenic and venous claudication are based on its pathology, sites of pain laterality, pain onset, and presenting symptom. The pathology of arterial claudication is described as stenosis of major lower limb arteries where muscle is identified as the site of pain usually the calf muscle but may affect thigh and buttock. Gradual onset after walking certain distance and symptom disappear after 1 to 2 minutes cessation of walking (Abdulhannan, Russell, and Homer-Vanniasinkam 2012; Davies et al. 2017; Hankey, Norman, and Eikelboom 2006; Walker et al. 2015).

In diagnosing PAD, the patient’s medical history is screened for risk factors and family history, and physical examination of the leg and ankle brachial index (ABI) are performed. ABI was developed and proposed as a definitive test for PAD in the early 1950s as a mean to distinct claudication from other leg pain such as spinal stenosis which has similar symptoms to claudication during exercise. ABI is a simple measurement of the ratio of systolic blood pressure at the ankle to that of the arm at rest and after exercise. A low ABI reading is suggestive of atherosclerosis of the lower extremities. A definitive cut off point for presence of PAD is generally accepted as an ABI <0.9. For patients with ABI <0.9, their extremities risk is assessed and classified into claudication or critical limb ischemia (CLI) based on their anatomical and physiological evaluation. Detailed procedure of PAD evaluation is shown in Figure 1.9.

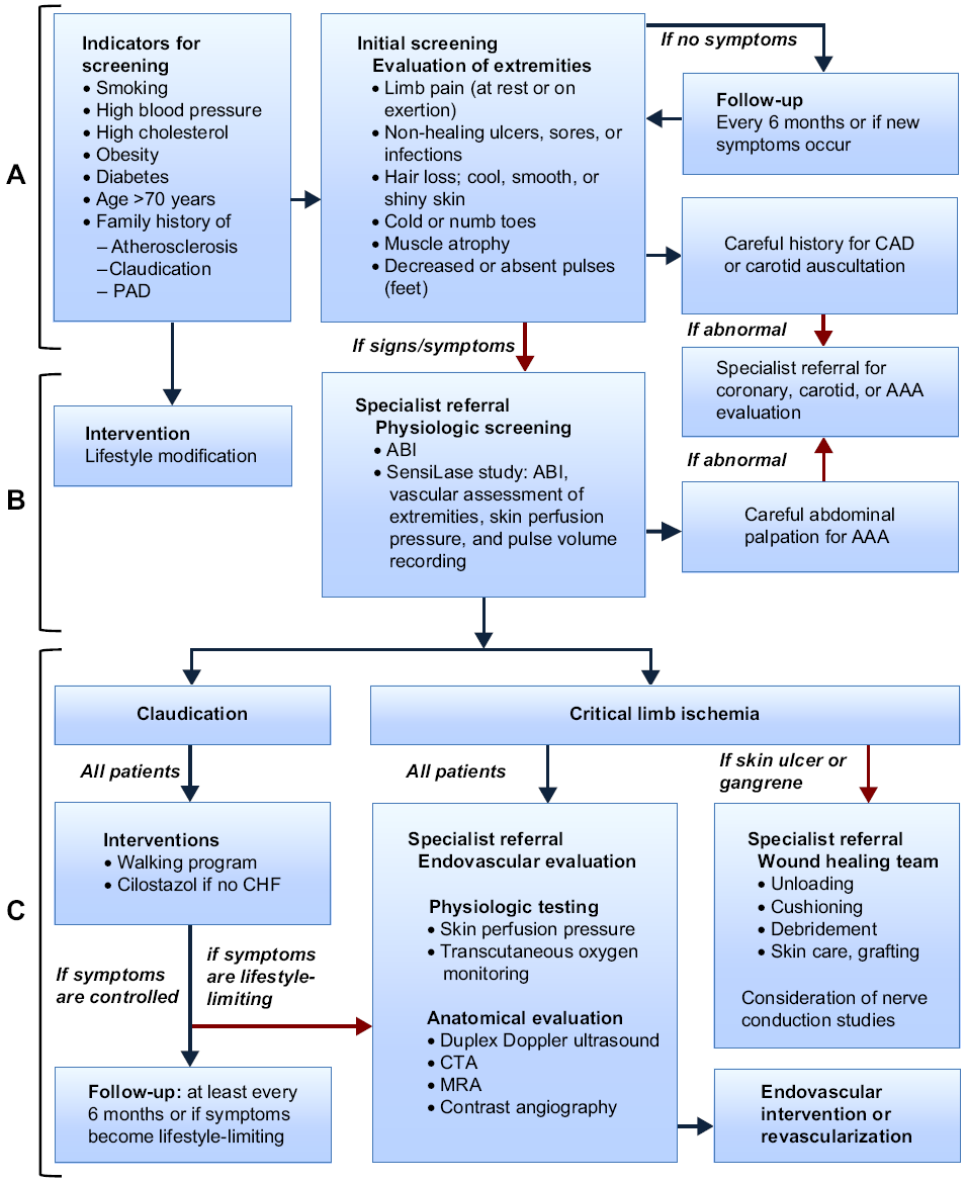

Figure 1.10 **<u>Diagnosis and management of PAD patients.</u>** The scheme illustrates patients that are at risk of PAD **(A)**, patients with symptoms of PAD **(B)**, patients diagnosed with PAD **(C)**. AAA: Abdominal aortic aneurysm; CHF: Congestive heart failure; CTA: Computed tomographic angiography; MRA: Magnetic resonance angiography (Walker et al. 2015).

1.3.2 Currently Applied Treatments and Prevention of PAD Progression

The currently applied treatments for PAD patients are aimed to reduce the risk of stroke and death, protection of the feet and legs to reduce the risk of ulceration and amputation, and to improve quality of life. The approaches utilised for treating patients with PAD are similar to CAD, where patients are first being managed through medical therapies (lifestyle changes and prescription drugs), followed with catheter based revascularisation (balloon angioplasty or stent deployment), and surgical based approach (reconstructive surgery via graft placement).

Medical therapies of PAD include management of risk factors such as smoking, dyslipidaemia, diabetes mellitus, hypertension, with lifestyle modifications and drug therapies. The two most relevant lifestyle changes in dealing with PAD are exercising regularly and cessation of smoking. PAD symptoms could be reduced and reversed by exercising regularly as recommended by National Institute for Health and Care Excellence (NICE) (Morley et al. 2018). Smoking had been proven to increase the risk of CVD and worsen PAD development, therefore cessation of smoking or nicotine replacement are recommended therapies for PAD patients (Lu and Creager 2004; Lu, Mackay, and Pell 2014; Sotoda et al. 2015). The American College of Cardiology/American Heart Association (ACC/AHA) recommendations for patients with PAD include a set of goals to manage risk factors such as: (a) for dyslipidaemia management a serum low-density lipoprotein (LDL) cholesterol goal reduced to 70 mg/dL with the prescription of statins; (b) blood pressure target at <140/90 mmHg for non-diabetic patients and <140/90 mmHg for diabetic patients with the help of antihypertensive agents including beta blockers; (c) standard target of Haemoglobin A_{1c} <7% in managing diabetic patients (Rooke et al. 2013; Hankey, Norman, and

Eikelboom 2006; Abdulhannan, Russell, and Homer-Vanniasinkam 2012). Antiplatelet (e.g. aspirin and clopidogrel) therapy is another medical management prior to endovascular and surgical approach with the consideration of anticoagulant (e.g. warfarin) for patients diagnosed with CLI.

Endovascular treatment of PAD is a catheter-based revascularisation via balloon angioplasty or stent deployment similar to the treatment for CAD as mention in section 1.2.2. The choice of stents is similar to those use in CAD treatment. When medical and endovascular approaches are inadequate or fail, open surgical revascularisation is utilised. When PAD affects a large surface area of the lower extremities the graft length required may be extensive (**Figure 1.10**). Unfortunately for PAD, IMA conduits are not suitable and the only available conduits are SVG or synthetic grafts. Therefore, fostering research on synthetic and alternative graft for the treatment of PAD, which results in the use of synthetic grafts such as Dacron and polytetrafluoroethylene (PTFE). Regrettably, patients with PAD are confronted with the fact that SVG and synthetic bypass blockage occurs in approximately 50% of grafts within 2-4 years.

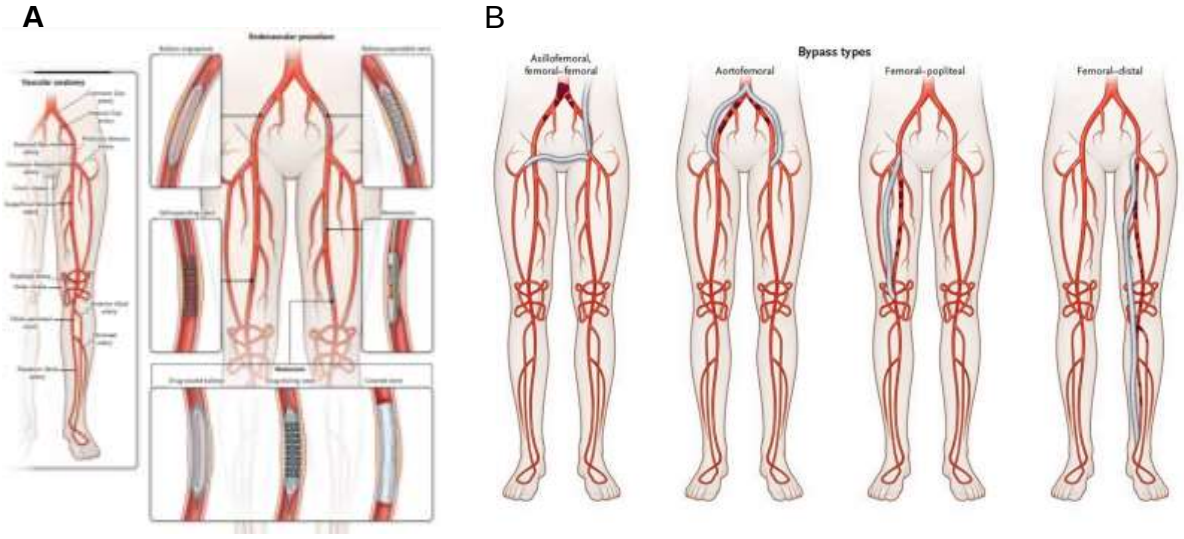

Figure 1.11 <u>Treatment of PAD.</u> (A) Endovascular approach via balloon angioplasty or stenting. **(B)** Surgical approach to bypass the blocked artery using either vein or synthetic graft (Creager, Beckman, and Loscalzo 2012).

Given the huge need to treat patients affected by severe CAD and/or PAD effectively, improving the outcome of bypass grafts using SVG (CAD) and synthetic grafts (PAD) is desirable. This has prompted the scientific community over the last decade to adopt a combination of tissue engineering and regenerative medicine technologies to investigate the feasibility of the production of conduits *in vitro* with arterial features that are suitable to treat CAD and PAD diseases.

1.4 Tissue Engineering and Regenerative Medicine

The term “Tissue Engineering” was coined in 1983 and was officially presented and defined at the Granlibakken conference in 1987 (Skalak and Fox 1988). The ‘Principles of Tissue Engineering and Methods of Tissue Engineering’ published in 1997 and 2002 (Lanza, Langer, and Chick 1997; Atala and Lanza 2002) are the

primary references for researchers embarking in this field. However, research which we now call tissue engineering (TE) can be tracked back to the 1970s. Even though this field is still in its infancy, the success stories are numerous and include clinical trials at various phases. Some tissues have been successfully engineered including skin, bone, cornea, cartilage and nerves (Levine 2007; Kay 2007; Hodges and Atala 2007; Setton, Bonassar, and Masuda 2007; Sambanis 2007; Smith and Sharpe 2007; Mansbridge 2007).

Tissue engineering is an ever-expanding field, and this is shown by the increase of related published articles in PubMed from just less than a thousand articles in 1990 to more than 70 000 articles to date. Tissue engineering is an alternative approach to drug therapy, gene therapy and whole organ transplantation. It attempts to replace cells that are missing within an otherwise functional tissue or organ, and hence it is considered part of regenerative medicine. The basic principle of tissue engineering involves three main components; biomaterials, cells and regulatory signals. This is called the tissue engineering triad (**Figure 1.11**).

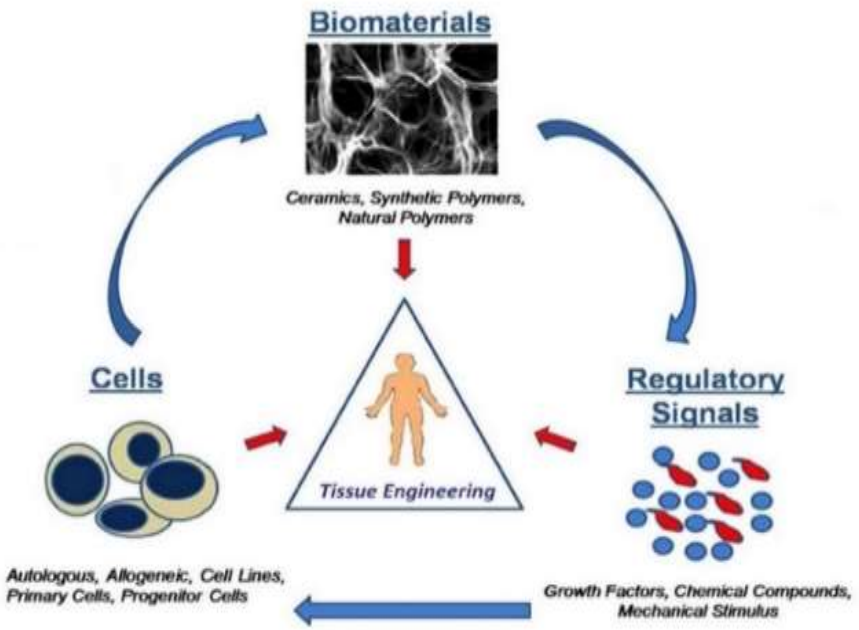

Figure 1.12 The tissue engineering triad. The triad consists of (a) biomaterials; to which the cells attach and migrate into and it provides supports for cell growth, (b) cells are the source of matrix remodelling and (c) regulatory signals that induce cell differentiation and tissue formation (Murphy et al. 2013)**.**

The most successful results in tissue engineering are perhaps related to skin. There are several “off-the-shelf” products available of engineered skin since the first FDA approved TransCyte in 1997, such as EpiDex, Dermagraft, Integra, Epicel, Alloderm and Xenoderm (Bello, Falabella, and Eaglstein 2001; Pape and Byrne 2000; Ortega-Zilic et al. 2010; Hafner, Kuhne, and Trueb 2006). In addition, promising results have been achieved in the areas of cartilage and bone tissue for example with the introduction of Carticel for replacement of damaged cartilage and Osteogenic Protein 1 (OP-1) Implant, for severe case of recalcitrant long bone non-unions (Ratcliffe 2011; Pelissier et al. 2014).

Theoretically any tissue could be engineered. However, every single component and the combinations need to be critically selected, analysed and the combination optimized. Skin, cartilage and bone have been successfully engineered from extensive research in each field and through interdisciplinary collaboration; medical, engineering and science researchers work together to produce a feasible product for patients. The tissue engineering concept has only been successful due to the interdisciplinary collaboration.

1.5 Tissue Engineered Vascular Grafts (TEVG)

The relationships between the components of the triad and the dynamics involved in combining them are studied independently or collectively by interdisciplinary groups. Pasneh-Tala and colleagues wrote a very comprehensive review on the tissue engineered vascular graft that covers the 3 TE triads; the past, present and future of TEVG in CABG (Pashneh-Tala, MacNeil, and Claeyssens 2015).

1.5.1 Biomaterial

The selection and construction of the biomaterial is a whole new field of research that stems from the tissue engineering field. The progression of the field has led to the term ‘biomaterial’ to be redefined from ‘a nonviable material used in a medical device, intended to interact with biological systems’; to ‘material intended to interface with biological systems to evaluate, treat, augment or replace any tissue, organ or function of the body’. There are a variety of factors to consider in producing a TEVG. Key factors to consider in designing a TEVG include biodegradability, mechanical

properties, scaffold architecture, manufacturing technology and biocompatibility (O'Brien 2011).

Early TEVG were designed using polymers such as polyethylene terephthalate (PET) (e.g. Terylene or Dacron) or PTFE (e.g. Teflon or Gore-Tex) (Chlupac, Filova, and Bacakova 2009). PTFE and Dacron were shown to be effective, although mostly at early and mid-term stage, feasible for large diameter (>5 mm) vessels such as those use for grafting of the aortic bifurcation, aorto-femoral, femoro-femoral and axillo-femoral (Chlupac, Filova, and Bacakova 2009; Peck et al. 2012). For example, this type of results were obtained in patients with ischemic limbs where grafting of naked PTFE grafts were performed in 822 patients with a mean age of 70 years and with equal gender distribution (Sauvage et al. 1986; Veith, Ascer, and Gupta 1986). Unfortunately, when used for some smaller diameter vessels (<5 mm), the mid- and long-term patency of these grafts was poor due to thrombogenicity and compliance mismatch (E. Niklason and S. Langer 1997; Edelman 1999; Desai, Seifalian, and Hamilton 2011).

Advances in synthetic TEVG design have led to the use of biodegradable scaffolds that support cell adhesion, cell repopulation on grafts, deposition of natural ECM proteins secreted from the recruited cells and thus create a naturally assembled TEVG by the host (Huang and Niklason 2014). These types of TEVGs are foreseen as the precursors of bioengineered vascular grafts that may be able to modulate the recipient's body to heal themselves. Polymers that could be degraded into harmless components and could be metabolised and eliminated by the host body such as

polyglycolic acid (PGA), were primarily used. Indeed, PGA could be absorbed and eliminated as water and carbon dioxide within 6 months *in vivo*; but it loses its mechanical strength within 4 weeks (Ravi and Chaikof 2010), with potential risk of graft rupture. Hence, to improve graft strength, safety and patency, biodegradation of PGA could be controlled/engineered via co-polymerization with other polymers. Poly-L-lactic acid (PLLA), polyhydroxyalkanoate (PHA), poly(lactic acid)/polycaprolactone (PLA/PCL) and polyethylene glycol (PEG) are such copolymerization products that are widely used to design more effective TEVGs (Ravi and Chaikof 2010). However, methodological refinement is required to achieve optimised manufacturing methods of TEVGs that could fulfil the rigid requirement of a good TEVG for human use.

Alternatively, a number of naturally derived scaffolds have been considered for designing effective TEVGs. Fibrin, chitosan, collagen and elastin have been used as the bases of biological scaffolds (Niklason et al. 1999; Zhang et al. 2006; Swartz, Russell, and Andreadis 2005). Tranquillo *et al.* and Andread *et al.* attempted using fibrin gel encapsulated with dermal fibroblasts, SMCs, ECs or ECs and SMCs progenitor cells, and subsequently implanted these in an ovine model (Huynh and Tranquillo 2010; Swartz, Russell, and Andreadis 2005). The purpose of cell encapsulation was to improve the mechanical properties of the natural scaffold to match those of native blood vessels. An additional advantage of this approach is that SMCs are the main contributors in synthesising the ECM in blood vessels.

Self-assembly has also been investigated as an alternative mode of producing TEVG. This is achieved in the form of sheet-based tissue engineering and more recently investigators have utilised cell printing (Huang and Niklason 2014). L'Heureux and colleagues were the first to design a TEVG via layers of cells sheets that were then

shaped into a tube using a mandrel (Peck et al. 2012; L'Heureux et al. 1993). Unfortunately, the entire process of producing a TEVG took up to 3 months, since 4 weeks are needed to produce the cell sheets and an additional 8 weeks required for the cells to be fused to the sheets (L'Heureux et al. 2001).

Therefore, the scientific community turned to the use of decellularised natural blood vessels; such as the SV, as a way to shorten the TEVG's manufacturing steps and duration. This is an excellent option providing a readily available naturally aligned vascular ECM, supplying a scaffold with good mechanical properties. This ECM can then be used in a variety of ways, for example to anchor seeded cells and organise them into tissues, coordinate cellular functions, allow cell migration, permit normal metabolism function and act as the base for signal transduction pathways for growth, differentiation, proliferation and gene expression. This option may require less lab-based processing, hence have greater translational potential. To this end, a selection of suitable blood vessels is available, with the source/donor being either autologous, or allogeneic or even xenogeneic. Rationally, an autologous source is more preferable to omit or lower translational application hurdles e.g. ethical approval process and immunological responses.

Of interest, whatever the biomaterial used, their mechanical properties such as burst pressure, suture retention strength and compliance are important aspect in designing a translatable TEVG. The target mechanical properties to emulate are either the artery to be replaced, or the graft with best patency, such as IMA or the more widely used SVG. For reference, the mechanical properties of IMA and SVG are as shown in Table

1.2. Burst strength is a measure of the graft's ability to withstand internal pressure which would be crucial in determining the patency of the graft *in vivo*. Whereas, the circumferential compliance is the ability of a graft to elastically expand and contract in the circumferential direction in response to a pulsatile pressure. IMA could withstand higher burst strength (3073 versus 2134 mmHg) but has a low suture retention strength (1.72 versus 1.92 N) and low compliance at 11.5 than 25.6 %/100 mmHg than SV (Pashneh-Tala, MacNeil, and Claeyssens 2015).

Table 1.2 Mechanical properties of IMA and SV used in CABG (Pashneh-Tala, MacNeil, and Claeyssens 2015).

Mechanical Properties	IMA	SV
Burst pressure (mmHg)	3073	2134
Suture retention strength (N)	1.72	1.92
Compliance (%/100 mmHg)	11.5	25.6

For synthetic TEVGs, while some mechanical parameters e.g. burst pressure could exceed those of IMA and SV, other parameters such as suture retention strength are reduced compared to IMA and SV (Johnson 2015). Interestingly, other synthetic material such as PCL and PTFE have high suture retention strength, but the burst pressure is not comparable to IMAs (Soletti et al. 2010; Nezarati et al. 2015).

Tranquillo *et al*. report that after seeding fibrin-based TEVGs *in vitro*, they decellularised the TEVG. The decellularised construct exhibited burst pressures above those of native vessels (5160 ± 680 mmHg before decellularisation and 4200 ±

180 mmHg after decellularisation). However, the suture retention strength was reduced compared to native vessels (see **Table 1.2**) with 0.58 ± 0.04 N and 0.60 ± 0.05 N before and after decellularisation, respectively (Syedain et al. 2014). Similar results were observed with synthetic TEVG as reported by Kim *et al.* where the suture retention strength of 1.5mm thick Poly (L-lactide-co-ε-caprolactone) (PLCL) scaffold was 10.28±1.69 N and ePTFE grafts with 9.02±0.45 N, which is way above the IMA and SV values but the compliance was 2.0±0.3 %/100 mmHg for 1.5 mm and 2.1±0.3 %/100 mmHg for ePTFE, which is below the native IMA and SV values (see **Table 1.2**)(Kim et al. 2013).

To date, there are no reports of TEVGs that possess all of the mechanical properties that closely resembling those of the IMA graft (Pashneh-Tala, MacNeil, and Claeyssens 2015) or other native arteries. It is also obvious that while the manufacturing of TEVGs from synthetic materials is favourable in terms of overall cost needed and availability of the material, the patency rates and long-term results of these grafts are not encouraging in terms of translation to bed-side with suboptimal mechanical strength values when compared to native vessels (Teebken and Haverich 2002).

1.5.2 Cells

The second component of the tissue engineering triad is the cells. To create a functional TEVG, incorporation of ECs and SMCs is considered desirable, since the cells are key constituents that regulate the homeostasis of blood vessels. Therefore, most attempts to produce TEVG include seeding of cells onto the biomaterial. The key

cell types within blood vessels are EC, vascular SMC and fibroblasts. These cells are organized in three layers within the vascular wall; the inner layer (tunica intima) composed mainly of EC, the middle layer (tunica media) composed mainly of SMCs and the outer layer (tunica externa/adventitia) is composed mostly of fibroblasts, as well as nerves and inflammatory cells (**Figure 1.12**). One of the differences between an artery and vein is the presence of prominent IEL and EEL in artery and not vein.

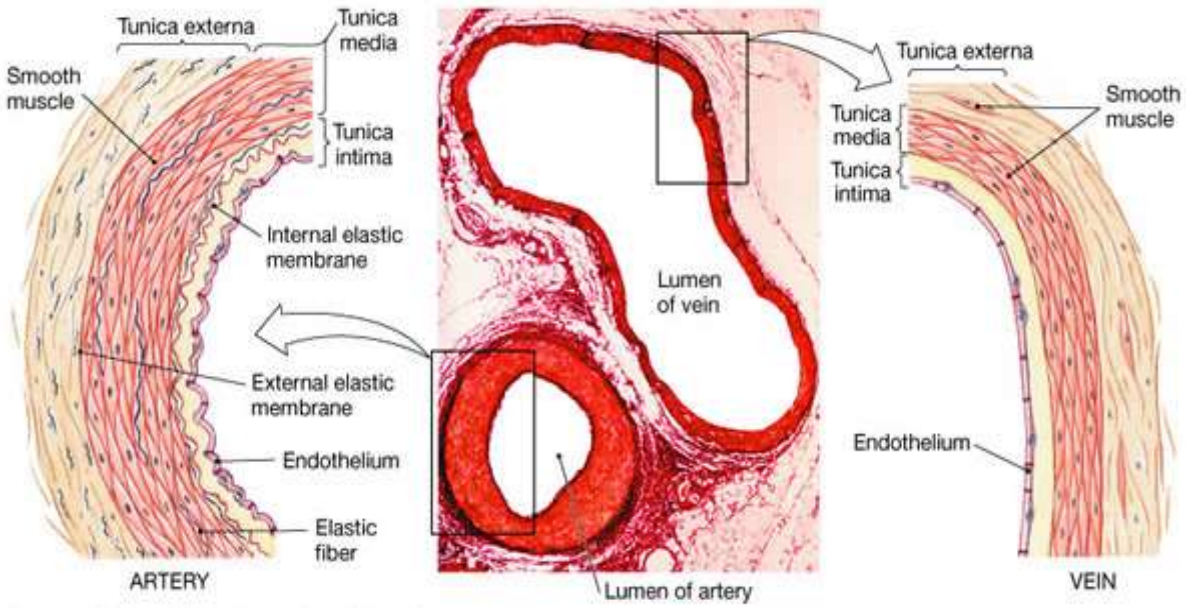

Figure 1.13 <u>Structure of Blood Vessels.</u> A micrograph showing the relative differences in wall thickness and schematic representation of the structure of an artery and a vein. They share the same general features, but the artery walls are generally thicker (Marieb and Hoehn 2015).

Interestingly, the cells in arteries and in veins are found to be genetically pre-determined even before the heart starts to beat (Castillo and Alvarez 2011). Apart from the local hemodynamic cues and cell localization, the predetermined cell fate could

also be contributing to the lower patency of venous grafts compared to arterial grafts. One such predetermining characteristic may be the proliferation of each cell type. SMC from veins for example are reported to have a higher proliferation rate than those from arteries (Turner et al. 2007; Waybill and Hopkins 1999; Waybill, Chinchilli, and Ballermann 1997; Kim et al. 2004; Wong, Nili, and Strauss 2005).

1.5.2.1 Endothelial Cells

ECs form a single layer of cells covering the lumen of vascular system hence representing the interface with circulating blood. ECs are the precursors in providing structural integrity of the blood vessel as they have the ability to produce elastin and form a selectively impermeable surface and thrombo-resistant wall. ECs also play a role in controlling blood flow and vessel tone via mechano-receptors that sense shear stress as a result of blood flow and facilitate the vasodilatation of blood vessels through signalling to surrounding cells to manage a flow change (Wagenseil and Mecham 2009; Nemeno-Guanzon et al. 2012). The ECs play a role in suppressing platelet activation, adhesion, and aggregation, leukocyte adhesion and SMC migration, proliferation (Lassance et al. 2012).

During embryogenesis, the fate of endothelial phenotype either arterial or venous; is determined even before circulation begins. Both types of ECs possess vascular endothelial growth factor receptor 2 (VEGFR2). During embryogenesis, the floor plate of the neural tube (NT) and notochord (Nc) work together and express sonic hedgehog (Shh) which in turn induce somites to increase the expression of vascular endothelial growth factor (VEGF). For arterial ECs, VEGF initiates a downstream activation of

Notch and ERK pathways thus leading to the expression of ephrinB2. Whereas in venous-fated ECs, the Notch and ERK activation is blocked by COUP-TFII, consequently leading to the expression of EphB4 (Lamont and Childs 2006; dela Paz and D'Amore 2009) (**Figure 1.13**).

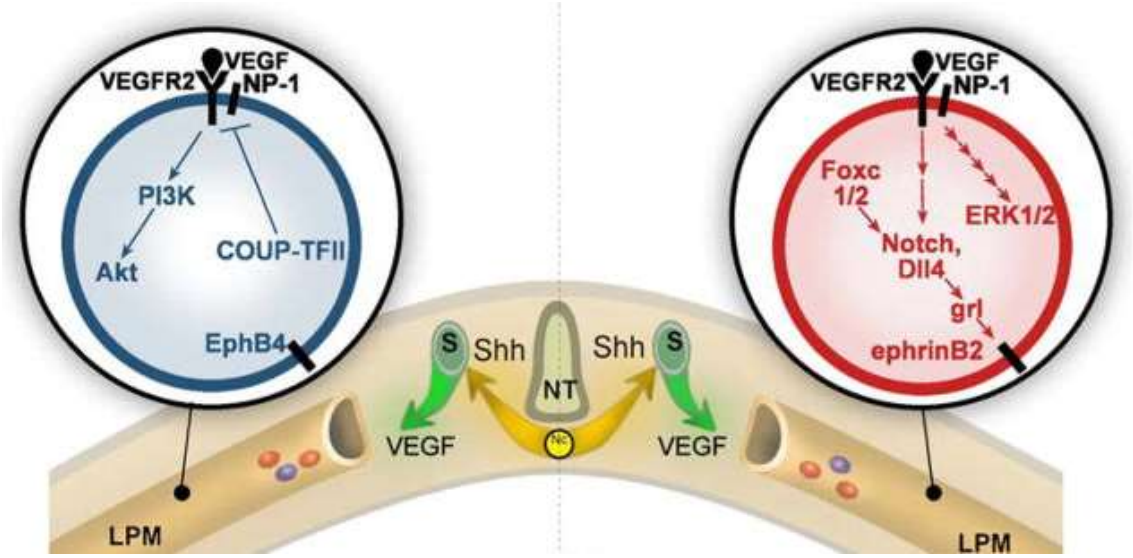

Figure 1.14 **Model of EC specification between arterial and venous.** The proposed cascade activation of genetic expression between arterial- and venous-fated endothelial cells based on a mouse and zebrafish experimental data (Lamont and Childs 2006).

Aside from the EC phenotypic specialisation in early embryonic development, another type of EC develops, called hemogenic EC, through a process named endothelial-to-hematopoetic cell transition (EHT) (Kanz et al. 2016; Chi et al. 2003; Adamo and Garcia-Cardena 2012). The idea that hematopoetic stem cells originate from the EC has been hypothesised since the last century but was just recently described through EHT. This cell transition is of great importance as it shows the transdifferentiation of

mature ECs to become hematopoetic stem cells that could potentially be a source of autologous cells for biomaterial cell repopulation in tissue engineering application.

The different gene expression of both mature arterial and venous EC has been reported. Arterial EC specific gene expression of connexin 40, delta-like 4, EphrinB2 and notch relate back to the embryonic development of EC as mention above. The same with venous EC with the expression of EphB4 and CoupTFII (dela Paz and D'Amore 2009). The differentiation of human mesenchymal stem cell (hMSC) to EC was done previously but the resulting EC-like cells express both Flk1, an arterial specific markers and Tie-2 which is a venous specific marker (Gang et al. 2006). VEGF and the Notch pathway was found to be a crucial determinant in the mechanism behind the phenotypic expression of these marker (Liu et al. 2003; Zhang et al. 2008). The promotion of stem cell differentiation through the manipulation of VEGF where higher VEGF in culture increase the expression of arterial EC markers e.g delta-like 4 and EphrinB2 and this arterialisation of EC could be reversed by inhibiting the Notch pathway (Aranguren et al. 2007; Zhang et al. 2008; Lanner, Sohl, and Farnebo 2007).

The genetic make-up of arterial and venous endothelial cells is recognised and the different physiological environment both phenotype was exposed too are apparent and contribute to the main function aside from their genetic make-up. The epigenetic factors involved in endothelial cell specification especially the influence of oxygen and hemodynamic flow in pushing specific cell type are not fully understood. Nonetheless, with low oxygen level, hypoxia induce factor (HIF) is activated thus producing more

VEGF that would leads to more arterialise EC specification (Silvestre and Mallat 2006; Yurugi-Kobayashi et al. 2006; Hirashima and Suda 2006).

1.5.2.2 Smooth Muscle Cells

The major function of SMCs is to synthesise and organise the ECM that provides the mechanical properties of the blood vessel (Wagenseil and Mecham 2009) as well as facilitating the contraction of the wall and thereby the progression of blood flow. During embryonic development, SMCs stem from the epicardial derived cells (EPDC) that undergo epithelial to mesenchymal transition (EMT) (Mikawa and Gourdie 1996; Kovacic et al. 2012). SMCs can take on one of three phenotypes in blood vessels that are termed “contractile or differentiated”, “synthetic or dedifferentiated” or “inflammatory” phenotype (Creager, Beckman, and Loscalzo 2012). These phenotypes are based on the SMC functions and cell marker expression (Shanahan, Weissberg, and Metcalfe 1993).

The contractile phenotype is the main one observed under normal physiological conditions. In culture, the contractile SMC has an elongated, spindle-shape morphology that express contractile protein expression e.g. smooth muscle myosin heavy chain (SM MHC) and smoothelin and express higher collagen I and IV (Rensen, Doevendans, and van Eys 2007). Contractile SMCs was found to have a low matrix-metalloproteinases (MMPs) which are responsible to breakdown matrix component such as collagen IV and laminin (LN) thus, higher tissue inhibitor of matrix metalloproteinase (TIMPs) (Beamish et al. 2010; Rzucidlo, Martin, and Powell 2007).

Under pathological conditions that cause disturbance of flow in the vessel, the change of phenotype from contractile to synthetic is observed (Majesky et al. 2011). Synthetic SMC has the “hills and valley’ *in vitro* culture morphology and they are found to be more proliferative, migratory, high MMPs and low TIMPs expression compared to their contractile counterpart (Beamish et al. 2010; Worth et al. 2001). These phenotypic expression was observed to be among the factors that causes hSV graft failure (Beamish et al. 2010; Kim et al. 2004; Orr et al. 2010). SMCs cultured *in vitro* in an extended period are synthetic in phenotype as opposed to contractile due to the absence of normal physiological signals to maintain the contractile phenotype (Proudfoot and Shanahan 2012; Thyberg 1996). The intermediate SMCs are called the inflammatory SMC (Hilenski and Griendling 2013) where the cells become motile and move towards the lumen causing a cascade of signalling pathway activation that can lead to intimal thickening and atherosclerosis (Yang et al. 1998; Orr et al. 2010).

There are factors that modulate the phenotypic expression of cells aside from genetic pre-programme cues. Factors such as environmental chemical, structural and mechanical signals that could be grouped as the regulatory signals (**Figure 1.15**). Therefore, it is important to use for arterial tissue engineering cells of arterial origin such as ECs and SMCs, especially to arterialise SV conduit ECM in a physiological condition that would maintain the cells arterial phenotype.

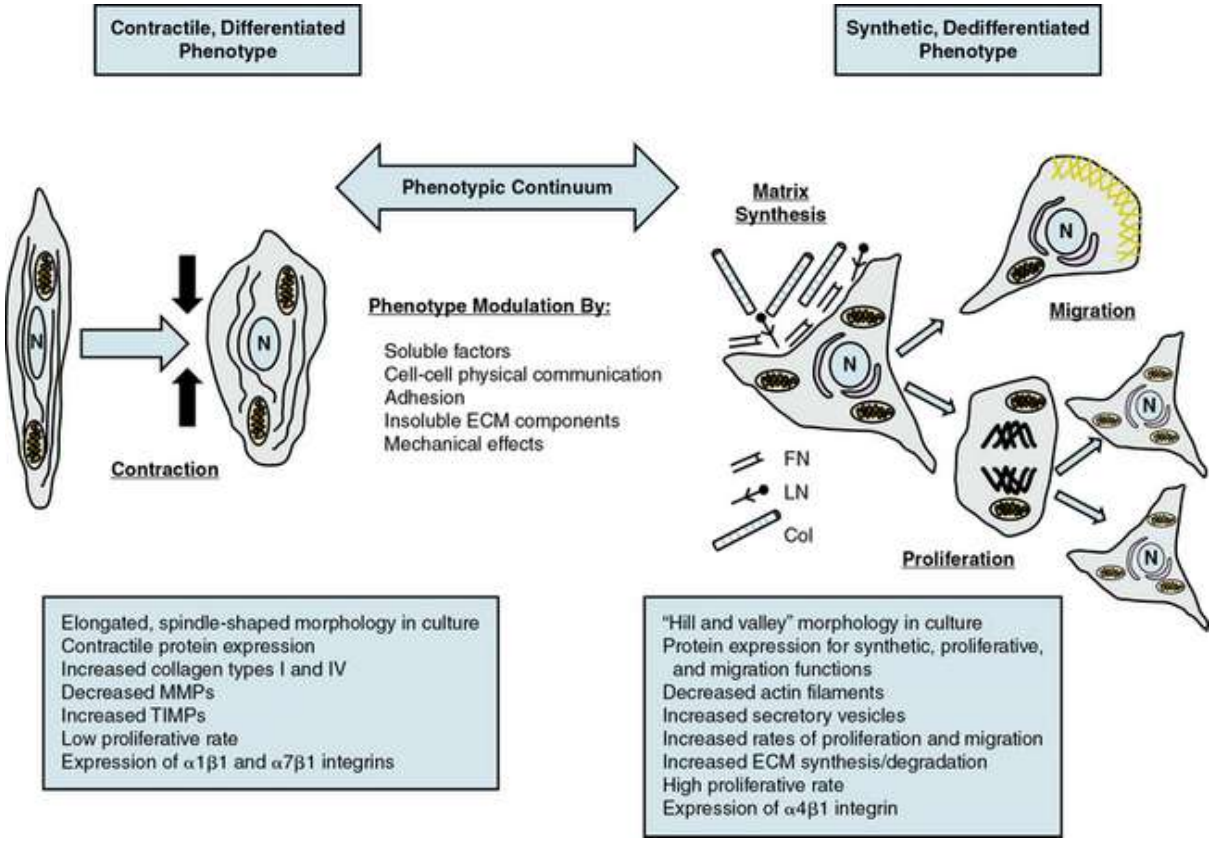

Figure 1.15 VSMC phenotypes. The three main VSMC phenotype with some of their characteristic and the regulatory signals involved; Col: collagen; ECM: extracellular matrix; FN: fibronectin; LN: laminin; MMPs: matrix metalloproteinases; TIMPs: tissue inhibitors of MMPs (Hilenski and Griendling 2013).

1.5.3 Regulatory Signals

The regulatory signals in tissue engineering include growth factors, chemical compounds and mechanical stimuli. Cell function is regulated by a combination of factors that include cell-cell interactions, ECM components, humoral factors, local chemical conditions and mechanical forces.

1.5.3.1 Humoral factors

Humoral factors include soluble and non-soluble factors in the circulation that affect the cell growth and differentiation. Growth inducing factors such as platelet-derived growth factors (PDGF), basic fibroblast growth factors (bFGF), epidermal growth factors (EGF) and insulin growth factors (IGF) activate signalling pathways when they bind to the receptor tyrosine kinases (RTKs) on the cell membrane surface(Yang et al. 1998). Other factors such as angiotensin II (AngII)(Touyz and Berry 2002; Griendling et al. 1997), cytokine transforming growth factor β (TGF-β)(Tsai et al. 2009; Suwanabol et al. 2012; Guo and Chen 2012) and members of the bone morphogenetic protein (BMP) family (Zhang et al. 2014; Willette et al. 1999; Perez et al. 2011) utilise another cascade of signalling pathways that promote the expression of genes to regulate the cell phenotype, in addition to cell growth, migration and apoptosis. These factors are applied *in vitro* and *in vivo* through their incorporation in the culturing media or intravenous (IV) delivery, respectively. Subsequently, the cells and tissue response has been studied to assist with understanding the importance of each factor in creating a TEVG, and how to manipulate them to get a suitable outcome (Fasciano et al. 2005; Libby and O'Brien 1983; Karakiulakis, Papakonstantinou, and Roth 2001; Thyberg 1996).

As shown in Figure 1.14, VSMCs phenotypic modulation is influenced by cell-cell and cell-matrix interactions. In the vascular bed, a balanced EC and SMC interaction are required to maintain their functions especially in response to injury or disease. Vascular endothelial cadherin (VE-Cad) for example is an important adhesion molecule of the EC adherent junction that plays a crucial role in preserving the endothelial barrier integrity (Corada et al. 1999; Flemming et al. 2015). By which the

lack-of or disturbance of VE-Cad leads to increase permeability of the endothelial barrier thus allowing invasion of immunocompetent and inflammatory cells e.g. macrophages, dendritic cells, T-cells etc. (Bobryshev et al. 1999). Therefore, by understanding the molecular modulation and processes involved in cell-cell interaction, a potential pharmacological therapy could be formulated to control the permeability of the endothelial layer and thus slowing down disease progression (George and Dwivedi 2004).

The vascular ECM is composed of a large number of matrix proteins (**Figure 1.16**) including; elastin, collagens, fibronectins, laminin and proteoglycans (Wagenseil and Mecham 2009; Bowers, Banerjee, and Baudino 2010). Various ECM components depicted in figure 1.16 has its own role in vascular regulation and maintenance. The two major matrix proteins that are essential in maintaining vascular mechanical properties are elastin and collagen. Elastin imparts the elasticity properties of the vessel while collagen is mainly responsible for imparting strength to the vessel wall. Hence, both elastin and collagen influence the vessel burst strength, suture retention strength and compliance. The ECM serves a variety of functions including maintaining the tube structure, regulating blood flow, providing a structure for attachment of cells and triggering certain signalling pathways that maintain the contractile phenotype of SMC and suppress proliferation and migration (Opitz et al. 2004).

Elastin was found to maintain the quiescent state of contractile VSMCs in normal physiological vasculature but when disrupted leads to phenotypic changes of VSMCs to the contractile phenotype that is proliferative and invasive (Shanahan, Weissberg,

and Metcalfe 1993), henceforth becoming the precursors of intimal thickening and atherosclerosis. The differences in glycosaminoglycan species in arterial and venous wall become one of the compounding factors that leads to lower hSV graft patency. Both arterial and venous vessel wall has the same amount of dermatan sulfate but arteries has significantly higher heparan sulfate than veins. GAGs species influence the LDL uptake in the vessel wall especially in injury site where the deposition of lipid will lead to the initiation of atherosclerosis formation (Leta, Mourão, and Tovar 2002; Sisto et al. 1990).

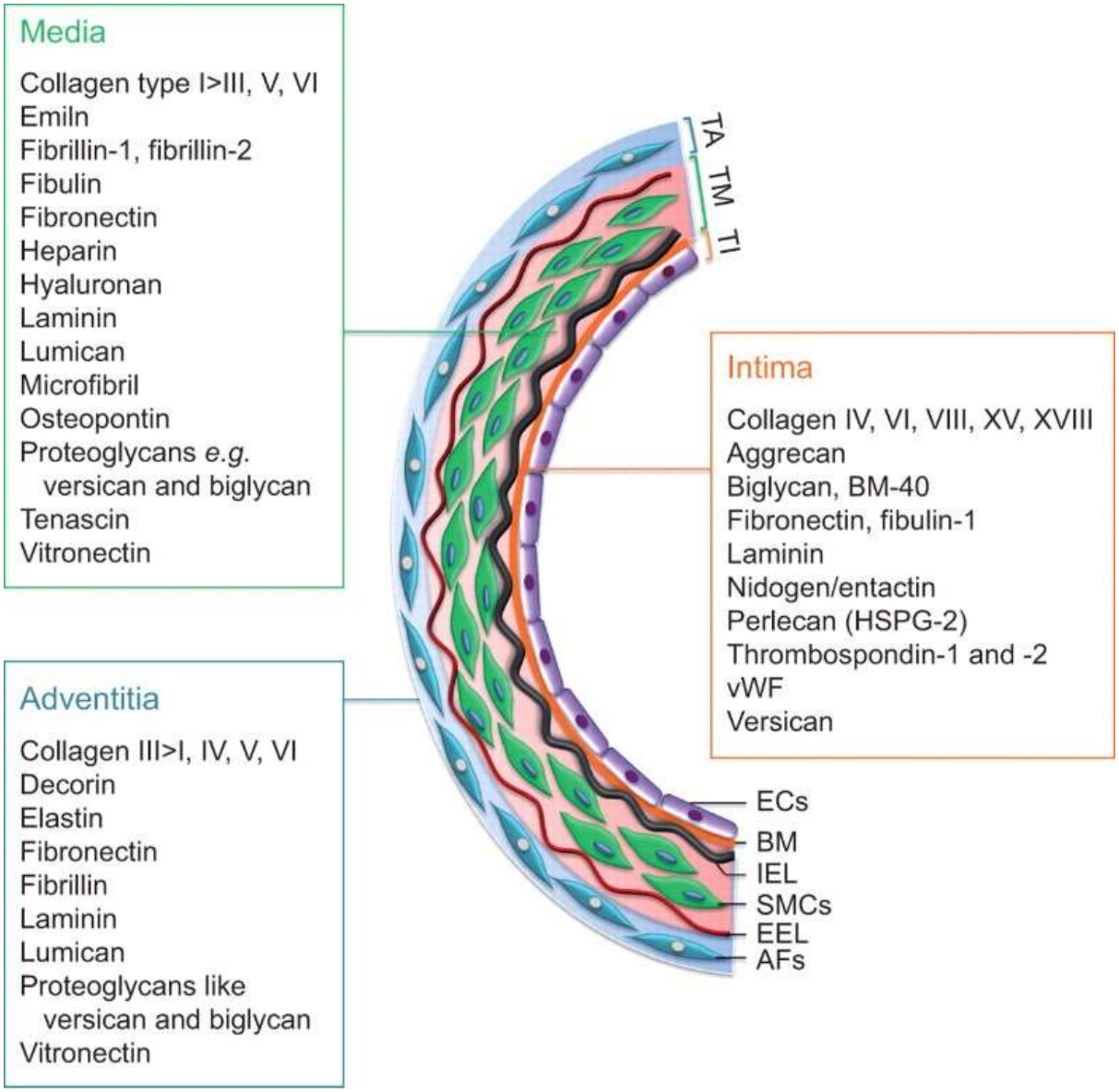

Figure 1.16 <u>Composition of the ECM within the arterial wall</u>. The vessel wall has a three-layered architecture: the tunica intima (TI), tunica media (TM) and tunica adventitia (TA). The arterial wall is composed of cells (endothelial cells (EC), smooth muscle cells (SMC) and adventitial fibroblasts (AFs)) and ECM (BM: basement membrane; IEL: internal elastic lamina; EEL: external elastic lamina; HSPG-2: heparan sulfate proteoglycan 2; vWF: von Willebrand factor)(Chelladurai, Seeger, and Pullamsetti 2012).

1.5.3.2 Mechanical factors

Various studies have been undertaken to understand the mechanics of blood flow and its implication on the cells and composition of the vasculature (Anwar et al. 2012; Muller-Marschhausen, Waschke, and Drenckhahn 2008; Li, Haga, and Chien 2005; Wang et al. 2001; Ives, Eskin, and McIntire 1986). Due to the viscosity of blood composed of both semisolid and liquid materials e.g. cells, proteins, lipoproteins and ions, the fluidity of blood does not always conform to the Newton's law of viscosity (Zaman et al. 2015). Therefore, understanding the mechanics of blood flow, especially in arterial circulation where the blood flows in a pulsatile fashion could not be explained with Poiseuille equations that need a laminar flow of a Newtonian fluid in a long cylindrical tubing with constant cross-section (Glagov et al. 1988).

Generally, the vascular system is exposed to two haemodynamic forces; cyclic strain or stress (including hydrostatic pressure) and shear stress. Cyclic strain take place when the vessel wall is distended by transmural pressure whilst shear stress is generated by the frictional forces of the blood flow (Birukov 2009). EC are exposed to both forces (shear and cyclic stress) whereas only cyclic strain influence SMCs as they are not in contact directly with the blood flow (**Figure 1.16**). Shear stress differs for both artery and vein based on their flow velocity differences; 10 – 40 dynes/cm^2 and 1 – 5 dynes /cm^2, respectively (dela Paz and D'Amore 2009). Under physiological condition, the cyclic strain is around 5-10%, whereas >20% is considered as the pathological stretch occurring in hypertension (Jufri et al. 2015).

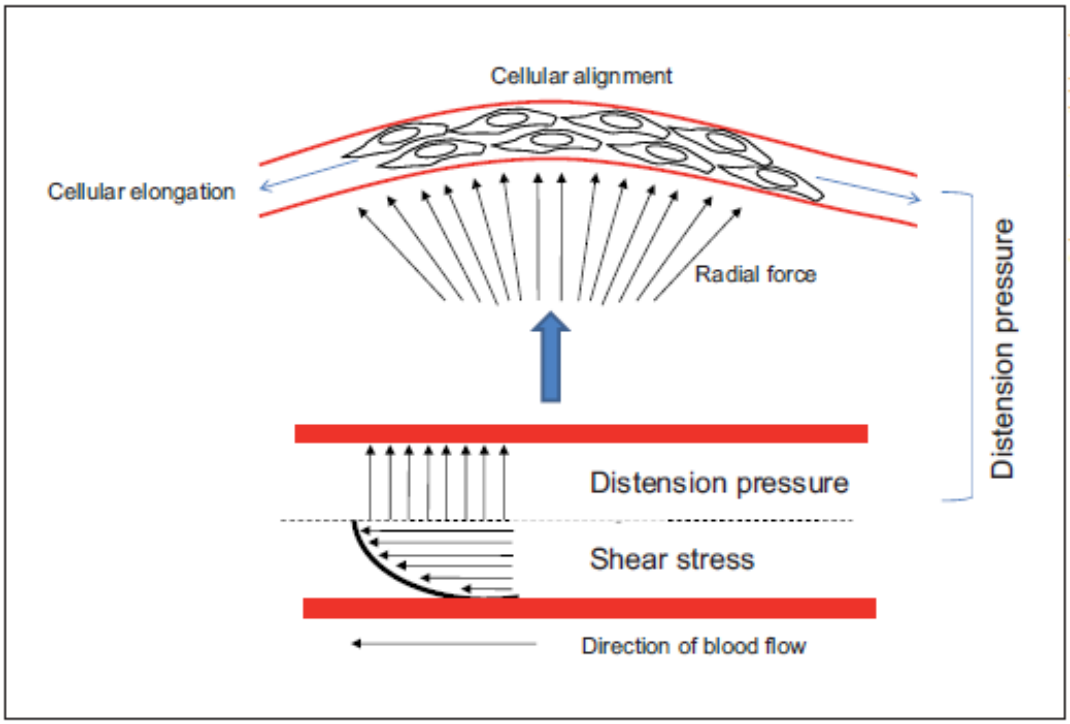

Figure 1.17 <u>Hemodynamic forces in vasculature.</u> Cyclic strain and shear stress acts on both ECs and SMCs thus influence the genetic and phenotypic regulation during physiological and pathological condition (Anwar et al. 2012).

Blood vessels are constantly exposed to blood flow; its mechanical forces and shear stress and these factors differ between arteries and veins. Therefore, when designing a TEVG, blood flow and shear stress are important mechanical factors to consider. Previous studies have investigated the role of mechanical stimuli in creating or maintaining an engineered tissue. Sun *et al.* observed higher proliferation rates of ECs and SMCs co-cultured on a PTFE conduit under 100 mmHg hydrostatic pressure for 7 days as compared to when exposed to zero pressure. Collagen deposition was also increased by exposure to the higher pressure (Sun et al. 2005). Kanda *et al*. found that SMC phenotype could be influenced by different types of stretch stress imparted

on the cell (Kanda, Matsuda, and Oka 1993). SMCs cultured under static conditions exhibited markers of the synthetic phenotype whereas under dynamic stress where they were periodically stretched and recoiled with 10% amplitude of relaxed scaffold length at 60 rpm frequency, more contractile markers were observed (Kanda, Matsuda, and Oka 1993).

For that reason, pre-conditioning the mechanical environment of the SV, which is a commonly used graft, would hopefully increase the graft patency. In summary, it is clearly apparent that the combination of all components of TE triads are of importance in designing effective TEVGs.

1.6 Thesis Rationale

1.6.1 Hypothesis

It was hypothesised that saphenous veins could be effectively decellularised to obtain an acellular matrix/scaffold to be used for *in vitro* and/or *in situ* tissue engineering and ultimately an arterial-like graft with improved long-term patency rates compared to autologous vein or synthetic conduits.

1.6.2 Project objectives

1.6.2.1 Overall Aims

1. Establish a reproducible protocol for effectively decellularization of human veins to create a human biological vascular scaffold.
2. Determine whether the decellularised human vein is mechanically suitable for arterial tissue engineering.
3. Investigate the biocompatibility of the decellularised human vein using cultured cells and peripheral whole blood (PWB).
4. Examine the behaviour of the decellularised human vein after implantation as a xenograft in a porcine model.

1.6.2.2 Specific Objectives

1. Validate an effective and reproducible decellularisation protocol for segments of human saphenous veins which yields an acellular human vascular extracellular matrix (ECM) for use as a scaffold.
2. Examine the effect of the decellularisation protocol on tissue integrity in terms of major ECM protein content (collagen, elastin and glycosaminoglycan.

3. Test the biocompatibility of decellularised saphenous veins using different cell types. Firstly, isolate, expand and characterise endothelial cells (ECs) and smooth muscle cells (SMCs) derived from porcine Carotid Artery (pCAs). Secondly, test the viability and proliferation of pECs and pSMCs from pCA on decellularised human saphenous vein scaffold *in vitro*. Finally, test the feasibility of porcine peripheral whole blood cell population to adhere, grow and differentiate on decellularised saphenous veins *in vitro*.
4. Assess re-cellularisation and patency of decellularised human saphenous veins when implanted as a xenograft in a porcine carotid artery interposition graft model.

2 MATERIALS, METHODS AND METHODOLOGY

2.1 Sample Collection and Processing

2.1.1 Human

Segments of surplus hIMA and hSV were collected from patients undergoing coronary artery bypass grafting (CABG) on completion of the procedure at the Bristol Heart Institute, Bristol, UK. The tissue was obtained in accordance with ethical standards of the local committee (REC. reference number: 10/H0107/63). The tissue segments were placed into a 50 mL Falcon tube containing sterile Dulbecco's modified Eagle's medium (DMEM) (D6421; Sigma); 200 µg/mL of Penicillin-Streptomycin (P4333-100ML, Sigma); 2 mM of GlutaMAX™-I Supplement (G7513-100ML, Sigma) and were transported to the laboratory for processing.

2.1.2 Pig

Segments of porcine carotid arteries (pCA) were collected from animals undergoing a termination procedure at the completion of other unrelated *in vivo* studies at the Translational Biomedical Research Centre, Bristol, UK. The tissue was obtained in accordance Home Office ethical standards (PPL number: 3002 854). The tissue segments were placed into a 50 mL Falcon tube containing sterile Dulbecco's modified Eagle's medium (DMEM) (D6421; Sigma) supplemented with; 200 µg/mL of Penicillin-Streptomycin (P4333-100ML, Sigma); 2 mM of GlutaMAX™-I Supplement (G7513-100ML, Sigma) and were transported to the laboratory for processing.

2.2 Human Saphenous Vein (hSV) - Decellularisation Protocol

2.2.1 Decellularisation Protocol Optimisation

Initially small segments of veins were used to determine the minimum concentration of SDS needed to achieve a successfully decellularised vein while preserving the integrity of the hSV extracellular matrix (ECM). Decellularisation was performed using a method previously described by Schaner et al.(Schaner et al. 2004) with a few modifications. Briefly, h-SV segments were obtained from the cannulated end of the h-SV. The vein was released from the cannula by cutting the silk suture to optimize the available vein length (approximately 5 cm). The vein segments were cut to approximately 1 cm in length using a scalpel then incubated in different concentrations (0.01; 0.025; 0.05; 0.075 and 0.1% (w/v)) of Sodium Dodecyl Sulphate (SDS) (S/5200/53; Fisher) in a 5 mL bijou tubes on a tube roller at 60 rpm (Stuart, UK) for 24 hours at room temperature. To wash the vein segments, they were transferred to a new bijou tube containing sterile Phosphate Buffer Saline (PBS: P4417-100TAB; Sigma) and incubated for 48 hours on a roller at room temperature with two changes of PBS every 24 hours. The processed vein segments were then used for analysis or stored in fresh PBS at 4°C until required. Two commercially available biological patches widely used for cardiac surgery (Supple Peri-Guard® (Synovis Life Technologies Inc.; PC-0608SN) and Porcine Pericardial Patch (BioIntegral Surgical Inc.; NRPP-05x05)) were used as controls. A segment of fresh unprocessed saphenous vein was retained as a control.

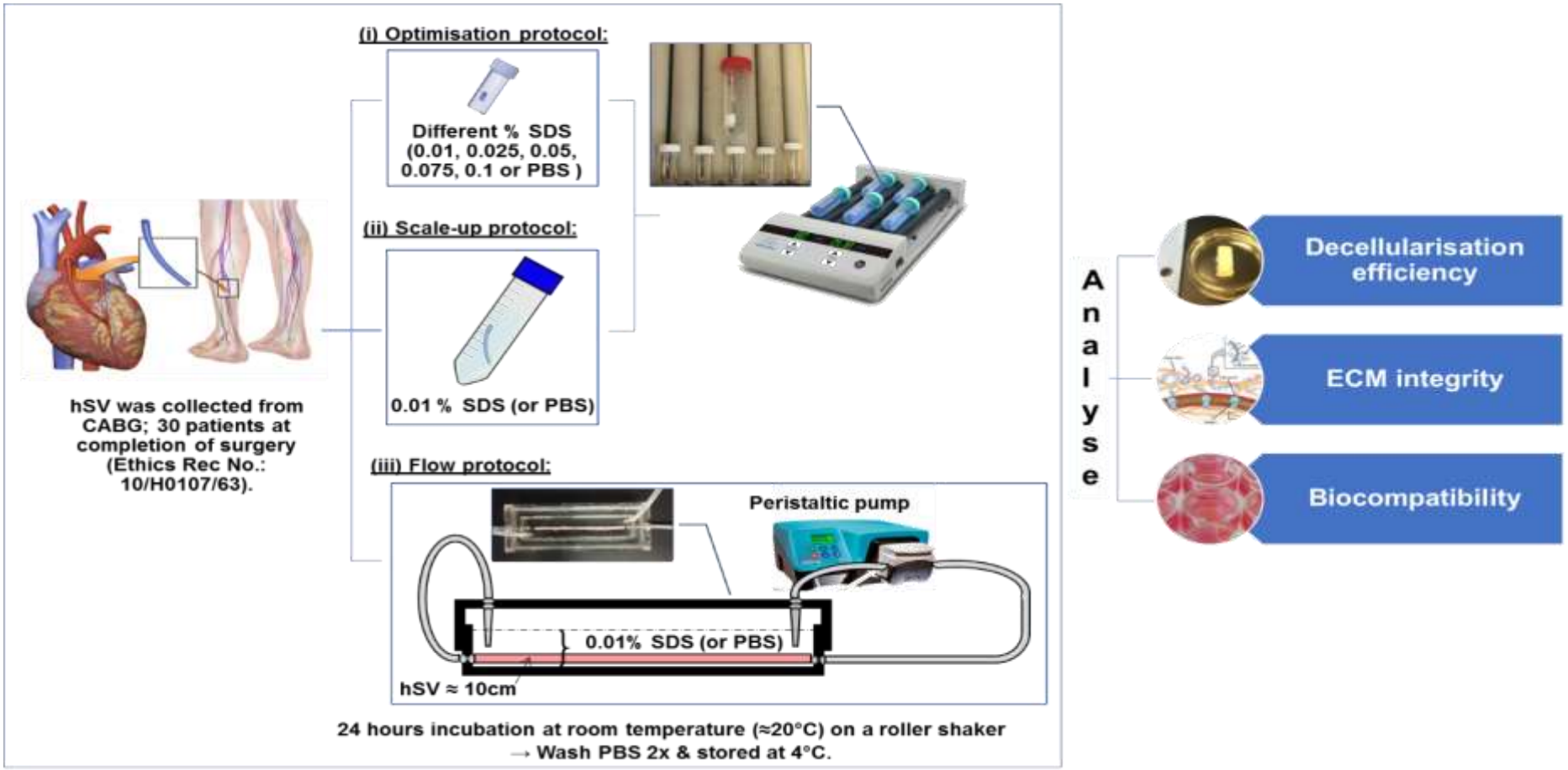

Figure 2.1 Decellularisation protocol set-up. (i) Optimisation protocol on a roller using different concentration of SDS (0.01, 0.025, 0.05, 0.075 and 0.1% (w/v) SDS). Decellularisation of larger vein segments; **(ii)** roller method **(iii)** flow method. All set-up is with the incubation in SDS for 24 hours at room temperature and followed with two 24 hour washes in PBS before analysis.

2.2.2 Decellularisation Protocol for larger vein segments; Roller method

After optimisation of decellularisation of small segments, it was attempted to scale-up the decellularisation protocol using larger vein segments ~4 cm in length in 40 mL 0.01% SDS. The efficacy of the decellularisation process was reassessed with histological and ECM analysis (**Figure 2.1 ii**).

2.2.3 Decellularisation Protocol for larger vein segments; Flow method

A modified technique of decellularisation using a flow system was assessed. SDS was circulated through the vein and also outside it to ensure thorough SDS exposure with the aim of enhancing decellularisation (**Figure 2.1 iii**). Segments of hSV (n=3) were divided into two ~4 cm lengths and a small piece of native tissue control was fixed in 10% formalin as a control. For the flow method, veins were cannulated at either end and the tubing and chamber primed with 120 mL 0.01% (w/v) SDS which flowed through the hSV and recirculated around the outside continuously 6 mL/min. For the roller method, the hSV was placed in a 50 mL Falcon tube in 40 mL SDS and rolled at 60 rpm. After 24 hours the vein segments were washed twice in PBS in the flow apparatus or in a fresh Falcon tube, respectively for 24 hours and then stored at 4°C until required.

2.3 Primary Cell Propagation

2.3.1 Collection of Human Internal Mammary Artery and Porcine Carotid Artery

Human internal mammary arteries (hIMAs) were harvested as a pedicle, which includes internal mammary vein, muscle, fascia and the surrounding adipose tissues. The distal segment of the hIMA is often discarded at the completion of surgery (on average >1 cm in length) and this surplus segment was utilised in this study. In a class II tissue culture hood, the IMA was identified and dissected from the surrounding tissues with scissors and forceps. Porcine carotid artery (pCA) specimens (about 3-5 cm length) were collected during termination procedures.

ECs and SMCs were extracted and propagated from h-IMA and pCA segments using a previously described method (Castronuovo Jr, Smith, and Price 2002; Yang et al. 1998) with a few modifications as described below.

2.3.2 Endothelial Cells Isolation and Expansion

Firstly, fibronectin-coated plate was prepared before tissue processing and cell isolation by dispensing 500 µL of 100 µg/mL fibronectin (F0895-1MG; Sigma) making sure to cover all surface area of one well of the 6-well plate and aspirating excess solution and was then left to dry in the hood for 30 minutes. After removal of most of the surrounding tissue from both hIMA and pCA, samples were cut longitudinally with scissors and pinned down with 19G needles, lumen facing up, on a sterile glass culture dish containing 5 mm thick set Sylgard gel. A scalpel was then lightly rubbed across the luminal surface to scrape off the endothelial cells. The endothelial cells on the tip of the scalpel were transferred into a 50 mL Falcon tube containing media (**Table 2.1 #1**) and subjected to centrifugation at 300 relative centrifugal force (rcf) for 5 minutes

at 37°C. The supernatant was discarded, and the pellet obtained was re-suspended with 1 mL of media (**Table 2.1 #1**) and seeded on a fibronectin-coated 6-well plate filled with another 1 mL of media (**Table 2.1 #1**) and then incubated in 5% CO_2 at 37°C. The cultures were examined after 3 days to assess cell grow and attachment with the culture media being changed every other day for the two weeks and then the culture was maintained with media changes twice a week until cells were 70-80% confluent before trypsinization for further analysis.

2.3.3 Smooth Muscle Cells Isolation and Expansion

The exposed medial layer of h-IMA and p-CA was then scored transversely near the ends with a scalpel and the medial layer was carefully peeled from the adventitia layer using forceps. The medial tissue was then finely cut into approximately 1 mm^2 explants using a scalpel, as described previously (Rodgerson et al. 2000). The explants were then transferred into a T25 flask and cultured in media as described in **Table 2.1 #1**. Explants were then incubated in 5% CO_2 incubator at 37°C for 3 weeks changing the media every other day. Detached SMC explants were removed with aspiration of media, and fresh culture media added once cells were observed to be proliferating on the surface of the flask. The culture was examined after 3 days to assess cell attachment and the culture media was changed every other day for the first three weeks and then the culture was maintained with media changes twice a week until cells were 70-80% confluent before trypsinization for further analysis.

2.3.4 Cell and Tissue Culture Maintenance, Sub-culturing and Cell Counting

Each cell type was maintained in their respective specific tissue culture medium as shown in **Table 2.1**.

Table 2.1 Culture media used for each respective cell lines.

#	Tissue source	Cell type/ Tissue type	Medium (Catalogue number , Supplier)
1	h-IMA and p-CA	Endothelial Cells and Smooth Muscle Cells	Dulbecco's modified Eagle's medium (DMEM) (D6421; Sigma) containing 10% (v/v) Fetal Bovine Serum (FBS) (10500064, Life Technologies); 200µg/mL of Penicillin-Streptomycin (P4333-100ML, Sigma); 2 mM of GlutaMAX™-I Supplement (G7513-100ML, Sigma);
2	hSV	Smooth Muscle Cells	Smooth Muscle Cell Growth Medium 2 (SMCGM2) containing 5% Fetal Calf Serum (FCS); 0.5 ng/mL Epidermal Growth factor (EGF); 2 ng/mL Basic Fibroblast Growth Factor (bFGF); 5 µg/mL Insulin (C-22062, PromoCell); 200 µg/mL of Penicillin-Streptomycin (P4333-100ML, Sigma)
3	Commercially acquired	hUVEC (C-12203; Promocell)	Endothelial Cell Growth Medium MV2 containing 2% (v/v) Fetal Calf Serum (FCS); 5 ng/mL Epidermal Growth factor (EGF); 10 ng/mL Basic Fibroblast Growth Factor (bFGF); 20 ng/mL Insulin-like Growth Factor (IGF); 0.5 ng/mL Vascular Endothelial Growth Factor 165 (VEGF 165); 1 µg/mL Ascorbic Acid; 22.5 µg/mL Heparin; 0.2 µg/mL Hydrocortisone (C-22022, PromoCell); 200 µg/mL of Penicillin-Streptomycin (P4333-100ML, Sigma)
4	Commercially acquired	ADSC (PT-5006; Lonza)	Dulbecco's modified Eagle's medium (DMEM) (D6421; Sigma) containing 10% (v/v) Fetal Bovine Serum (FBS) (10500064, Life Technologies); 200µg/mL of Penicillin-Streptomycin (P4333-100ML, Sigma); 2 mM of GlutaMAX™-I Supplement (G7513-100ML, Sigma);

#	Tissue source	Cell type/ Tissue type	Medium (Catalogue number , Supplier)
5	hSV	Native and decellularised hSV organ culture	**Wash medium**: 25 mM Hepes-buffered RPMI 1640 supplemented with 2 mM L-glutamine, 8 µg/mL gentamicin, 100 IU/mL penicillin and 100 µg/mL streptomycin (42401018; Life Technologies) **Culture media**: Sodium bicarbonate-buffered RPMI 1640 supplemented with 30% FCS, 2mM L-glutamine, 8 µg/mL gentamicin, 100 IU/mL penicillin, 100 µg/mL streptomycin, (31870025; Life Technologies) and 10 µM bromodeoxyuridine (BrdU) (B5002; Sigma)

Cell cultures were trypsinized once cultures reached 70-80% confluency. Cells were washed with PBS and then were incubated with 0.05% (v/v) Trypsin/EDTA (15400-054, Life Technologies) at 37°C for 2 minutes. The culture plate was then gently agitated, and the bottom of the culture flasks and plates were tapped to aid cell detachment. An equal volume of fresh media was added to inactivate Trypsin/EDTA. The cell suspension was transferred to a 50 mL Falcon tube and subjected to centrifugation at 300 rcf for 5 minutes at 37°C. The supernatant was discarded, and the pellet obtained was re-suspended with tissue culture media. Cells were then counted on a Countess® Automated Cell Counter (Life Technologies, UK). Briefly, 10 µL of cell suspension was mixed with 10 µL of 0.4% (v/v) Trypan Blue Stain (T10282; Life Technologies). 10 µL of this solution was then inserted into each chamber of a Countess Chamber Slide (C10228; Life Technologies) and analysed by the cell counter. The number of viable cells calculated was used for subsequent cell seeding.

2.4 Histological Analysis

Tissue samples were fixed overnight in 10% (w/v) neutral buffered formalin, NBF (HT501128, Sigma) and stored in PBS at 4°C before processing in the Shandon Excelsior ES Tissue Processor (Thermo Scientific, UK) and paraffin-wax embedding using the Shandon Histocentre™ 3 Embedding Center (Thermo Scientific, UK). Sections of 3-5 µm were cut using a microtome and placed on Superfrost Plus (10149870; Fisher) microscope slides. The slides were stored at room temperature and incubated at 37°C for 20 minutes prior to further analysis.

2.4.1 Hematoxylin and Eosin (H&E) staining

H&E staining was used to detect nuclei in decellularised tissue segments. H&E was performed using an automated staining machine, Varistain 24-4 Shandon™ (Thermo Scientific, UK). Coverslips were mounted on stained slides using DPX mountant (100503-836; VWR). Samples were viewed with a bright field microscope and images captured using the ImagePro software.

2.4.2 Morphological analysis

Low-powered field images were taken at 10 to 40X magnification to quantify the wall thickness and lumen diameter using ImageJ software. Wall thickness of transverse sections were measured and presented as mean ± SEM. Lumen perimeter is measured, and diameter calculated using the following formula;

$$\text{Lumen diameter} = \frac{\text{Circumference}}{\pi}$$

2.4.3 Decellularisation percentage analysis

All nuclei (stained blue) present in the intima, media and adventitia of high-powered fields (400X magnification) were counted automatically using a macro in ImageJ software. Four quadrants in four transverse sections (total of 16 high-power fields) were averaged for each untreated venous control (n=10) and for each decellularised (n=10) vein segment. The percentage of decellularisation was calculated using the following formula:

$$\text{Percent of decellularisation} = \frac{\text{Nuclei count for fresh control} - \text{nuclei count for processed vein}}{\text{(nuclei count for control vein)}} \times 100\%$$

2.4.4 Elastin Van Gieson (EVG) staining

EVG staining was used to visualise and semi-quantitate elastin composition in tissue samples before and after the decellularisation process. EVG staining was performed using an automated staining machine, Varistain 24-4 Shandon™ (Thermo Scientific, UK). Coverslips were mounted on stained slides using DPX mountant (100503-836; VWR) and samples were viewed with a bright field microscope. Images were captured using the ImagePro software. The area occupied by elastin (purple/black colour) per high-powered field (400X magnification) was measured by pixel counting using ImageJ software. Four areas in four transverse sections (total of 16 high-power fields) were averaged for each fresh native control (n=10) and each processed vein (n=10).

The percentage content of elastin was calculated using the following formula:

$$\text{Percent fibres} = \frac{\text{Average EVG positive area per high-power fields}}{\text{total area of high-power fields}} \times 100\%$$

2.4.5 Picrosirius Red (PSR) staining

Picrosirius red staining enables visualisation and semi-quantitative measurement of collagen fibres in tissue samples. The slides were dewaxed and rehydrated by immersing in three changes of Clearene (3803600E; Surgipath) for 5 minutes each and then were rehydrated in three changes of 100% Industrial Methylated Sprits (IMS) for 5 minutes each, followed by 90% IMS for 3 minutes and lastly in 70% IMS for another 3 minutes. Finally, the slides were placed in distilled water for 3 minutes to complete the rehydration step before followed by incubation in picrosirius red (365548; Sigma) for one hour. Slides were then washed in two changes of acidified water (0.005% (v/v) glacial acetic acid (537020; Sigma) in distilled water). Most of the water was then removed by shaking the slides vigorously. Slides were then dehydrated in three changes of 100% ethanol, cleared in xylene and then mounted with DPX mountant (100503-836; VWR).

Samples were viewed with a bright field microscope and images were captured using the ImagePro software. The area occupied by collagen (red) on a pale-yellow background per high-powered field (400X magnification) was measured by pixel counting using ImageJ software. Four areas in four transverse sections (total of 16 high-power fields) were averaged for each fresh native control (n=10) and for each

processed vein (n=10). The percentage content of collagen was calculated using the following formula:

$$\text{Percent collagen content} = \frac{\text{Average PR positive area per high-power fields}}{\text{total area of high-power fields}} \times 100\%$$

2.4.6 Alcian Blue

Alcian Blue was utilised to visualise and as a semi-quantitative measurement of glycosaminoglycans (GAGs) in tissue samples. The slides were dewaxed and rehydrated. Briefly, slides were immersed in three changes of Clearene (3803600E; Surgipath) for 5 minutes each and then were rehydrated in three changes of 100% Industrial Methylated Sprits (IMS) for 5 minutes each, followed by 90% IMS for 3 minutes and lastly in 70% IMS for another 3 minutes. Finally, the slides were placed in distilled water for 3 minutes to complete rehydration.

The slides were then incubated in alcian blue (A5268; Sigma) solution for 30 minutes and then washed in running tap water for 2 minutes followed by a quick rinse in distilled water. The nuclei were then counterstained in nuclear fast red (N8002; Sigma) solution for 5 minutes and washed in running tap water for 1 minute. Slides were then dehydrated in three changes of 100% ethanol, cleared in xylene and then were mounted using DPX (100503-836; VWR).

Samples were viewed with a bright field microscope and images were captured using the ImagePro software. The area occupied by GAGs (blue) per high-powered field (400X magnification) was measured by pixel counting using ImageJ software. Four areas in four transverse sections (total of 16 high-power fields) were averaged for each fresh control (n=10) and each processed vein (n=10). The percentage content of GAGs was calculated using the following formula:

$$\text{Percentage GAG content} = \frac{\text{Average Alcian blue positive area per high-power fields}}{\text{total area of high-power fields}} \times 100\%$$

2.5 Picogreen Assay

The deoxyribonucleic acid (DNA) content of native vein and vein segments subjected to the decellularisation protocol (each treatment group; n=10) was quantified by the Quant-iT Picogreen Assay (P11496; Life Technologies), as previously described (Vavken, Joshi, and Murray 2009; Böer et al. 2015; Quint et al. 2012). Quant-iT™ PicoGreen® dsDNA reagent is an ultra-sensitive fluorescent nucleic acid stain for quantitating double-stranded DNA (dsDNA) in solution. Detecting and quantitating small amounts of DNA as little as 25 pg/mL of dsDNA.

DNA from fresh tissue was extracted using the salting-out method as described by Miller, et al. with minor modifications (Miller, Dykes, and Polesky 1988). Briefly, tissue samples of approximately ≈10 to 25 mg were cut into small pieces using a scalpel. The samples were then transferred into 1.5 mL microcentrifuge tubes and 600 µL of TNES buffer and 50 µL of Proteinase-K (20 mg/mL) added. After mixing by inverting

the tubes several times the samples were incubated overnight at 50ºC or until the tissue were completely lysed. The tubes were occasionally mixed by inverting the tubes. 167 µL of 6 M NaCl was added to the lysed samples and vigorously mixed for 20 seconds. The tubes were then subjected to centrifugation at full speed ≈14,000 rpm for 10 minutes at room temperature. The supernatants were then transferred to new, labelled 1.5 mL microcentrifuge tubes and 800 µL of cold 100% ethanol added and then the tubes were inverted a couple of times to mix. The DNA was precipitated out of solution by incubation at -20ºC for a few hours or overnight. The samples were then subjected to centrifugation at 14,000 g for 20 minutes at 4ºC. The supernatants were then removed by pipette while taking care not to dislodge the pellet of DNA. The DNA pellets were then washed with 700 µL of 100% ethanol by gentle inversion. The ethanol was poured off and the tubes were briefly centrifuged to keep the DNA pellet at the bottom of the tube. A further wash with 70% ethanol was performed as described for 100% ethanol. The samples were then allowed to air dry for 30 minutes. As soon as the samples were dry, the DNA pellets were re-suspended in 200 µL of Tris-EDTA, pH 7.5.

Subsequently 1 µl of extracted DNA for each sample in duplicate was transferred to wells of a black chimney µClear® flat bottom 96 Well Microplates (655090; Greiner). A duplicate of standard curve with a range of 0 (blank), 1, 10, 100, 1000 ng/mL prepared from 2 µg/mL Lambda DNA standard in 1X TE (10mM Tris-HCl, 1mM EDTA, pH 7.5) was also added to the 96 well plate. 100 µL of diluted PicoGreen reagent (1:200 in 1X TE buffer) was added to each standard and sample. The microplate was covered with aluminium foil and incubated at room temperature for 2-5 minutes. The DNA content was quantified by reading on a microtiter plate fluorescence reader

(413.3020; FLUOstar® Optima) at excitation of 485 nm and measurement at 520 nm. A reference standard graph where Absorbance (Abs) was plotted against known Lambda DNA Concentration (ng/mL) was used to calculate the DNA content of the test samples.

2.6 Hydroxyproline Assay

The hydroxyproline content of native vein and vein segments subjected to the decellularisation protocol (each treatment group; n=10) was quantified using a Hydroxyproline Assay Kit (MAK008; Sigma) according to the manufacturer's instructions. Hydroxyproline was used as a measure of collagen content in the tissue samples, as described previously (Meyer et al. 2006; Stegemann and Stalder 1967). Hydroxyproline (4-hydroxyproline) is a non-proteinogenic amino acid formed by the post translational hydroxylation of proline. Hydroxyproline is a major component of collagen, where it serves to stabilize the helical structure and because hydroxyproline is largely restricted to collagen, hence it is a good indicator for collagen content in tissue. The hydroxyproline content of both wet tissue samples and paraffin wax embedded was quantified.

2.6.1 Wet tissue Sample Extraction

Approximately 10 mg of tissue was cut into small pieces using a scalpel and then transferred to a 2.0 mL polypropylene tube containing 100 µL of water. After vortexing 100 µL of concentrated hydrochloric acid (HCl, ~12 M: 320331; Sigma) was added and then the tube was placed on a heating block at 120°C overnight to hydrolyse the tissue. The following day 30 µL of the supernatant was then transferred in duplicate to

a well of a 96 well flat bottom microplate which was then placed in a 60°C oven to dry the samples for 3 hours.

2.6.2 Paraffin Wax Embedded Sample Extraction

Using a microtome 10 µm of paraffin wax embedded tissue was cut and then transferred to a 1.5 mL polypropylene tube containing 100 µL of water. After vortexing for 100 µL of concentrated hydrochloric acid, HCl ~12 M (320331; Sigma) was added and then the tube was placed on a heating block at 120°C overnight to hydrolyse the tissue. The following day 30 µL of the supernatant was then transferred to a well of a 96 well flat bottom microplate and placed in a 60°C oven to dry the samples for 3 hours.

2.6.3 Sample analysis

The assay reagent and standard curve were prepared just prior to the start of the assay. A duplicate standard curve range of 0 (blank), 0.2, 0.4, 0.6, 0.8, and 1.0 µg/well was then prepared in the same 96 well microplate from diluted standard solution (0.1 mg/mL Hydroxyproline). For every reaction and standard well, a mix of 6 µL of Chloramine T Concentrate and 94 µL of Oxidation Buffer was added and then the plate was incubated at room temperature for 5 minutes. Subsequently for each well, 50 µL of (Dimethylamino) benzaldehyde (DMAB) concentrate was mixed with 50 µL of Perchloric Acid/Isopropanol Solution and added to the well and mixed via pipetting. The plate was incubated for 90 minutes at 60°C. The hydroxyproline concentration was determined by the reaction of oxidized hydroxyproline with DMAB, which resulted in a colorimetric product that was quantified by a microtiter plate reader (24200;

DYNEX Technologies) at 570 nm. A reference standard graph where Absorbance (Abs) was plotted against the Hydroxyproline concentration was used to calculate the hydroxyproline content (mg/mL) of the test samples, which correlates to the collagen content. The concentration in wet tissue was expressed as µg/mg wet tissue and in paraffin wax embedded tissue the concentration was expressed as ng/µg total protein.

2.7 Fastin Elastin Assay

The elastin content of native vein and decellularised vein segments (each treatment group; n=10) was quantified by the Fastin Elastin Assay Kit (F2000; BioColor) according to the manufacturer's instructions. The Fastin Elastin Assay is a quantitative dye-binding method for the analysis of elastin extracted from biological materials(Lü et al. 2009; Lee, Stolz, and Wang 2011). The Fastin Elastin Assay is able to measure insoluble cross-linked elastin that are extracted from tissue in the form of soluble cross-linked polypeptide elastin fragment; α-elastin. The α-elastin content from both wet tissue samples and paraffin wax embedded were analysed.

2.7.1 Wet tissue Sample Extraction

Approximately 10 mg of wet tissue was cut into small fragments and placed into centrifuge tubes. 500 µl of 0.25 M oxalic acid was then added into each sample tube. Tubes were then placed tissue on a heating block at 100ºC for 60 minutes with loosened tube caps. The tubes were removed from the heat and cooled to room temperature before they were subjected to centrifugation at 10,000 rcf for 10 minutes. The supernatant was transferred using a pipette into a new labelled tube. Another 500 µl of 0.25 M oxalic acid was then added to the residual tissue in the tubes and heated

again for another 60 minutes. Three heat extractions with 0.25 M oxalic acid were performed to ensure complete solubilisation of the tissue elastin.

2.7.2 Paraffin Wax Embedded Sample Extraction

Using a microtome 10 µm paraffin wax embedded tissue was cut using a microtome and transferred to a 1.5 mL polypropylene tube. 500 µl of 0.25 M oxalic acid was added to each sample tube. Tubes were then placed tissue on a heating block at 100ºC for 60 minutes with loosened tube caps. The tubes were removed from the heat and cooled to room temperature before they were subjected to centrifugation at 10,000 rcf for 10 minutes. The supernatant was transferred using a pipette into a new labelled tube. Another 500 µl of 0.25 M oxalic acid was then added to the residual tissue in the tubes and heated again for another 60 minutes. Three heat extractions with 0.25 M oxalic acid were performed to ensure complete solubilisation of the tissue elastin.

2.7.3 Sample analysis

A set of 1.5 mL microcentrifuge tubes were labelled for reagent blanks (0.25M oxalic acid), α-elastin standard at 0.025, 0.05 and 0.1 µg/mL in 0.25M oxalic acid and all test samples. 500 µL of Elastin Precipitating Reagent was added to each tube and briefly vortexed to mix contents before incubation for 10 minutes to complete the precipitation of elastin at room temperature. The tubes were then subjected to centrifugation at >10,000 rcf for 10 minutes. The supernatant was discarded, and all excess fluid was removed by tapping the inverted tube onto a single thickness absorbent paper towel. 1 mL of Dye Reagent was added to all tubes. The tube contents were mix by inverting the tubes and dispersing the elastin precipitate using a vortex mixer. The tubes were

incubated for 90 minutes on a shaker at room temperature. The tubes were then subjected to centrifugation at >10,000 rcf for 10 minutes. The supernatant that contained unbound dye was discarded and most of the remaining fluid was remove from the tube by tapping the lip of the tube onto an absorbent paper towel. A reddish-brown deposit which was composed of the elastin-dye complex at the bottom wall of the tube could be observed.

250 µl of Dye Dissociation Reagent was added to each tube followed by vortexing to release the dye into solution. Vortex mixing was repeated after 10 minutes so as to ensure all bound dye has been released into solution. 250 µl of each sample was transferred to a well of a 96 well flat bottom microplate. The elastin content of the assayed samples was determined by the amount of bound dye released from the elastin which was quantified by a microtiter plate reader (24200; DYNEX Technologies) at 490 nm. A standard curve where Absorbance (Abs) was plotted against known Elastin Concentration (µg/mL) was used to determine the elastin content of the test samples. The concentration in wet tissue was expressed as µg/mg wet tissue and in paraffin wax embedded tissue the concentration was expressed as ng/µg total protein.

2.8 Glycosaminoglycan Assay

The sulfated proteoglycans and glycosaminoglycan (GAG) content of native vein and vein segments subjected to the decellularisation protocol (each treatment group; n=10) was quantified by the Blyscan Assay Kit (B1000; BioColor) according to the manufacturer's instructions. The Blyscan Assay is a quantitative dye-binding method

for the analysis of sulfated polysaccharide component of proteoglycans or the protein-free sulfated glycosaminoglycan chains extracted from biological materials (Lü et al. 2009; Lee, Stolz, and Wang 2011). The α-elastin content from both wet tissue samples and paraffin wax embedded were analysed.

2.8.1 Wet tissue Sample Extraction

Approximately 20 to 50 mg of wet tissue was cut into small fragments and placed into centrifuge tubes. 1 mL of Papain Extraction Reagent (consist of: 0.2M sodium phosphate buffer, (Na2HPO4 – NaH2PO4), pH 6.4; 400 mg sodium acetate; 200 mg EDTA, disodium salt; 40 mg cysteine HCl and 250 µL of a papain suspension, containing about 5 mg of the enzyme (P3125; Sigma-Aldrich)) was then added. The microcentrifuge tubes were then placed in a heated block at 65°C overnight. After digestion, the tubes were subjected to centrifugation at 10,000 rcf for 10 minutes and the supernatant was removed for further analysis in the protocol below (2.8.3).

2.8.2 Paraffin Wax Embedded Sample Extraction

Using a microtome 10 µm paraffin wax embedded tissue was cut and transferred to a 1.5 mL polypropylene tube. 1 mL of Papain extraction reagent (consist of: 0.2 M sodium phosphate buffer, (Na_2HPO_4 – NaH_2PO_4), pH 6.4; 400 mg sodium acetate; 200 mg EDTA, disodium salt; 40 mg cysteine HCl and 250 µL of a papain suspension, containing about 5 mg of the enzyme (P3125; Sigma-Aldrich) was then added. The micro-centrifuge tubes were then placed in a heated block at 65°C overnight. After digestion, the tubes were subjected to centrifugation at 10,000 rcf for 10 minutes and the supernatant was removed for further analysis in the protocol below (2.8.3).

2.8.3 Sample analysis

A set of 1.5 mL microcentrifuge tubes were labelled for reagent blanks (deionised water), glycosaminoglycan standards (1.0, 2.0, 3.0, 4.0 and 5.0 µg/mL in deionised water) and all test samples. 1 mL of Blyscan dye reagent was added to each tube and the content was mixed by inversion and then the tubes were placed in a gentle mechanical shaker for 30 minutes. The tubes were then subjected to centrifugation at 12,000 rcf for 10 minutes. The tubes were carefully inverted, allowed to drain and then the inverted tube was gently tapped on a paper tissue to remove remaining liquid droplets from the tubes. Then 500 µL of dissociation reagent was added to the tubes. The tubes were vortexed for 10 minutes to release the bound dye into solution. The tubes were then subjected to centrifugation at 12,000 rcf for 5 minutes. 200 µL of each sample was transferred to individual wells of a 96 micro well plate. The plate was then read at 630 nm using a microtiter plate reader (24200; DYNEX Technologies). GAG concentrations were calculated from the standard curve. The concentration in wet tissue was expressed as µg/mg wet tissue and in paraffin wax embedded tissue the concentration was expressed as ng/µg total protein.

2.9 Total protein Assay

Normalisation of the ECM protein extracted was done with the Pierce Detergent Compatible Bradford Assay (23246, ThermoFisher). Due to the use of SDS which is in fact a detergent in the decellularisation protocol, this assay kit is used to omit the interference in the reading. Just as in normal Bradford method, Coomasie dye binds to protein and cause a shift in colour from green to blue at 595 nm.

2.9.1 Sample extraction

All ECM proteins (collagen, elastin and GAGs) tissue extract from Section 2.6 to 2.8 were used for total protein quantification.

2.9.2 Sample analysis

A set of 1.5 mL microcentrifuge tubes were labelled for reagent blanks (deionised water), Bovine Serum Albumin (BSA) standards (as shown in manufacturer's manual concentration range from 2.5 to 25 µg/mL in deionised water) and all test samples.

150 µL of each standard or unknown sample are dispense into the appropriate microplate wells. Followed by addition of 150 µL of Pierce Detergent Compatible Bradford Assay Reagent to each well, and each sample were mix with reagent. Plate were then incubated for 10 minutes at room temperature. The absorbance was then measured at 595 nm with a microtiter plate reader (24200; DYNEX Technologies). The average 595 nm measurement for the blank replicates were subtracted from the 595 nm measurements of all other individual standard and unknown sample replicates. A standard curve was plotted with the average blank-corrected 595 nm measurement for each BSA standard vs. its concentration in µg/mL. The protein concentration was estimated using the standard curve for each unknown sample.

2.10 AlamarBlue® Cell Viability

Resazurin is an oxidation-reduction indicator that changes colour and has enhanced fluorescence as a result of cellular metabolic reduction. AlamarBlue® works similarly

to MTT assay. Viable cultured cells continuously convert resazurin to resofurin thus increasing the overall fluorescence and the colour of the tissue media of the cultured cells.

2.10.1 Cells cultured in tissue culture plates

Cells (ADSC, HUVEC and hSV SMC) were seeded at 5.0 x 10^4 cells/well in a 96 well plate and were incubated in 5% CO_2 at 37°C. After 24 hours, the tissue culture media was discarded and 100 µl of respective tissue culture media as shown in Table 2.1 supplemented with 10% (v/v) AlamarBlue® (DAL1100; Qiagen) was added and the plate was incubated for another 24 hours in 5% CO_2 at 37°C.

2.10.2 Cells cultured in cell crowns

Decellularised vein segments were cut longitudinally with scissors to expose the luminal surface and a 4mm disc was punched-out using a biopsy punch (PUNC010; Premier Healthcare & Hygiene Ltd.). The discs were then attached onto 96 well plate CellCrowns™ (Z682004-6EA; Sigma) with the luminal surface facing up, prior to placing into the 96 well cell culture plate as shown in **Figure 2.3**. The discs were then pre-conditioned overnight with the cell specific tissue culture media for the cell type that was to be seeded (refer to **Table 2.1**). Cells were seeded at 5.0 x 10^4 cells/well and the Cell Crowns were incubated in 5% CO_2 at 37°C. After 24 hours, the media was discarded and 50 µl of tissue culture media supplemented with 10% (v/v) AlamarBlue® (DAL1100; Qiagen) was added and the plate was incubated for another 24 hours in 5% CO_2 at 37°C. The tissue culture media was collected after 24 hours and transferred to a new 96 well plate.

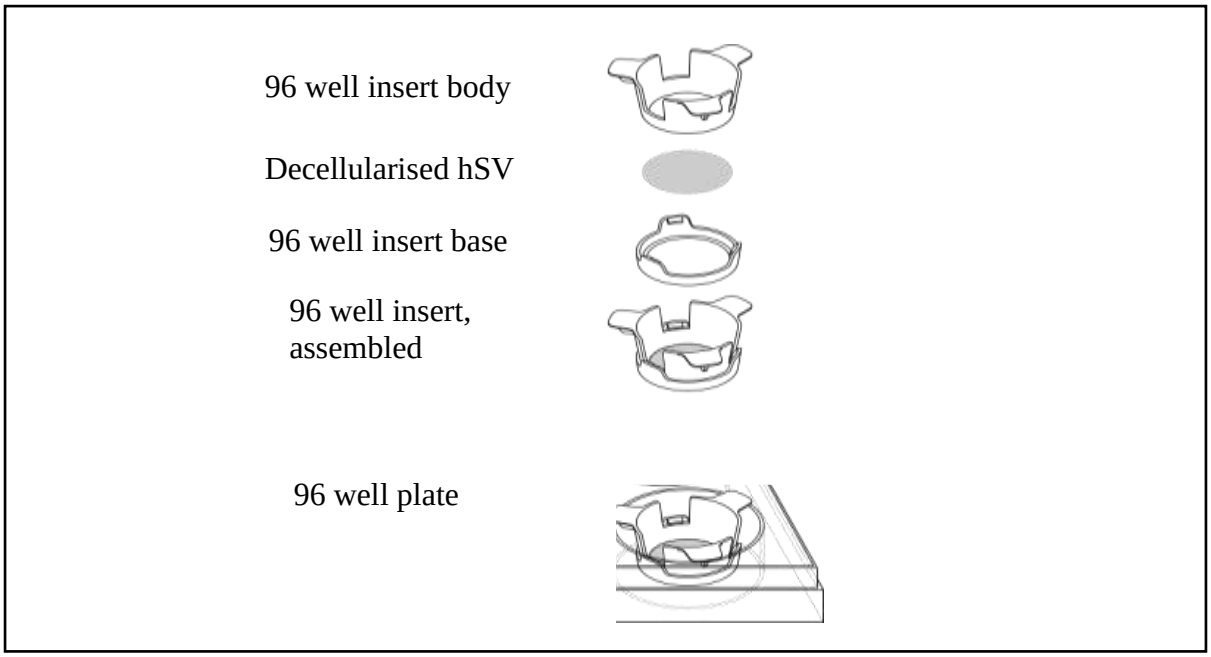

Figure 2.2 Schematic diagram of CellCrown™ apparatus used in 96 well plates. Discs of dellularise hSV were placed in CellCrowns which were inserted into 96 well plates prior to cell seeding.

2.10.3 Sample analysis

The absorbance was read using a microtiter plate reader (24200; DYNEX Technologies) at the lower wavelength filter (570 nm) and at the higher wavelength filter (595 nm). Readings from both lower and higher wavelengths were recorded to ensure an accurate method for deriving the amount of reduced AlamarBlue® present in each sample. The absorbance of 50 µl tissue culture media only was also measure at both lower and higher wavelengths.

The absorbance value of tissue culture media only was subtracted from the absorbance values of AlamarBlue® in tissue culture media in contact with cell to calculate the absorbance of oxidized AlamarBlue®; AO_{LW} = absorbance of oxidized form at lower wavelength, and AO_{HW} = absorbance of oxidized form at higher wavelength. The correction factor (R_O) was calculated using this formula: $R_O = AO_{LW}/AO_{HW}$.

Therefore, the percent of reduced AlamarBlue® (AR_{LW}) was calculate using this formula: $AR_{LW} = A_{LW} – (A_{HW} \times R_O) \times 100$.

Accordingly, the percent difference between treated and control cells in cytotoxicity/proliferation assays was determine using this formula:

Percent difference in reduction =

$$\frac{(A_{LW} – (A_{HW} \times R_O) \text{ for test well})}{(A_{LW} - (A_{HW} \times R_O) \text{ positive growth control})} \times 100\%$$

For better result presentation of cytotoxicity/proliferation, a reference standard graph where the percent difference in reduction (using the formula above) was plotted against the seeding density of each cell type was used to calculate the total number of cells present in the test samples.

2.11 Methylene Blue Assay

SDS was used for decellularisation and its cytotoxicity was proven via action in disruption of cells. The methylene blue (MB) two-phase titration method is a rapid and efficient method for determining the concentrations of anionic surfactants. SDS is the main ingredient in many detergent products consequently the MB assay is used for detecting SDS in the environment (Hayashi 1975). It was critical to detect the level of SDS in the effluent and hSV tissue after the decellularisation protocol. Firstly, to demonstrate the effectiveness of the washing steps and secondly to show that the decellularised tissue were biocompatible for cells to grow on.

2.11.1 Effluent samples

The assay was modified from Zvarova et. al. where an aliquot of 1 mL of effluent was collected after each solution change (0.01% SDS, wash 1 and wash 2) and kept at 4° until the analysis (Zvarova et al. 2016).

2.11.2 Tissue extract sample

The assay was modified from Mathapati et. al. where approximately 50 mg of decellularised hSV was crushed under liquid nitrogen using a pestle and mortar. 1ml of distilled water was added to the homogenised tissue and the 3 mL of 100% ethanol was added. The samples were subjected to centrifugation at 140 000 rcf for 10 minutes (Mathapati et al. 2010). The supernatant was collected into newly labelled tubes and kept in 4°C until the analysis.

2.11.3 Sample Analysis

A set of 1.5 mL microcentrifuge tubes were labelled. 50 µL of reagent blanks (DPBS), SDS standards (0, 0.00001, 0.00005, 0.0001, 0.0005, 0.001, 0.005, 0.01 % w/v in DPBS) and all test samples was added to tubes. 50 µL of Methylene Blue; 0.0125% w/v (M6900; Sigma) was then added to the tubes and the tubes were vortexed vigorously. Next, 200 µL of chloroform was then added. The tubes were vortexed for 1 minute and then the tubes were incubated for 30 minutes, at room temperature. A two-phase layer was observed and 150 µL of the bottom layer was transferred into a 96-well polypropylene (PP) plate (736-0122; VWR). The plates were then immediately read at 630 nm using a microtiter plate reader (24200; DYNEX Technologies).

2.12 Agarose Gel Electrophoresis

The minimum criteria of decellularisation is less than 200 base pair (bp) dsDNA in decellularised tissue (Crapo, Gilbert, and Badylak 2011). To determine the size of the DNA content of decellularised hSV DNA fragments were extracted from decellularised tissue and gel electrophoresis was completed to examine the size of DNA. Agarose gel (0.5% (w/v)) was prepared by dissolving 1 g of agarose powder (MB1200; Melford) in 1X TAE buffer (consist of: 40 mM Tris, 20 mM acetic acid, 1 mM EDTA (B49; Sigma-Aldrich)) and with 200 µL SYBR™ Safe stain (S33103; Invitrogen) by heating in a microwave. The molten agar was cooled to ≈ 60°C before pouring into the gel tray with well comb in place. Molten agar was allowed to solidify for 30 minutes.

Once the gel was set, it was placed in the electrophoresis tank and the tank was filled with 1X TAE buffer until the gel was submerged. The first well was then loaded with 5 µL HyperLadder™ 50 bp (BIO-33054; Bioline Reagents Ltd.) and subsequent wells were loaded with a mix of samples with loading dye (1:5 dilution). Electrical leads were then appropriately attached, and the set-up was then run at ~80 to 100V for about 30 minutes. The gel was then transferred to be visualised and analysed using with Gel Doc™ XR$^+$ System and Quantity One® 1-D analysis software (Bio-Rad Laboratories, Inc., UK).

2.13 Click-IT® Plus EdU Cell Proliferation Assay

Proliferation of ECs and SMCs from porcine carotid artery in the presence of different concentration of SDS was quantified with the Click-iT EdU Alexa Fluor 555 Imaging Kit (C10638; Life Technologies). ECs or SMCs were seeded separately in 96 well tissue culture treated plates (655090; Greiner Bio-One Ltd.) at a seeding density of 100 000 cell/cm^2 and allowed to grow overnight. Cells were then cultured with tissue culture media with 2% (v/v) FBS overnight to suppress proliferation. The cells were then exposed to different SDS concentrations in tissue culture media with 10 µM EdU overnight. Cells were then washed twice with PBS and fixed using 3% (v/v) paraformaldehyde in PBS for 15 minutes. After rinsing with 3% (v/v) BSA in PBS twice, cells were permeabilised at room temperature for 20 minutes with 0.5% (v/v) Triton-X100 in PBS. The staining solution was prepared according to the manufacturer's instructions but adapted to smaller volume for 96 well plates.

The Click-iT Plus reaction cocktail were prepared as follows: 88 µL 1X Click-iT reaction buffer, 2 µL copper protectant, 0.25 µL Alexa Fluor picolyl azide and 10 µL reaction buffer additive were mixed in the listed order to make a final volume of 100.25 µL for each well. At the end of permeabilisation incubation, 0.5% (v/v) Triton-X100 in PBS was discarded, and the cells were washed twice with 3% (v/v) BSA in PBS. Each well was added with 50 µL of Click-iT Plus reaction cocktail prepared earlier (and within 15 minutes of preparation for optimal reaction results). The plate was protected from light with aluminium foil and incubated for 30 minutes at room temperature. Wells were then washed twice with 3% (v/v) BSA in PBS followed by a wash with PBS. Nuclei staining was performed with 2 µg/mL of Hoechst 33342 in PBS, 50 µL was dispense in each well and incubated for another 30 minutes at room temperature protected from light. Wells were then washed twice with PBS and wet mounting media Fluoromount-G (00-4958-02; Life Technologies) was added before imaging was performed using the EVOS FL Cell Imaging System at medium-powered field (medium power fields = 200X magnification). Five views of each well under the medium power field were captured and nuclei counting using ImageJ software. Proliferation was determined with cells grown under normal media served as a positive control with 100% proliferation. The percentage of proliferation was calculated using the following formula:

$$\text{Percent of proliferation} = \frac{\text{Positive nuclei (red) count after 48 hours}}{\text{All nuclei (red and blue) count after 48 hours}} \times 100\%$$

2.14 BrdU incorporation in Organ Cultures

In order to ascertain that the decellularised vein did not harbour viable cells, the number of proliferating cells in hSV was determined by Bromodeoxyuridine (BrDU) incorporation within organ cultures of decellularised hSV. Native un-decellularised hSV served as a positive control. Surplus hSV was cut into segments; a 2 cm length was immediately processed for organ culture and the rest was decellularised in a tube placed on a roller as described previously as described in Section 2.2.2. The segment isolated for organ culture was placed in a petri dish filled with wash medium (detailed in **Table 2.1**). A piece of 0.5 cm length was fixed in 10% formalin for 24 hours and placed in PBS before processing, to be used as an untreated control (Day 0).

The rest of the tissue was cleaned by removing as much of adventitial layer as possible. Using scissors, the untreated hSV and decellularise hSV were then cut longitudinally to expose the luminal surface. The opened untreated hSV and decellularised hSV were transferred luminal surface uppermost onto a piece of plastic mesh in a small glass petri dish coated with 5mm thick set Sylgard resin and pinned down using a minute pins at all four corners. The vein was then cultured in 5 mL of tissue culture media (detailed in **Table 2.1**) for 14 days with tissue culture media change every 2 to 3 days. At the end of two weeks, the vein was fixed in 10% formalin for 24 hours and kept in PBS before further processing.

All collected fixed tissue samples;

a) positive control tissue (un-decellularised)
    i. untreated with BrdU and fixed on Day 0
    ii. treated with BrdU and fixed on Day 14

b) decellularised tissue

   i. untreated with BrdU and fixed on Day 0

   ii. treated with BrdU and fixed on Day 14

were stored in PBS before further processing protocol in the Shandon Excelsior ES Tissue Processor (Thermo Scientific, UK) and paraffin wax embedding using the Shandon Histocentre™ 3 Embedding Center (Thermo Scientific, UK). Sections of 3-5 µm were cut using a microtome and placed on Superfrost Plus (10149870; Fisher) microscope slides. The slides were stored at room temperature and incubated at 37°C for 20 minutes prior to staining.

The slides were dewaxed and rehydrated as follows: slides were immersed in three changes of Clearene (3803600E; Surgipath) for 5 minutes each and then rehydrated in three changes of 100% (v/v) Industrial Methylated Sprits (IMS) for 5 minutes each, followed by 90% (v/v) IMS for 3 minutes and lastly in 70% (v/v) IMS for 3 minutes. Finally, the slides were placed in distilled water for 3 minutes.

The slides were then incubated in 3% (v/v) hydrogen peroxide, H_2O_2 (H3410; Sigma) for 5 minutes at room temperature and then washed twice with PBS. The slides were then incubated in 10 mM citrate buffer pH 6.0 for 20 minutes in a boiling water bath. The slides were allowed to cool at room temperature before washing twice with PBS. The surrounding sections were wiped dry with paper tissue and sections were marked with a wax pen. Slides were incubated in 50 µL of 8.6 µg/mL mouse anti-BrdU IgG (B2531; Sigma) diluted in 1% (v/v) horse serum in 1% (v/v) BSA/PBS for 90 minutes at 37°C or overnight at 4°C. Slides were then washed four times with PBS before

addition of 50 µL biotinylated horse anti-mouse IgG in 1% (v/v) BSA/PBS diluted 1 in 200 for 30 minutes. After washing four times with PBS, 50 µL of Extravidin™-HRP (E2886; Sigma) diluted 1 in 200 with 1% (v/v) BSA/PBS was added to each section and incubated for 30 minutes at room temperature. After four washes with PBS, each section was incubated with 250 µL of Fast DAB Peroxidase Substrate (D4293; Sigma) for 10 minutes at room temperature. Slides were washed with distilled water and counter-stained with Mayer's haematoxylin for 30 seconds. Final washing with tap water was performed before mounting slides with VectaMount Permanent Mounting Medium (H-5000; Vector Laboratories).

Sections were viewed with a bright field microscope and images were captured using the ImagePro software. All positive nuclei (stained brown) and negative cells (stained blue) in the intima, media and adventitia, seen via high-powered field (high power fields = 400X magnification) were counted automatically using a macro in ImageJ software. Four quadrants in four transverse sections (total of 16 counts) were averaged for each un-decellularised control (n=5) and decellularised (n=5) vein segments. The percentage of proliferation was calculated using the following formula:

$$\text{Percent of proliferation} = \frac{\text{Positive nuclei (brown) count at day 14}}{\text{All nuclei (brown and blue) count at day 14}} \times 100\%$$

2.15 Surgical Procedures for Porcine Implant

Surgical implants were undertaken by a team of clinical experts lead by Professor Raimondo Ascione in accordance with Home Office, Clinical, and Good Laboratory Practice Monitoring Authority (GLP MA) standards at the Translational Biomedical Research Centre, University of Bristol, Bristol, UK under Project Licence Number 30/3064 (**Figure 2.3 A and B**). Large White Landrace female pigs weighing between 55 to 65 kg were put on 75 mg aspirin daily for 1 week before surgery. After an overnight fast, the pigs were sedated, anaesthetised, and ventilated by standard clinical protocols, similar to that used in clinical practice. A venous catheter was inserted through an ear vein and used for continuous administration of saline and anaesthetic drugs. Continuous monitoring of ECG, systemic blood pressure, body temperature, and peripheral saturation was performed throughout according to established protocols (Theisen and Grundy 1987; Snider and Vincenzoni 2001; Allain et al. 2005). All animals were anesthetized with an intramuscular injection of ketamine (20 mg/kg), which was followed by an intravenous injection of thiopentone (20 mg/kg).

Anesthesia was achieved by using diazepam (1 mg/kg), fentanyl (15 µg/kg for initial dose and 50 µg/kg/h for maintenance), and propofol (1 mg/kg for initial dose and 6 mg/kg/h for maintenance). Animals were placed in a supine position and an endotracheal tube was inserted for mechanical ventilation, which started with 10 mL/kg tidal volume, 15/min frequency, 100% of oxygen, and 0 mmHg of end-expiratory pressure. To obtain favourable arterial carbon dioxide tension ($PaCO_2$) (35.0–45.0 mm Hg) and pH (7.35–7.45), tidal volume was changed before surgery. Following heparinisation, activated clotting time (ACT) values were maintained above 300 throughout the surgery.

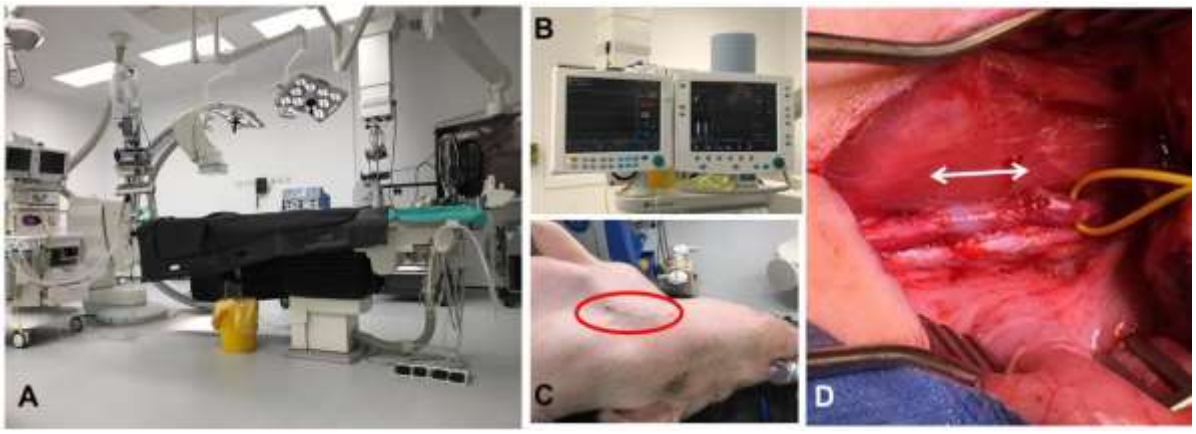

Figure 2.3 Arterial Porcine Xenografting Procedure Set-up. (A) Hybrid Preclinical Theatre at TBRC Bristol. **(B)** full monitoring of vital signs during surgery; **(C)** healed surgical wound at 4 weeks post implant of acellular hSV; **(D)** Acellular hSV implanted in carotid artery position (white arrow).

Following skin prepping according to clinical standards using Betadine solutions, an 8-10 cm skin incision was made in the neck, 2.5 cm on the right lateral side to the midline. The right carotid artery was then exposed and isolated with vessel loops as shown in **Figure 2.4C**.

Doppler ultrasound of native vessel was performed at clinical standard where colour doppler was used to record the systolic and diastolic blood flow velocity and the M-Mode was used for wall compliance were recorded as shown in **Figure 2.5**. After a bolus of 100 IU/kg heparin intravenously, the carotid artery was clamped proximally and distally of the anastomotic sites. A 0.5 to 1 cm segment of the native carotid artery was then excised as control. The tissue was sectioned into three pieces, one piece

was placed in 10% formalin, one piece was place in 4% paraformaldehyde, and the last piece was snap frozen in liquid nitrogen.

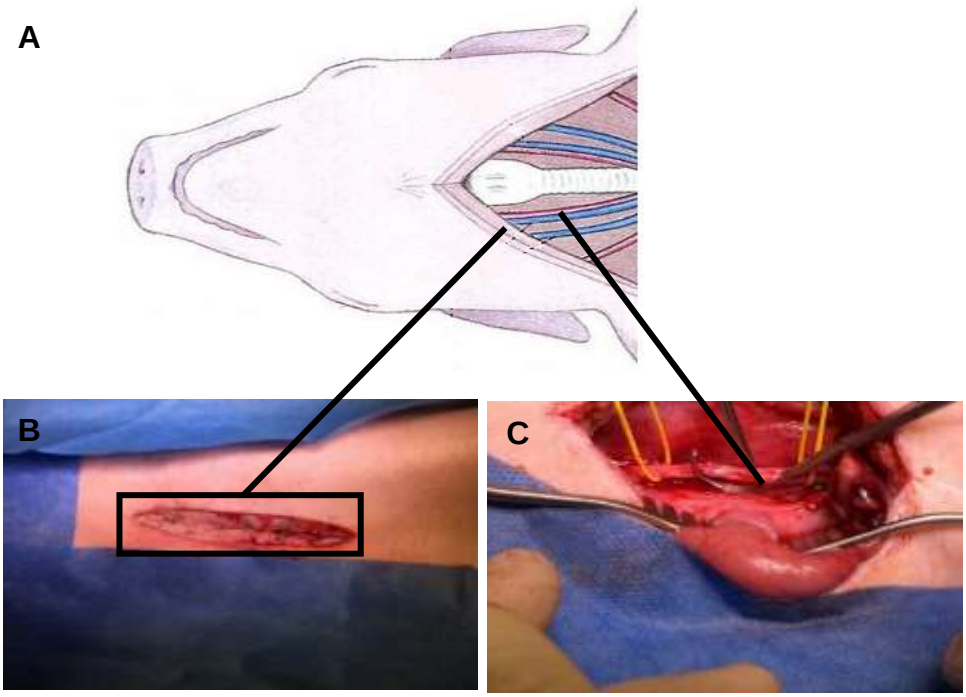

Figure 2.4 Surgical procedure to expose right carotid artery. (A) Anatomic illustration of the location of the porcine right carotid artery. **(B)** 8 to 10 cm neck skin incision. **(C)** Right carotid artery exposed and isolated with vessel loops.

A **B**

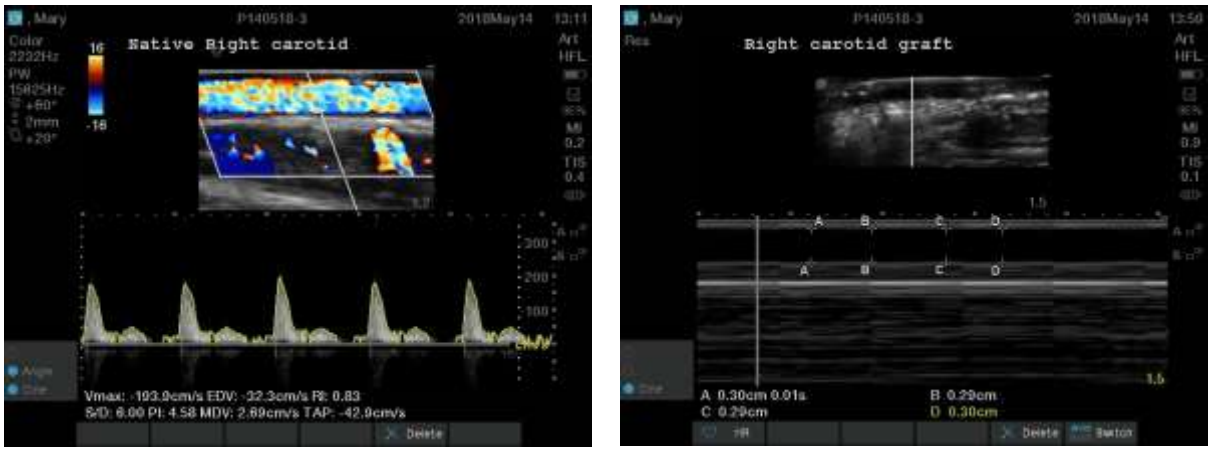

Figure 2.5 Doppler ultrasound observation of a native vessel. (A) Colour Doppler was used to record the systolic and diastolic blood flow velocity and **(B)** M-Mode was used for wall and lumen observation.

The decellularised hSV was sutured in place with end-to-end anastomoses performed with 7-0 polypropylene material (Ethicon, US) by a senior surgeon using 3.5 magnification surgical loupes (see **Figure 2.5**). On completion, the vascular clamps were removed to permit perfusion. The patency was assessed by checking the flow across the graft directly as well as by checking the transmission of the pulsatile flow distal to the implant. In addition, doppler ultrasound scanning of the implanted graft was recorded similar as shown in **Figure 2.5**. After 30 minutes of observation the surgical incision was closed in layers using biodegradable clinical sutures. The skin was sprayed with an antiseptic spray according to the veterinary clinical practice. Heparin was not reversed.

Animals were taken to the recovery room, monitored and extubated according to standard protocols within 30 to 60 minutes. Post-operative pain control was established as stated by clinical protocols. Animals were administered on 75 mg/day (for the first three implants) and 300 mg/day (for the latest three implants aspirin with food from four hours post-surgery until termination. Animals were then transferred to their maintenance areas, kept in groups for the following four weeks and fed standard porcine diet *ad libitum*. Daily monitoring was undertaken as per routine practice by a veterinary technician. After 1 month and after an overnight fast, the pigs were sedated, anaesthetised, and ventilated by standard clinical protocols. Under controlled and sterile conditions the implanted grafts were exposed and subjected to additional follow-up vascular doppler scanning as shown in **Figure 2.6**. Following administration of 5000 UI of heparin the right CA were clamped and 5 to 6 cm long segments were explanted, inclusive of the hSV segments. The vascular grafts were excised and transported to the laboratory in 50 mL facon tube fill with 40 mL of PBS. The tissue was sectioned into three pieces, one piece was placed in 10% formalin, one piece was placed in 4% PFA, and the last piece were snap frozen in liquid nitrogen. The animal was then terminated according to HO regulations.

A B

Figure 2.6 Doppler ultrasound observation of implanted graft. (A) Colour doppler was used to record the systolic and diastolic blood flow velocity and **(B)** M-Mode was used for wall and lumen observation.

2.16 Peripheral whole blood collection

Large White Landrace female pigs weighing between 55 to 65 kg were sedated, anaesthetised, and ventilated by standard clinical protocols, and right external jugular vein and carotid artery were exposed as described in section 2.15. The pig's vein was punctured with 16 G needle on the Compoflex® Blood Bag for collection of whole blood in anticoagulant citrate phosphate dextrose adenine solution (CPDA-1) and about 500 to 600 mL whole blood were collected from each pig (PS11150; Fresenius Kabi). Blood bag was then transferred to the laboratory for further processing where the whole blood was transferred to a 200 mL sterile media bottle and used for the bioreactor experiment or diluted with 2% (v/v) FBS/PBS (10500064, Life Technologies) as shown in Figure 2.7.

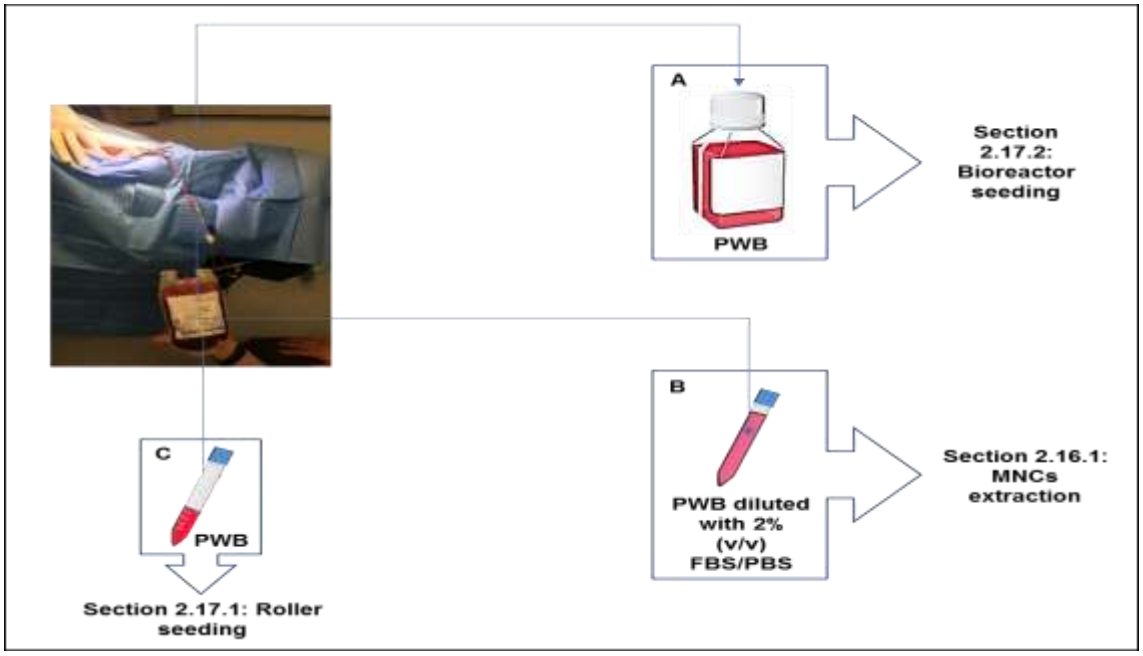

Figure 2.7 Pig peripheral whole blood collection and processing. (A) 200 mL of PWB was transferred into 250 mL sterile media bottle and were later use for bioreactor reseeding experiment. **(B)** 15 mL of PWB was diluted with 2% (v/v) FBS/PBS and were used to extract MNCs. **(C)** 5 mL of PWB was transferred into 15 mL tube and then later use for the roller reseeding experiment.

2.16.1 Mononuclear cell fraction extraction

SepMate™ 50 tube (15460, StemCell Tech.) was prepared by adding 15 mL of density gradient medium, Ficoll® Paque Plus (GE17-1440-02, Sigma) to the bottom of the tube through the central hole in the insert. Then, 15 mL of diluted whole blood (refer to Figure 2.7 ii) was carefully added on the side of the SepMate™ tube that was placed vertically. The tubes were then subjected to centrifugation at 1200 rcf for 10 minutes at room temperature with the break on. The centrifugation will separate the sample based on density gradient which result in 3 distinct layer as shown in Figure 2.8. The

top layer which contains MNCs were then quickly (<2 seconds) poured into a new falcon tube. The plasma and MNCs collected were then used for seeding experiment.

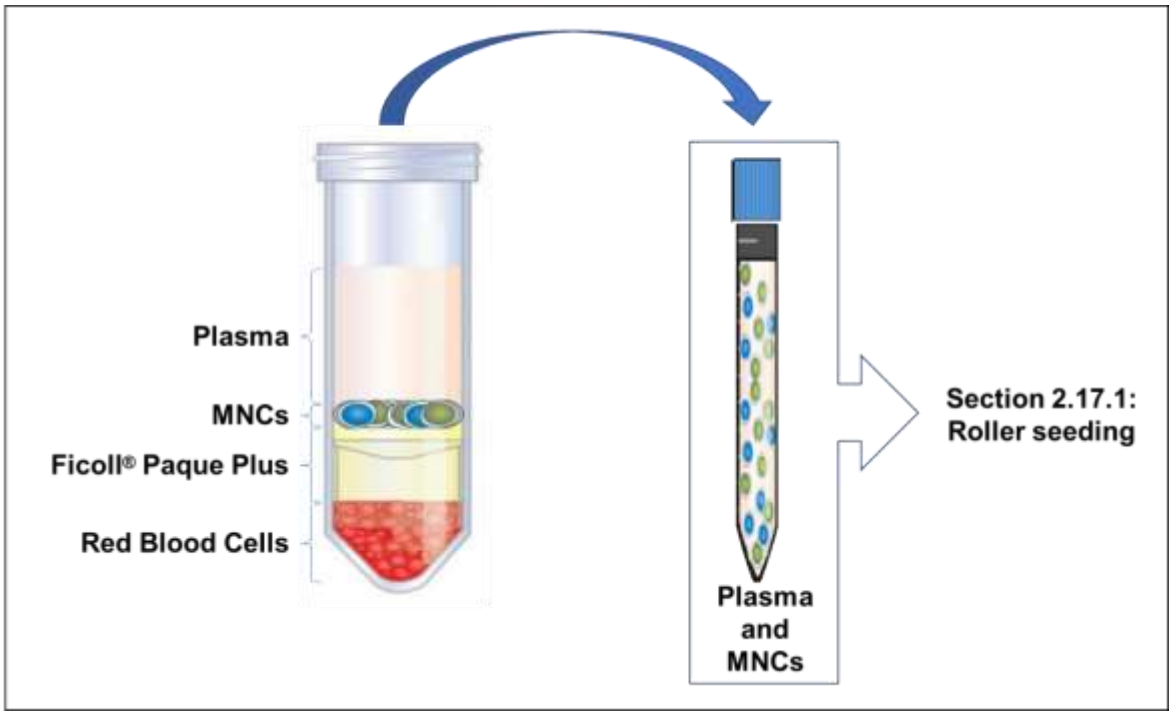

Figure 2.8 Porcine plasma and MNCs extraction and collection. Plasma and MNCs collected through density gradient centrifugation in SepMate™ 50 tube was collected in a 15 mL tube and later used in roller reseeding protocol.

2.17 Recellularisation Experiment

A few experiments were designed to assess the feasibility of using PWB to repopulate the decellularised scaffold.

2.17.1 Roller Seeding Protocol

First, a simple set-up was employed by placing the decellularised hSV in a cylindrical tube containing sufficient PWB or mononuclear cells (MNC) to submerge the scaffold and sealed with a filtered cap to allow gas exchange. The filled tubes were then placed on an angled roller, at 10 rpm in the incubator at 39°C, 5% CO_2 for 48 hours.

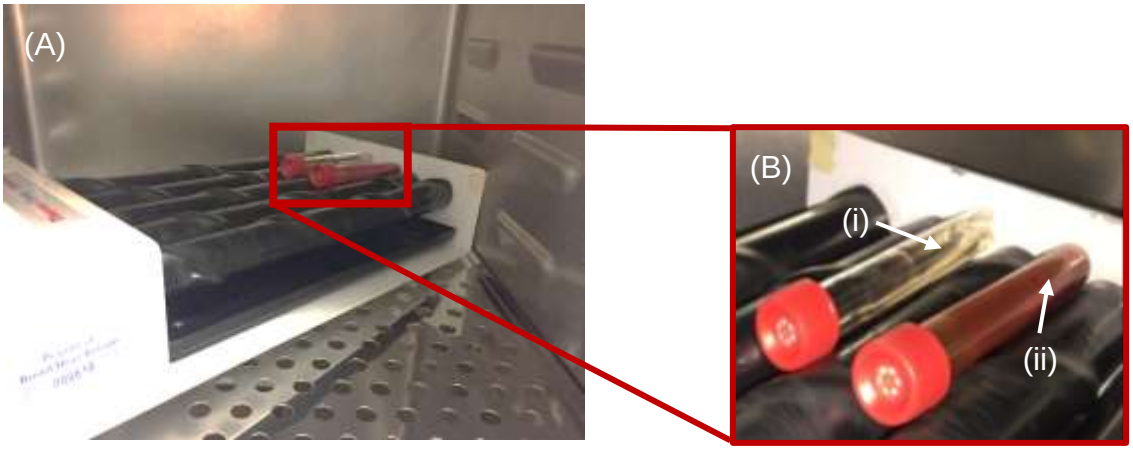

Figure 2.9 Decellularised vein seeding using a roller at 10 rpm in the incubator at 39°C, 5% CO_2 for 48 hours. (A) MNCs in plasma and PWB were placed with decellularised hSV scaffolds in cylindrical tubes fitted with filtered cap to allow gas exchange (**B)** Close-up view of the decellularised vein in filtered cap tubes filled with (i) MNCs in plasma extracted from PWB and (ii) PWB.

2.17.2 Bioreactor Seeding Protocol

On the other hand, a second method utilised a bioreactor system set up in the incubator at 39°C, 5% CO_2, where decellularised veins were mounted on a holder in a chamber filled with media and PWB was circulated at either low or high flow 25 or 200 mL/minute for 48 hours.

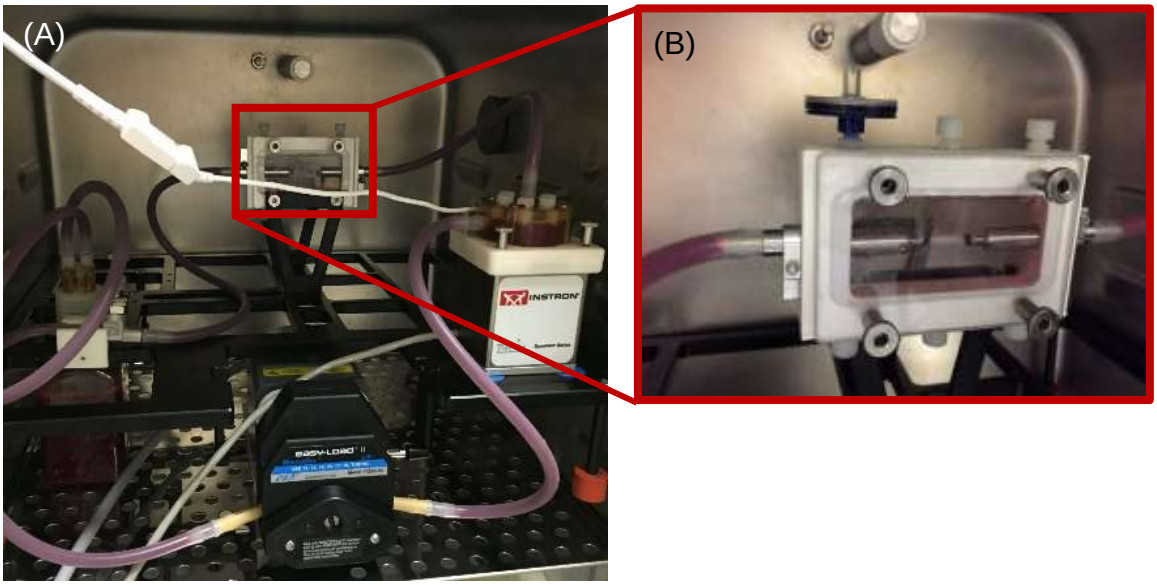

Figure 2.10 Decellularised vein seeding using a bio-reactor at 39°C, 5% CO_2 for 48 hours. (A) Bioreactor set-up to perfuse blood through decellularised veins at either low or high flow; 25 or 200 mL/minute respectively for 48 hours. **(B)** Close-up view of the decellularised vein mounted in the bioreactor chamber.

2.18 Immunostaining

2.18.1 Immunocytochemistry

Cells, either ECs or SMCs were seeded separately in 96 well tissue culture treated plates (655090; Greiner Bio-One Ltd.) at a seeding density of 100 000 cell/cm^2 and allowed to grow overnight. Cells were then washed twice with PBS and fixed using 3% (v/v) paraformaldehyde in PBS for 15 minutes. Cells were rinsed with 3% (v/v) BSA in PBS twice. Triton-X100 (concentration according to each antibody as shown in Table 2.2) in PBS was added to wells and the plate was incubated for 10 min at room temperature. Wells were then washed twice with PBS before incubation with primary antibody according to the cell type (refer to **Table 2.2**) at 4°C. Wells were washed twice with PBS before incubation with secondary antibody for 1 hour at room temperature. Wells were then washed twice with PBS. Nuclei staining was performed with Hoechst 33342 for another 30 minutes at room temperature whilst plate was protected from light with aluminium foil. Wells were then washed twice with PBS and aqueous mounting media Fluoromount-G (00-4958-02; Life Technologies) was added before imaging was performed using the EVOS FL Cell Imaging System at medium-powered field (medium power fields = 200X magnification). Five views of each well under the medium power field were captured and positive cells and nuclei counted using ImageJ software. Antibodies and dilutions used are listed in **Table 2.2**.

2.18.2 Immunohistochemistry

Decellularised tissue re-seeded with cells was stained with different antibodies for different cell specific markers e.g. ECs were stained with CD31 and SMCs were identified with □-smooth muscle actin. Additionally, tissues collected after *in vivo*

explants were also stained with cells specific marker to investigate the localisation of different cell types within the re-cellularised graft.

Tissue samples were fixed overnight in 10% formalin and store in PBS before processing in the Shandon Excelsior ES Tissue Processor (Thermo Scientific, UK) and paraffin wax embedding using the Shandon Histocentre™ 3 Embedding Center (Thermo Scientific, UK). Sections of 3-5 µm were cut using a microtome and placed on Superfrost Plus (10149870; Fisher) microscope slides. The slides were stored at room temperature and incubated at 37° for 20 minutes prior to analysis. Slides were dewaxed and rehydrated as follows: slides were immersed in three changes of Clearene (3803600E; Surgipath) for 5 minutes each, and then were rehydrated in three changes of 100% (v/v) IMS for 5 minutes each, followed by 90%(v/v) IMS for 3 minutes and lastly in 70% (v/v) IMS for another 3 minutes. Finally, the slides were placed in distilled water for 3 minutes.

The slides were incubated in 10 mM citrate buffer pH 6.0 for 20 minutes in a boiling water bath and were then allowed to cool at room temperature before washing twice with PBS. The surrounding sections were wiped dry with tissue paper and sections were mark with a wax pen. Slides were incubated in blocking buffer (5% (v/v) BSA and 0.1% (v/v) Triton in PBS) for 30 minutes at room temperature. Excess buffer was removed before incubation in primary antibody (as shown in Table 2.2) overnight at 4°C. Slides were washed three times with PBS before incubation with secondary antibody (refer to Table 2.2) for 1 hour at room temperature whilst protected from light with aluminium foil. Slides were then washed three times with PBS and cover-slipped

with ProLong® Gold Antifade Mountant with DAPI (P36931; Thermo Fisher Scientific). Imaging was performed with a fluorescent microscope and images were captured using the ImagePro software at high-powered field (high power fields = 400X magnification) for a descriptive analysis.

2.19 Statistical Analysis

For analysis of data in two groups statistical analysis was performed with a Student's two-sample t-test, assuming equal variances. One-way analysis of variance (ANOVA) was used to identify significant differences between three or more groups with post hoc comparison. Two-sided P values less than 0.05 indicated statistical significance. Numeric values are presented as the mean ± SEM. Reported n represents the number of individual cultured grafts tested (not repeat segments of the same graft).

Table 2.2 Details of reagents used in both immunocytochemistry (ICC) and immunohistochemistry (IHC).

Antibodies/stain	Species	Working dilution	Permeabilisation step	Catalogue number	Company
Primary antibodies/stain:					
Anti-Actin, α-Smooth Muscle-Cy3™	Mouse	ICC: 1/400 IHC: 1/400		C6198	Sigma
Anti-smooth muscle, Myosin heavy chain 11	Rabbit	ICC: 1/250 IHC: -	0.3% (v/v) Triton-X100 for 10 mins	ab53219	Abcam
Anti-Vimentin	Mouse	ICC: 1/200 IHC: -		ab8979	Abcam
Anti-Periostin	Rabbit	ICC: 5 µg/mL IHC: -		ab83739	Abcam
Anti-CD31	Rabbit	ICC: 1/20 IHC: 1/20		ab28364	Abcam
Anti-VE-Cadherin	Rabbit	ICC: 1/400 IHC:		ab33168	Abcam
Anti-Von Willebrand Factor	Rabbit	ICC: 1/400 IHC: -	0.1% (v/v) Triton-X100 for 10 mins	ab6994	Abcam
Biotinylated Dolichos Biflorus Agglutinin (DBA)	Horse Gram seeds (plant)	ICC: 1/200 IHC: 1/200		B-1035	Vector Laboratories
Anti-eNOS	Rabbit	ICC: 1/200 IHC: -		ab5589	Abcam
Mouse IgG_1, Isotype Control	Mouse	ICC: 1/200 IHC: 1/200		MAB002	R&D Systems
Rabbit IgG, Isotype Control	Rabbit	ICC: 1/400 IHC: 1/400		A11008	Life Technologies

Antibodies/stain	Species	Working dilution	Permeabilisation step	Catalogue number	Company
Secondary antibodies/stain:					
Goat anti-Rabbit IgG, Alexa Fluor 488	Goat	ICC: 1/400 IHC: 1/400		A11029	Life Technologies
Streptavidin, Alexa Fluor™ 488 conjugate	-	ICC: 1/200 IHC: 1/200		10164762	Life Technologies
Goat anti-Mouse IgG1, Alexa Fluor 488	Goat	ICC: 1/200 IHC: 1/200		A21121	Life Technologies
Nuclei stain:					
Hoechst 33342	-	ICC: 1/2000		H1399	Life Technologies

3 DECELLULARISATION OF HUMAN SAPHENOUS VEIN FOR USE AS A GRAFTING CONDUIT

3.1 Introduction

Decellularisation is a method used to remove the cellular component whilst retaining tissue extracellular matrix (ECM). It is considered that removal of the cellular component reduces the likelihood of immune rejection when used in clinical transplantation. This technique has been applied to produce various decellularised tissues and organs for transplantation including skin tissue, pericardium, heart valve (Fu et al. 2014; Guyette et al. 2014; Crapo, Gilbert, and Badylak 2011). Decellularisation is of interest as has enhanced biocompatible compared to synthetic materials and the production is less time consuming than the synthetic alternatives. In simple terms, decellularisation is achieved by removing all the cells from a given tissue and the resultant acellular scaffold is then available for various biomedical purposes.

A review of the literature reveals that the set of criteria accepted by the scientific community which defines effective decellularisation include: (i) lack of detected nuclear material in a decellularised tissue section when stained with haematoxylin and eosin (H&E), (ii) <50 ng DNA per mg dry weight of ECM and (iii) <200 bp of dsDNA fragment length (Crapo, Gilbert, and Badylak 2011; Rambol et al. 2018; Kargar-Abarghouei et al. 2018; Wilson et al. 2013; Destefani, Sirtoli, and Nogueira 2017).

To achieve effective decellularisation, several methods have been developed based on mechanical, chemical and biological approaches that are used either alone or in combination (e.g. mechanical-chemical, chemical-biological, mechanical-biological or mechanical-chemical-biological). Combination approaches have been tested since it

was considered that a single method approach may yield sub-optimal decellularisation (Crapo, Gilbert, and Badylak 2011; Azhim et al. 2011). The selection of method is also dictated by the type and size of tissue or organ to be decellularised. For example, decellularisation of a whole heart, as opposed to a piece of vein, requires a more robust protocol given the obvious qualitative and quantitative differences in cellular and structural composition.

Since the ultimate aim of this project was to decellularise human saphenous vein for clinical application, the simplest protocol consisting of various concentrations of sodium dodecyl sulphate (SDS) was selected. Following treatment with SDS the decellularisation efficacy was evaluated by examining the residual cellular components. In addition, the integrity of extracellular matrix and the mechanical strength of the resultant scaffold was determined. Of note, SDS, otherwise known as sodium lauryl sulphate or sodium lauryl sulphate (SLS), is a detergent commonly used in personal hygiene products as well as domestic and industrial cleaning products. The structure of SDS structure is shown in **Figure 3.1 A** (Kim et al. 2016). It acts an emulsifying agent because of its negatively charged functional group making it an anionic surfactant that acts on the plasma cell membrane thus disrupts cell structure and stability (**Figure 3.1 B**) (Seddon, Curnow, and Booth 2004). Previous studies report that the efficacy of decellularisation using SDS is determined by the type/or size of tissue targeted and the concentration used (Syed et al. 2014; Gilpin et al. 2014; Fitzpatrick, Clark, and Capaldi 2010; Wu et al. 2015).

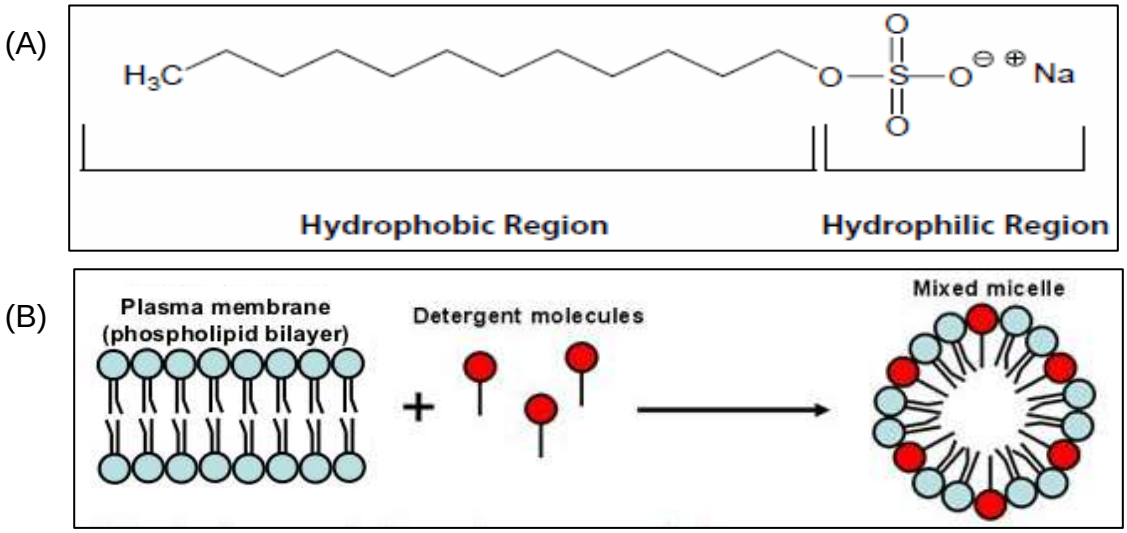

Figure 3.1. **SDS used in the decellularisation protocol. (A)** The structure of SDS illustrating its hydrophobic and hydrophilic regions. **(B)** The action of SDS (detergent) on the plasma cell membrane enabling it to disrupt the cell phospholipid bilayer through forming mixed micelle.

SDS is also used as a cell lysis buffer because as in addition to disrupting the plasma membrane structure, it also binds to and eventually denatures proteins by unfolding the protein 3-dimensional formation rendering them linear. Consequently, it is vital to optimise the exposure time and concentration of SDS on the tissue to be decellularised to avoid undesirable destruction of the tissue.

It was hypothesised that saphenous veins could effectively be decellularised using SDS and that the resultant acellular matrix scaffold could be used for *in vitro* and/or *in situ* tissue engineering for arterialisation. The ultimate goal of this process was to create an arterial-like vein graft with better long-term patency rates of saphenous

veins. To achieve this aim, a combination of mechanical and chemical decellularisation as describe by Schaner and colleagues was adopted (Schaner et al. 2004). In this chapter, the effectiveness of the decellularisation protocol, its effect on tissue integrity including ECM composition, biocompatibility of resultant tissue with cells for the purpose of recellularisation and feasibility of *in situ* recellularisation as a xenograft implant in *in vivo* porcine model of carotid replacement surgery was investigated.

3.2 Results

3.2.1 Decellularisation of human Saphenous Vein (hSV)

In brief, the decellularisation protocol included a 24-hour incubation of hSV in SDS at room temperature, followed by washing twice with PBS for 24 hours with PBS (as illustrated in **Figure 3.2**).

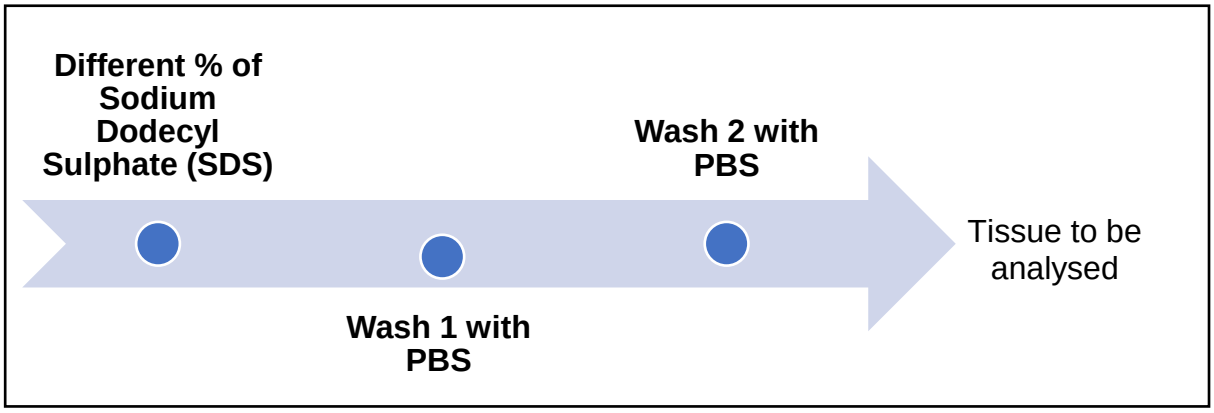

Figure 3.2 Decellularisation protocol. Decellularisation of hSV were done with different SDS concentration for 24 hours followed by two PBS washes every 24 hours for 48 hours on a roller at 60 rpm in room temperature.

3.2.2 Effectiveness of decellularisation protocol

The effectiveness of the decellularisation protocol is conventionally determined through the evaluation of cell numbers (most commonly by quantification of nuclei) remaining in the ECM scaffold following decellularisation (Crapo, Gilbert, and Badylak 2011). Therefore, the number of nuclei remaining on the ECM was quantified using H&E staining. It was demonstrated that incubation in 0.05% (w/v) SDS resulted in almost complete elimination of nuclei (95 ± 12%) whereas no nuclei were observed in the vein segments treated with 0.075 and 0.1% (w/v) SDS (100 ± 0.01% and 100 ± 0.16%, respectively). Of note, 0.01 - 0.025% (w/v) SDS achieved lower decellularisation (65 ± 8%) than 0.1% (w/v) SDS (69 ± 9%) despite a significant reduction in the number of` nuclei compared to the control vein segments (**Figure 3.3 A**).

A visual comparison of the SDS-treated tissue was made with two commercially available decellularised grafts including CorMatrix® ECM® for vascular repair and No-React® Porcine Pericardial Patch. Nuclei in 0.01% (w/v) SDS revealed faded as compared to the native hSV that act as a control (**Figure 3.3 B: shown by arrow**). The commercially available grafts contained noticeably more nuclei than that of dhSV segments subjected to the SDS treatment (**Figure 3.3 C**).

(A)

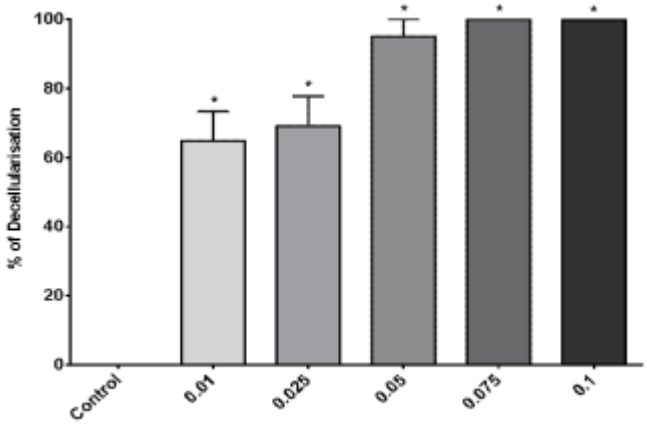
% of Decellularisation
100
80
60
40
20
0
Control
0.01
0.025
0.05
0.075
0.1
SDS %

(B)

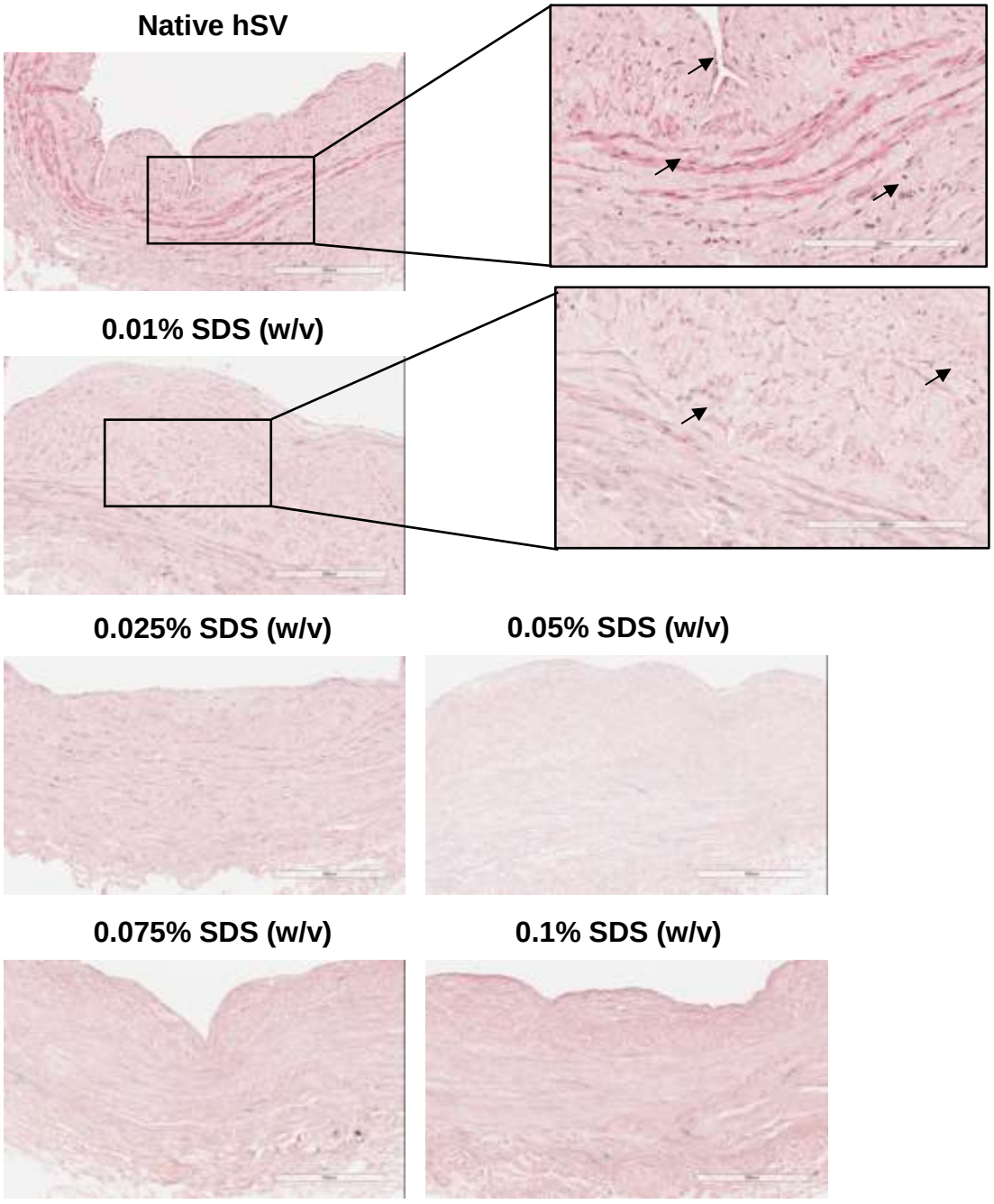
Native hSV
0.01% SDS (w/v)
0.025% SDS (w/v)
0.05% SDS (w/v)
0.075% SDS (w/v)
0.1% SDS (w/v)

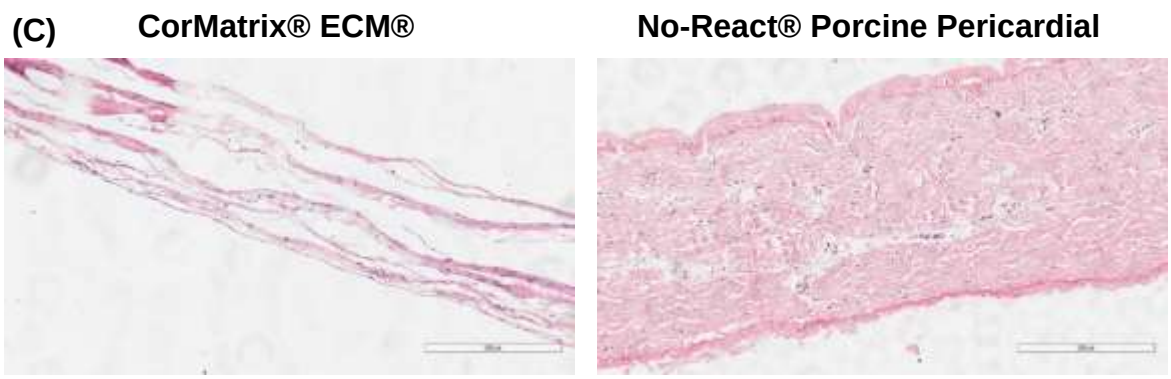

Figure 3.3 Efficiency of the decellularisation protocol with various SDS concentrations. Decellularisation protocol optimisation using 0.01, 0.025, 0.05, 0.075 and 0.1% SDS (w/v) compared to native control hSV. **(A)** Percentage of decellularisation was calculated by quantifying the nuclei (purple-black) in H&E stained paraffin wax embedded sections of decellularised compared to native veins. Values are presented as mean ± SEM, 1-way ANOVA, Dunnett's multiple comparisons test, * indicates $p<0.001$, $n=6$. **(B)** Representative images of decellularised and native veins stained with H&E. **(C)** Commercially available grafts; CorMatrix® ECM® for vascular repair and No-React® Porcine Pericardial Patch stained with H&E. Collagen and muscle are pink, cytoplasm is purple-red and nuclei are purple-black. Scale bars represent 300 µm and 200 µm for 100X and 200X magnifications respectively. Arrows indicate some of the detected nuclei (purple-black).

The H&E staining showed that although a low number of nuclei are detectable after SDS treatment, qualitative observation shows the decellularisation protocol achieved better decellularisation compared to commercial biological patches. Indeed, the H&E staining showed that the lowest concentration of SDS used (0.01% (w/v) significantly reduced the number of detectable nuclei compared to the native vein. The PicoGreen assay, which quantifies dsDNA was also utilised to assess decellularisation efficiency. The results showed that there was no significant reduction of dsDNA in all decellularised hSV. Therefore, indicated that the decellularisation protocol does not eliminate dsDNA (**Figure 3.4 A**).

DNA samples extracted from native and 0.01% (w/v) SDS decellularised hSV samples were subjected to gel electrophoresis, to ascertain the size of dsDNA in the tissues after decellularisation protocol. The size of the dsDNA detected in both native hSV and 0.01% (w/v) SDS decellularised hSV was >1000 bp but it was noted that dramatically lower amounts of dsDNA were detectable in the decellularised hSV compared to native hSV. Contrasting to the PicoGreen analysis, which may be due to the fact that PicoGreen could detect smaller DNA fragments that could not be detected on the gel electrophoresis (**Figure 3.4 B**).

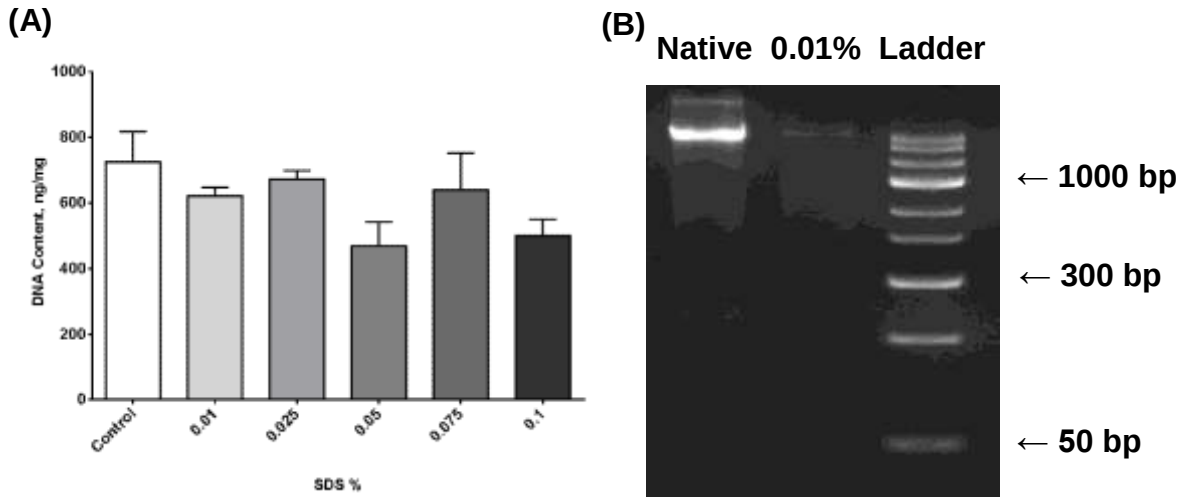

Figure 3.4 Effect of SDS treatment on DNA content. (A) PicoGreen assay to quantify dsDNA on each group of decellularised and native tissues. Values are presented as mean ± SEM, 1-way ANOVA, Dunnett's multiple comparisons test, n=6. **(B)** Representative gel electrophoresis image of native hSV (Native) and 0.01% (w/v) SDS decellularised hSV (0.01%).

To determine whether viable cells remained in the treated vein segments, BrdU incorporation within organ cultures of treated and untreated veins was quantified. BrdU incorporation indicative of proliferation was observed in 81 ± 4% cells within native hSV organ culture. In contrast, BrdU incorporation and thereby proliferation was not detected in decellularised hSV. This confirmed that cell proliferation did not occur within decellularised veins, hence confirming viable cells did not remain after the decellularisation protocol (**Figure 3.5**).

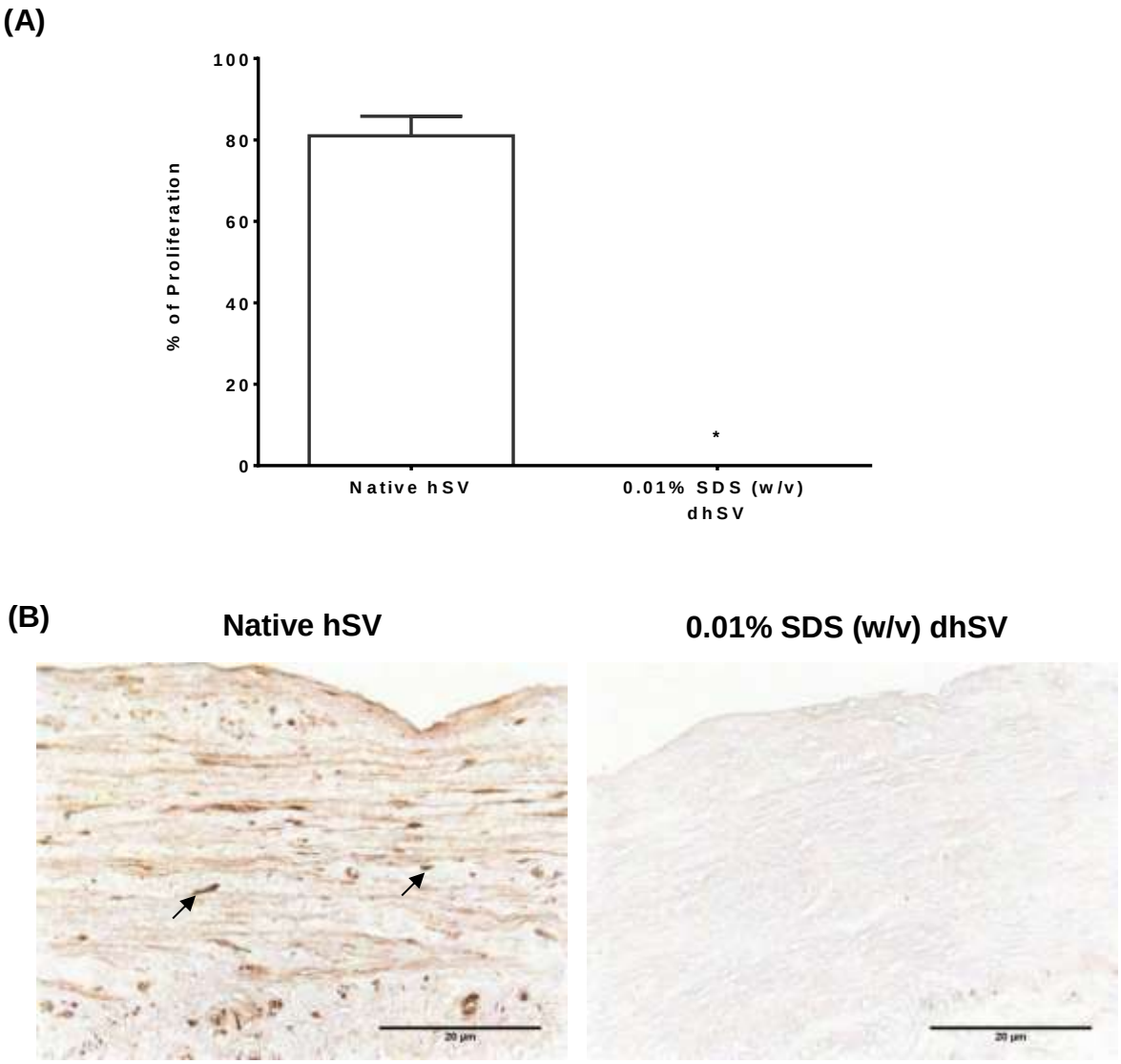

Figure 3.5 Detection of proliferating cells in organ cultures. (A) The percentage of proliferating cells was calculated by quantifying the number of nuclei with BrdU incorporation (brown) using peroxidase-based immunohistochemical BrdU-detection within native hSV and 0.01% (w/v) SDS decellularised hSV. Values are presented as mean ± SEM, * indicates $p<0.0001$, paired t-test, two-tailed, n=5. **(B)** Representative images of native hSV and 0.01% (w/v) SDS decellularised hSV sections subjected to immunohistochemistry for BrdU at 200X magnification. Scale bar represent 20 µm and applies to both panels. Arrows indicate some of the positive cells.

3.2.3 Effect of decellularisation protocol on hSV ECM structural integrity

The structural integrity of the decellularised vein segments is of key importance in terms of safety aspects for future transplantation of these decellularised scaffolds into the arterial circulation in a large animal preclinical model resembling human arterial size and anatomy. In addition to confirmation of decellularisation, demonstration of structural integrity is critical before implanting as a graft or attempting to reseed the decellularised vascular scaffolds with arterial cells. Hence, to confirm integrity the main structural components of the ECM including collagen, elastin and GAGs content within the decellularised vein segments were examined and compared with native vein.

To assess ECM content picrosirius red (PSR), elastin van Geison (EVG) and alcian blue staining were first performed to quantify the percentage of vein composed of collagen, elastin and GAGs, respectively. As histological staining is only representative of 3 µm section of the whole tissue, specific protein assays for collagen, elastin and GAGs and normalised with total protein content were also performed using paraffin embedded segments. Both approaches yielded similar results (**Figure 3.6 to 3.8 A and B**). Using histological staining and colour pixel quantification it was determined that over 60% of the vein section was composed of collagen. Treatment with SDS at any concentration did not significantly reduced the amount of collagen (**Figure 3.6A and C**). Hydroxyproline assay of native hSV shows it is consisting of 0.8 ng/µg collagen. Using the same assay, collagen content however was significantly reduced by 40% in vein segments treated with 0.05, 0.075 and to 0.1% (w/v) SDS, than native vein (**Figure 3.6B**). Native hSV were observed to be composed of 30% elastin from quantification using colour pixel histological staining. No significant difference in elastin content of decellularised hSV as compared to native with a

variable outcome was also observed (**Figure 3.7A and C**). Whereas almost 80% of native hSV were of GAGs. The decellularisation protocol doesn't seems to affect the GAGs content in decellularised hSV (**Figure 3.8A and C**). Due to the variability of the colour pixel quantification, Elastin and GAGs content in the tissues was further detected using Fastin Elastin™ and Blyscan™ assay. Native hSV showed they are consisting of 8 ng/µg and 1.7 ng/µg of elastin and GAGs, respectively. The same assays were done with decellularised tissue and shows that the SDS doesn't affect both elastin and GAGs (**Figure 3.7 and 3.8B**).

(A)

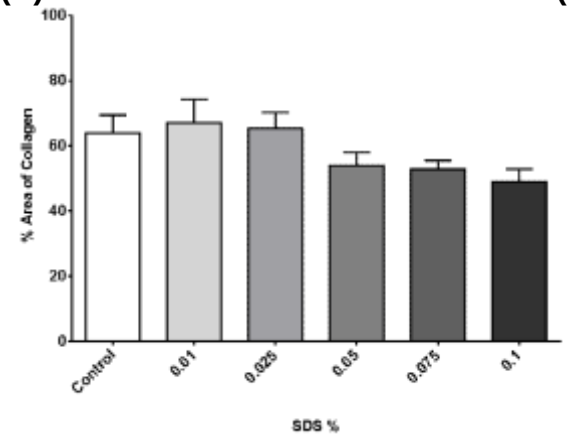

(B)

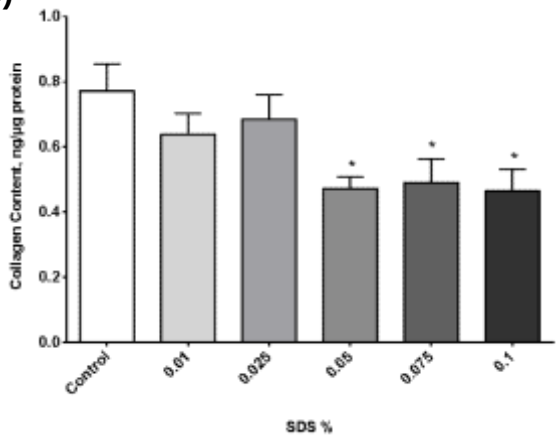

(C) Native hSV (Control)

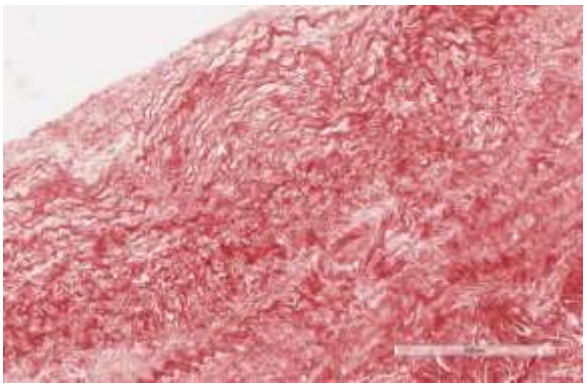

0.01% SDS (w/v)

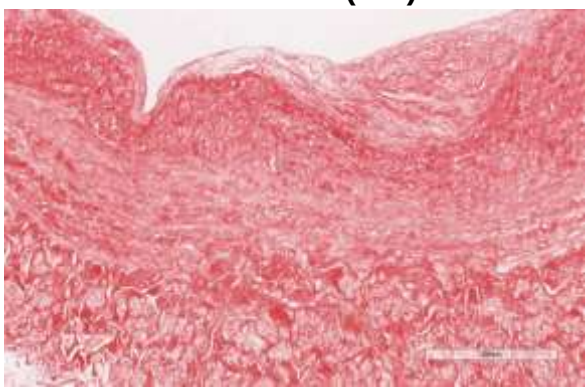

0.025% SDS (w/v)

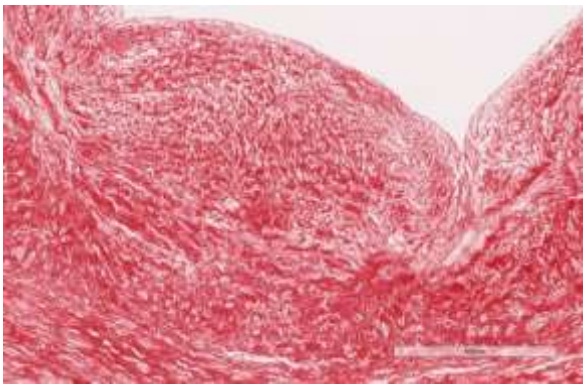

0.05% SDS (w/v)

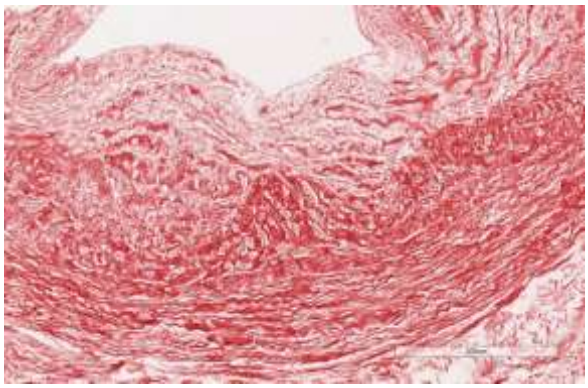

0.075% SDS (w/v)

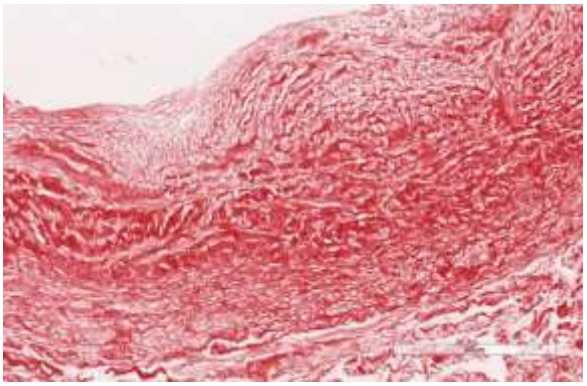

0.1% SDS (w/v)

Figure 3.6 Collagen content after decellularisation. (A) The percentage of collagen was determined by counting the red pixels within the PSR stained decellularised and native vein segments. Values are presented as mean ± SEM, 1-way ANOVA, Dunnett's multiple comparisons test, n=6. **(B)** Quantification of collagen content using the hydroxyproline assay. Values are presented as mean ± SEM, * indicates $p<0.05$, 1-way ANOVA, Dunnett's multiple comparisons test, n=6. **(C)** Representative images for each group of decellularised and native tissues at 100X magnification. Collagen is stained red. Scale bars represent 300 µm.

(A)

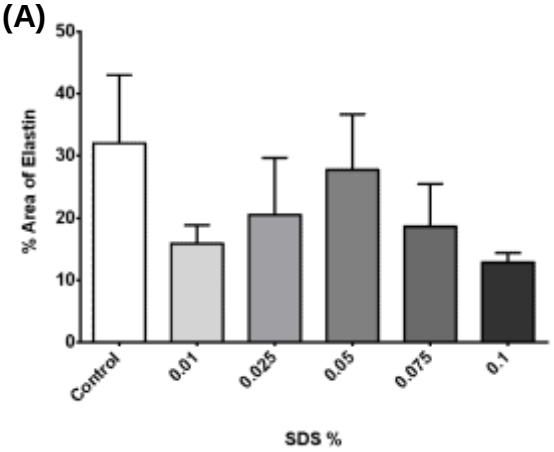

(B)

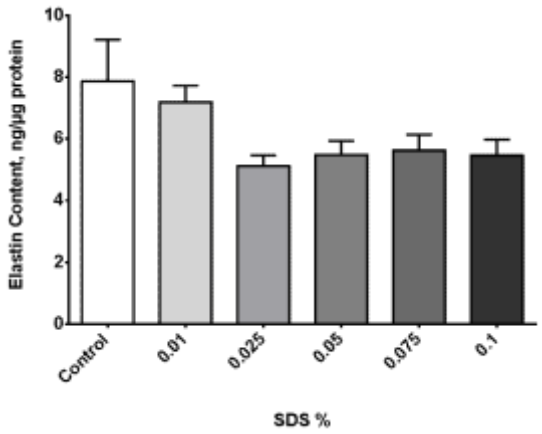

(C) Native hSV (Control)

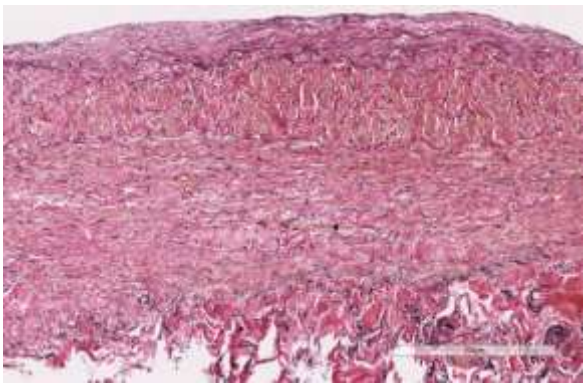

0.01% SDS (w/v)

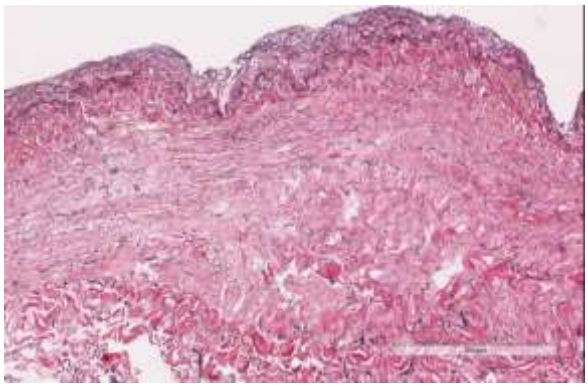

0.025% SDS (w/v)

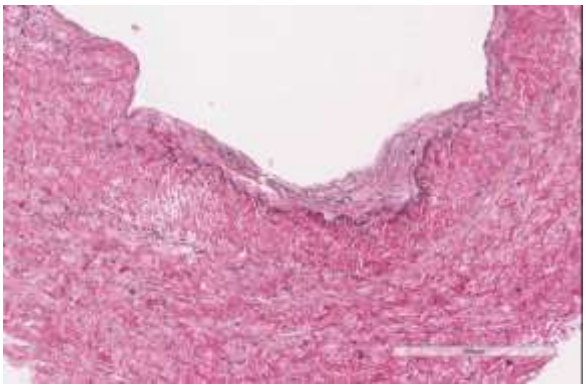

0.05% SDS (w/v)

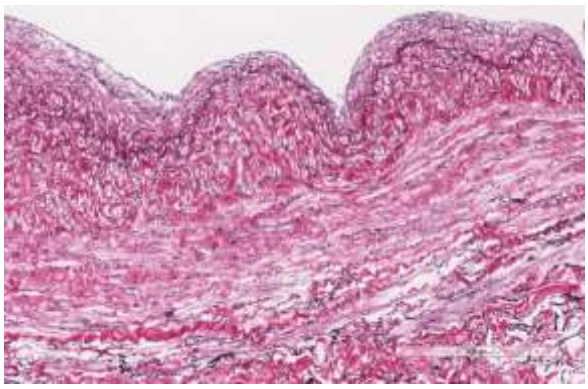

0.075% SDS (w/v)

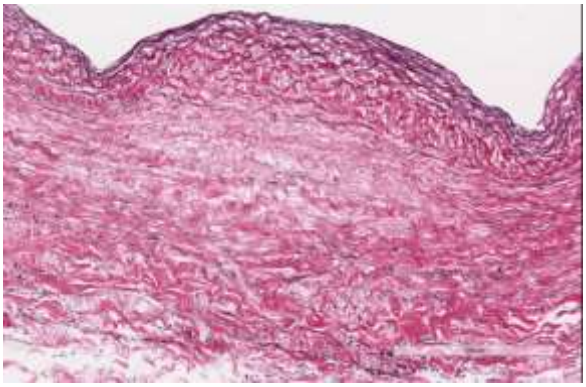

0.1% SDS (w/v)

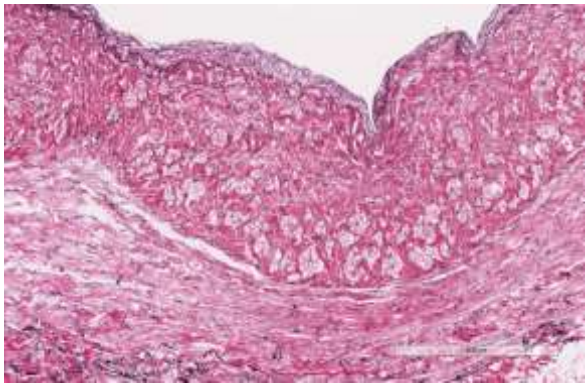

Figure 3.7 Elastin content after decellularisation. (A) The percentage of elastin was determined by counting the purple/black pixels within the EVG stained decellularised and native vein segments. Values are presented as mean ± SEM, 1-way ANOVA, Dunnett's multiple comparisons test, n=6. **(B)** Quantification of elastin content using the Fastin Elastin™ assay. Values are presented as mean ± SEM, * indicates $p<0.05$, 1-way ANOVA, Dunnett's multiple comparisons test, n=6. **(C)** Representative images for each group of decellularised and native tissues at 100X magnification. Elastin is stained purple/black. Scale bars represent 300 µm.

(A)

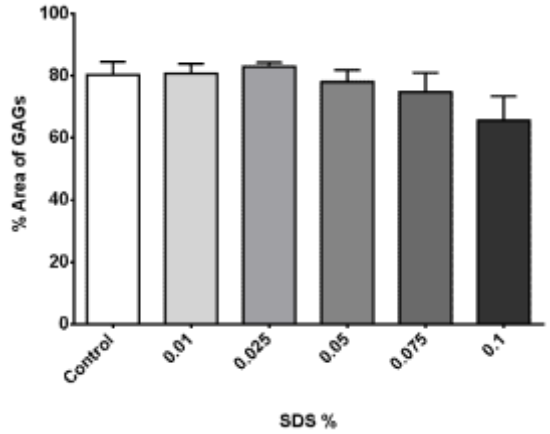

(B)

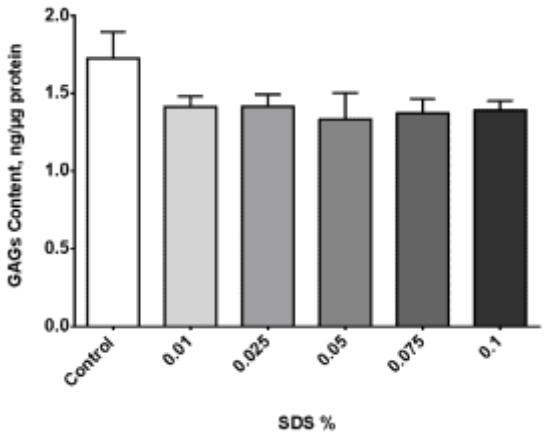

(C) Native hSV (Control)

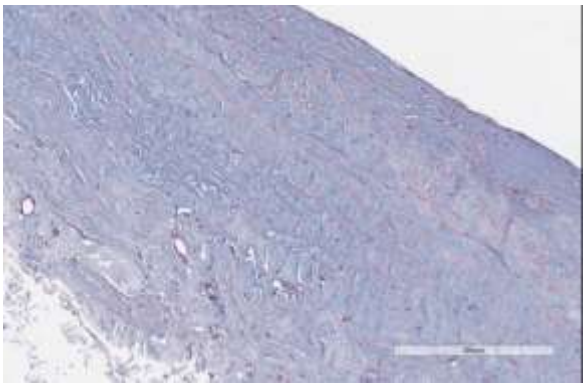

0.01% SDS (w/v)

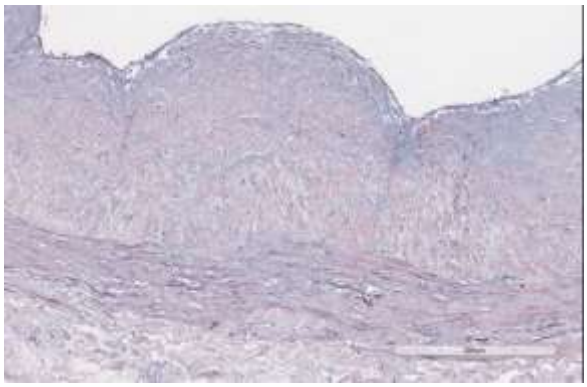

0.025% SDS (w/v)

0.05% SDS (w/v)

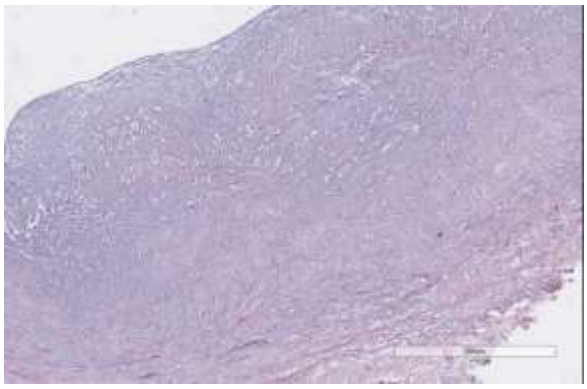

0.075% SDS (w/v)

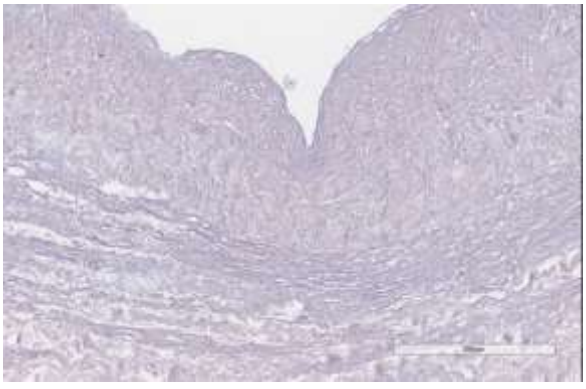

0.1% SDS (w/v)

Figure 3.8 GAGs content after decellularisation. (A) The percentage of GAGs was determined by counting the purple-blue pixels within the EVG stained decellularised and native vein segments. Values are presented as mean ± SEM, 1-way ANOVA, Dunnett's multiple comparisons test, n=6. **(B)** Quantification of GAGs content using the Blyscan™ assay. Values are presented as mean ± SEM, * indicates $p<0.05$, 1-way ANOVA, Dunnett's multiple comparisons test, n=6. **(C)** Representative images for each group of decellularised and native tissues at 100X magnification. GAGs are stained purple-blue, nuclei are stained red and cytoplasms are stained pink. Scale bar represent 300µm.

3.2.4 Effect of Decellularisation Protocol on hSV ECM Mechanical Properties

Mechanical properties of the decellularised graft was taken into consideration hence samples were sent to Amrita Centre for Nanoscience, India for an ISO accredited testing; n=5 control human saphenous veins, decellularised saphenous veins and porcine carotid arteries where burst strength and compliance test were done. No significant differences were observed on both burst strength and compliance of human saphenous veins, decellularised saphenous veins and porcine carotid arteries therefore the decellularised hSV were deemed suitable for porcine model carotid artery implantation.

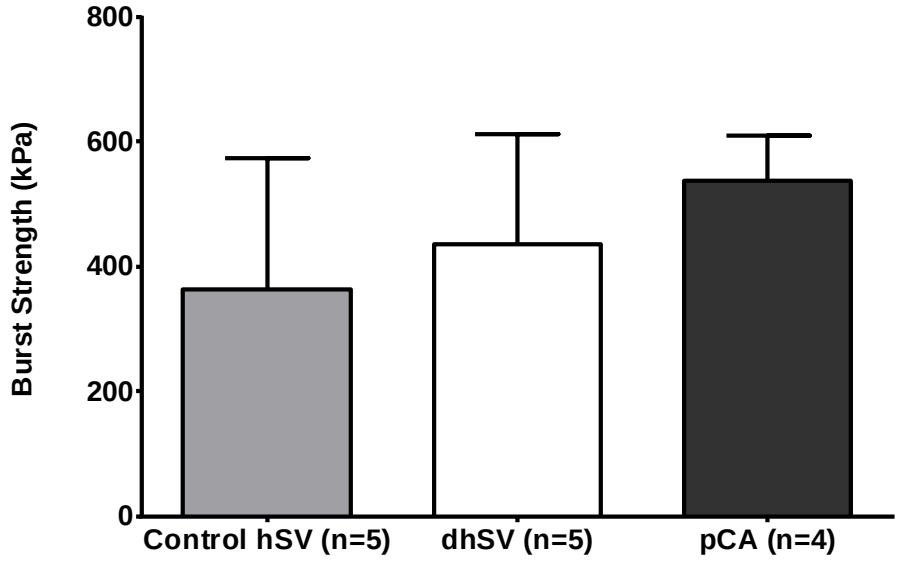

Figure 3.9 Grafts burst strength (kPa). Native hSV, 0.01% SDS w/v decellularised hSV and pCA segments burst strength comparison. Values are presented as mean ± SEM, 1-way ANOVA, Tukey's multiple comparisons test, n=5.

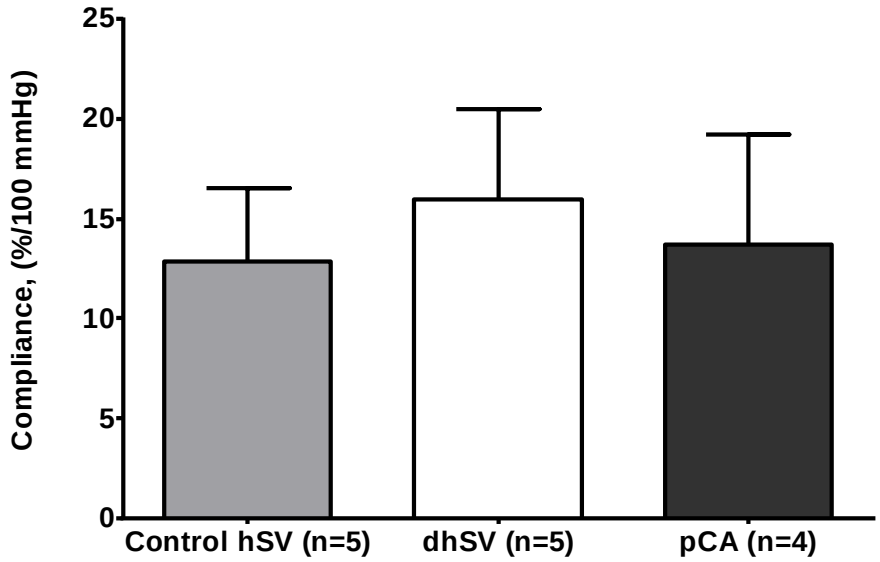

Figure 3.10 Grafts compliance test (%/mmHg). Native hSV, 0.01%SDS w/v decellularised hSV and pCA segments burst strength comparison. Values are presented as mean ± SEM, 1-way ANOVA, Tukey's multiple comparisons test, n=5.

3.2.5 Biocompatibility of decellularised tissue

As one goal is to reseed the decellularised vein scaffolds with arterial cells either *in vitro*, *ex vivo* or *in vivo*, the scaffold must facilitate adhesion and viability of seeded cells. Thus, confirmation of biocompatibility of the decellularised veins is an important.

SDS as an anionic detergent, is cytotoxic to cells, with the potential to disrupt the plasma cell membrane. Therefore, methylene blue assay was performed on the effluent from the PBS washes and the decellularised vein to analyse whether the SDS washing-out protocol was effective in removing SDS from the tissue.

It was observed that the first washing step significantly reduced SDS content by 10 fold compared to the initial 0.01% (w/v) SDS effluent (**Figure 3.11**). Further washing

steps significantly reduced the SDS concentration in the effluent a further 100 fold. The SDS content within the vein tissue showed that further washes did extract all SDS and the remaining concentration of SDS was 0.002% (w/v) SDS.

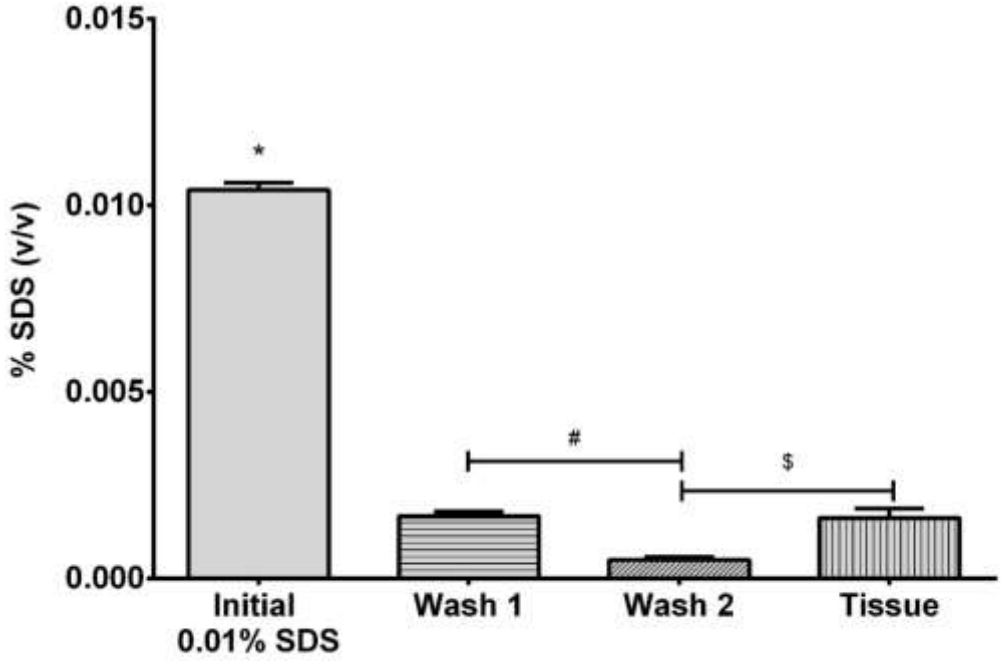

Figure 3.11 Effectiveness of the removal of SDS in the decellularisation protocol. The concentration of SDS in the effluent after each wash step and in the hSV tissue after treatment with 0.01% (w/v) SDS was quantified using methylene blue that detects SDS. Values are presented as mean ± SEM, * indicates $p<0.05$ vs. wash 1, wash 2 and tissue, and # and $ indicates $p<0.05$ vs. wash 1 and wash 2, respectively, Repeated measure 1-way ANOVA, Tukey's multiple comparisons test, n=6.

To assess biocompatibility, hSV segments were treated with 0.01% (w/v) SDS, as this concentration significantly reduced the number of nuclei and had the least effect on ECM integrity and collagen content as described above (see **3.2.2** and **3.2.3**).

Following washing with PBS twice described above, the hSV scaffolds were seeded with ADSCs, HUVECs and hSV SMCs. The cell number was quantified with the AlamarBlue® assay at 24 and 72 hours after seeding. A total of 5,000 cells was seeded in every well. With all three cell types less than 4,000 adherent and viable cells were detected after 24 hours incubation, illustrating the decellularised scaffold provided a suitable surface for the seeded cells. Interestingly, the number hSV SMCs almost doubled between 24 and 72 hours post seeding suggesting good biocompatibility of the decellularised hSV scaffold for this cell type (**Figure 3.12**). In contrast, the number of HUVECs and ADSCs did not significantly increase between 24 and 72 hours.

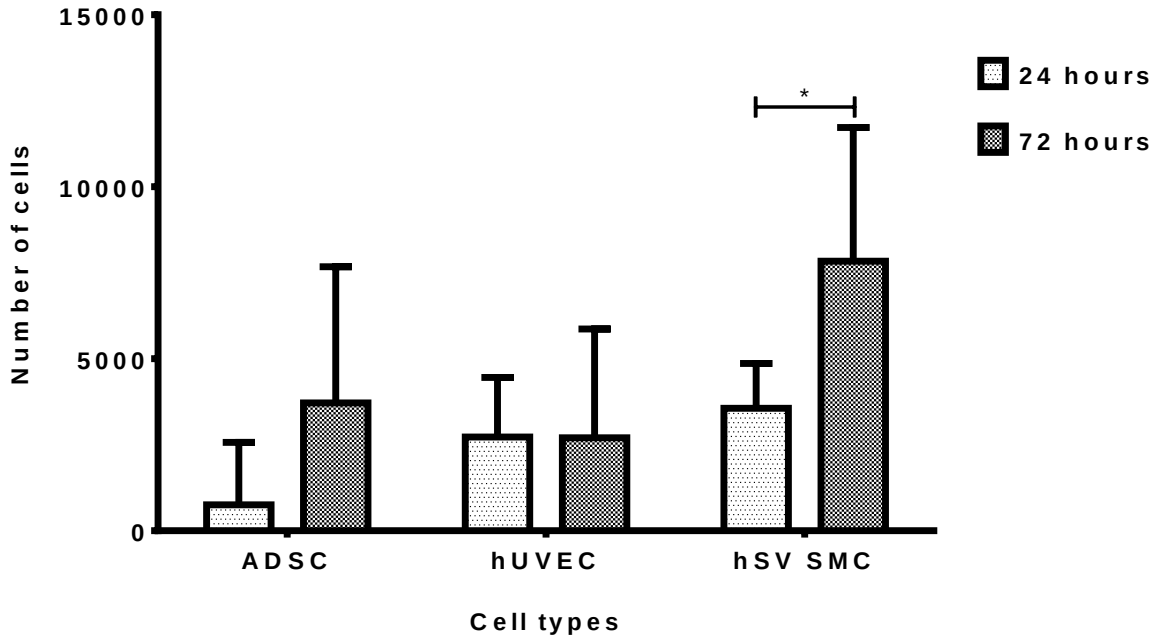

Figure 3.12 Assessment of biocompatibility using the cell viability assay. 0.01% (w/v) SDS decellularised vein segments were seeded with ADSCs, hUVECs and hSV SMCs and cultured for 24 and 72 hours. The cell number was estimated with the Alamar Blue assay. Values are presented as mean ± SEM, * indicates $p<0.05$, Repeated measure 2-way ANOVA, Bonferroni's multiple comparisons test, n=6.

3.2.6 Implantation of decellularised human saphenous veins as a xenograft in a porcine model

With confirmation of *in vitro* biocompatibility and integrity, to the next aim was to confirm mechanical strength and examine recellularisation *in vivo*. Decellularised hSV was implanted as a xenograft into a porcine model of carotid artery replacement at clinical standards. The aim was to induce *in situ* re-cellularisation of the decellularised hSV scaffolds by host cells and assess at 4 weeks after implantation with a focus on patency rate, thrombogenesis, suturability, flow dynamics, wall thickness, structural and cellular content.

The result of this first wave of pilot *in vivo* implants showed excellent feasibility of suturing all of the hSV at surgery. In addition, there was excellent suturability (passing through of the fine 7-0 prolene stitches and no oozing or bleeding from the suture line following arterial reperfusion with systemic arterial pressure maintained at normal physiological standards). In addition, there was excellent transmission of arterial pulse across the decellularised hSV when assessed by finger palpation in all three arterial implants with confirmation of patency at 30 minutes post reperfusion. Also, there was no obvious mismatch in lumen diameter and wall thickness between decellularised hSV and pCA pre-implantation. Similar observation was done right before extraction of decellularised hSV graft. Pulsatility of the graft pre-explantation were observed in the first 2 explant and the rhythm were observed dampen down in the last graft. High pressure blood flow through the graft in the first graft but not the latter two. The lumen diameter of the patent graft in the pCA appeared expanded outward and dilated reaching almost twice the lumen diameter of the native pCA with no apparent wall thickness differences. Macroscopic observation of the second explant shows

expansion of the lumen similar to the first explant but the graft was occluded. Further staining of the post-implant pCA proximal to the graft shows the formation of atherosclerosis plaque. Whilst in the third graft, the formation of thrombus was detected in the lumen of the pCA proximal to the graft (**Figure 3.13**).

Post-implantation, the collagen content of the hSV graft was not significantly different to the decellularised vein prior to implantation or pre- and post-implant pCA (**Figure 3.14 A**). Collagens were observed to be in evenly distributed layers in the vascular wall in all pre-implant tissue and post-implant pCA. Interestingly, all hSV graft explant shows more irregular distribution of collagen with most of them concentrated in the adventitia layers (**Figure 3.14 B**). Similar observation was noted with elastin content as that of collagen content (**Figure 3.15**). The GAG content of pCA and hSV was similar pre-implantation and at explant, but a significantly increased amount of GAGs was detected when comparing post-explant pCA levels compared to pre-implant hSV (**Figure 3.16**).

Marked *in situ* repopulation by host cells was apparent within the hSV when explanted from the CA position. Identification of the different cell types repopulating the decellularised veins was attempted through immunostaining for proteins that are well recognised as specific cell type markers (SMCs: αSMA and SM-MHC, ECs: DBA, CD31 and eNOS, macrophage/monocytes: CD203 and fibroblasts: vimentin). Sections of the native pCA removed at implantation of the decellularised hSV and sections of the pre-implant decellularised hSV were also subjected to immunostaining for these markers.

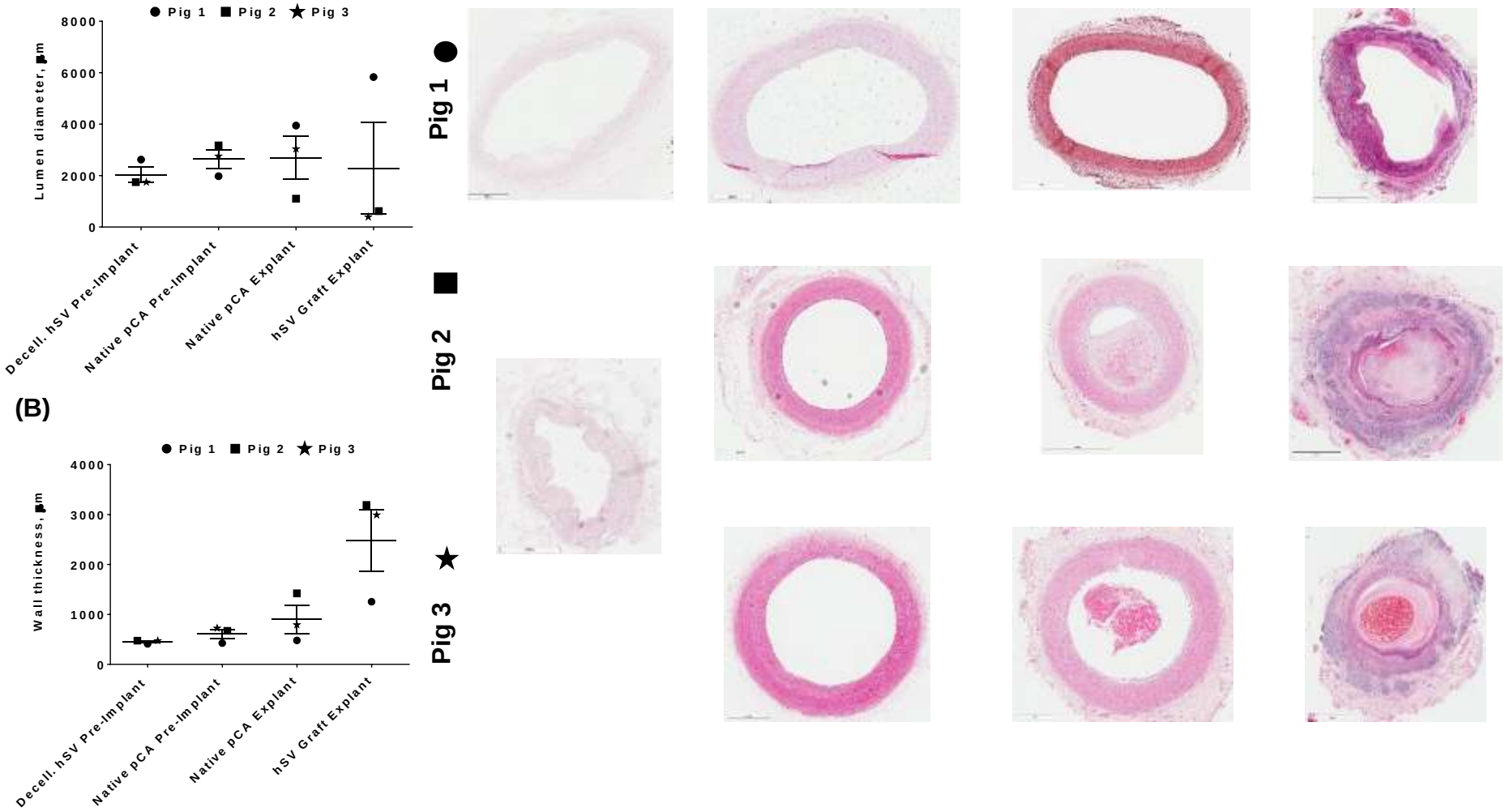
(A)
Pig 1
Pig 2
Pig 3
Lumen diameter, µm
8000
6000
4000
2000
0
Decell. hSV Pre-Implant
Native pCA Pre-Implant
Native pCA Explant
hSV Graft Explant
(B)
Pig 1
Pig 2
Pig 3
Wall thickness, µm
4000
3000
2000
1000
0
Decell. hSV Pre-Implant
Native pCA Pre-Implant
Native pCA Explant
hSV Graft Explant
(C) Decellularised hSV
Pre-implant pCA
Post-implant pCA
hSV Graft Explant
Pig 1
Pig 2
Pig 3

Figure 3.13 Structural characteristics of pCA and decellularised vein pre- and post-implant. (A) Lumen diameter pre- and post-implant of pCA and 0.01% (w/v) SDS decellularised hSV. Values are presented as mean ± SEM, Repeated measure 2-way ANOVA, Sidak's multiple comparisons test, n=3. **(B)** Wall thickness pre- and post-implant of pCA and 0.01% (w/v) SDS decellularised hSV. Values are presented as mean ± SEM, Repeated measure 2-way ANOVA, Sidak's multiple comparisons test, n=3. **(C)** H&E images for pre- and post-implant of pCA and 0.01% (w/v) SDS decellularised hSV. Collagen and muscle are stained pink, cytoplasm is stained purple-red, nuclei are purple-blue and red blood cells stained cherry red. Scale bars are indicated on images.

(A)

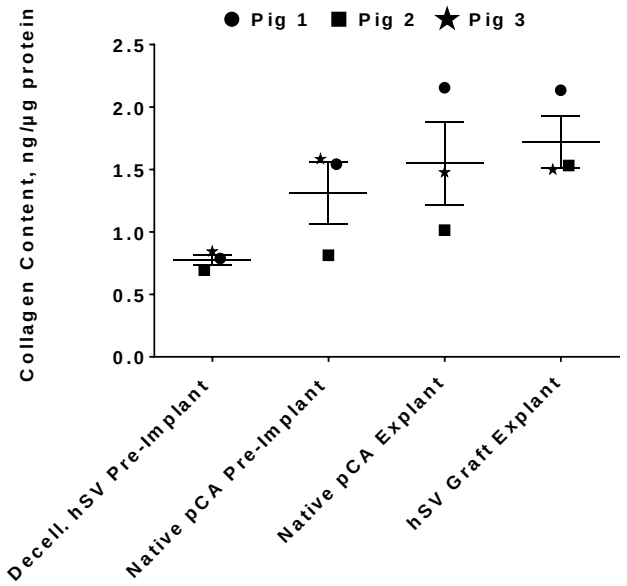

Figure 3.14 Collagen content of pCA and decellularised vein pre- and post-implant. (A) Quantification of collagen content within pre- and post-implant of pCA and 0.01% (w/v) SDS decellularised hSV using hydroxyproline assay. Values are presented as mean ± SEM, Repeated measure 2-way ANOVA, Sidak's multiple comparisons test, n=3. **(B)** PSR images for pre- and post-implant of pCA and 0.01% (w/v) SDS decellularised hSV where collagen is red on a pale-yellow background at 200X magnification. ●; ■ and ★ indicate explants from pig 1, 2 and 3 respectively. Scale bar represent 300 µm.

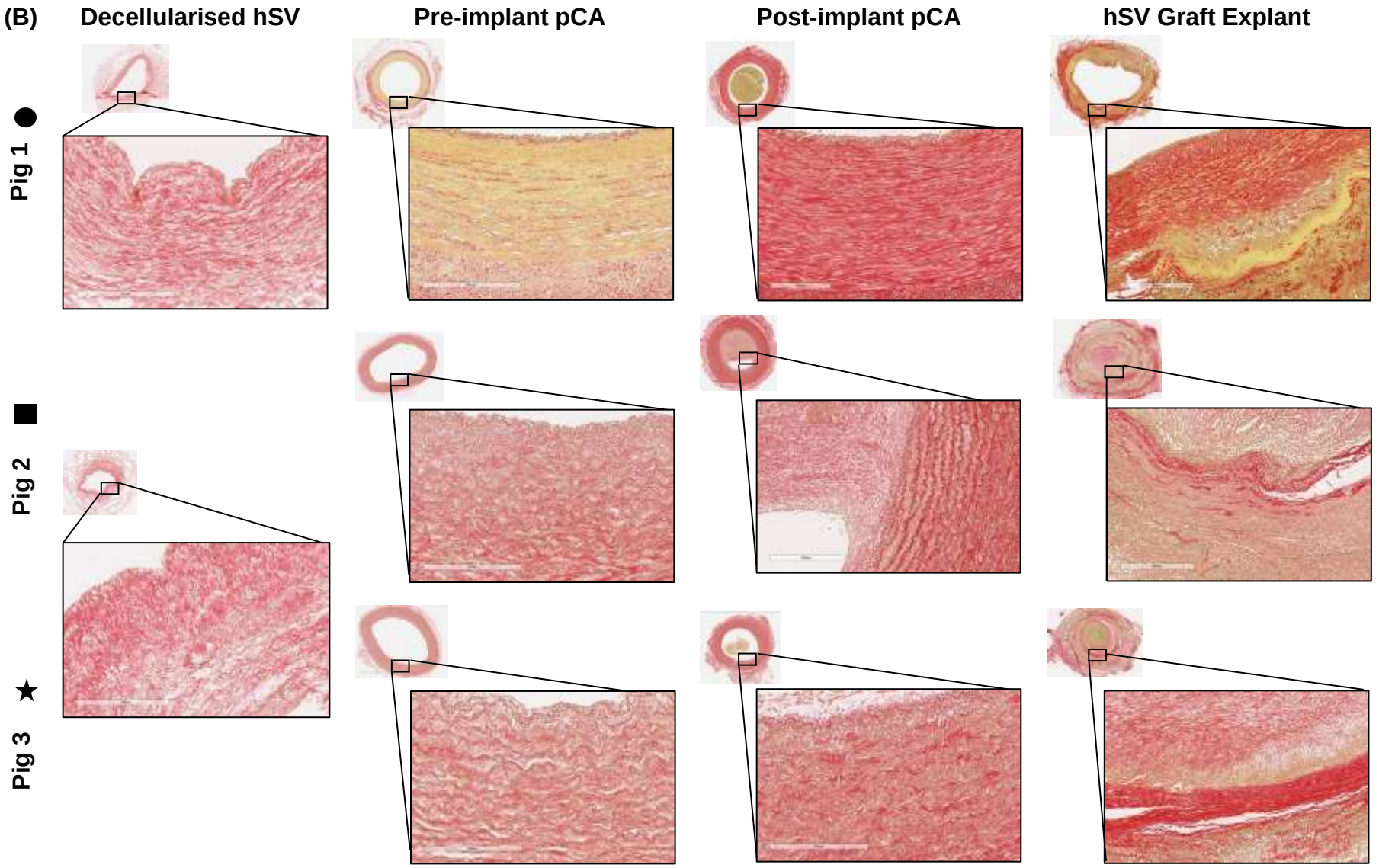
(B)
Decellularised hSV
Pre-implant pCA
Post-implant pCA
hSV Graft Explant
Pig 1 ●
Pig 2 ■
Pig 3 ★

(A)

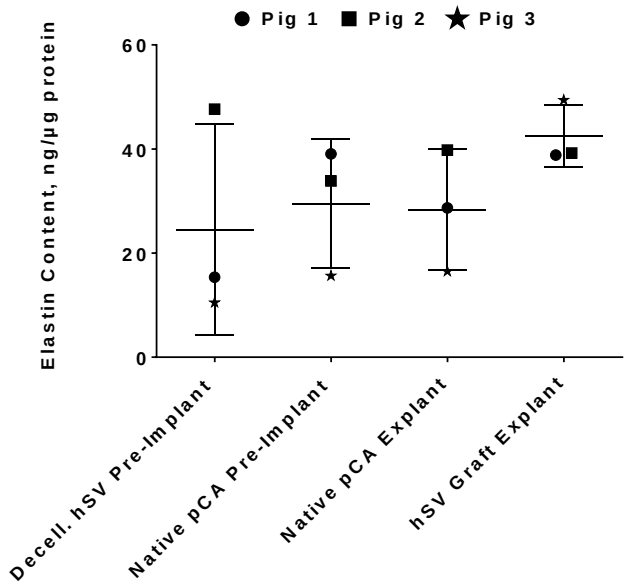

Figure 3.15 Elastin content of pCA and decellularised vein pre- and post-implant. (A) Quantification of elastin content within pre- and post-implant of pCA and 0.01% (w/v) SDS decellularised hSV using Fastin Elastin™ assay. Values are presented as mean ± SEM, Repeated measure 2-way ANOVA, Sidak's multiple comparisons test, n=3. **(B)** EVG images for pre- and post-implant of pCA and 0.01% (w/v) SDS decellularised hSV where elastic fibres are stained purple-black, collagen is red and other tissue elements are yellow) at 200X magnification. ●; ■ and ★ indicate explants from pig 1, 2 and 3 respectively. Scale bar represent 300 µm.

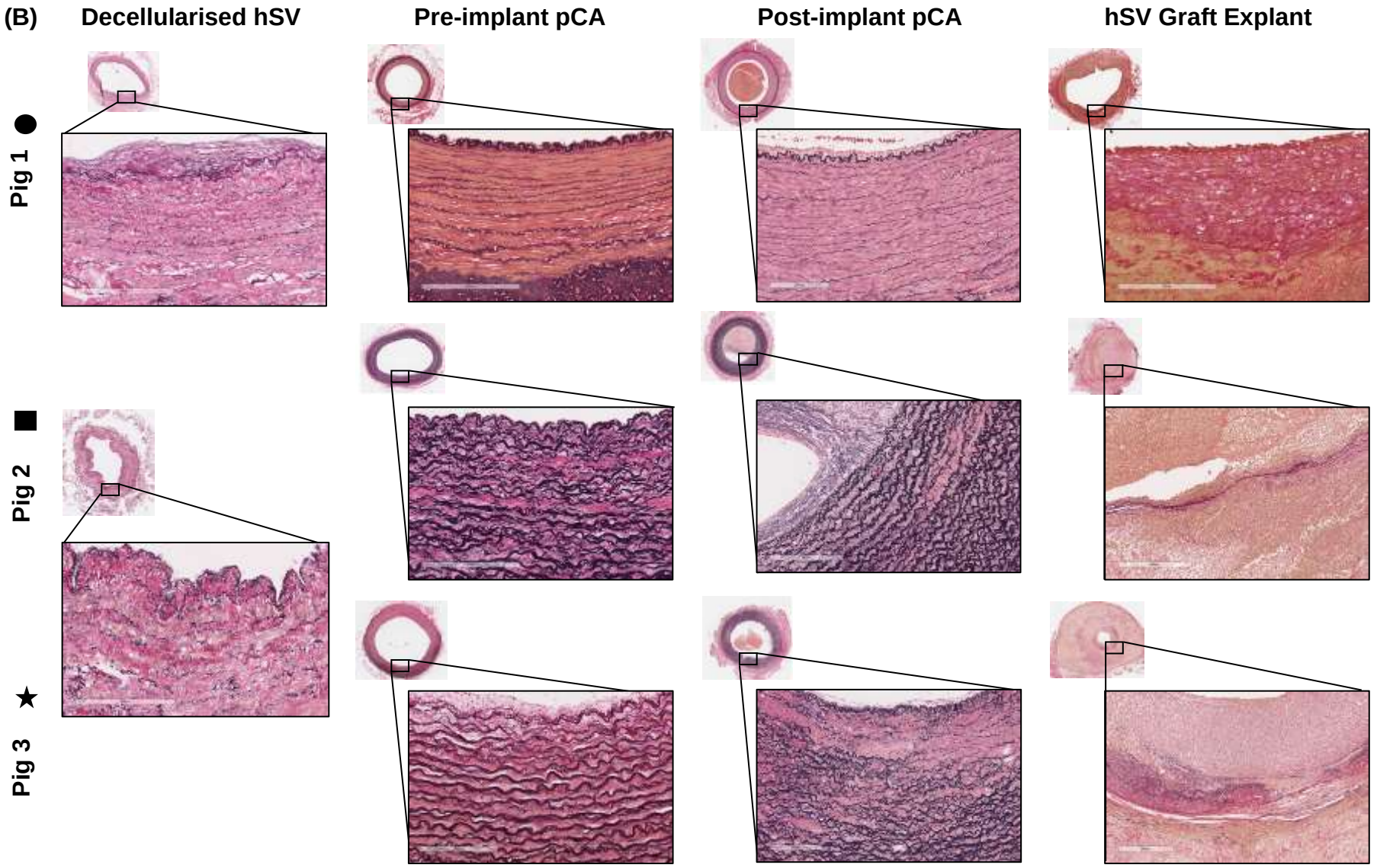
(B)
Decellularised hSV
Pre-implant pCA
Post-implant pCA
hSV Graft Explant
Pig 1 ●
Pig 2 ■
Pig 3 ★

(A)

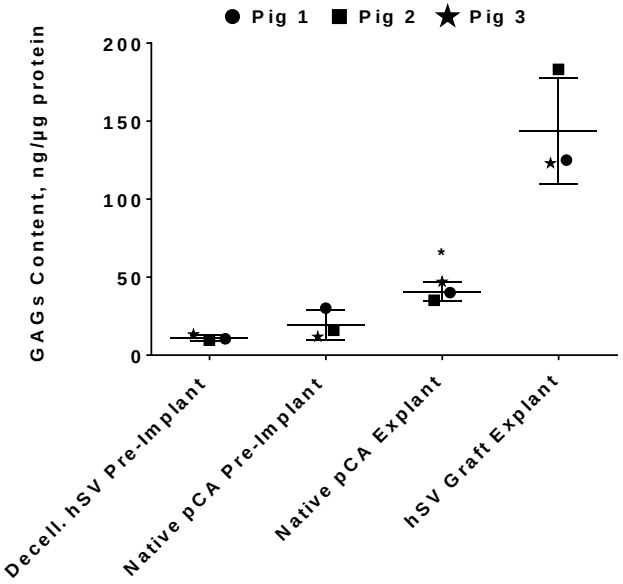

Figure 3.16 GAGs content of pCA and decellularised vein pre- and post-implant. (A) Quantification of GAGs content within pre- and post-implant of pCA and 0.01% (w/v) SDS decellularised hSV using Blyscan™ assay. Values are presented as mean ± SEM, Repeated measure 2-way ANOVA, Sidak's multiple comparisons test, n=3. **(B)** GAGs images for pre- and post-implant of pCA and 0.01% (w/v) SDS decellularised hSV where GAGs are stained purple-blue, nuclei are stained red and cytoplasm are stained pink at 200X magnification. ●; ■ and ★ indicate explants from pig 1, 2 and 3 respectively. Scale bar represent 300 µm.

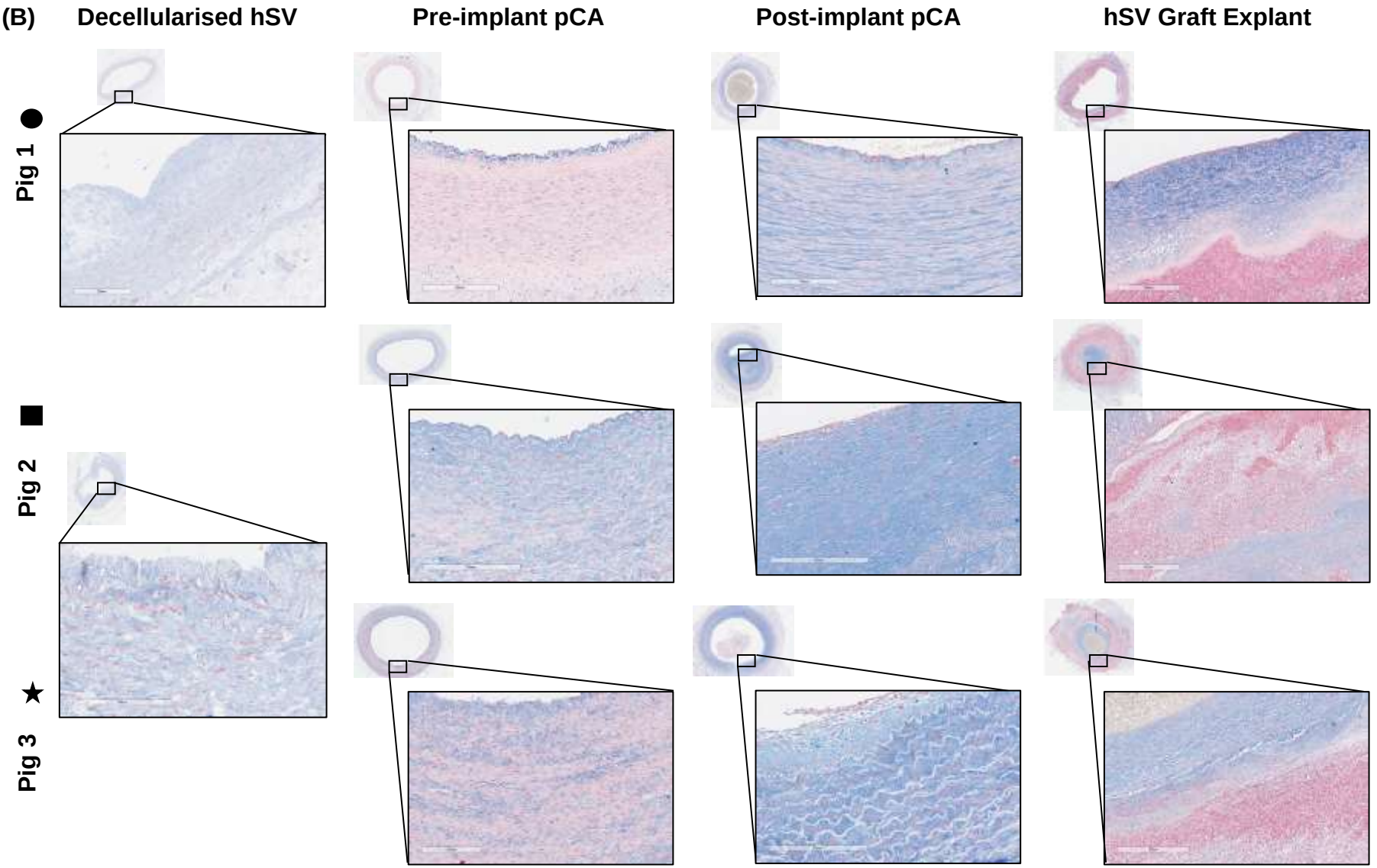
(B)
Decellularised hSV
Pre-implant pCA
Post-implant pCA
hSV Graft Explant
Pig 1 ●
Pig 2 ■
Pig 3 ★

Initial dual immunostaining of all hSV explant resulted in the detection on neovascularisation in all hSV graft positively stained with both DBA and αSMA localised in the adventitial later of the grafts (**Figure 3.17**). DBA was initially used due to limited established porcine antibodies. The immunostaining was then followed with other antibodies that has reacts with porcine antigens was established and optimised e.g. αSMA, SM-MHC, CD31, eNOS, CD203 and vimentin. Isotype control for each antibody showed that the antibodies are specific as all the IgG control used shown negative staining (**Figure 3.18-3.20A**). Porcine CA was used as a positive control tissue and decellularised hSV pre-implant was used as a comparison.

Interestingly, αSMA was detected in the decellularised tissue but not CD31 (**Figure 3.18A**). ECs layers on the patent graft luminal surface from the first explant were observed but not as brightly stained as DBA. CD31 were also detected to be less as compared to DBA. Adventitial neovascularisation was also confirmed with CD31 staining (**Figure 3.18B**). Vimentin which is a fibroblast marker was detected in pCA but not in decellularised hSV (**Figure 3.19A**). Vimentin was also detected in the patent graft but not in the occluded grafts. On the other hand, eNOS was observed within the wall and not on the lumen (**Figure 3.19B**). SM MHC reconfirmed αSMA observation where the decellularised hSV was stained positive. Pig spleen was used as a positive control for CD203 which is a macrophage/monocyte marker (**Figure 3.20A**). CD203 and SM MHC were detected in all grafts wall and especially in and around the neovessels (**Figure 3.20B**).

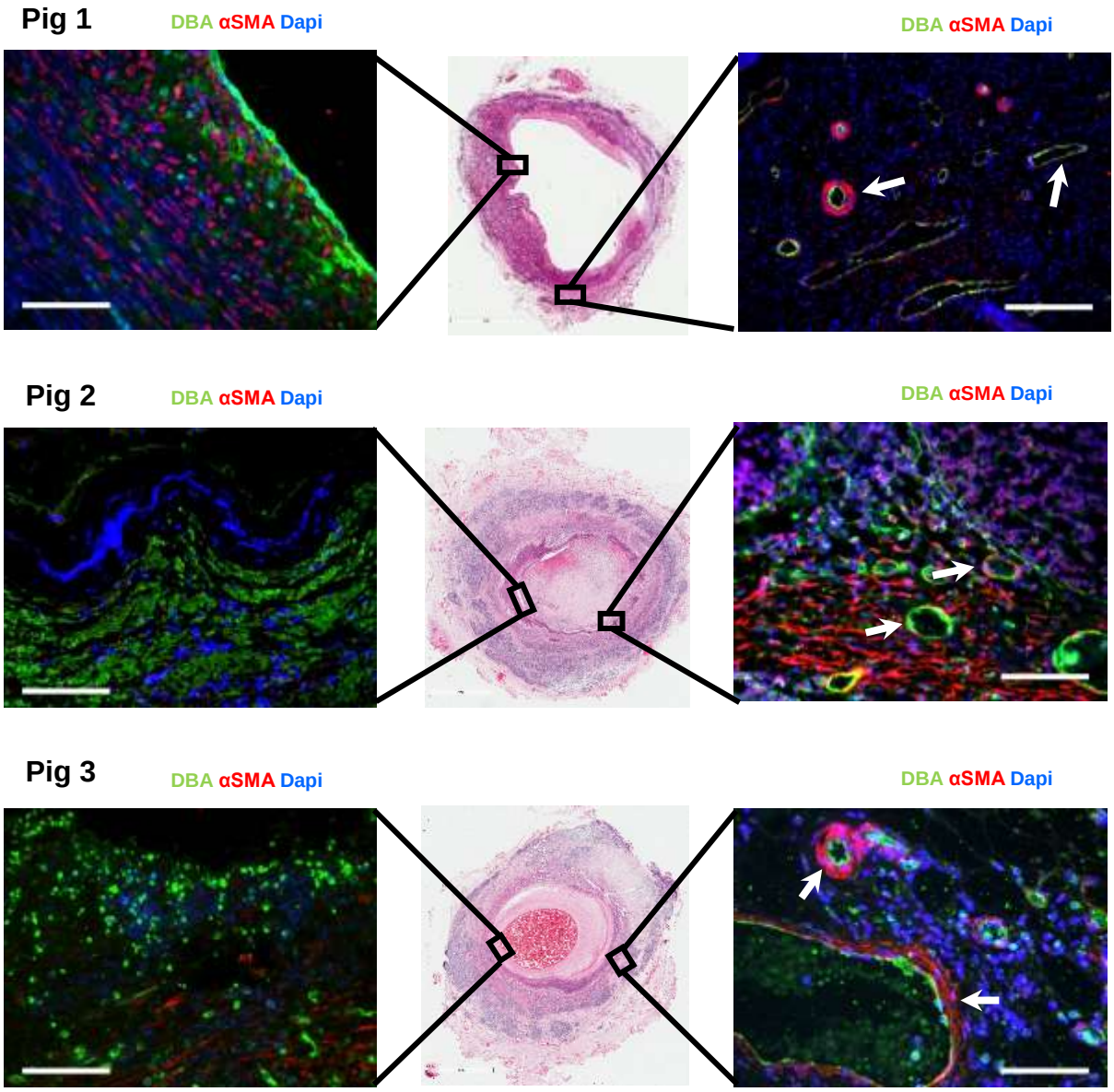

Figure 3.17 Xenograft immunohistochemistry screening staining. Representative images of dual immunostaining on 3-micron slices of xenograft explants stained with both DBA and αSMA to identify cells in the explants with H&E stained explants ring to show localisation. All tissues were nuclear stained with DAPI (blue), αSMA (red) and DBA (green) at 400X magnification. White arrow shows neovascularisation. Scale bar represent 80 µm and 3 mm for IHC and H&E images; respectively.

(A)

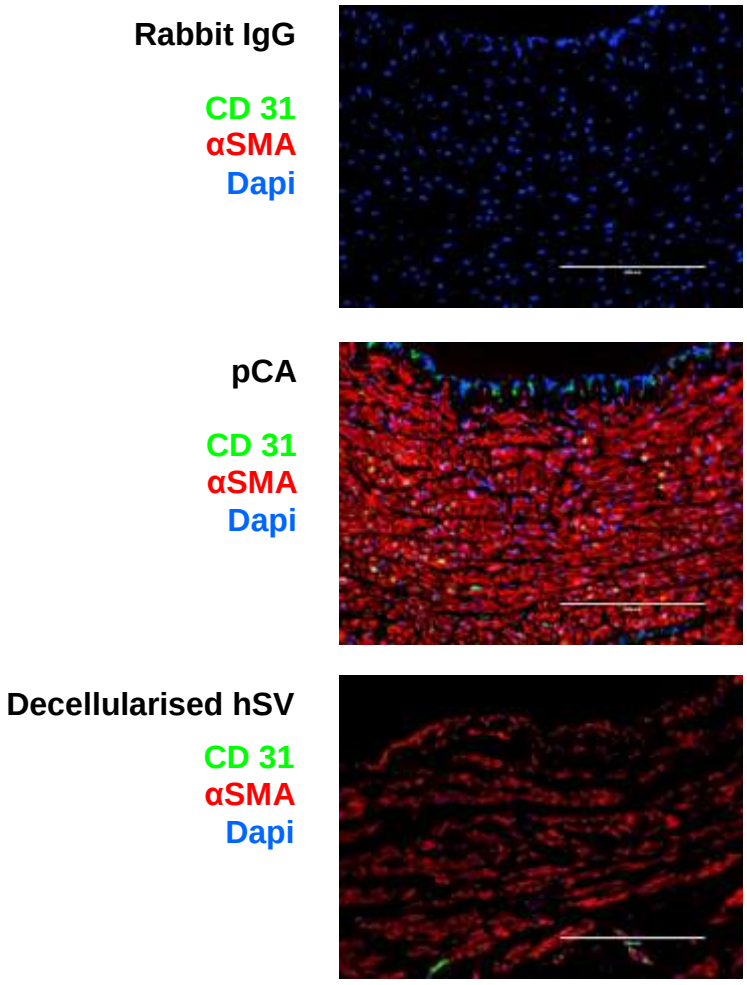

Figure 3.18 Immunostaining for cell type markers: CD31 and αSMA. (A) Control tissue; pre-implant pCA and 0.01% (w/v) SDS decellularised hSV stained with EC and SMC marker; CD31 and αSMA respectively with rabbit IgG as antibody negative control. **(B)** Representative images of dual immunostaining on 3-micron slices of xenograft explants stained with both CD31 and αSMA to identify cells in the explants. All tissues were nuclear stained with DAPI (blue), αSMA (red) and CD31 (green) at 200X magnification. White arrow shows neovascularisation and green arrow head shows CD31 positive cells on the lumen. Dotted lines indicate lumen surface. Scale bar represent 200 µm.

(B)

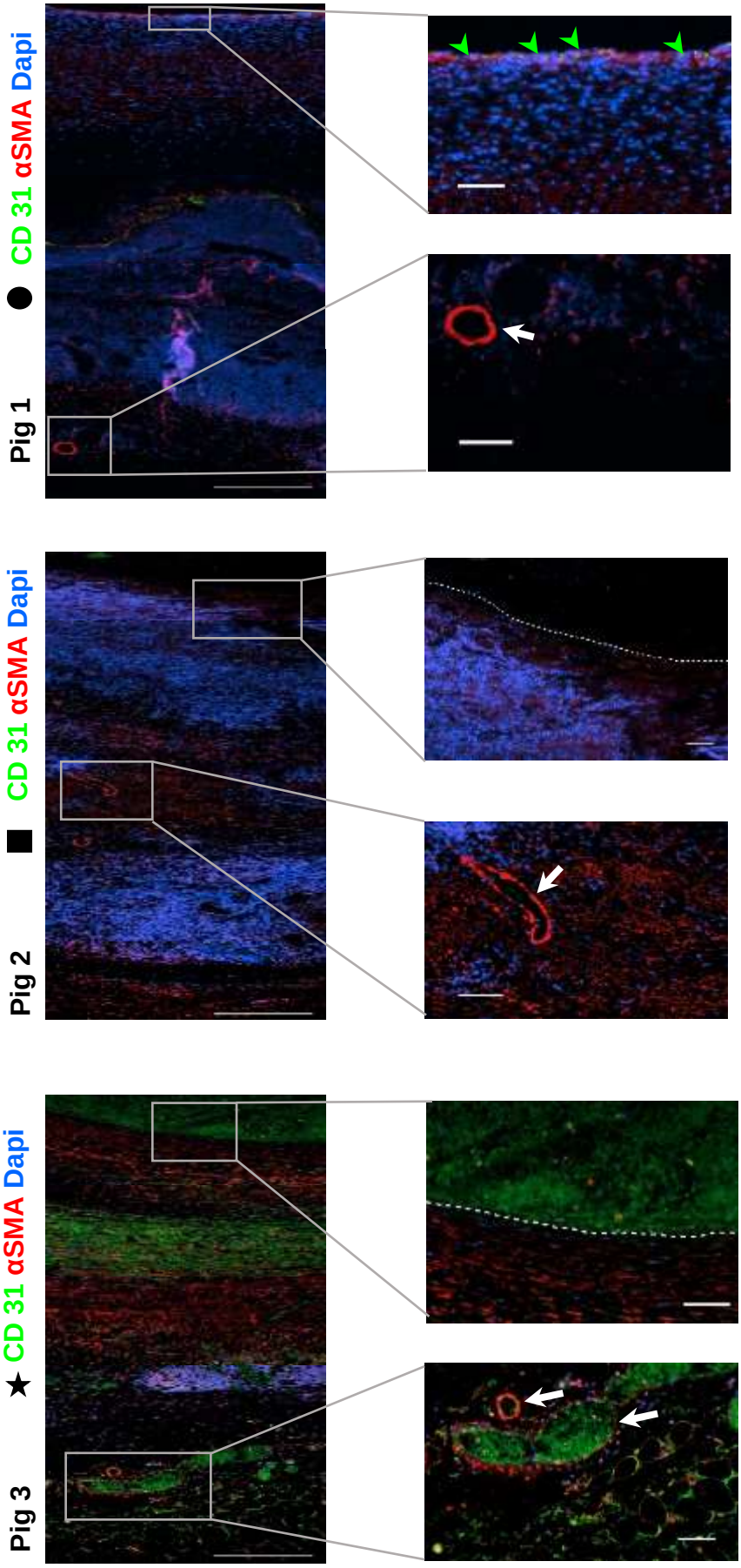

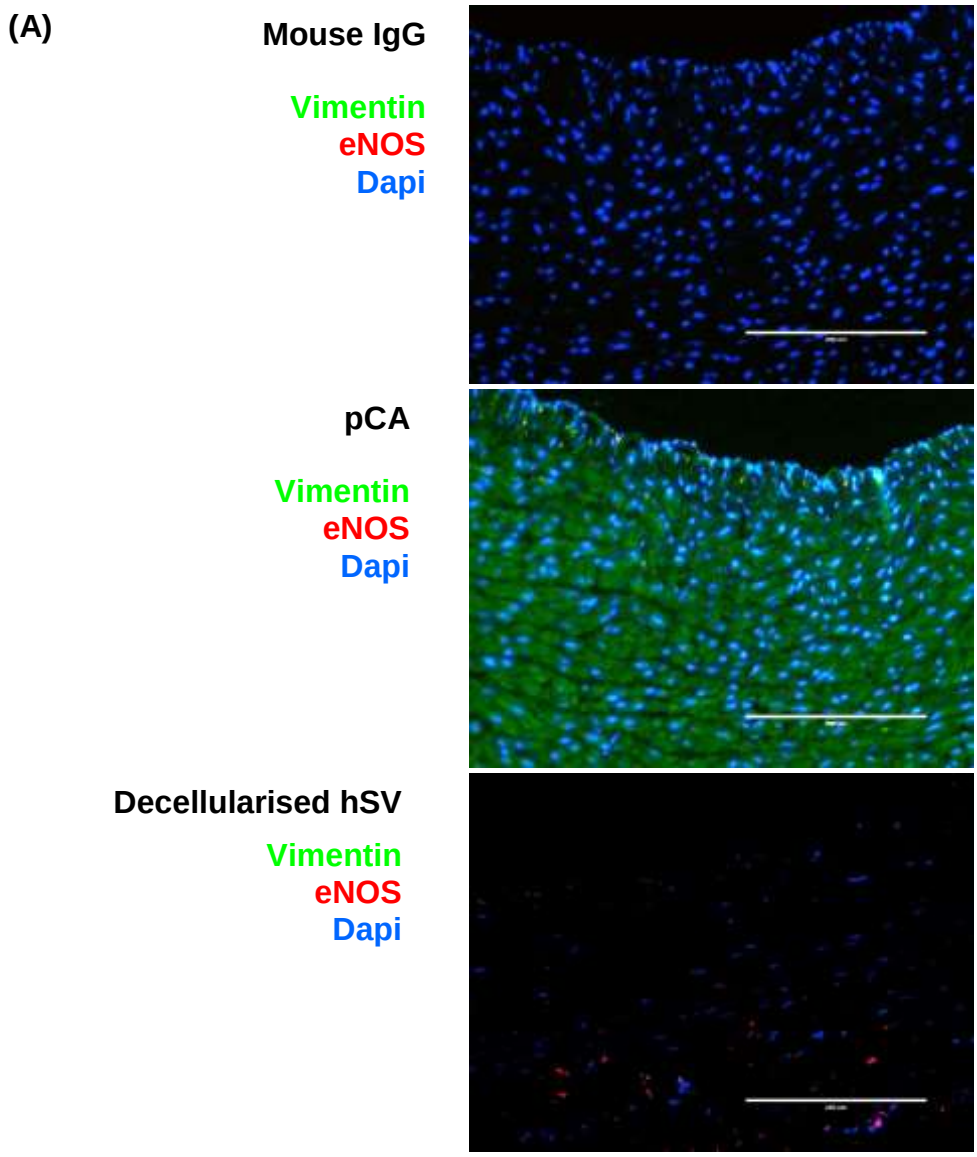

Figure 3.19 Immunostaining for cell type markers: vimentin and eNOS. (A) Control tissue; pre-implant pCA and 0.01% (w/v) SDS decellularised hSV stained with EC and fibroblast marker; eNOS and Vimentin respectively with mouse IgG as antibody negative control. **(B)** Representative images of dual immunostaining on 3-micron slices of xenograft explants stained with both eNOS and Vimentin to identify cells in the explants. All tissues were nuclear stained with DAPI (blue), eNOS (red) and Vimentin (green) at 200X magnification. Dotted lines indicate lumen surface. Scale bar represent 200 µm.

(B)

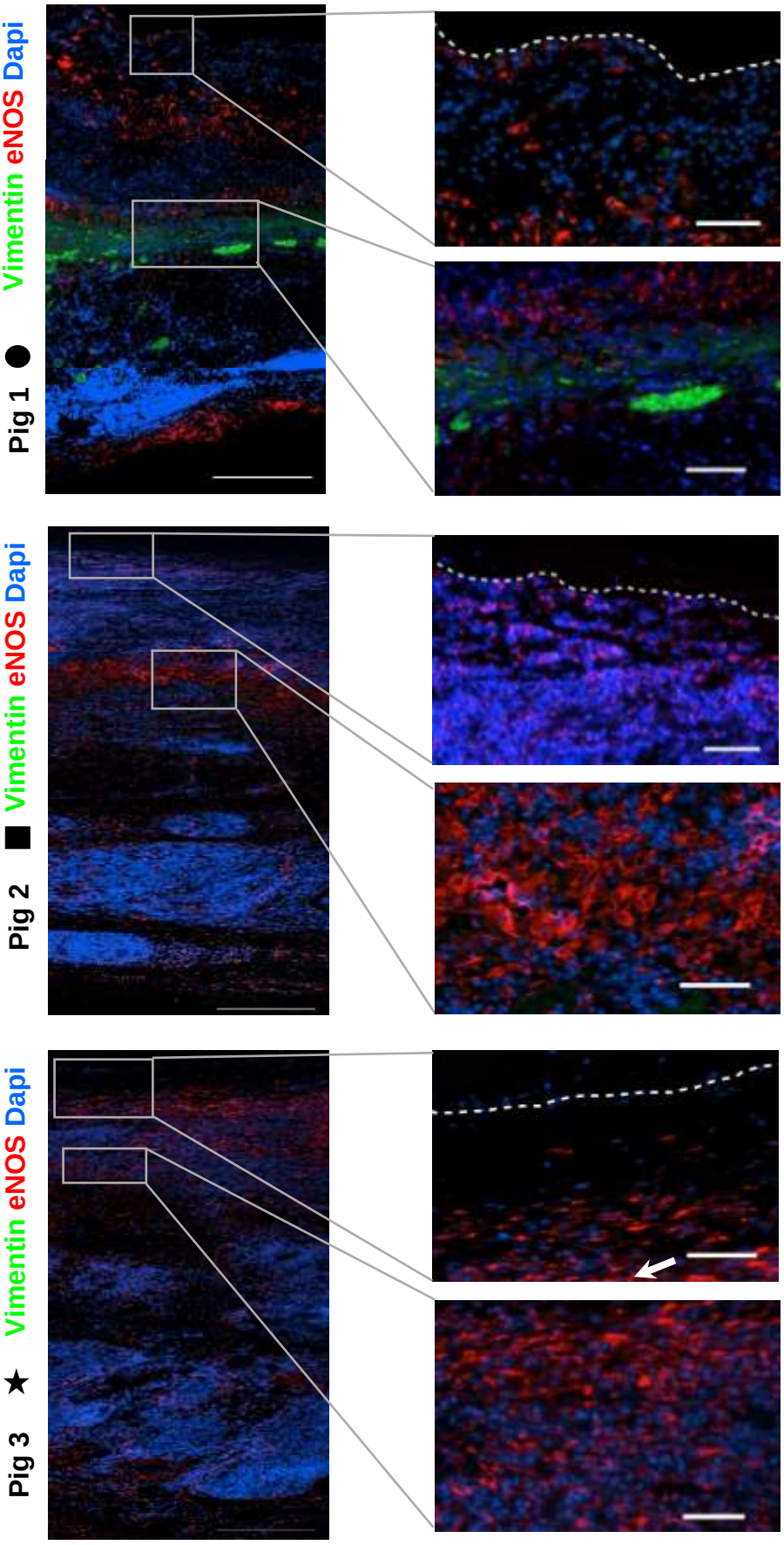
Vimentin eNOS Dapi
Pig 1 ●
Vimentin eNOS Dapi
Pig 2 ■
Vimentin eNOS Dapi
Pig 3 ★

(A)

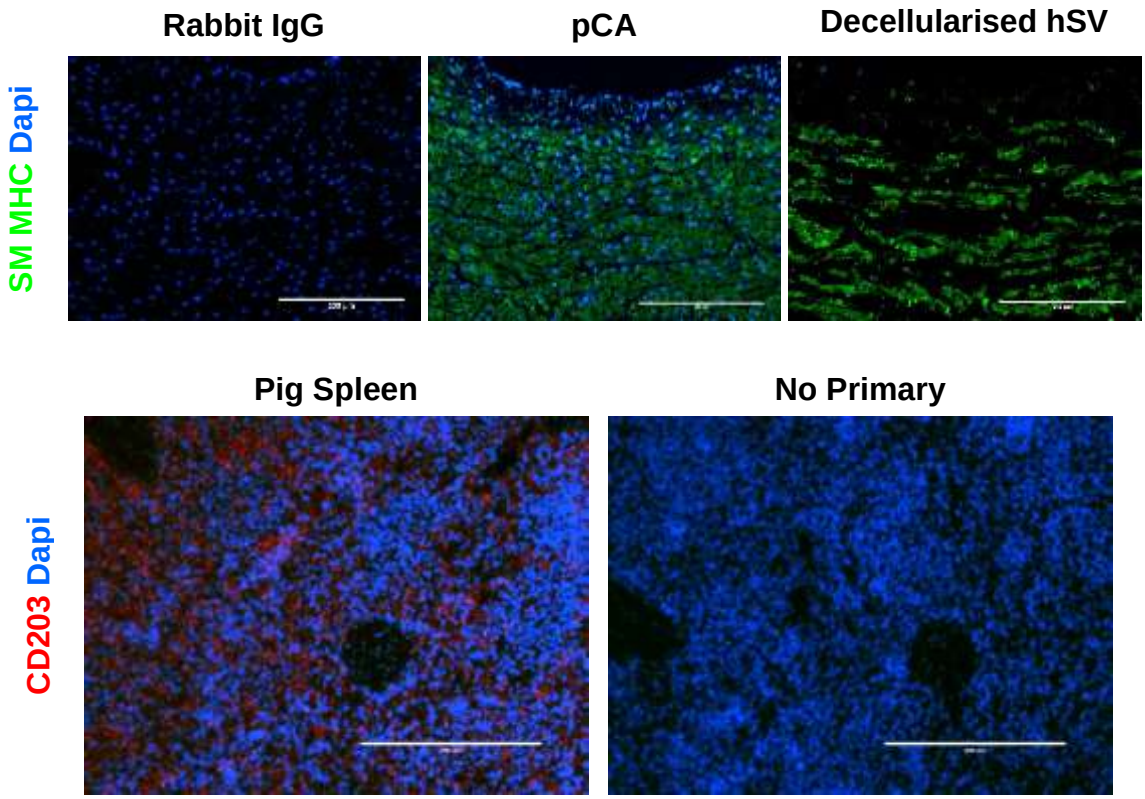

Figure 3.20 Immunostaining for cell type markers. (A) Control tissue; porcine spleen, pre-implant pCA and 0.01% (w/v) SDS decellularised hSV stained with macrophage/monocyte and SMC marker; CD203 and SM MHC respectively with no primary antibody as negative control. **(B)** Representative images of dual immunostaining on 3-micron slices of xenograft explants stained with both CD203 and SM MHC to identify cells in the explants. All tissues were nuclear stained with DAPI (blue), CD203 (red) and SM MHC (green) at 200X magnification. White arrow shows neovascularisation and red arrow head shows CD203 positive cells in neovessels. Dotted lines indicate lumen surface. Scale bar represent 300 µm.

(B)

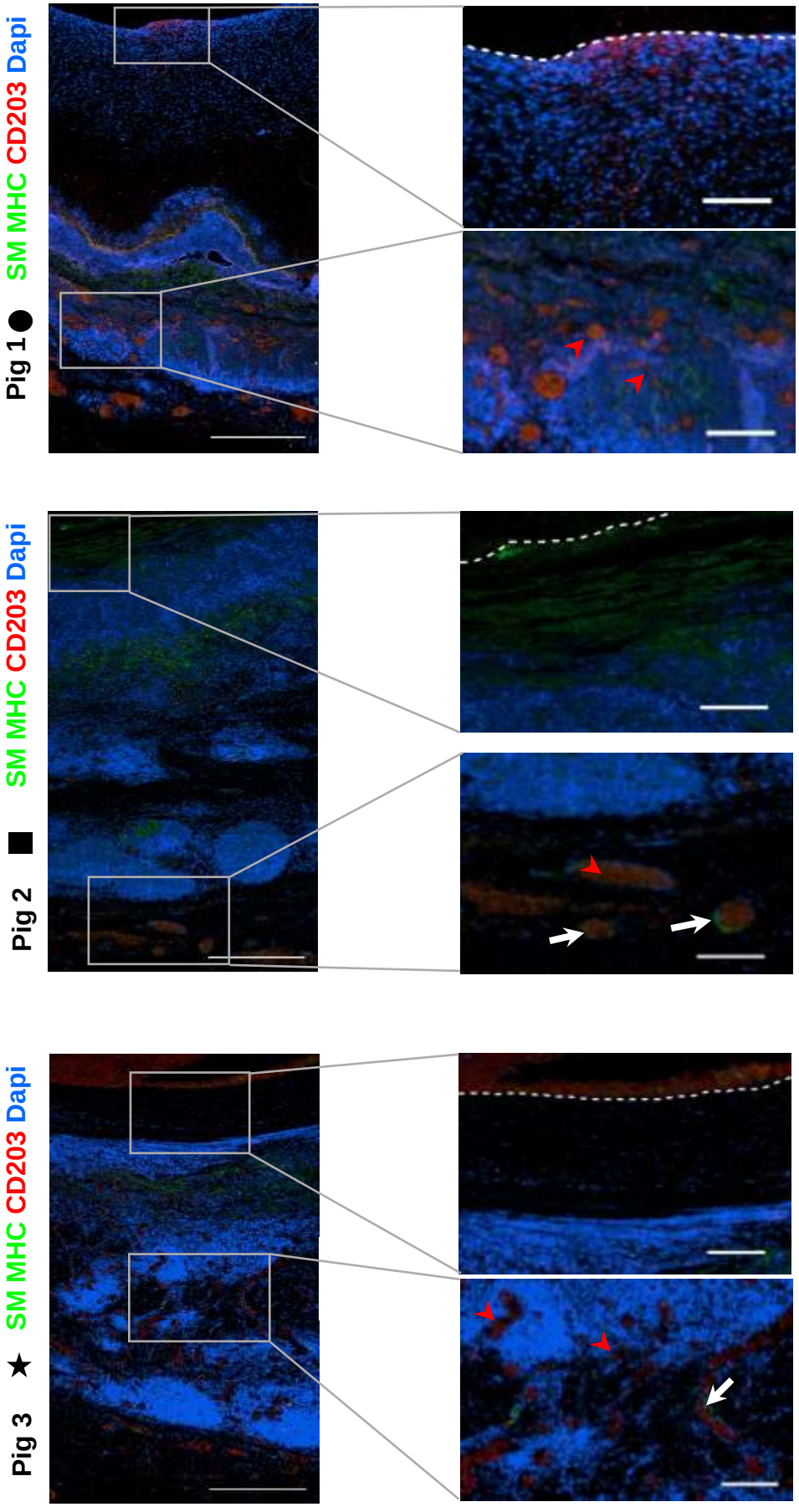
Pig 1 ●
SM MHC CD203 Dapi
Pig 2 ■
SM MHC CD203 Dapi
Pig 3 ★
SM MHC CD203 Dapi

3.3 Discussion

Grafting of autologous saphenous veins (SV) onto blocked coronary arteries has been widely utilised since its inception in 1962 by Sabiston *et al.* (Kakos et al. 1972; Endo 2000). Saphenous veins (SVs) are a common conduit for CABG in patients with coronary atherosclerosis and for peripheral vascular grafting in patients with ischemic limbs. Unfortunately, following CABG the patency rate of SVs is reported be only about 50% at 10 years after implantation, as compared to 95% of internal mammary artery (IMA) (de Vries et al. 2016; Taggart 2013). The patency rate of SV grafts used for peripheral vascular disease is even lower, with the rate of occlusion being >50% at 2 to 4 years post-surgery.

This project was undertaken to test the hypothesis that decellularised hSV is a suitable scaffold for arterial grafting. The properties of the venous graft are not ideal for arterial blood flow dynamics and this likely contributes to early vein graft thrombosis (15-20% at 1 year) and later on to reduced SV patency as a result of late vein graft failure. Hence, decellularisation of SV was undertaken (with future arterialisation in mind) using a simple protocol that combine both chemical (SDS) and mechanical (agitation) method. The effects of this protocol on the SV cellularisation and composition were analysed, along with its patency following arterial grafting in a porcine model.

The optimal SDS concentration used in the decellularising protocol was established using segments of human SV left over from CABG surgery. These segments were taken to the laboratory where they were decellularised using different concentrations of SDS. Almost 65% of decellularisation was achieved with 0.01% (w/v) SDS. This

was considerably higher than previously reported by Schaner *et al.* who reported that 0.01% SDS achieved only 32% decellularisation with hSV (Schaner et al. 2004).

The effectiveness of the decellularisation protocol was further analysed by quantifying the dsDNA content in decellularised hSV as compared to native hSV. This results of the PicoGreen assay demonstrated that the amount of dsDNA was not reduced by SDS treatment. However, agarose gel electrophoresis showed that the majority of the high molecular weight DNA was lost by treatment with 0.01% (w/v) SDS. Presumably the dsDNA was fragmented by the SDS and remained in the vein as small fragments of <50 bp. Others have reported that almost 90% of DNA was eliminated using SDS to decellularise porcine myocardium, porcine heart valve, porcine small intestine submucosa and porcine and human lung (O'Neill et al. 2013; Zhou et al. 2010; Syed et al. 2014). However, these studies used higher concentrations of SDS ranging from 0.1 to 1 % (w/v) SDS. To demonstrate that all venous cells were killed by the SDS treatment and illustrate that the residual dsDNA was not contained within viable human venous cells, cell proliferation was examined. Organ cultures of native and decellularised hSV were performed. These confirmed that proliferation did not occur in the decellularised hSV. Thus confirmed that the protocol used produced a hSV scaffold without viable cells despite remnants of DNA which is predominantly low molecular weight.

In terms of ECM integrity following decellularisation, Schaner *et al.* showed that treatment with 0.075% (w/v) SDS did not significantly affect the amount of collagen in decellularised hSV, but elastin content was significantly decreased (Schaner et al.

2004). In this previous study, the ECM content was quantified in sections stained by EVG and the percentage area occupied by both collagen and elastin calculated. This approach gave a significantly lower collagen content as the collagen area overlapping elastin were excluded thus underestimating the collagen content as reported by Masugi *et. al* (Masugi et al. 2018). In this chapter, collagen and elastin content in decellularised hSV was quantified via PSR and EVG, respectively. This showed similar results to those reported by Schaner and colleagues in terms of collagen despite using a different approach. However, the findings presented in this chapter clearly demonstrate that the content of elastin was not affected by any of the SDS concentrations tested (0.01-0.1% w/v SDS), hence confirming better preservation of hSV ECM integrity compared to the previously published study.

The discrepancies in terms of decellularisation effectiveness and protein quantification between the findings in this chapter and the published data from Schaner and co-workers may be due to differences in the decellularisation protocol used. Decellularisation was performed using 0.075% (w/v) SDS in a shaking water bath at 37°C for 15 hours by Schaner *et al*., while in this study decellularising was performed using 0.01% (w/v) SDS at room temperature (~27°C) for 24 hours in SDS on a roller followed by two PBS washes. The lower concentration of SDS and the less extreme treatment of the vein may be responsible for the observed results of improved preservation of ECM integrity in terms of protein content. Additionally, GAGs content was also analysed via AB staining. No significant effects on GAG content was detected as a result of decellularisation protocol compared to the native vein.

In addition to the histological staining analysis, assays for specific ECM proteins were undertaken. The aim was to confirm our findings with multiple approaches since in published articles various groups uses different types of assays and quantification (de Castro Bras et al. 2013; Crapo, Gilbert, and Badylak 2011; Gilpin and Yang 2017; Guyette et al. 2014; Lin et al. 2018). Moreover, using these differing approaches the findings varied and with some contradicting others as reviewed by Bruyneel and Carr (Bruyneel and Carr 2017). The collagen assay using larger tissue segments revealed that collagen content was significantly decreased with 0.05, 0.075 and 0.1% (w/v) SDS, whereas elastin and GAGs content were not affected. Specific protein assays were considered to give a more accurate estimation of the ECM proteins after decellularisation as compared to using simple staining methods. The simple staining methods provide a snap-shot of single 5 µm tissue slices whereas for the specific assays, ~100 µm slices were used hence lowering potential measurement error.

Moving on to mechanical properties of a vascular graft, two most important criteria are the burst strength and circumferential compliance. These test is an important indicator of a graft suitability before proceeding with *ex vivo* (bioreactor) or *in vivo* model. Normal arterial blood pressure at systolic are between 90-140 mmHg and at diastolic at 60-90 mmHg. This test is done at a lower pressure of 110 mmHg the highest pressure of 150 mmHg where the internal radius at the specified pressure. Literature search shows that the compliance of saphenous veins is higher than that of internal mammary artery (IMA). Therefore, the low percentage of compliance recorded by decellularised veins could be negligible as long as it is near to the compliance of IMAs.

Table 3.3 Mechanical properties of internal mammary artery graft and saphenous vein graft used in CABG as compared to decellularised veins.

Mechanical Properties	*IMA	*SV	Decellularised SV
Burst pressure (kPa)	410	285	436
Compliance (%/100 mmHg)	11.5	25.6	8.23

*IMA and SV data obtained from (Pashneh-Tala, MacNeil, and Claeyssens 2015).

The mechanical testing results was compared to a review data paper by Pasneh-Tala et al. (**Table 3.1**), shows that the results obtained are closer to that of an IMA burst strength and compliance. Therefore, proves that the decellularised veins mechanical properties are suitable to be used as a graft *ex vivo* and *in vivo*.

Given the toxicity of SDS, it was important to determine the efficiency of removal of SDS from the hSV scaffold following the decellularisation protocol. The SDS content in the effluents after each PBS wash and in the tissue at the end of decellularisation protocol was quantified, as previously described (Zvarova et al. 2016; Mathapati et al. 2010). The first PBS wash was deemed to be efficient in removing the SDS as the second wash did not eliminate any additional amount of SDS from the tissue. The amount of SDS detected in the tissue after the washing steps was very low (0.002%). The biocompatibility of the decellularised hSV scaffold was directly examined by seeding different cell types (ADSCs, hUVECs and hSV SMCs) on to the scaffold and their viability in terms of proliferative capacity was assessed. It was observed that adherent cells were detected with all three cell types at 24 hours and importantly viable cells were still detected 72 hours after seeding. The cell type with the lowest number of adhered cells 24 hours after seeding was ADSCs. Interestingly, only with hSV SMCs

there was a significant increase in cell numbers detected between 24 and 72 hours. This highlights the suitability of these scaffolds for the adherence of various cell types and also illustrates that these scaffolds facilitate proliferation of hSV SMCs. As vascular ECs are a unique type of cells that are highly sensitive to contact inhibition. Therefore, the reseeding outcome was expected as hUVEC will exit cell cycle and do not grow and proliferate once they come into contact with each other and fully covered the surface area in a monolayer (Suzuki et al. 2000; Olyslaegers et al. 2013; Lampugnani and Dejana 1997; D'Amore 1992).

The results to this point demonstrate that treatment with 0.01% (w/v) SDS yields a hSV scaffold that is devoid of viable cells and in which DNA is fragmented but without a significant impact on ECM integrity. Therefore, it was considered appropriate to test the feasibility of the decellularised vein as a xenograft in a porcine arterial grafting model. This was achieved through bilateral (arterial and venous) implantation of decellularised hSV from two different individual into three different pigs. All implants showed no lumen mismatched between native pCA and decellularised hSV, with excellent surgical feasibility and suturability, and without rupture or anastomotic pseudo-aneurysm.

The first arterial implant was patent at four weeks, however, there was expansion/dilation of the graft to almost twice the original lumen size, resembling an aneurysm formation. Vein to artery allograft implantation has been previously reported in a canine model. It was demonstrated that graft patency was 100% after two weeks with no graft dilation, rupture or anastomotic false aneurysm (Schaner et al. 2004).

After the first implant showed a patent but dilated graft, the next two implants were performed with decellularised hSV from the same individual grafted into two different animals. After four weeks both implants were occluded. The evaluation of structural differences between decellularised hSV and pCA pre- and post-implantation showed no apparent differences in terms of collagen, elastin and GAGs content. However, this preliminary result need future validation due to the low number of implants performed in this study.

The cells repopulating the grafts were also analysed by staining for specific EC and SMC proteins that cross react with both human and pig tissue. All of the decellularised grafts showed considerable infiltration of host cells. Martin et. al, reported a very relevant study where they implanted autograft, allograft and decellularised vein in canine model and shows that better outcome of decellularised allograft than allograft. Their vein to artery allograft also shows no endothelialisation at eight weeks post implantation (Martin et al. 2005). The first implant was patent; endothelial cells were observed on the luminal surface when assessed with CD31 antibody although less apparent than DBA staining. CD31 and eNOS were detected in the wall of two latter occluded explant grafts and inside the neovessels lumen area similar to where CD203, a macrophage marker was observed. As both CD31 and eNOS markers also play a role in inflammatory mechanism the observation was not unusual as macrophages also express eNOS and CD31 (Woodfin, Voisin, and Nourshargh 2007; Privratsky, Newman, and Newman 2010; Cirino, Fiorucci, and Sessa 2003; Kim et al. 2009; Connelly et al. 2003). When the explant was stained with DBA, a distinct staining was observed on the luminal surface of the patent graft. This demonstrates regeneration of new endothelium from the host cells as DBA is a glycoprotein exclusively used for

the identification of endothelial cells of porcine origin (Darr et al. 1990; Zhang, Smith, and Charnock-Jones 2002; Scruggs et al. 2015; Loesch et al. 1997). DBA also identified the presence of angiogenesis in all explanted grafts. The role of this glycoprotein is perceived crucial in the expression of adhesion molecules on endothelial cells as discussed by Scott and Patel (Scott and Patel 2013).

αSMA and SM MHC proteins were more abundant in the second and third implant and less obvious in the first graft which was patent. It is important to note that these SMC markers detected cell remnants within the decellularised hSV prior to implantation so it is possible that some of the protein detected in the graft at four weeks may be of human origin rather than due to re-population of the scaffold. It is possible that the human cell remnants may promote cell infiltration via immune response and encourage re-population (Sanders et al. 2017). ECM from biological materials that are used in tissue engineering have been reported to cause an innate and acquired immune response by the host (Allman et al. 2002; Allman et al. 2001; Keane et al. 2012; Daly et al. 2012). The overall mechanism of the host response to any implanted biological materials includes but is not just limited to T-lymphocytes and macrophages (Badylak and Gilbert 2008). The balance between inflammation due to immune response and tissue remodelling need to be achieved in order to ensure a successful in vivo xenograft implantation.

The last two explants were occluded and showed thrombus formation which resulted in total occlusion of the xenograft. Therefore, our use of anti-thrombotic agent post-surgery was reviewed. All the animals received 75 mg aspirin pre and post-operative

procedures with food, which is the recommended human dose by the American College of Cardiology/American Heart Association (ACC/AHA) (Pearson et al. 2002). This is due to the cardio protective benefit of aspirin to inhibit COX-1 enzymes. which promotes platelet aggregation and vasoconstriction through the inhibition of prostaglandins and thromboxane A_2 (Goldman et al. 1988; Schror 1997; Warner, Nylander, and Whatling 2011). However, pigs have a higher metabolic rate compared to humans, hence a higher dose of aspirin may be necessary to achieve a clinically meaningful platelet inhibition. As such, it was concluded that for future preclinical implants a higher dose of aspirin should be utilised.

3.4 Conclusion

To summarise, this chapter presents results of decellularisation optimisation showing that with as low as 0.01% (w/v) SDS it is possible to decellularised up to 65% of hSV without any remaining viable cells or any effect on the ECM proteins. However, it was noted that although DNA was fragmented the DNA content was not significantly reduced and SMC proteins remained in the scaffold. Importantly, the resultant decellularised hSV contained only low levels of SDS and was biocompatible with different cell types. In addition, one out of three hSV scaffolds implanted as a xenograft in an arterial porcine drafting model *in vivo* was patent at four weeks and was positive for a marker of luminal endothelial coverage. Unfortunately, two arterial implants were occluded at the same time point, suggesting a refinement of methods as well as anti-platelet drug regimen may be needed. While these results are interesting and confirm the feasibility of this approach, they also suggest the need for further refinements some of which will be explored in the next chapter.

4 SEEDING OF HSV SCAFFOLDS WITH CELLS FROM PORCINE CAROTID ARTERY AND PERIPHERAL WHOLE BLOOD (PWB)

4.1 Introduction

The implantation experiments described in the previous chapter revealed that the decellularised hSV was not suitable as a conduit. Consequently, it was considered whether seeding with appropriate cell types would result in improved grafting outcomes. Suitable possible cell sources from the literature were considered. There are a number of different options such as stem cells from either embryonic, mesenchymal or hematopoietic origin and induced pluripotent stem cells (iPCs) (Adamo and Garcia-Cardena 2012; Akashi 2002; Comenzo and Berkman 1995). Moreover, it was recognised that autologous cell sources may be considered more favourable to alleviate future transplantation complications (Mirensky et al. 2010; Pashneh-Tala, MacNeil, and Claeyssens 2015; La and Tranquillo 2018; Ong et al. 2017). Therefore, initially internal thoracic/mammary artery (hIMA) were salvaged from CABG surgery with the aim of isolating SMCs and ECs. Subsequently, SMCs and ECs were isolated from pCA. The aim was to determine the feasibility of seeding differentiated SMCs and ECs on to the hSV scaffold. Unfortunately, due to the limited tissue availability of surplus hIMA and the difficulty in culturing and expanding ECs *in vitro,* insufficient hIMA ECs were propagated, despite successful culture of SMCs. Henceforward, pCAs were utilized to determine the feasibility of the use of arterial origin cells for seeding onto the scaffold.

Additionally, the use of peripheral whole blood (PWB) was assessed as a potential autologous cell source. Circulating endothelial progenitor cells (CEPC) and blood

outgrowth endothelial cells (BOEC) are among cell populations that are of interest (Ormiston et al. 2015; Martin-Ramirez et al. 2012; Asahara, Kawamoto, and Masuda 2011). CEPC and BOEC are both cells isolated from the peripheral blood that could be the same population of cell but due to lack of consistency in the scientific community the same population of cells has several other name. Therefore, a consensus in naming the cells are in need and as suggested by Medina *et. al.* to have a more consistent reporting of the type of cells and avoiding confusion (Medina et al. 2017; Hagensen, Vanhoutte, and Bentzon 2012; Asahara, Kawamoto, and Masuda 2011; Ormiston et al. 2015; Punshon et al. 2008).

Numerous reports on both cell type have described the ability of these cells to form colonies of mature endothelial cells *in vitro,* although having different proliferative capacity (Tagawa et al. 2015; Powell et al. 2005; Patel, Donovan, and Khosrotehrani 2016; Campioni et al. 2013). In this chapter PWB as a cell source for cell seeding of the scaffold was examined using a bioreactor as an *ex vivo* circulating model. Therefore, two of the tissue engineering components; cells and regulatory signals (specifically, mechanical stimulus) were applied to achieve re-cellularisation.

4.2 Results

4.2.1 Propagation of cells from Porcine Carotid Arteries

ECs and SMCs were extracted and isolated from pCA as described in chapter 2.

4.2.1.1 ECs and SMCs from pCA *in vitro*

Cultured ECs showed the characteristic morphology of ECs with the 'cobble-stone' appearance *in vitro* (**Figure 4.1 A**). Positive staining was observed with biotinylated Dolichos Biflorus Agglutinin (DBA) and detection of platelet endothelial cell adhesion molecule (PECAM), also known as cluster of differentiation (CD31), using immunocytochemistry (**Figure 4.1 B** and **C)**. pCA ECs also expressed vascular endothelial Cadherin (VE Cad), von Willebrand factor (vWF), and endothelial nitric oxide synthase (eNOS) proteins as shown in **Figure 4.1 D** and **E**.

SMCs isolated from pCAs exhibited the characteristic 'spindle-shape' morphology observed with SMC *in vitro* (**Figure 4.2 A**). pCA SMCs also expressed □-smooth muscle cells (αSMA), smooth muscle myosin heavy chain (SM MHC) and vimentin (**Figure 4.2 B – D**).

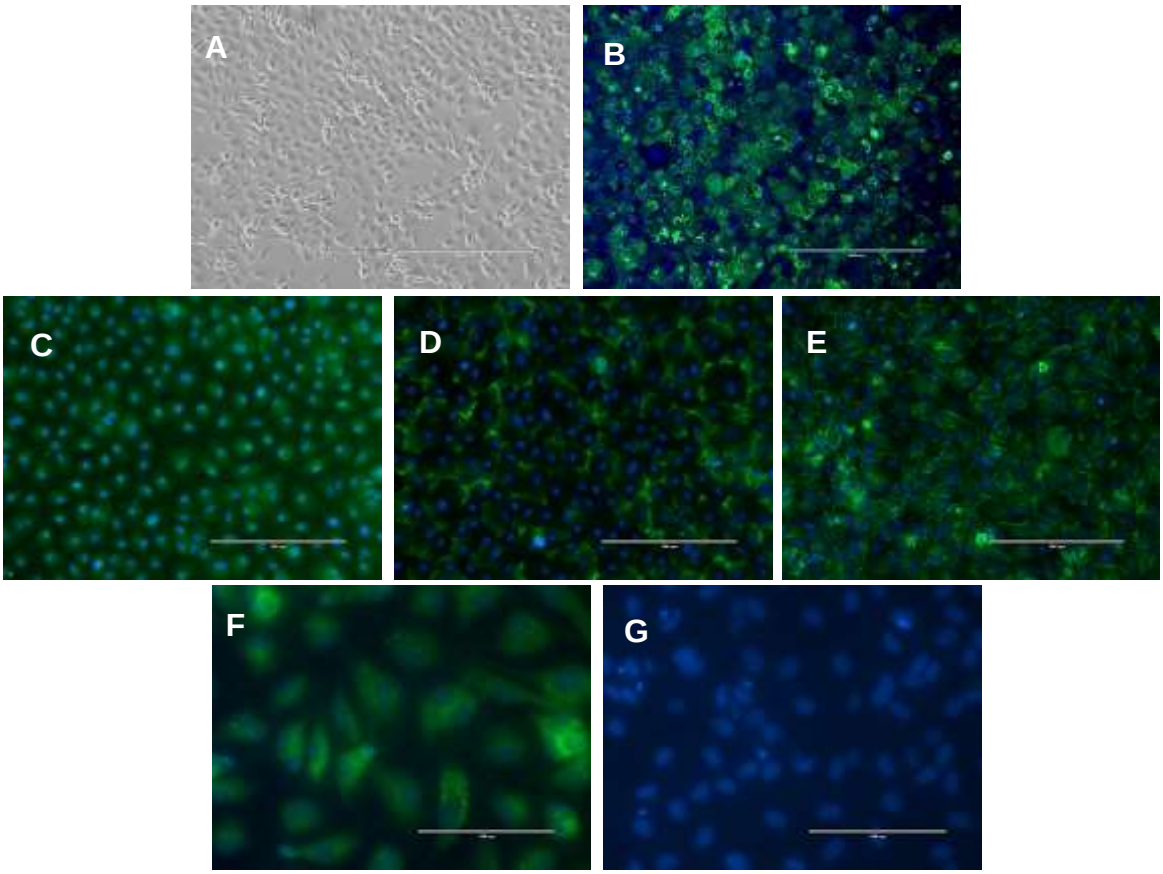

Figure 4.1 pCA EC morphology and characterisation. (A) ECs propagated from pCAs *in vitro*. **(B)** pCA ECs stained with the endothelial specific marker DBA. Immunofluorescence detection of endothelial specific proteins (green): CD31/PECAM **(C)**, VE Cad **(D)**, vWF **(E)** and eNOS **(F)** in pCA ECs. **(G)** IgG control. Nuclei are stained blue with DAPI in **(B)** – **(G).** Scale bars in **(A)** – **(E)** represent 300 µm. Scale bars in **(F)** and **(G)** represent 100 µm.

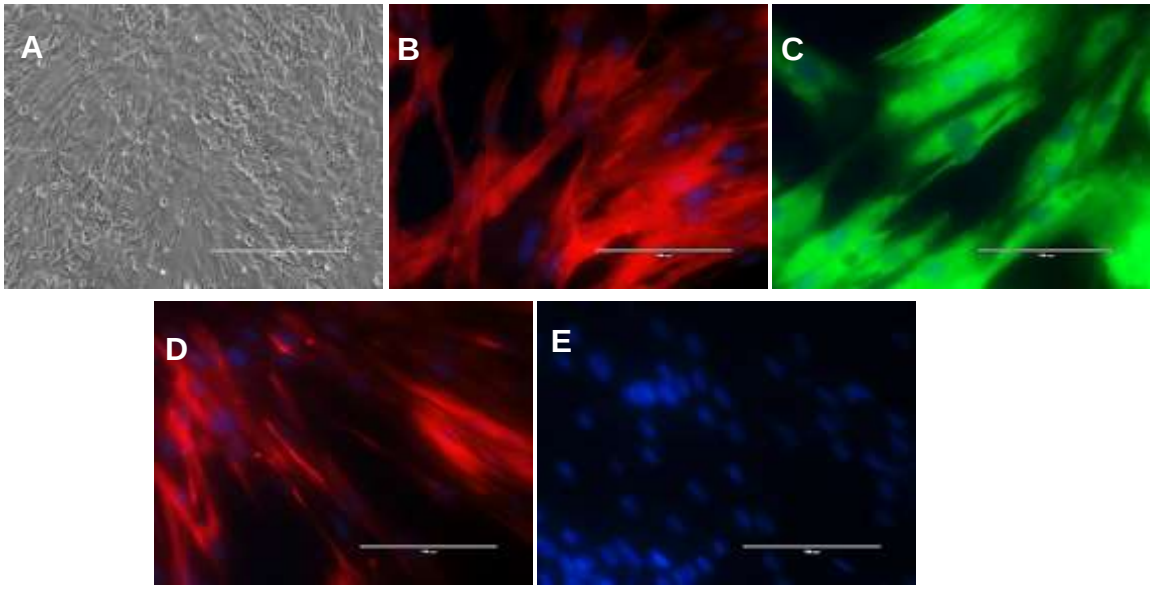

Figure 4.2 pCA SMC morphology and characterisation. (A) SMCs propagated from pCA. Scale bar represent 300µm. Immunofluorescence detection of smooth muscle specific proteins: αSMA - red **(B)** SM MHC – green, **(C)** and vimentin - red **(D). (E)** IgG control. Nuclei are stained blue with DAPI in **(B)** – **(E).** Scale bars in **(A) - (E)** represent 100 µm.

4.2.1.2 Effect of SDS on pCA EC and SMC viability and proliferation

SDS is known to be cytotoxic to cells and therefore, the AlamarBlue™ assay was used to assess the effect of four hours of exposure to SDS on pCA EC and SMC number. The AlamarBlue™ assay utilises the cell's ability to reduced resazurin to resofurin and therefore acts as an indicator of cell health and viability. The subsequent proliferation of both cell types was then quantified by measuring EdU incorporation after 24 hour exposure to SDS.

The cytotoxic threshold is set at 70% critical viability compared to the normal cell culture medium as suggested by ISO 10993:5 (Standard, I. Biological Evaluation of Medical Devices: Tests for *in vitro* cytotoxicity) (ISO 2009). pCA EC viability was not affected with SDS concentrations up to 0.0025% (w/v) (**Figure 4.3 A**). However, pCA EC proliferation was significantly impaired at ≥0.0025% (w/v) SDS (**Figure 4.3 B**). In contrast, with pCA SMCs, the viability was significantly affected at ≥0.01% (w/v) SDS whereas its proliferation was significantly affected 0.0025% SDS (w/v) (**Figure 4.4**).

(A)

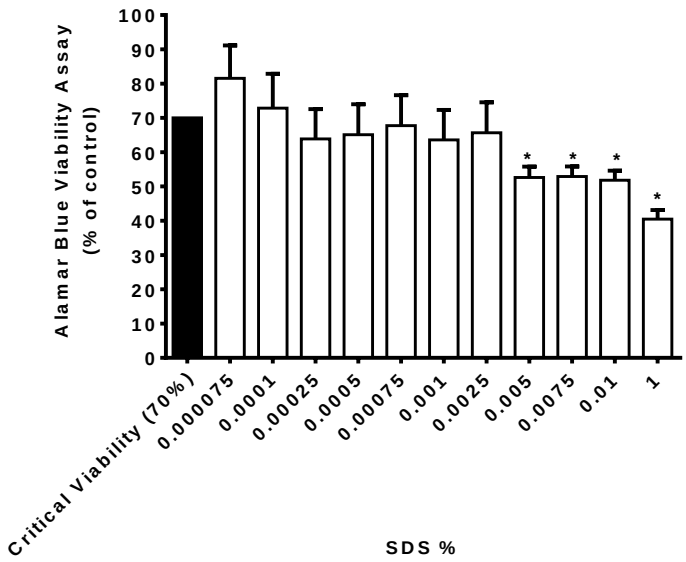

(B)

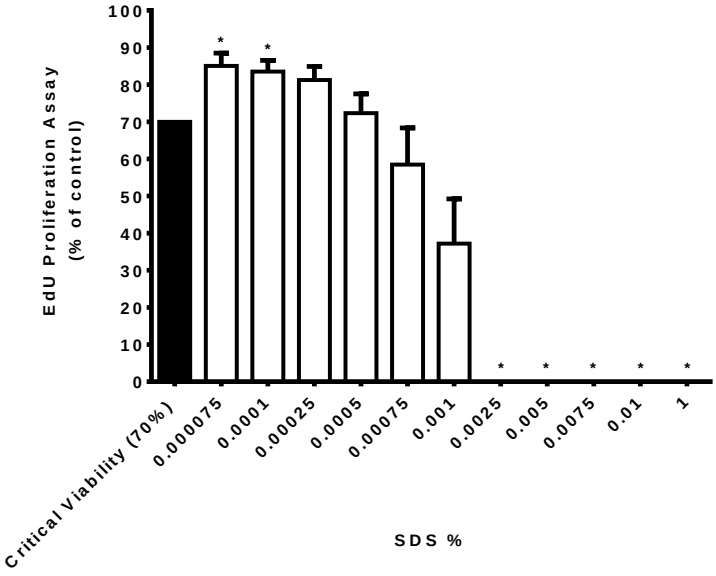

Figure 4.3 pCA EC viability and proliferation after exposure to SDS at different concentrations. (A) pCA EC viability when exposed to different concentration of SDS was assess using AlamarBlue™ after 4 hours exposure. Values are presented as mean ± SEM, 1-way ANOVA, Dunnett's multiple comparisons test, * indicates $p<0.01$, n=8. **(B)** Proliferation was quantified by counting positive nuclei labelled with EdU (pink) and total nuclei number (blue). Values are presented as mean ± SEM, 1-way ANOVA, Dunnett's multiple comparisons test, n=8.

(A)

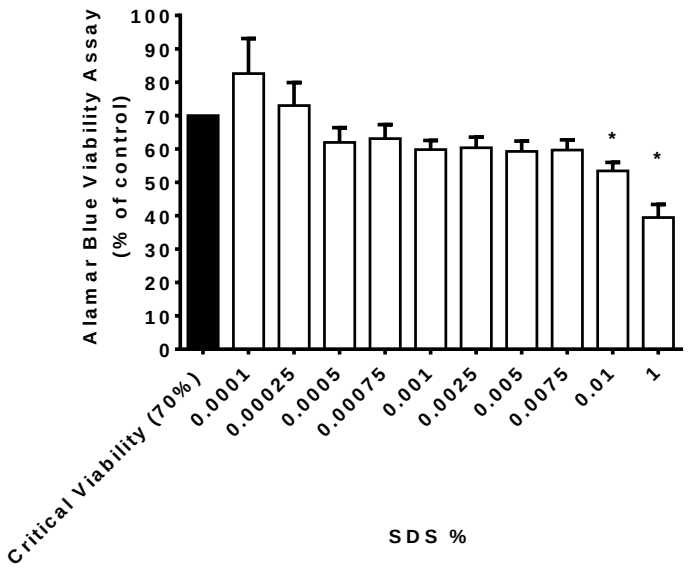

(B)

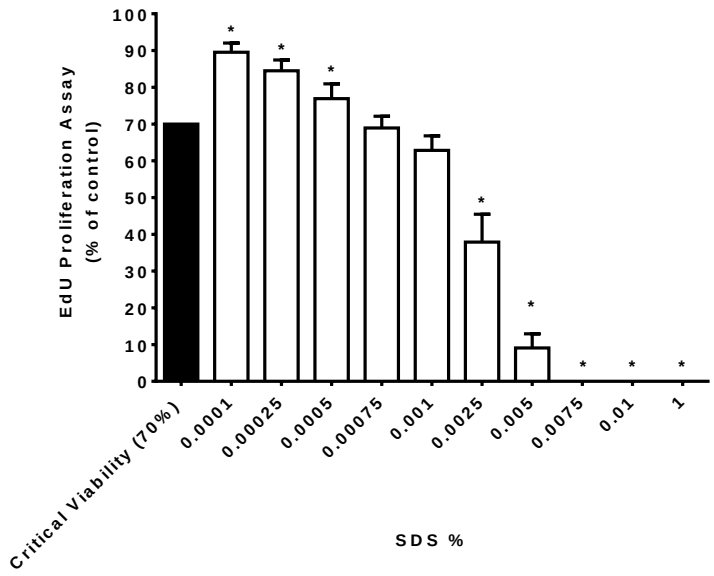

Figure 4.4 pCA SMC viability and proliferation after exposure to SDS at different concentration. (A) pCA SMC viability when exposed to different concentration of SDS was assess using AlamarBlue™ after 4 hours exposure. Values are presented as mean ± SEM, 1-way ANOVA, Dunnett's multiple comparisons test, * indicates $p<0.01$, n=6. **(B)** Proliferation was quantified by counting positive nuclei labelled with EdU (pink) and total nuclei number (blue). Values are presented as mean ± SEM, 1-way ANOVA, Dunnett's multiple comparisons test, n=6.

4.2.2 Decellularised hSV recellularisation

4.2.2.1 PWB versus MNC cell seeding – roller set-up

Seeding of decellularised hSV was attempted with both PWB and MNC for 48 hours on a roller set-up as described in methods (**Section 2.17.1**). Nuclei were detected in both PWB and MNC seeded decellularised hSV (**Figure 4.5 C** and **D**) and quantification of this preliminary data suggests higher numbers of cells were detected with MNC however statistical analysis could not be performed as only two replicates were performed (**Table 4.1**).

Table 4.1 Re-cellularisation percentage calculated from H&E stained sections. Values are presented as mean ± SEM, n=2.

Seeding cell source	Mean ± SEM; n = 2
MNC	84.87 ± 0.3072
PWB	49.82 ± 30.28

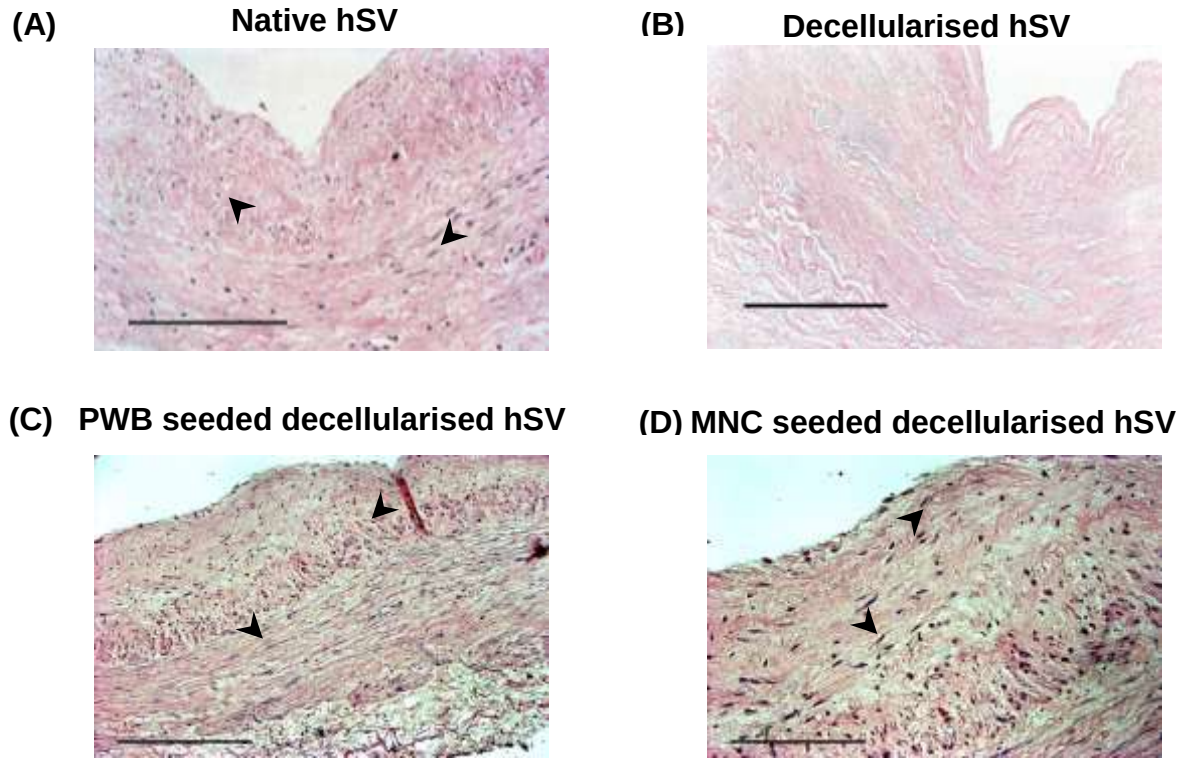

Figure 4.5 PWB versus MNC roller seeding of decellularised hSV. Representative image of **(A)** native hSV prior to the decellularisation protocol and **(B)** 0.01% (w/v) SDS decellularised hSV subjected to roller decellularisation protocol. Decellularised hSV after incubation with PWB **(C)** and MNC **(D)** at 200X magnification. Scale bar represent 200 µm. Arrows indicate some of the detected nuclei (purple-black).

4.2.2.2 PWB cell seeding – flow set-up

The first experiment with the bioreactor system was set with a flow rate similar to resting coronary blood flow of 200 mL/minute (Boron and Boulpaep 2008; Ramanathan and Skinner 2005). Unfortunately, after 24 hours, it was observed that the blood flowing through the system was a dark red colour that suggested that the blood had become deoxygenated. In addition, leakage was detected and the chamber holding the veins was filled with blood (**Figure 4.6**). Nonetheless, the vein was taken

out and analysed. Histological analysis revealed that clotted blood was present in the centre of the graft (**Figure 4.6 A** and **B iii**). It was noted that the lumen area was slightly enlarged after perfusion for 24 hours in the bioreactor. The graft wall appeared denser from H&E staining and the wall was thinner after the perfusion in the bioreactor.

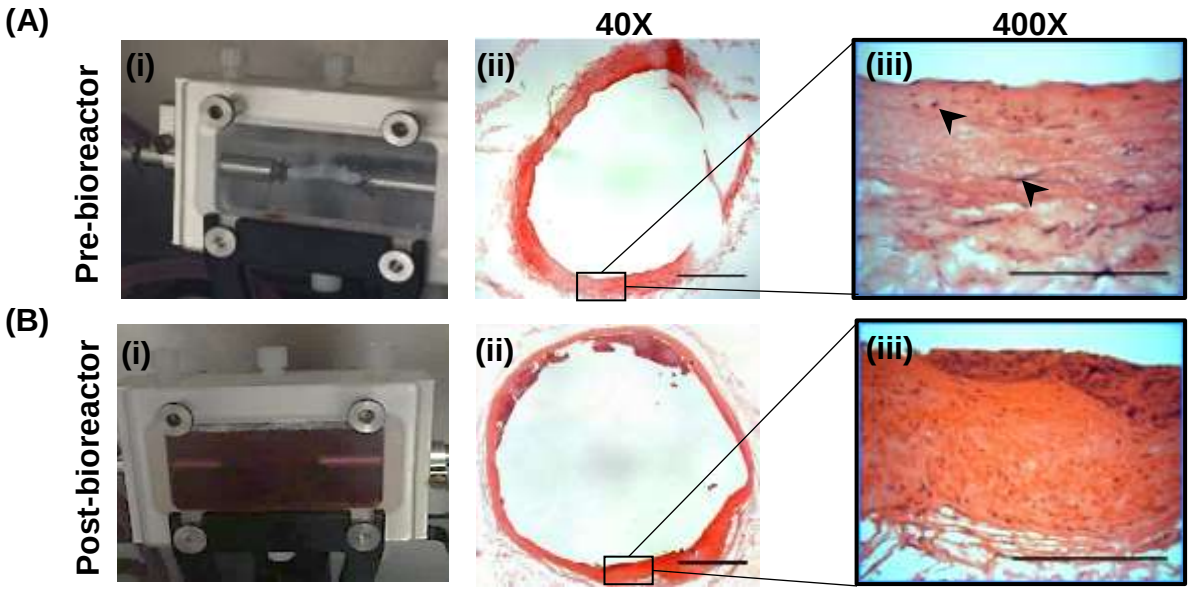

Figure 4.6 Perfusion of decellularised hSV with PWB at 200 mL/minute for 24 hours. 0.01% (w/v) SDS decellularised hSV subjected to roller decellularisation protocol**, (A)** Pre-bioreactor and **(B)** Post-bioreactor. **(i)** Bioreactor chamber pre- and post-perfusion at 200 mL/minute. H&E sections at **(ii)** 40X magnification and **(iii)** 200X magnification. Scale bar represent 200 and 20 µm for 40X and 400X magnification respectively. Arrows indicate some of the detected nuclei (purple-black).

Seeding of decellularised hSV was also attempted with PWB for 48 hours using the bioreactor set-up as described earlier (**Section 2.17.2**). After flowing PWB through decellularised hSV at 25 mL/minute, that the number of nuclei in the decellularised tissue was low and appeared less than prior to seeding, suggesting that the process

of flowing fluid through the scaffold removed donor cell debris. It was noticeable that the tissue ECM was more disrupted after 48 hours in the bioreactor than prior to flowing fluid through the scaffold (**Figure 4.6**).

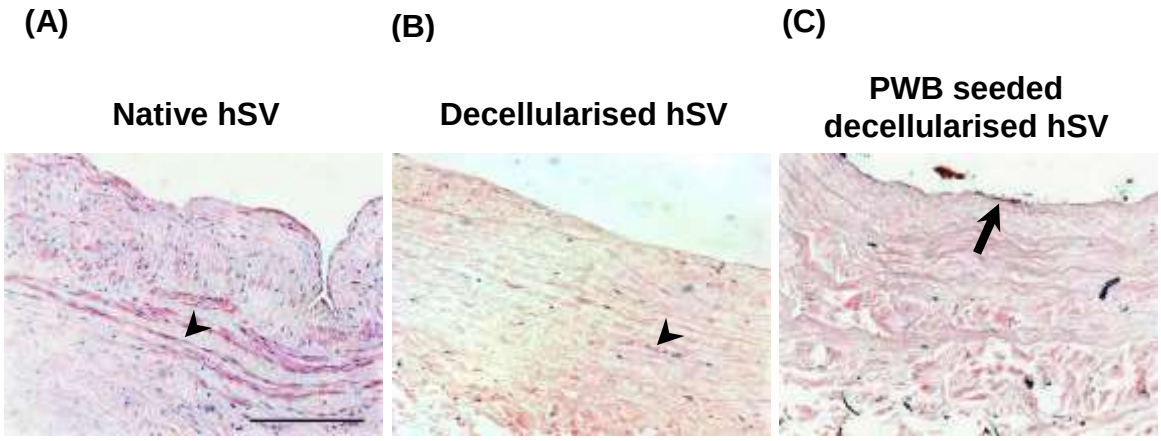

Figure 4.7 Perfusion of decellularised hSV with PWB at 25 mL/minute for 48 hours. H&E stained sections of **(A)** Native hSV prior to decellularisation protocol, **(B)** 0.01% (w/v) SDS decellularised hSV subjected to roller decellularisation protocol **(C)** 0.01% (w/v) SDS decellularised hSV after perfusion with PWB at 25 mL/minute in bioreactor at 200X magnification. Scale bar represent 200 µm and applies to all panels. Arrows indicate some of the detected nuclei (purple-black).

4.3 Discussion

The findings from the porcine arterial xenograft implantation reported in chapter 3 showed mixed results, where one out of three implants was patent and the other two were occluded. This strengthened the proposition that seeding of the decellularise scaffold with arterial cells would improve graft patency. Therefore, possible sources of arterial cells were investigated. Isolation of EC and SMC from small segments of surplus hIMA but with little success due to the limited amount of surplus tissue available. With the intention in implanting decellularise hSV in the porcine model, therefore the isolation and expansion of both pCA ECs and SMCs was attempted. All analysis was undertaken with primary *in vitro* cultured cells that are no more than passage 5 (P_5) and all cells still expressed their immunophenotypical and ultrastructural features and showed no obvious signs of de-differentiation.

Prior to seeding of cells onto the scaffolds which contain residual amounts of SDS (0.002% (w/v), see **3.2.4**) the effect of SDS on pCA EC and SMC viability and proliferation was crucial. SDS is an anionic detergent that acts on the cell membrane and is largely used in molecular research to extract cellular content (Woldringh and van Iterson 1972; Tukmachev et al. 1979). At high SDS concentrations SDS has the capability to denature proteins and is used for studying protein folding and conformation (Xu and Keiderling 2004; Parker and Song 1992; Sun et al. 2015). Even though, SDS is widely use to decellularised tissue and organs, limited reports determine the cytotoxicity of SDS on mammalian cells with the decellularisation protocol. Mathapati *et al.* reported the presence of residual SDS in tissue after a decellularisation protocol and suggested that with 0.1% (w/v) SDS this equates to 16 mg of SDS in 20 g of implanted saphenous vein which is less than 125 mg that would

be sufficient to cause toxic effect to the human system in general (Mathapati et al. 2010). However, the effect of the localised concentration of SDS in the scaffold on cell seeding capacity and proliferation has not been established. Therefore, Zvarova *et al.* analysed the level of cytotoxicity of SDS on several different representative human cell types commonly used in lung recellularisation and showed that the cytotoxicity threshold varied according to cell types. They reported that human pulmonary vascular endothelial cells has the lowest cytotoxicity threshold at 0.00012% SDS (w/v) (Zvarova et al. 2016). Consequently, determination of pCA EC and SMC (or any other future cells to be use in recellularisation of decellularised hSV) cytotoxicity threshold need to be established before moving forward with recellularisation.

As a result, both pCA ECs and SMCs cytotoxic threshold is shown to be at 0.0025% (w/v) SDS taking into account both viability and proliferation of cells. ECs are more susceptible to lower SDS concentration, but they would be in contact with SDS only on the basolateral cell surface as they are expected to repopulate the luminal surface of the vein. On the other hand, SMCs are anticipated to invade the tissue and repopulate the medial layer of the vein scaffold, hence it is likely that they will be exposed to more of the residual SDS that is trapped inside the scaffold after decellularisation protocol.

The susceptibility of cells towards any surfactant are not just based on the surfactant critical micelle concentration (CMC) but also on the cell membrane arrangement and polarisation (Inacio et al. 2011). As shown in previous chapter the level of SDS detected in the tissue after the decellularisation protocol were at 0.002% (w/v) SDS

(see **3.2.4)**, similar to level of cytotoxic threshold of both pCA EC and SMC. The data also shows that after 48 hours of exposure to 0.001% (w/v) SDS, about 30% of pCA EC were observed to be able to proliferate (**Figure 4.3B**). In a dynamic environment, EC would be exposed to shear stress which would change the alignment of EC in the direction of flow and this is achieved with the change of cell polarisation (Wojciak-Stothard and Ridley 2003). Therefore, it is important that EC needed to be first established *in vitro* before being exposed to a dynamic environment. This is done and presented in the next chapter as a proof of biocompatibility (**Figure 5.4**).

Other sources of cells for seeding were also explored. Since the discovery of stem cells in peripheral blood between 1960 to 1970s, the potential use of peripheral blood in diverse disease therapies has been considered (Tripura and Pande 2013; McCredie, Hersh, and Freireich 1971; Martin-Ramirez et al. 2012; Goodman and Hodgson 1962). In the context of tissue engineering and regenerative medicine research the potential use of peripheral blood derived cells to recellularise vein grafts especially decellularised xenograft or allograft with autologous PWB has been investigated (Rambol et al. 2018; Olausson et al. 2014; Punshon et al. 2008). PWB has been used in combination with a dynamic seeding both *in vivo* or *ex vivo* (Tripura and Pande 2013; Rambol et al. 2018; Olausson et al. 2012). Hence, the ability of PWB and PWB-derived cells to repopulate the decellularised hSV was considered.

Initially decellularised vein scaffolds were rolled in either PWB or MNC isolated from PWB (see Section 2.16). PWB consists of a whole range of blood cells including; red blood cells (RBC), white blood cells (WBC), and platelets. Whereas, MNC isolated

from PWB consists mainly of lymphocytes and monocytes. The use of PWB eliminated the initial step of MNC isolation but has the downfall of being a mixture of cell types some of which may not be useful for seeding of the scaffold and may interfere with the repopulation of decellularised hSV. The preliminary results showed that both conditions resulted in increased numbers of nuclei throughout the decellularised scaffold. More cells appeared to be present in the decellularised hSV seeded with MNC than those perfused with PWB. This may be due to the ratio of PWB to MNC used being 1:2 therefore more cells were present in the MNC preparation than in PWB. To be able to directly compare the recellularisation procedures, it would be advisable to dilute the PWB to achieve the same concentration of cells. Unfortunately, this was not done due to time limitation, thus more assays and analysis with optimisation in terms of time, temperature and rolling speed of the seeding protocol are required.

A dynamic seeding protocol was also examined using PWB for seeding the decellularised hSV in a bioreactor. In setting up the bioreactor system itself, a lot of hurdles were faced, e.g. part malfunctions, system failure, and deoxygenation of whole blood when it was perfused for 24 hours. In the first run of the bioreactor system with a flow of 200 mL/minutes was used that equates to a pressure of about 250 – 350 mmHg in the bioreactor system. The resultant tissue was observed to have an expanded lumen size and the scaffold wall appeared denser (compacted). Noting the high pressure of the bioreactor system that would induce high shear stress to the scaffold, perfusion of decellularised hSV at a lower flow rate was also attempted. Olausson *et al.* previously implemented a very low flow at 2 mL/minute of PWB for 48 hours (Olausson et al. 2014), but our system could not generate a flow rate as low as

2 mL/minute, hence we adapted the flow to the lowest the system could manage at 25 mL/minute.

The bioreactor system ran for 48 hours with laminar flow at 25 mL/minute at 39°C. Filters were introduced on the chambers to allow gas exchange and the blood was changed after 24 hours to minimise the likelihood of deoxygenation that was previously observed. The histological analysis showed that perfusion of the PWB through the decellularised vein scaffold did not enable large numbers of PWB cells to enter the scaffold however it did appear to remove some of the donor cell nuclei and debris. This may be due to a range of reasons, such as fluid drags and the effect of gravity within the system as higher flow rates could impart shear stress to the scaffold but lower flow rates may cause sedimentation of PWB cells in the system before reaching the scaffold (Marin et al. 2017).

4.4 Conclusion

In summary, a number of cell sources were considered for their suitability to seed decellularised hSV scaffolds. The use of ECs and SMCs from pCA were the most feasible cell source to prove the concept of recellularisation with arterial cells on decellularised hSV in porcine arterial xenografting. However, utilisation of PWB and its derivative cells are seen to be more feasible for translational application. The preliminary studies have revealed some success in seeding scaffolds with cells. A more detailed understanding and knowledge of various interdisciplinary fields e.g. rheology, mechanical stimulation etc. are vital in adapting the bioreactor system to

recellularise any grafts in the future and overcome difficulties and limitations with the current approach.

5 DECELLULARISATION LARGER SEGMENTS OF HUMAN SAPHENOUS FOR *IN VIVO* TESTING

5.1 Introduction

In this chapter a methodological upgrading of the protocol of hSV decellularisation was attempted. In keeping with the previous protocol described in Chapter 2 Subsection 2.2.1, this modified protocol also included 24-hour incubation of hSV in SDS at room temperature, followed by washing twice with PBS for 24 hours (as shown in **Figure 3.1**). The modification consisted of using a flow system where SDS was circulated through the vein and around the outside of the vein at a flow of 6 mL/min to ensure exposure of all parts of the hSV to SDS. The set up for this modified decellularisation protocol is shown in Figure 2.1 iii. In brief, veins were cut into 2 segments with one segment being cannulated at either end with the tubing and the chamber primed using 120 mL of 0.01% (w/v) SDS. As a comparison, the other segment of the same hSV was placed in a 50 mL universal in 40 mL of 0.01% (w/v) SDS and rolled at 60 rpm (**Figure 2.1 ii**). In both protocols the veins were exposed to SDS for 24 hours.

5.2 Results

5.2.1 Decellularisation of hSV using a flow-based system

As reported for the initial protocol of hSV decellularisation, the effect of the flow-based system versus the roller-based system was evaluated. The following parameters were assessed: cell content, tissue integrity (focussing on ECM composition), biocompatibility of the resultant scaffold for seeding of cells for the purpose of recellularisation, and the feasibility of *in vivo* recellularisation by host cells as a xenograft in the porcine carotid artery model.

5.2.2 Effectiveness of decellularisation protocol

The effectiveness of the decellularisation was determined with several assays including H&E staining, dsDNA quantification using the PicoGreen assay and gel electrophoresis of DNA fragments. The two decellularisation protocols were compared and showed that the percentage of decelluarisation achieved was significantly greater with the roller protocol than with the flow apparatus (**Figure 5.2 A**). As observed in chapter 3 (**Section 3.4**), the DNA content was not affected by treatment with SDS using either protocol (**Figure 5.2 B** and **C**). Gel electrophoresis revealed similar results in the amount of dsDNA where neither protocol affected the dsDNA (**Figure 5.2 C**).

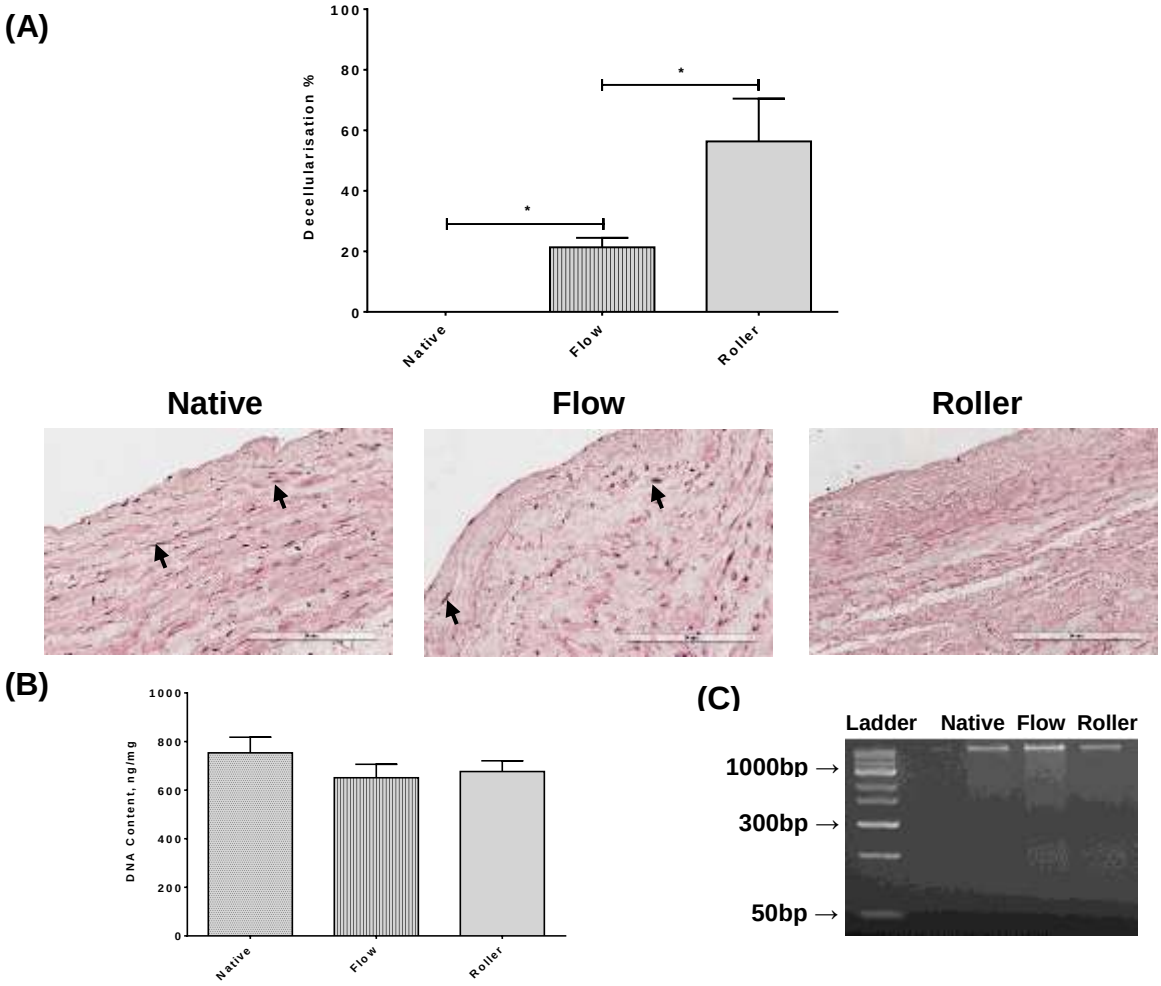

Figure 5.1 Effectiveness of decellularisation: flow vs. roller protocols. (A) The percentage of decellularisation was calculated by quantifying the nuclei (blue) in H&E stained sections of decellularised and native veins. Values are presented as mean ± SEM, 1-way ANOVA, Dunnett's multiple comparisons test, * indicates $p<0.01$, n=6. Representative images of native hSV and 0.01% SDS (w/v) flow versus roller decellularised hSVs are shown. Arrows indicate some haematoxylin stained nuclei. Scales bar represent 300 µm. **(B)** PicoGreen assay quantification of dsDNA from 0.01% SDS (w/v) flow versus roller decellularised and native hSVs. Values are presented as mean ± SEM, 1-way ANOVA, Dunnett's multiple comparisons test, n=6. **(C)** Representative gel electrophoresis image of native hSV and 0.01% SDS (w/v) flow versus roller decellularised and native hSVs.

5.2.3 Effect of decellularisation protocol on tissue integrity

The impact of the two protocols on the ECM integrity was analysed. Since it is established that the specific assay gave better representation in presenting the ECM integrity as shown in section 3.2.3. Therefore, only quantitative ECM protein assays were done and they showed that collagen, elastin and content were not significantly reduced compared to the native hSV using either protocol (**Figure 5.2 A-C**). Specific staining for each ECM components were done as a qualitative observation (**Figure 5.2 A-C**). Collagen and elastin were observed to be lesser in the flow decellularisation protocol than in the native and roller protocol. No apparent differences could be observed with the GAGs content in all tissue (native vs flow vs roller).

(A)

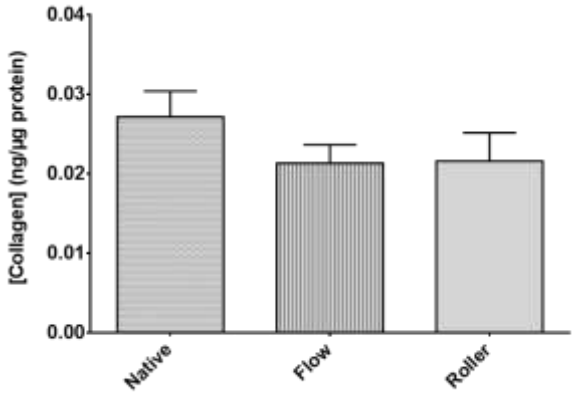

Native Flow Roller

Figure 5.2 ECM protein content after decellularisation with flow and roller protocols. (A) Quantification of collagen, **(B)** elastin and **(C)** GAGs content using Hydroxyproline, Fastin Elastin™ and Blyscan™ assays, respectively. Values are presented as mean ± SEM, * indicates $p<0.05$, 1-way ANOVA, Dunnett's multiple comparisons test, n=6. Representative images for ECM proteins of flow versus roller decellularised and hSVs. PSR (collagen is red), EVG (elastic fibres are stained purple-black, collagen is red and other tissue elements are yellow) and alcian blue (GAGs are stained blue, nuclei are stained red and cytoplasm are stained pink). Scale bar represent 300 µm.

(B)

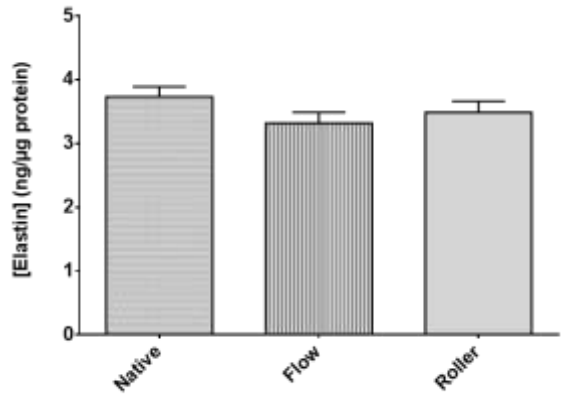

Native Flow Roller

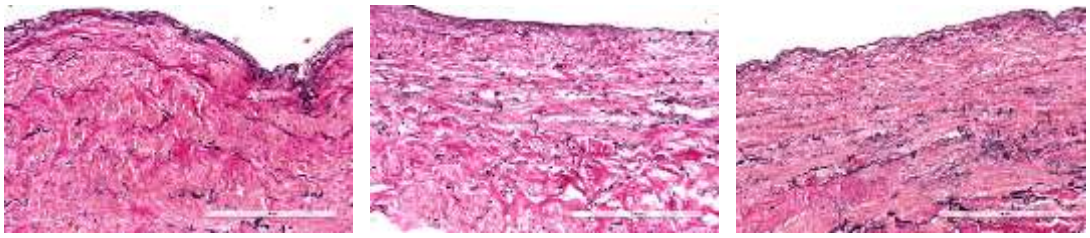

(C)

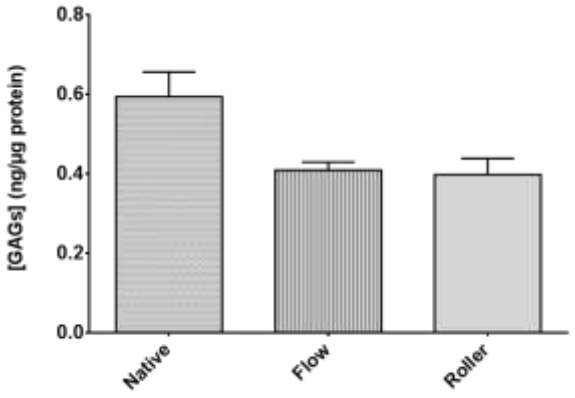

Native Flow Roller

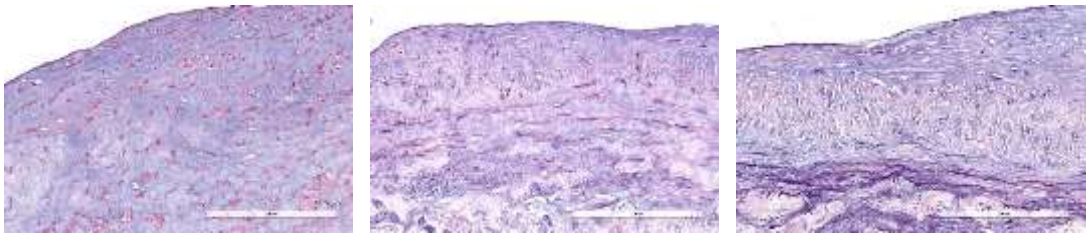

5.2.4 Biocompatibility assay of decellularised tissue

As shown in chapter 3, the first washing step for both protocols significantly reduced the SDS content by 10 times as compared to the initial 0.01% (w/v) SDS effluent followed by another 100 times reduction of SDS content in the second washing effluent. The amount of SDS detected in the tissue after decellularisation was similar in both methods of either flow or roller-based protocol. The results reconfirm the results obtain in the previous chapter with SDS detection at 0.002%, 0.002% and 0.0005% for first wash, second wash and in the tissue, respectively.

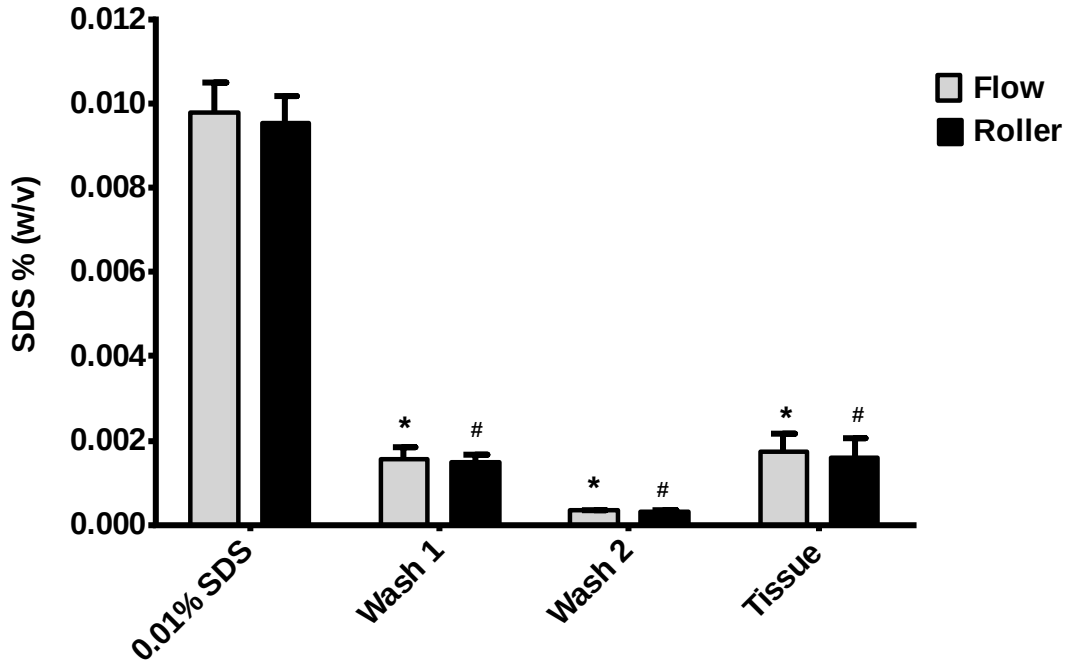

Figure 5.3 Effectiveness of the removal of SDS in the decellularisation protocol

The concentration of SDS in the effluent for both protocols after decellularisation with 0.01% (w/v) SDS and the residual amount in SV tissue at the end of the decellularisation protocol was determined using the methylene blue assay. Values are presented as mean ± SEM, repeated measure 2-way ANOVA, Sidak's multiple comparisons test, * indicates $p<0.01$, n=8.

The decellularised hSVs from both decellularisation protocols were then seeded with pCA ECs for 48 hours. Formalin fixed hSVs were stained with H&E (**Figure 5.5 A**) and subsequently immunostained for EC and SMC markers; CD31 and αSMC, respectively (**Figure 5.5 B**). Native hSVs before decellularisation were used as controls (**Figure 5.4 A i**). The pCA ECs seeded could be observed on both H&E (**Figure 5.4 A ii** and **iii**) and IHC images with green arrow heads showing nucleated ECs (**Figure 5.4 B ii** and **iii**). The decellularised hSV showed there are left over nuclei in decellularised hSV and they are stained positive with αSMA; indicated by red arrow and nuclei with blue arrow (**Figure 5.4 B i**). This observation shows that pCA EC could survive on decellularised hSV regardless of the decellularisation protocol employed. More nuclei are detected in the wall of roller decellularised hSV and some CD31 with nuclei staining in the wall of roller decellularised hSV (**Figure 5.4 B iii**). This might be due to the cells migrating through the bottom of CellCrown and repopulate the tissue from the bottom.

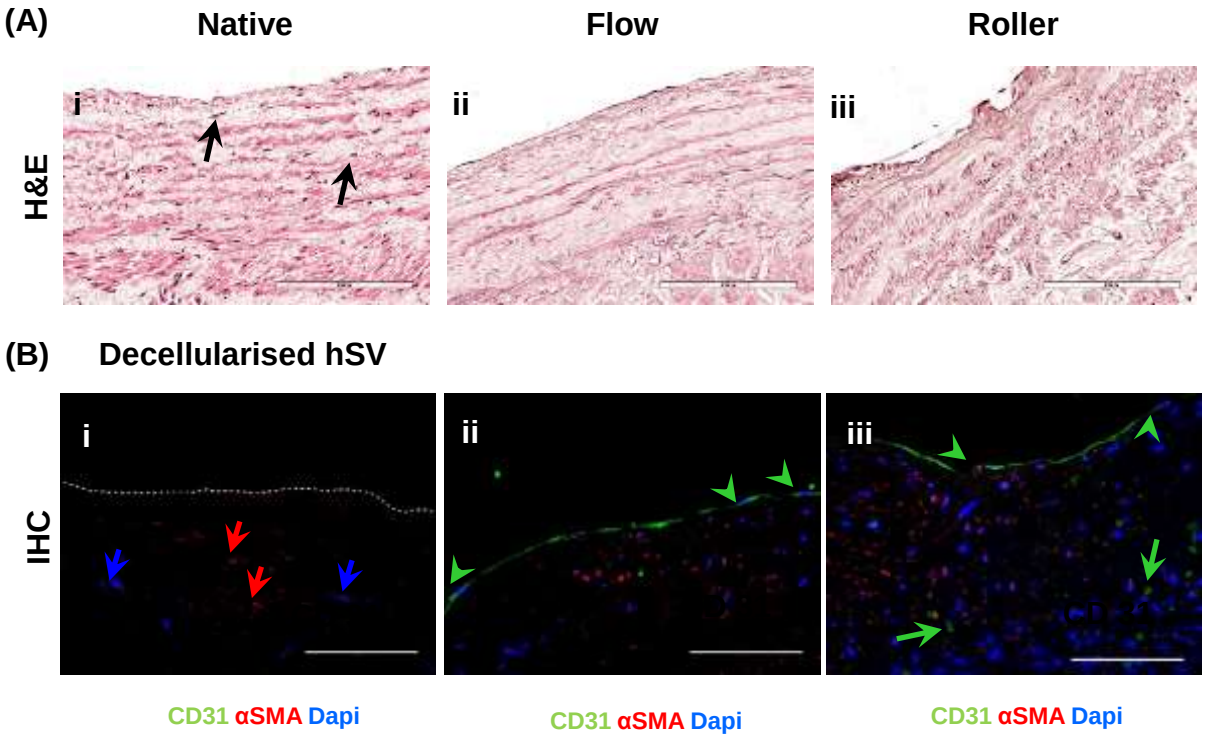

Figure 5.4 Assessment of biocompatibility using EC seeding and histological analyses. (A) Representative images of H&E stained sections of **(i)** native hSV, **(ii)** flow and **(iii)** roller decellularised hSVs that were seeded with pCA EC for 48 hours. Black arrow showing nuclei. Scale bars represent 200 µm. **(B)** Representative images of dual immunohistochemistry for αSMA (red arrow) and CD31 (green arrow head and arrow) in **(i)** decellularised hSV; and the seeded **(ii)** flow and **(iii)** roller decellularised hSVs. Nuclei are stained with DAPI (blue arrow). Scale bars represent 100 µm. n=5.

5.2.5 Implantation of decellularised human saphenous veins as a xenograft in a porcine model

The comparisons undertaken with a limited number in each group suggested that the flow-based protocol of decellularisation was not superior to the roller-based system. The only tangible translational benefit associated with the flow-based protocol of decellularisation is that this system allowed to decellularise longer segment of veins, something of key importance when undertaking aorto-coronary or peripheral bypass grafts.

Three decellularised hSV subjected to roller decellularisation protocol with 0.01% (w/v) SDS were implanted as a xenograft in the porcine model. As 2/3 of previous carotid implants showed severe luminal thrombosis resulting in complete occlusion, in this subsequent group of *in vivo* implants a more aggressive anti-platelet dose of aspirin of 300 mg/day was employed from 4-hour post-surgery until termination. This approach was thought to be more appropriate and in line with current clinical practice.

In addition, vascular Doppler evaluation was undertaken for functional evaluations. Doppler ultrasound was used before and after implantation of the scaffold to determine patency, flow dynamics, and wall thickness, whereas in the previous study, patency was determined manually by confirming persistence of distal pulse in artery verified by the surgeon.

Doppler readings of flow velocities and indices were assessed and compared soon after surgical post-implant and just before pre-explant at termination (n=2, one graft was occluded) to see the changes soon after graft implantation and before the graft

was explanted. Doppler spectrum of the carotid artery shows a low resistance pattern (<0.7) with sufficient diastolic antegrade flow post implantation in all pigs (**Figure 5.5**). On the other hand, the pre-explant reading varies between animals. The first hSV graft was occluded. The second hSV graft has almost similar RI index post-implantation and pre-explantation (0.6 and 0.61; respectively). Whereas, the RI index in the third graft increased 1.6 times higher at pre-explantation; 1.01 than at post-implantation; 0.65 (**Figure 5.6**).

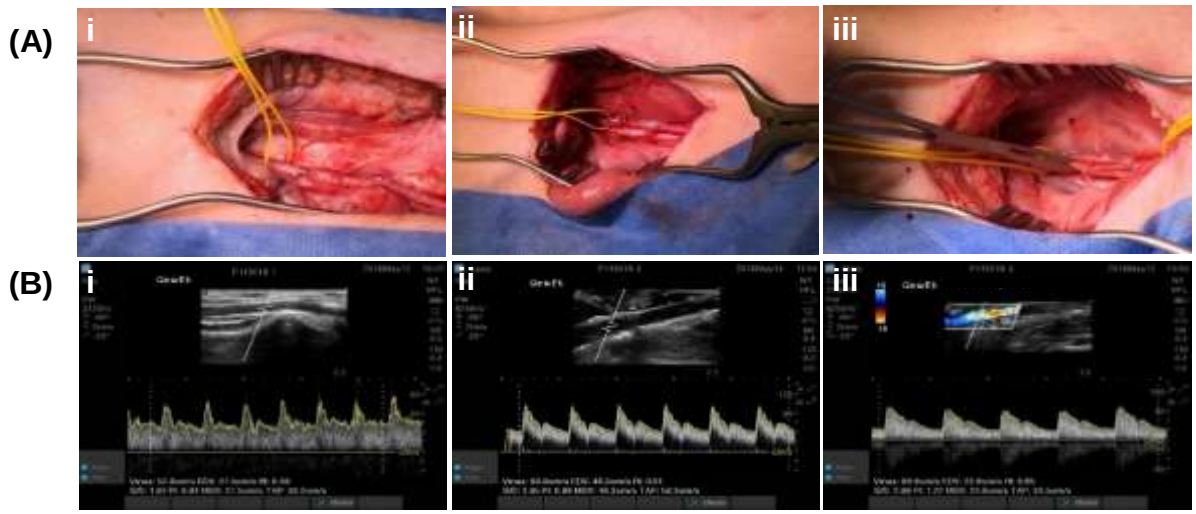

Figure 5.5 Post-implant observation. (A) Gross morphology of the 0.01% (w/v) SDS decellularised hSVs immediately after implantation within the carotid artery. **(i)** first graft, **(ii)** second graft and **(iii)** third graft. **(B)** Doppler ultrasound screen capture of the flow velocity of each graft. Maximum systolic velocity; Vmax, mean diastolic velocity; MDV, end-diastolic velocity; EDV, resistivity index; RI, pulsatility index; PI and systolic/diastolic ratio; S/D.

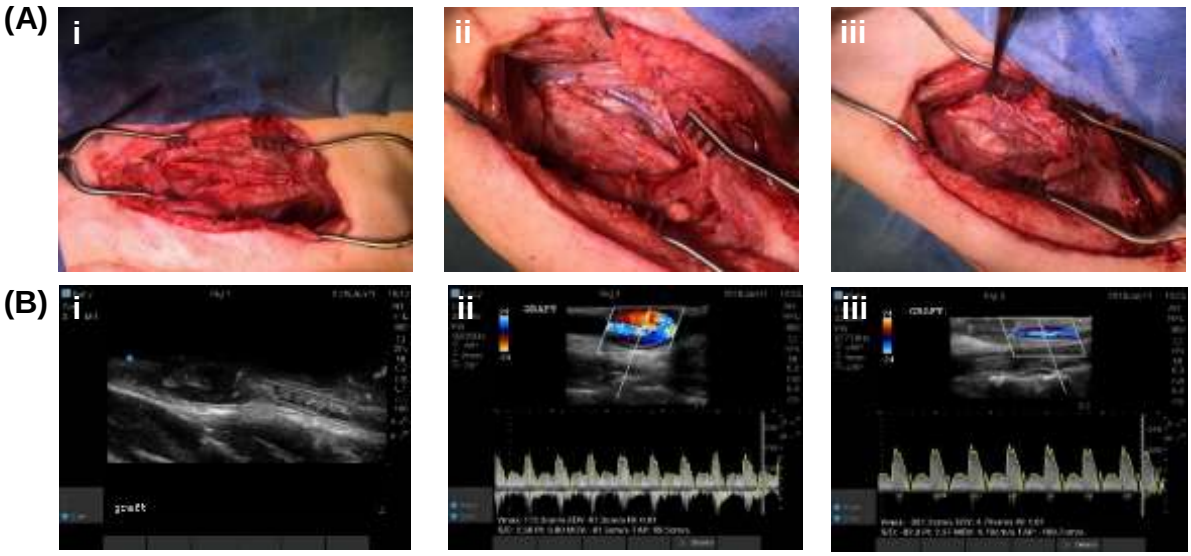

Figure 5.6 Pre-explant observation at 4 weeks. (A) Gross morphology of the 0.01% (w/v) SDS decellularised hSVs immediately before the graft was extracted. **(i)** first graft, **(ii)** second graft and **(iii)** third graft. **(B)** Doppler ultrasound screen capture of the flow velocity of each graft before extraction. Maximum systolic velocity; Vmax, mean diastolic velocity; MDV, end-diastolic velocity; EDV, resistivity index; RI, pulsatility index; PI and systolic/diastolic ratio; S/D.

Summary of Doppler based flow velocities for native pCA, post-implantation and pre-explantation are shown in Table 5.1. There are no significant differences observed in all flow velocities and waveforms between the decellularised hSV right after implantation and before the graft being taken out. The Doppler in situ lumen measurement shown in Table 5.1 corroborate later H&E lumen diameter analysis as shown in Figure 5.7A. At explantation, Doppler reading of the native pCA proximal and distal to the graft and inclusive of the middle of the graft are presented in Table 5.2 (occluded graft recorded as 0). Maximum velocity (V_{max}) of the pCA proximal to the

graft are observed to be significantly lower as compared to the velocities in the graft and distal to the graft (**Table 5.2: V_{max}**).

Table 5.1 Flow velocities and waveforms at post-implant and pre-explant graft procedures.

	Native pCA (n=2)	Post-implant graft (n=2)	Pre-explant graft (n=2)
V_{max} (cm/s)	155 ± 39	141 ± 51	180 ± 107
EDV (cm/s)	38 ± 5	54 ± 16	72 ± 43
MDV (cm/s)	23 ± 20	54 ± 16	32 ± 30
TAP (cm/s)	51 ± 8	56 ± 15	83 ± 53
S/D	4 ± 2	2 ± 0.2	1.7 ± 0.8
RI	0.7 ± 0.1	0.6 ± 0.04	0.4 ± 0.2
PI	3 ± 2	1 ± 0.09	2 ± 0.2
ID (cm)	0.5 ± 0.1	0.3 ± 0.01	0.3 ± 0.3
OD (cm)	0.6 ± 0.2	0.4 ± 0.03	0.4 ± 0.3

Maximum systolic velocity: Vmax, mean diastolic velocity: MDV, end-diastolic velocity: EDV, resistivity index: RI, pulsatility index: PI, systolic/diastolic ratio: S/D, internal diameter: ID and outer diameter: OD.

Table 5.2 Flow velocities and waveforms at pre-explant comparing native pCA proximal to the graft, hSV graft and distal to the graft procedures.

	Proximal pCA	hSV graft	Distal pCA
V_{max} (cm/s)	35.9 ± 12	*180 ± 106	*171 ± 118
EDV (cm/s)	13 ± 6	71 ± 43	14 ± 12
MDV (cm/s)	15 ± 7	32 ± 29	14 ± 12
TAP (cm/s)	15 ± 8	84 ± 53	74 ± 50
S/D	3 ± 0.4	2 ± 0.8	29 ± 27
RI	0.8 ± 0.2	0.4 ± 0.2	0.6 ± 0.3
PI	5 ± 3	2 ± 1	1 ± 0.7
ID (cm)	0.4 ± 0.1	0.3 ± 0.3	0.3 ± 0.2
OD (cm)	0.5 ± 0.1	0.4 ± 0.3	0.3 ±0.2

Maximum systolic velocity: Vmax, mean diastolic velocity: MDV, end-diastolic velocity: EDV, resistivity index: RI, pulsatility index: PI, systolic/diastolic ratio: S/D, internal diameter: ID and outer diameter: OD. * indicates $p<0.05$, 2-way ANOVA, Bonferroni's multiple comparisons test, n=3.

Additionally, histology was performed to analyse the graft structure and composition. The lumen diameter calculated from fixed tissues corroborate the Doppler ultrasound reading taking into account *in situ* measurements which is under perfusion and up to 30% shrinkage of tissue due to tissue fixation and processing. Of note, the lumen diameter and wall thickness were similar of the decellularised hSV, pre-implant and

post-implant pCA are similar (**Figure 5.7 A** and **B**) although the velocities were noted to be significantly different between flow in the pCA proximal to the graft and within the grafts onward. All three explants gave differing but interesting results. The first graft was occluded whereas the other two grafts were both patent at 4 weeks post-surgery. These two grafts however, showed obvious differences in structure and composition and flow velocity from the Doppler evaluation. Noticeably, the second graft was dilated with a larger lumen diameter compared with that of the native artery and the hSV at implant. The third graft was also patent but showing a lumen diameter more similar to that of the native pCA or hSV at implant. In all grafts the wall thickness was increased. Of note, ECM protein assays for ECM proteins (collagen, elastin and GAGs) showed no apparent differences between decellularised hSV and pCA pre- and post-implant (**Figure 5.8 – 5.10)**.

H&E staining shows marked cell infiltration in all graft wall (**Figure 5.11 i**). The explanted grafts were then subjected to immuhistolochemistry to identify cell types markers as in chapter 3 (SMC: αSMA and SM MHC, EC: CD31 and eNOS, macrophage/monocytes: CD203 and fibroblast: vimentin). Immunostaining of all three grafts with the EC specific antibodies revealed the presence of CD31 and eNOS positive cells (EC) in the medial layer of the grafts (**Figure 5.11**). A streak of CD31 positive staining could be observed on the section of the lumen (**Figure 5.11B iii**).

Of note, αSMA was detected in the medial layer of graft 4 and 6, despite the first graft being occluded and the third graft showing a thick wall (**Figure 5.11 A iii and C iii**). As observed in the first set of implants, these might be donor cell remnants from the

implanted decellularised hSV as previously observed (**Figure 3.14**). Additionally, faint staining for αSMA was noted in the graft 2, which was also patent (**Figure 5.11 B iii)**.

Vimentin which is a fibroblast and synthetic SMC marker was not detected in the three grafts (**Figure 5.11 v**). CD203 which is a marker for macrophage/monocyte for swine was also not detectable in all three graft (**Figure 5.11 iv**). Noteworthy, the detection of neovascularisation in the adventitial layer of the grafts as shown in Figure 5.11 A iv and B iv (white arrow).

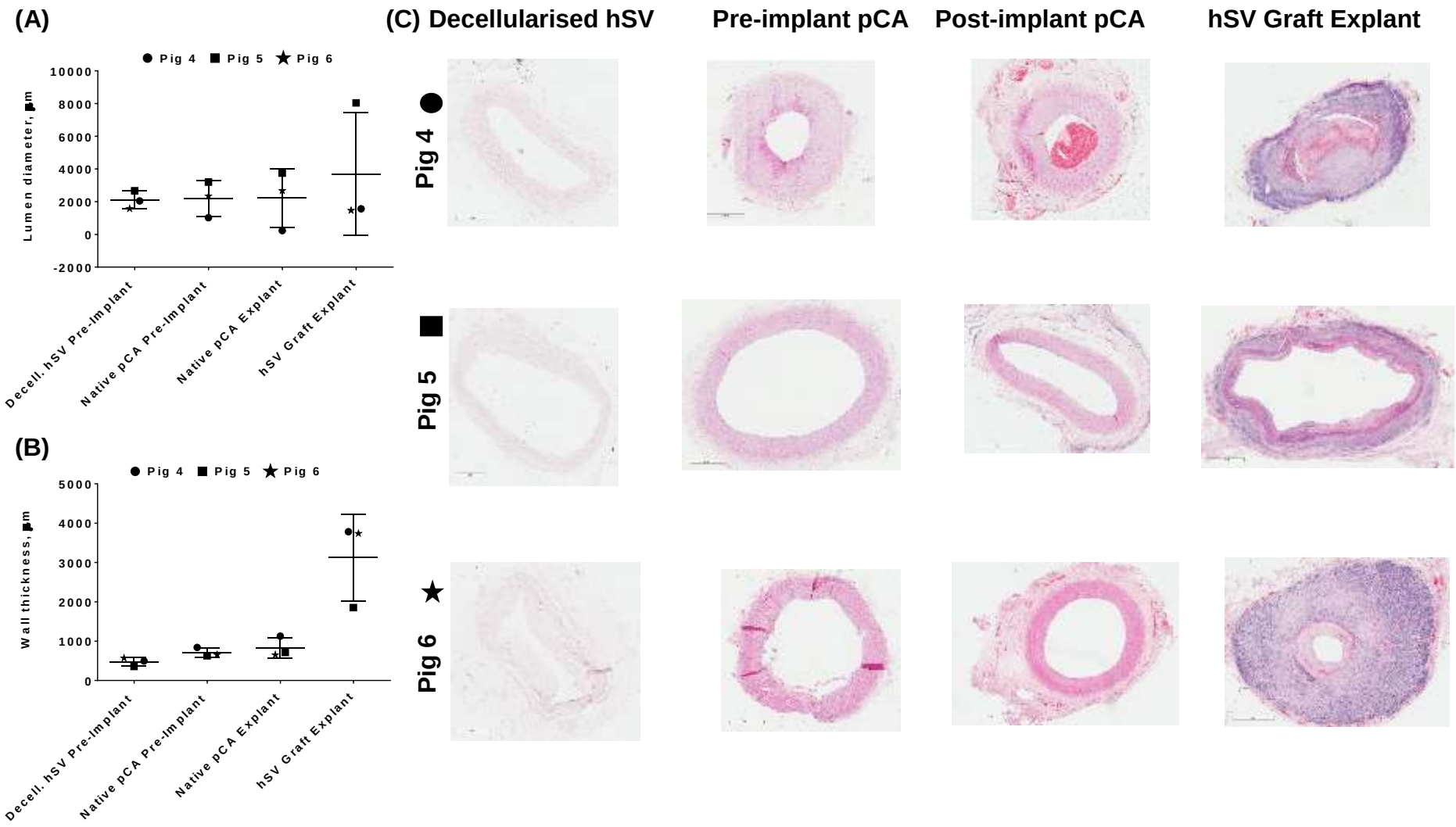
(A)
Pig 4
Pig 5
Pig 6
Lumen diameter, µm
10000
8000
6000
4000
2000
0
-2000
Decell. hSV Pre-Implant
Native pCA Pre-Implant
Native pCA Explant
hSV Graft Explant
(B)
Pig 4
Pig 5
Pig 6
Wall thickness, µm
5000
4000
3000
2000
1000
0
Decell. hSV Pre-Implant
Native pCA Pre-Implant
Native pCA Explant
hSV Graft Explant
(C) Decellularised hSV
Pre-implant pCA
Post-implant pCA
hSV Graft Explant
Pig 4
Pig 5
Pig 6

Figure 5.7 Structural characteristics of pCA and decellularised vein pre- and post-implant. (A) Lumen diameter pre- and post-implant of pCA and 0.01% (w/v) SDS decellularised hSV and. Values are presented as mean ± SEM, Repeated measure 2-way ANOVA, Sidak's multiple comparisons test, n=3. **(B)** Wall thickness pre- and post-implant of pCA and 0.01% (w/v) SDS decellularised hSV. Values are presented as mean ± SEM, Repeated measure 2-way ANOVA, Sidak's multiple comparisons test, n=3. **(C)** H&E images for pre- and post-implant of pCA and 0.01% (w/v) SDS decellularised hSV. Collagen and muscle are stained pink, cytoplasm is stained purple-red, nuclei are purple-blue and red blood cells stained cherry red. ●; ■ and ★ 4, 5 and 6 indicate explants from pig 4, 5 and 6 respectively. Scale bars are indicated on images.

(A)

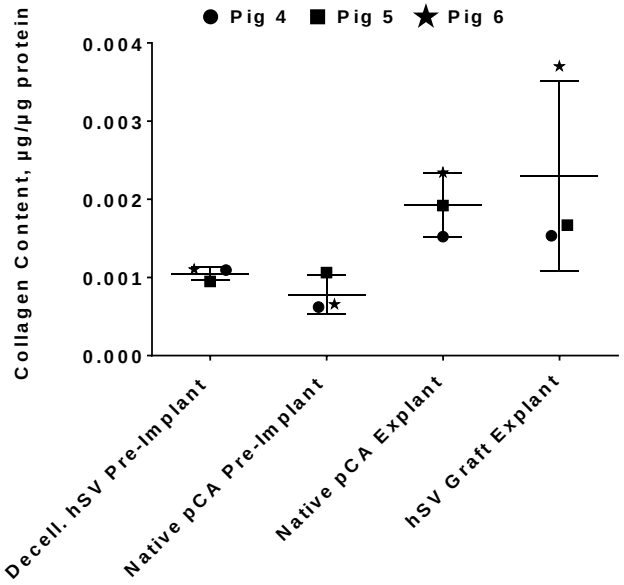

Figure 5.8 Collagen content of pCA and decellularised vein pre- and post-implant. (A) Quantification of collagen content within pre- and post-implant of pCA and 0.01% (w/v) SDS decellularised hSV using hydroxyproline assay. Values are presented as mean ± SEM, Repeated measure 2-way ANOVA, Sidak's multiple comparisons test, n=3. **(B)** PSR images for pre- and post-implant of pCA and 0.01% (w/v) SDS decellularised hSV where collagen is red on a pale-yellow background at 200X magnification. ●; ■ and ★ indicate explants from pig 4, 5 and 6 respectively. Scale bar represent 300 µm.

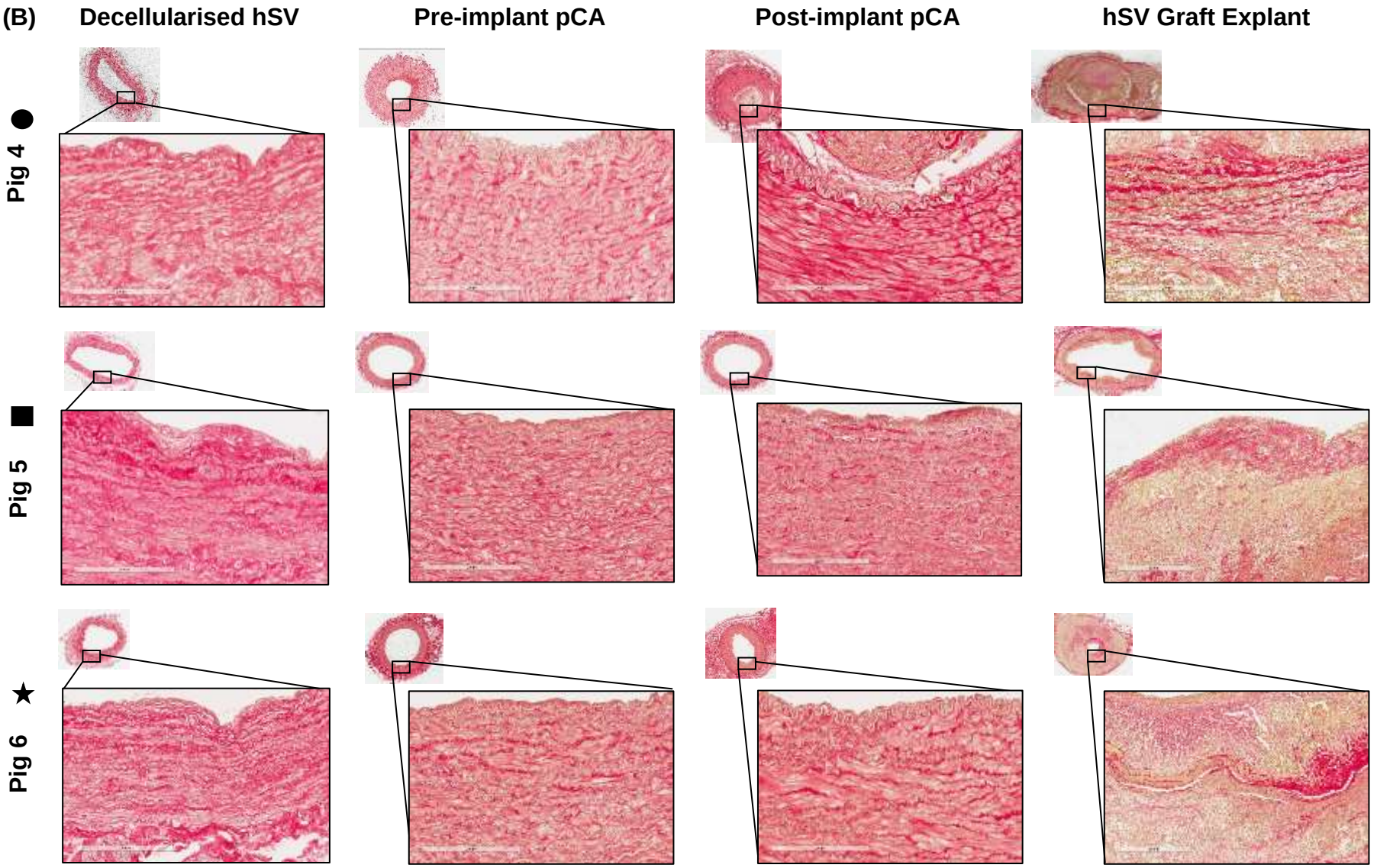
(B)
Decellularised hSV
Pre-implant pCA
Post-implant pCA
hSV Graft Explant
Pig 4 ●
Pig 5 ■
Pig 6 ★

(A)

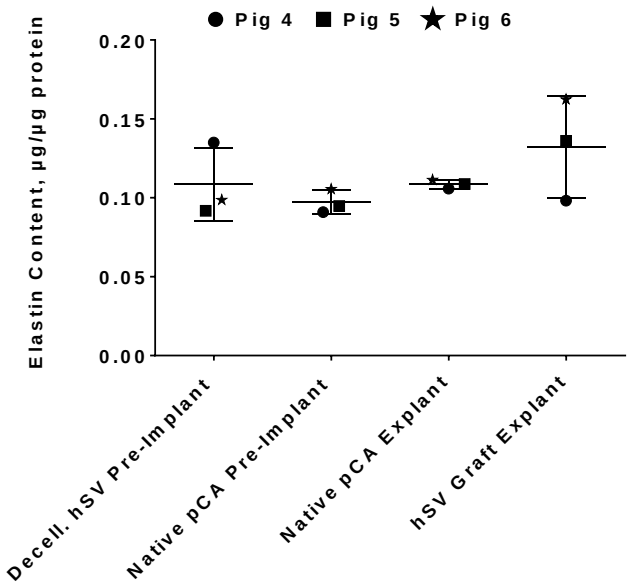

Figure 5.9 Elastin content of pCA and decellularised vein pre- and post-implant. (A) Quantification of elastin content within pre- and post-implant of pCA and 0.01% (w/v) SDS decellularised hSV using Fastin Elastin™ assay. Values are presented as mean ± SEM, Repeated measure 2-way ANOVA, Sidak's multiple comparisons test, n=3. **(B)** EVG images for pre- and post-implant of pCA and 0.01% (w/v) SDS decellularised hSV where elastic fibres are stained purple-black, collagen is red and other tissue elements are yellow) at 200X magnification. ●; ■ and ★ indicate explants from pig 4, 5 and 6 respectively. Scale bar represent 300 µm.

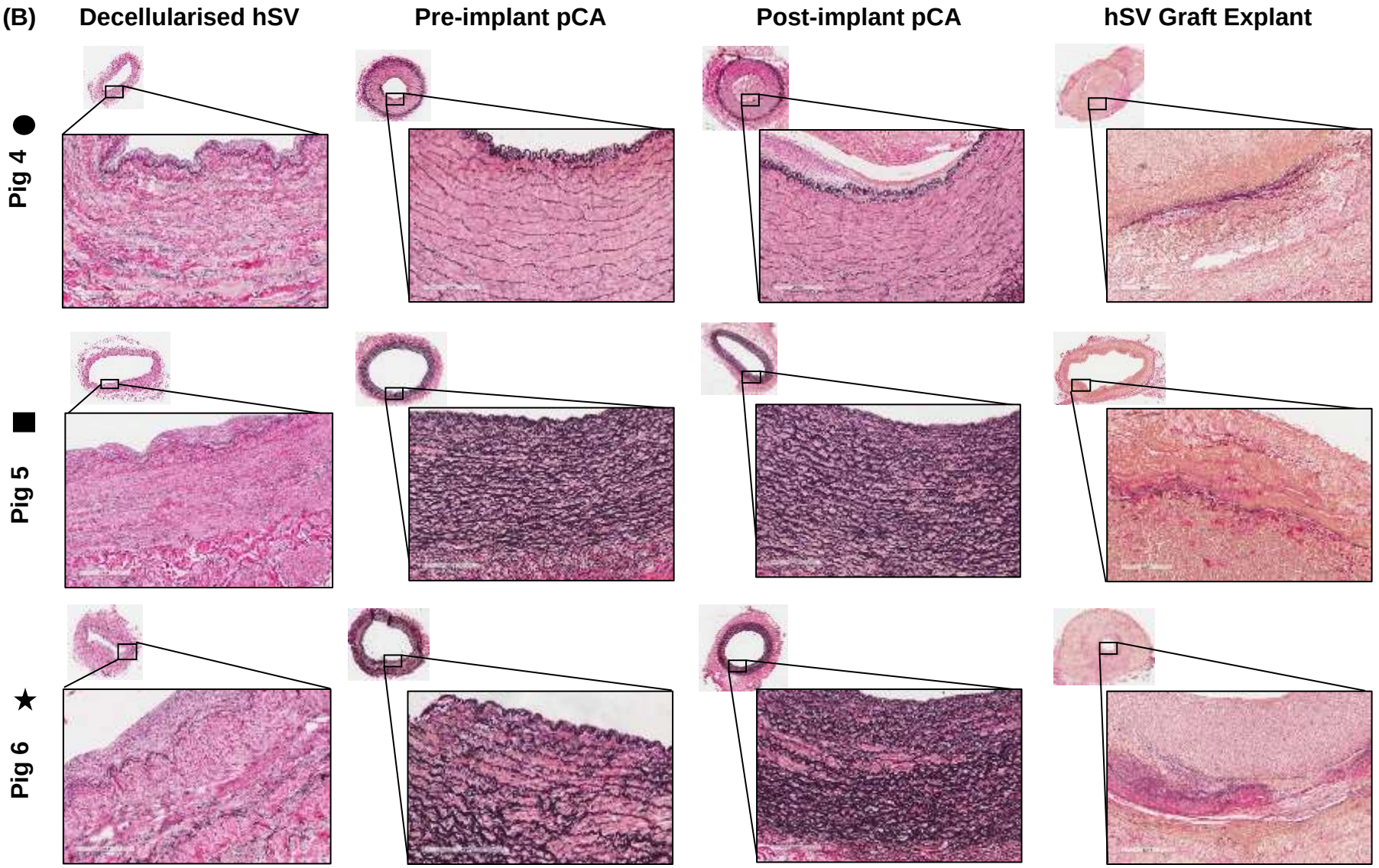
(B)
Decellularised hSV
Pre-implant pCA
Post-implant pCA
hSV Graft Explant
Pig 4 ●
Pig 5 ■
Pig 6 ★

(A)

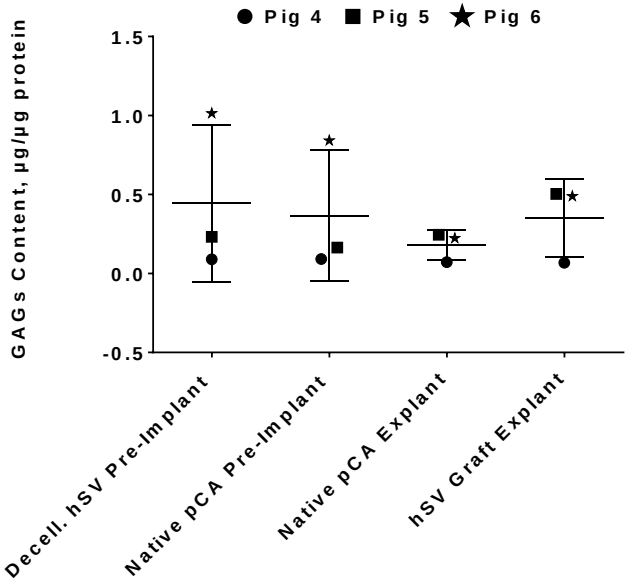

Figure 5.10 GAGs content of pCA and decellularised vein pre- and post-implant. (A) Quantification of GAGs content within pre- and post-implant of pCA and 0.01% (w/v) SDS decellularised hSV using Blyscan™ assay. Values are presented as mean ± SEM, Repeated measure 2-way ANOVA, Sidak's multiple comparisons test, n=3. **(B)** GAGs images for pre- and post-implant of pCA and 0.01% (w/v) SDS decellularised hSV where GAGs are stained blue, nuclei are stained red and cytoplasm are stained pink at 200X magnification. ●; ■ and ★ indicate explants from pig 4, 5 and 6 respectively. Scale bar represent 300 µm.

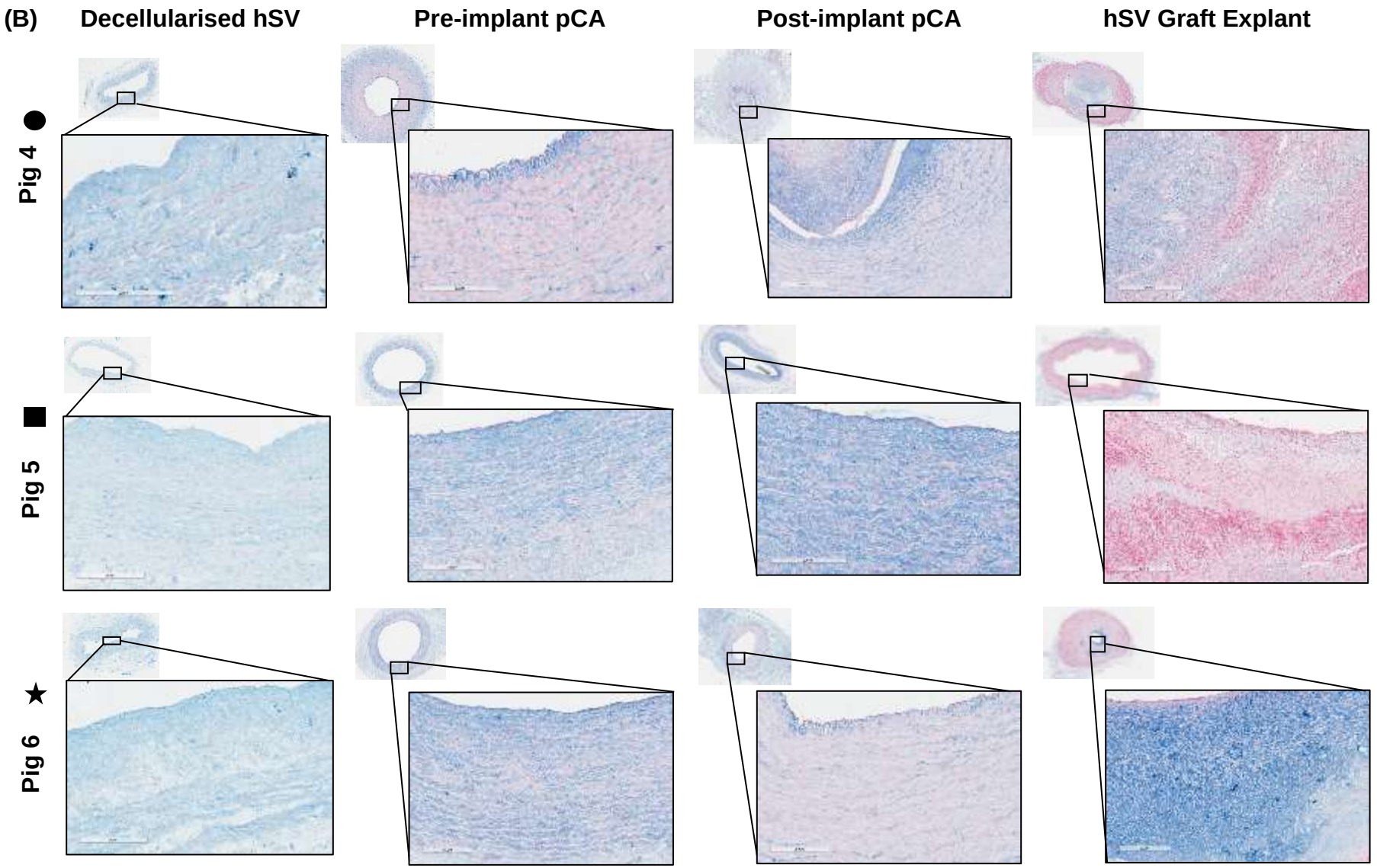
(B)
Decellularised hSV
Pre-implant pCA
Post-implant pCA
hSV Graft Explant
Pig 4 ●
Pig 5 ■
Pig 6 ★

(A) Pig 1

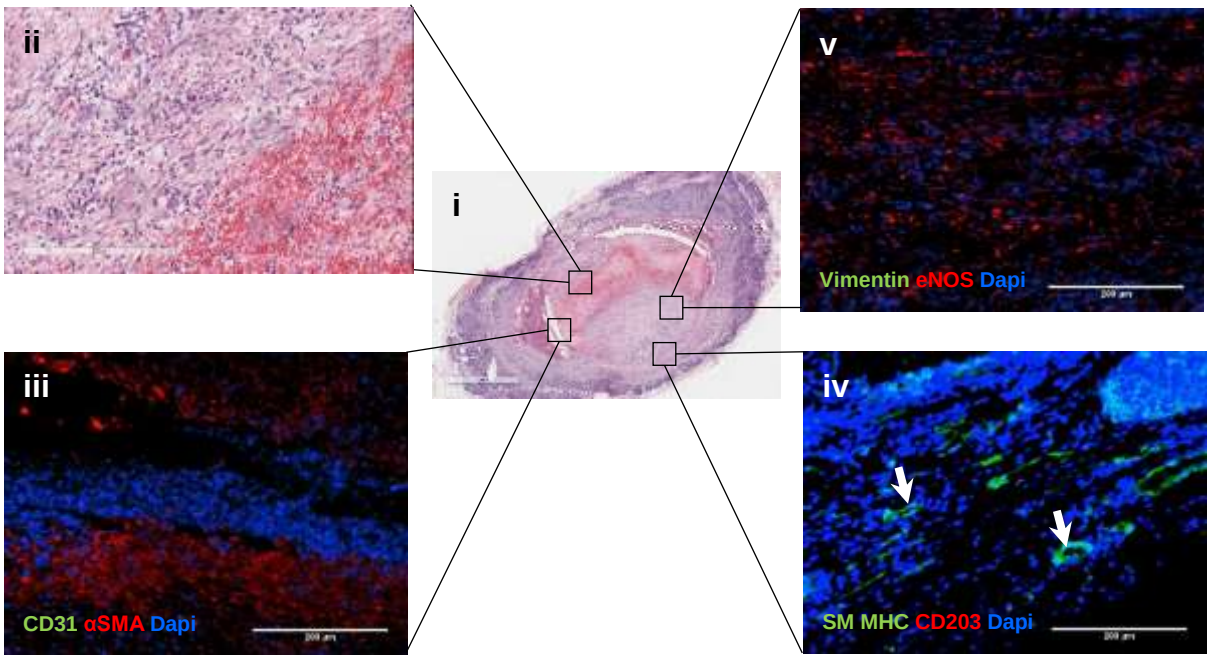
ii
i
v
Vimentin eNOS Dapi
iii
CD31 αSMA Dapi
iv
SM MHC CD203 Dapi

(B) Pig 2

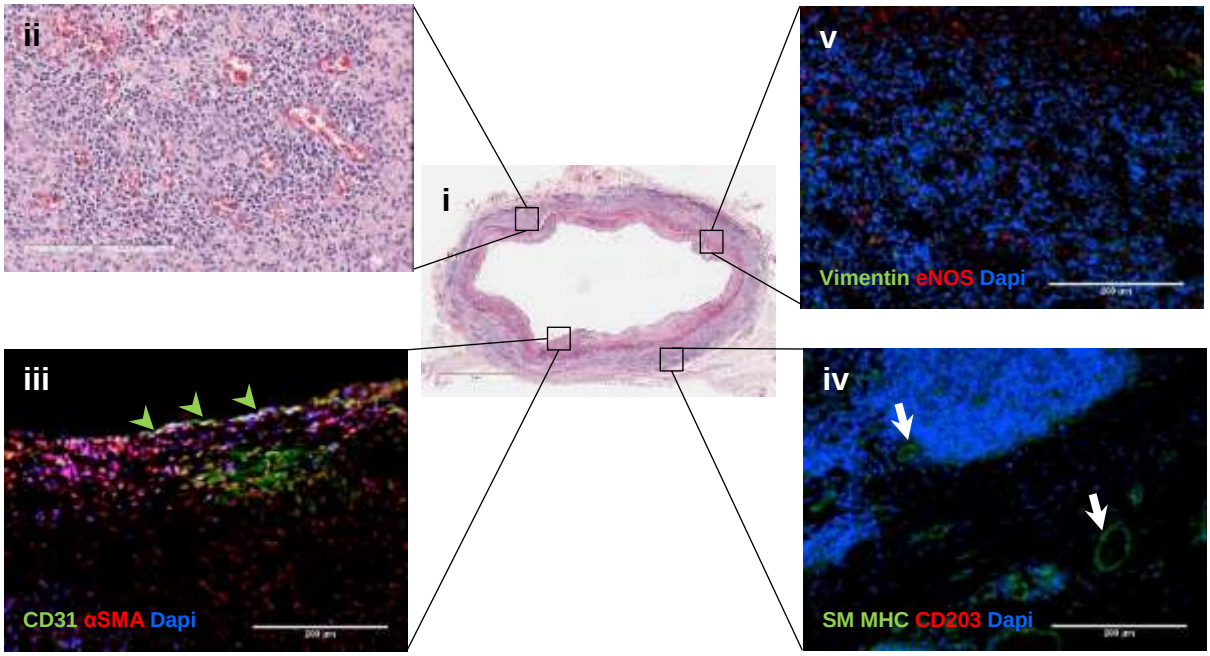
ii
i
v
Vimentin eNOS Dapi
iii
CD31 αSMA Dapi
iv
SM MHC CD203 Dapi

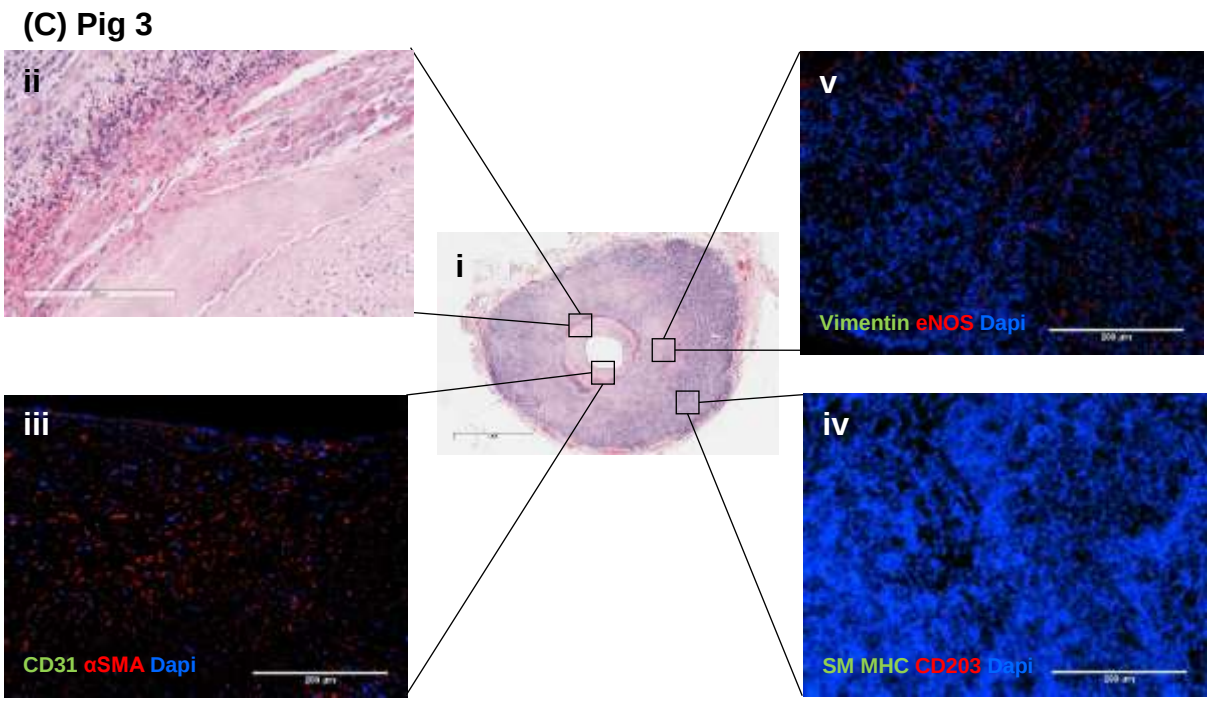

Figure 5.11 Xenograft immunohistochemistry screening staining. Representative images of dual immunostaining on 3-micron slices of xenograft explants stained with both EC and SMC marker to identify cells in the explants with **(i)** H&E stained explants ring to show localisation and **(ii)** cell infiltration (nuclei are stained purple black). All slides were nuclear stained with **(iii)** αSMA (red) and DBA (green); **(iv)** SM MHC (green) and CD203 (red); **(v)** Vimentin (green) and eNOS (red) with nuclei stained DAPI (blue), at 200X magnification. Green arrow indicates CD31 positive cells. White arrow shows neovascularisation. Scale bar represent 200 µm for both high magnification IHC and H&E images and 3 mm for lower magnification H&E images.

Discussion

Perfusion systems have been employed to decellularise a range of whole organs, for example heart, lung, liver (Gilpin et al. 2014; Wu et al. 2015; Gerli et al. 2018). This approach provides a more thorough exposure to the detergent utilised for decellularisation of tissues. Therefore, a simple perfusion system was used in this chapter as a comparison with the previous decellularisation protocol using a roller, with the aim to obtain a more translational decellularised hSV that when implanted *in vivo* would gave a more effective and consistent outcome. Decellularisation was achieved with the perfusion system but with no apparent differences with the previously employed roller decellularisation protocol in terms of decellularisation efficiency, DNA elimination, ECM integrity and biocompatibility. Subsequent experimental work is required to further enhance the decellularisation protocol. It is possible that increasing the flow rate would help in increasing the decellularisation efficiency of the flow decellularisation protocol and this could be attempted in the future. One advantage of using the perfusion system is the ability to decellularise longer segments of hSV and this would be advantageous in terms of preparing a graft for use in CABG. The guidelines for vein harvest are based on the artery occlusion to be bypassed. The shortest vein needed for grafting at the left anterior descending artery is at least 10 to 15 cm whereas the longest would be 20 cm to be grafted at the posterolateral artery (Barner and Farkas 2012; Barner 2013).

The biocompatibility of the resultant scaffolds was proven via pCA EC reseeding on the decellularised hSV *in vitro*. The purpose of the xenografting was to assess the patency and the repopulation of the scaffold *in vivo* by host cells. Three *in vivo* implants

of decellularised hSV were prepared with the roller decellularisation protocol and implanted with improved antiplatelet therapy. This overall approach aimed to improve the graft patency by reducing the likelihood of thrombus formation, and thus prevent graft occlusion (Goldman et al. 1988; Stein et al. 2004; Poston et al. 2006). Aspirin was given with a daily dose of 300 mg for a week before surgery and from 4-hour post-surgery, daily until termination as opposed to 75 mg daily aspirin in the first batch of three decellularised hSV implants. The outcome of all three implants varied, and given the limited number of implants undertaken it is not possible to reach firm conclusions on the differences observed between the first and the second group of *in vivo* implants.

Doppler ultrasonography has widely been used to assess various vascular diseases (Cooperberg 1992; Vriens et al. 2001; Jahromi et al. 2005). Doppler ultrasound observation verified the patency of graft immediately after implantation. Dynamic information of blood flow was crucial in analysing the spectral waveform and may assist in predicting future outcome of the implants. Doppler ultrasound readings of the native right carotid arteries didn't deviate from the reference range reported by other groups for several other species e.g. minipig, dogs, cows, and human (Jung et al. 2010; Cooperberg 1992; Vriens et al. 2001; Jahromi et al. 2005; Braun and Fohn 2005; Svicero et al. 2013). The degree of stenosis, based on values suggested by North American Consensus Criteria (NACC) where value of peak systolic velocity (PSV) at <125 cm/s for 50% stenosis, >230 cm/s for 70% stenosis and >400 cm/s for ≥90% stenosis showed that even the values of native pCA are >150 cm/s which if according to NACC has a degree of stenosis between 5 to 69% (Grant et al. 2003). It is important to note that the pre-explanted and post-explanted graft has a high V_{max} value of 142

cm/s and 180 cm/s which falls in the same interpretation with native pCA according to NACC (Cooperberg 1992; Grant et al. 2003; Jahromi et al. 2005). Therefore, the baseline reference level captured in these experiments for this particular model will be helpful for future implant studies.

Histological staining results proved that there was no lumen mis-match between the decellularised hSV and the pre-implant pCA at the time of surgical implantation. Persistent change in vessel size in atherosclerosis were apparent hence the term arterial remodelling was coined to describe these changes because in the presence of stable lesion, arterial remodelling and not plaque size is the main determinant of lumen size (Sipahi et al. 2006; Ward et al. 2000). The wall thickness increased in all grafts although only one showed an increased lumen diameter which is similar to the first batch of grafts. Thus, the expansion of grafts is in agreement to the arterial remodelling where a compensatory dilatation of vessels occurs to accommodate any plaque formation without any lumen loss (Glagov et al. 1987; Glagov et al. 1988; Sipahi et al. 2006; Davies 2000; Murphy and Angelini 2004). Collagen, elastin and GAGs showed no differences pre- and post-implantation and between native pCA shows the suitability of the graft as a xenograft.

Histological staining showed a marked infiltration of host cells into the wall of the scaffold. Endothelial markers CD31 and eNOS were detected in all grafts predominantly within the wall at level of the medial layers. As discussed in earlier chapters, both markers are also expressed in inflammatory cells, hence highlighting the inflammatory response of host cells to the vein xenografts (Kim et al. 2009;

Connelly et al. 2003). SMC markers, especially αSMA were apparent in all graft explants along with many nuclei. It is hard to confirm whether these SMC are remnants of human cells after decellularisation or new SMC derived from recruited host cells. Of note, we observed αSMA in the decellularised hSV before surgical implant as shown initially in chapter 3. There is the possibility of SMC invasion from porcine host cells through the anastomosis region as demonstrated by Liang *et. al* in studying the neointima formation in arteriovenous fistulas that was attributed to SMC from the artery side of the fistula (Liang et al. 2015). Vimentin staining was not detectable suggesting that the cells were fibroblasts or synthetic SMCs that are associated with the venous phenotype (Asada et al. 2005; Beamish et al. 2010; Worth et al. 2001; Zhou et al. 2007).

It has been demonstrated that initially, recellularisation of any graft, be it synthetic or biological, leads to marked macrophage recruitment, representing the host immune response to the foreign tissue implanted (Kim et al. 2009; Badylak 2014). This triggering of immune response may be beneficial. The tissue engineering and regenerative medicine research communities are looking at this matter in a positive light as macrophage recruitment is seen as a means to recellularisation of any graft especially biological grafts (Badylak and Gilbert 2008; Badylak 2014; Moroni and Mirabella 2014). The subsequent aim after macrophage recruitments and graft infiltration are directing the macrophage phenotype from pro-inflammatory (M1) to anti-inflammatory (M2) (Novak and Koh 2013; Lech and Anders 2013; Badylak 2014; Wynn and Vannella 2016).

The swine macrophage/monocyte marker CD203 was initially chosen as it is expressed when monocytes differentiate into macrophages. However, CD203 has been used to identify macrophages with M2 polarisation (Singleton et al. 2016; Jacobsen et al. 2016; Franzoni et al. 2017). M2 macrophages are associated with the anti-inflammatory and cell repair function which are the main subtype of macrophages that would be beneficial in the repopulation of the graft and direct tissue remodelling and regeneration of the decellularised graft. CD203 staining was not detected in the wall of the grafts. Therefore, other macrophage marker regardless of their phenotype like CD68, CD163 or CD80 would be of use here but was not possible due to limited availability of suitable antibodies that recognise porcine antigens (Badylak et al. 2008; Fairbairn et al. 2013).

5.3 Conclusion

This chapter showed that the two decellularisation protocols used are reasonably effective in decellularisation without damaging the ECM integrity. There were no apparent differences in effectiveness between the two approaches however, except for the capacity of the flow decellularisation apparatus to accommodate longer lengths if vein which would be beneficial toward translations of this protocol for CABG applications. No obvious improvement in the group with 300 mg aspirin vs the 75 mg used in the previous pilot study, no conclusive inference can be made with this increase of antiplatelet therapy and any benefits it may imposed. Nonetheless, future implants should employ the higher dose of antiplatelet therapy which is at par with the current clinical practise in humans. Finally, for the porcine arterial xenografting, vascular Doppler ultrasound analysis was a very effective functional scan in assessing graft patency *in vivo*. A baseline reading of control pigs could be established to get a better degree of stenosis extrapolation.

6 GENERAL DISCUSSION AND FUTURE WORK

6.1 General discussion

The emergence of tissue engineering and regenerative medicine (TERM) approaches facilitates the idea of ‘From Bench to Bedside’ research towards the translational stage. The multidisciplinary nature of TERM allows the collaborative effort between science, medicine and engineering to a common goal in treating diseases and saving patients lives. For that reason, in this thesis the tissue engineering framework that encompass three components which are biomaterial, cells and signalling was adopted in the project. Starting off with the biomaterial it was assessed whether it is possible to increase the patency of the SV, which is the most commonly used bypass graft for coronary and peripheral applications. It is well established that IMA grafts have significantly higher patency than SV grafts and numerous reasons for the difference in patency have been identified. Aside from the anatomical and the physiological differences, the phenotype of the cells within the arterial and venous grafts differ (dela Paz and D'Amore 2009; Hirashima and Suda 2006; Kim et al. 2004) .

Therefore, the hypothesis was to remove the cellular materials from SVs and obtain a vascular ECM which could be utilised an ‘acellular’ graft or seeded with cells prior to implantation. One might suggest an alternative approach whereby the venous cells could be arterialised with the hemodynamic forces mimicking the arterial system consequently might increase vein graft patency. Haemodynamic forces may have an impact on directing the change of cell from venous to arterial phenotype, although their mechanistic role in vascular tissue engineering need to be elucidated further. The possibility of *in vivo* arterialisation of veins is disputed by the findings of Kuto *et al*.,

who reported that vein graft adaptation does not change the molecular identity of the vein to an artery as vein grafts lost their venous markers but did not gain any arterial markers (Kudo et al. 2007). These findings are further corroborated by Berard *et al*. in their *ex vivo* perfusion system (Berard et al. 2013). These findings confirm that the genetic make-up of mature cells are pre-determined during development. Hence, decellularising human veins into acellular vascular scaffolds and re-seeding the decellularised ECM with arterial cells possibly under dynamic conditions was deemed a suitable aim. In keeping with this rationale, the ECM or any TEVG should be re-seeded with cells that either come from *in vivo* arterial origin or are derived from any available pluripotent or multipotent cells *in vitro*. It is proposed that this approach may achieve an arterialised conduit with an improved patency through remodelling of the graft towards arterial characteristics.

The decellularisation of veins has been performed previously, and used particularly for allografts and xenografts (Martin et al. 2005; Ketchedjian et al. 2005; Schaner et al. 2004). The efficacy of a decellularisation protocol is generally based on assessing the amount of residual donor cell nuclei and quantifying the DNA content after decellularisation, while other cellular debris (including plasma cell membrane, and cytoplasmic proteins) are neglected (Crapo, Gilbert, and Badylak 2011). Most reports of decellularisation approaches cover very little quantitative results and focus more of a representative qualitative staining images (Bruyneel and Carr 2017). Thus, in this study a quantitative approach was utilised wherever possible to enable the decellularisation protocol efficacy to be accurately assessed.

The use of decellularised ECM has potential benefits over synthetic scaffolds as the ECM scaffold facilitates and inhibits recruitment of various cell types, and can undergo remodelling, which are features lacking in synthetic grafts. The characteristic of ECM mediated constructive remodelling includes the degradation of ECM proteins that can release signalling molecules, modulate the inert immune response and promote recruitment of endogenous stem cells (Voytik-Harbin et al. 1997; Robinson et al. 2005; Badylak and Gilbert 2008; Reing et al. 2009; Vorotnikova et al. 2010; Hammond et al. 2011; Badylak 2014). Matrix-bound nanovesicles (MBVs) have been demonstrated to be an integral and functional component of ECM bioscaffolds which are released via constructive remodelling (Huleihel et al. 2016). MBVs promote the M2-like anti-inflammatory macrophage phenotype and T cells towards the Th2-like immune response that stimulate remodelling rather than rejection (Allman et al. 2001; Huleihel et al. 2016). MVBs are similar to exosomes which is a subset of extracellular vesicles (EVs) (van Niel, D'Angelo, and Raposo 2018). MVBs, like EVs, have a varied cargo including microRNA (miRNA), cytokines, chemokines, proteins, and lipids (Choi et al. 2015; Maas, Breakefield, and Weaver 2017). It has been shown that the contents of EBVs play some positive roles in the regulation of immune response (Robbins and Morelli 2014).

It is possible that MBVs contribute at least in part to the variable *in vivo* porcine arterial xenograft results. After analysing the initial 3 xenografts, an improvement of the decellularisation protocol was thought to be necessary, to eliminate any residual DNA as it was the possible culprit for the adverse outcome. Although the lack of EC coverage could feasibly lead to large thrombus formation. A modified protocol was

established, but to no avail as the perfusion decellularisation protocol rendered similar results to the roller decellularisation protocol in terms of DNA content and ECM integrity. However, the perfusion decellularisation proved to be more effective that the roller decellularisation protocol as it permitted the use of a longer segment of hSV, something critical for future possible translation to bedside. The results from the porcine arterial xenografts confirmed that the cell infiltration inside the grafts. Granting that no evidence was shown in this project due to limitation in optimising working porcine cell markers, the immune response of host cells to the graft may be due not just to remnants of DNA in the graft but also be mediated by MBVs in the ECM. Previous studies have highlighted that residual DNA and cell debris mediate the host macrophage infiltration into the graft (Sanders et al. 2017; Wong et al. 2008). The host immune response will direct macrophages into the graft, and cytokine, chemokines, miRNAs released from MBVs may direct the polarisation of macrophages to the anti-inflammatory phenotype (M2) that contribute to tissue remodelling (Lech and Anders 2013; Badylak 2014).

From the six xenografts a 50% success rate was recorded which is low compared to other reported large animal model arterial xenograft transplantation studies with 100% patency at 3 and 5 months in an ovine model and at 10 months in a canine model (Clarke et al. 2001; Affonso da Costa et al. 2004). Long-term implantations of seeded grafts would be beneficial to ascertain the progress of arterial remodelling in the porcine model used in this study and eliminate and enhance the repopulation of the grafts. Preclinical testing with short-term implantations often used in small animal models with as short as 2 weeks evaluations and larger animal models usually are

done longer (Lopez-Soler et al. 2007; Gui et al. 2009; Xiong et al. 2013; Negishi et al. 2015; Amensag et al. 2017). The increase of aspirin as an antiplatelet therapy in the second pilot study was initially thought to improve the implantation protocol but the outcome of the implantation is not conclusive due to too small n number.

It is commonly perceived that *ex vivo* seeding of ECM scaffolds has potential for recellularisation of the graft and creation of an arterialised vein before surgical implant (Quint et al. 2011; Kaushal et al. 2001; Villalona et al. 2010). By reseeding the graft *ex vivo* to create an endothelial lining in the lumen, the patency of the graft could be preserved as demonstrated by Yang *et al.* where native grafts and reseeded acellular allografts produced 100% patency after 6 months, but only 50% of naked acellular grafts were patent (Yang et al. 2009). Hence, a variety of recellularisation techniques have been developed to achieve the best recellularisation, be it static or dynamic seeding (Mirensky et al. 2010; Punshon et al. 2008; Villalona et al. 2010; Yang et al. 2009). Static seeding includes injecting, dripping or bathing cells onto the decellularised ECM. The static method has as the benefit that it is the simplest application, hence easier to manipulate and thus more feasible for translation and most economical. Static seeding was undertaken in this project to assess the biocompatibility of the decellularised hSV with pCA ECs where decellularised tissue was fixed on a CellCrown™ insert to hold the tissue and then cells were seeded on top of the tissue hence preventing the migration of cell onto the culture plate. This method worked for a small piece of the tissue but scaling up of this approach to reseed the whole decellularised lumen will present a challenge.

Alternatively, the use of a dynamic system presents a more comprehensive approach in reseeding an acellular vascular graft. The dynamic environment that a bioreactor system provides with different variables that could be manipulated such as the flow pattern, may be vital in the arrangement of ECs on the surface of the acellular graft. Aligning ECs on the luminal surface will prevent the adhesion of monocytes and therefore should improve graft patency (Shin et al. 2016; Huang et al. 2013). The bioreactor system is widely used in TERM research as a combinatory approach using cells, scaffolds and regulatory signalling to achieve a functional tissue (Nieponice et al. 2008; Schulte et al. 2014; Catto et al. 2014; Pashneh-Tala, MacNeil, and Claeyssens 2015).

In exploiting the bioreactor system, PWB was used as a cell source due to limited number of primary pCA ECs that could be extracted from arteries and the time needed to expand the cell culture to achieve enough number to be used in the system. The aim was to prove that PWB contains cells that could potentially recellularise the decellularised vein similar to described by Olausson *et al.* (Olausson et al. 2012; Olausson et al. 2014). Unfortunately, there was insufficient time to optimise the utilisation of the bioreactor system e.g. the flow, pressure for this project. The results were based on several attempts that were successful but not comparable as they utilised differing protocols. But based on the bioreactor attempts that were successful, it was noted that high flow with high pressure (200 mL/minute, 250-350 mmHg) resulted in a slight increase of lumen diameter and more compact decellularised hSV wall. Whereas, lower flow with slightly lower pressure (25 mL/minute, 100-200 mmHg)

did not affect the tissue appearance and therefore appears more suitable in terms of seeding of cells for future studies.

The reason for utilising the high flow, was first to mimic the flow condition in the internal carotid artery which is reported as 238.84 mL/min (Oktar et al. 2006). Unfortunately, the PWB perfusion in the bioreactor system at high flow did not show any cells attached on the lumen surface, and instead blood clots were observed. The flow was then decreased to 25 mL/minute but the resultant tissue still did not show any cell attachment except for a few streaks of red blood cells. This might suggest that even lower flow rates are needed. Olausson *et al.* in their recellularisation process applied a very low flow at 2 mL/minute which is equivalent to 0.6 dyne/cm^2. Their decision to use such a flow rate was based on various report of fluid shear stress at this level move the differentiation of endothelial progenitor cells to endothelial-like cells and the expression of these cells towards arterial endothelial cell (Obi et al. 2012; Ankeny et al. 2012; Egorova et al. 2012; Adamo and Garcia-Cardena 2012; Obi et al. 2009; Yamamoto et al. 2003). Further optimisation is therefore needed on the system to circumvent the problem of gravity and sedimentation of cells early on in the system before reaching the chamber where the graft is mounted.

6.2 Overall findings and conclusion

Development of new arterial-like vascular conduits for coronary and peripheral bypass grafting surgery is desirable to overcome the limitations of currently available biological and/or synthetic grafts and thereby reduce the incidence of early thrombosis, late intimal thickening and infection. One alternative is to use arterialised decellularised venous scaffolds. The aim of this PhD project was to assess the feasibility and suitability of hSV decellularisation as a way to obtain an effective biological acellular scaffold for vascular grafting.

We identified an optimal low SDS concentration (0.01%) to decellularise short segments of hSVs (~0.5cm), but this approach was not effective in removing nuclei when using ~4cm long hSVs. However, a modified flow technique of decellularisation was established with successful decellularisation of longer hSV segments, with translational potential. Biocompatibility and integrity of decellularised hSVs were evaluated. Methylene blue assay detected only trivial residual concentrations of SDS after decellularisation. This was biocompatible as this residual amount of SDS did not affect the viability of porcine carotid artery endothelial cells (pCA ECs) to populate the acellular hSV (AlamarBlue) and to proliferate (EdU proliferation assays). The ECM integrity of acellular hSVs was assessed by quantifying major ECM proteins (collagen, elastin and GAGs). Results revealed that decellularisation with ≤0.01% (v/v) SDS did not have a significant impact on the ECM content. The feasibility, safety and capacity of acellular hSVs to act as an end-to-end anastomoses in pigs without immunosuppression was tested. This pilot study showed that porcine carotid artery

xenograft of decellularised hSV was feasible and safe, with 50% graft patency rate at 4 weeks and signs of *in situ* vascular tissue engineering by host cells.

In conclusion, taken together, this project suggests that effective decellularisation of hSV is feasible, safe and reproducible as potential acellular vascular scaffolds. Acellular hSVs may be used as vascular acellular scaffolds either for *in situ* vascular engineering by host cells or following *ex vivo* manipulation before implantation. However, this approach need significant refinement and warrants further future investigations.

REFERENCES

Abal, M., J. M. Andreu, and I. Barasoain. 2003. 'Taxanes: microtubule and centrosome targets, and cell cycle dependent mechanisms of action', *Curr Cancer Drug Targets*, 3: 193-203.

Abdulhannan, P., D. A. Russell, and S. Homer-Vanniasinkam. 2012. 'Peripheral arterial disease: a literature review', *Br Med Bull*, 104: 21-39.

Adamo, L., and G. Garcia-Cardena. 2012. 'The vascular origin of hematopoietic cells', *Dev Biol*, 362: 1-10.

Affonso da Costa, F. D., P. M. Dohmen, S. V. Lopes, G. Lacerda, F. Pohl, R. Vilani, M. B. Affonso Da Costa, E. D. Vieira, S. Yoschi, W. Konertz, and I. Affonso da Costa. 2004. 'Comparison of cryopreserved homografts and decellularized porcine heterografts implanted in sheep', *Artif Organs*, 28: 366-70.

Ahmed, H. M., M. J. Blaha, K. Nasir, J. J. Rivera, and R. S. Blumenthal. 2012. 'Effects of physical activity on cardiovascular disease', *Am J Cardiol*, 109: 288-95.

Akashi, K. 2002. '[Potential usefulness of hematopoietic stem cells in regenerative medicine]', *Nihon Ronen Igakkai Zasshi*, 39: 246-52.

Ali, Z. A., R. Gao, T. Kimura, Y. Onuma, D. J. Kereiakes, S. G. Ellis, B. Chevalier, M. T. Vu, Z. Zhang, C. A. Simonton, P. W. Serruys, and G. W. Stone. 2018. 'Three-Year Outcomes With the Absorb Bioresorbable Scaffold: Individual-Patient-Data Meta-Analysis From the ABSORB Randomized Trials', *Circulation*, 137: 464-79.

Allain, R., L. K. Marone, J. Meltzer, and G. Jeyabalan. 2005. 'Carotid endarterectomy', *Int Anesthesiol Clin*, 43: 15-38.

Allman, A. J., T. B. McPherson, S. F. Badylak, L. C. Merrill, B. Kallakury, C. Sheehan, R. H. Raeder, and D. W. Metzger. 2001. 'Xenogeneic extracellular matrix grafts elicit a TH2-restricted immune response', *Transplantation*, 71: 1631-40.

Allman, A. J., T. B. McPherson, L. C. Merrill, S. F. Badylak, and D. W. Metzger. 2002. 'The Th2-restricted immune response to xenogeneic small intestinal submucosa does not influence systemic protective immunity to viral and bacterial pathogens', *Tissue Eng*, 8: 53-62.

Ambrose, John A., and George Dangas. 2000. 'Unstable Angina', *Archives of Internal Medicine*, 160.

Amensag, S., L. Goldberg, K. A. O'Malley, D. S. Rush, S. A. Berceli, and P. S. McFetridge. 2017. 'Pilot assessment of a human extracellular matrix-based vascular graft in a rabbit model', *J Vasc Surg*, 65: 839-47 e1.

Anderson, J. L., and D. A. Morrow. 2017. 'Acute Myocardial Infarction', *N Engl J Med*, 376: 2053-64.

Ankeny, R. F., C. J. Ankeny, R. M. Nerem, and H. Jo. 2012. 'Maturing EPCs into endothelial cells: may the force be with the EPCs: focus on "Fluid shear stress induces differentiation of circulating phenotype endothelial progenitor cells"', *Am J Physiol Cell Physiol*, 303: C589-91.

Anwar, M. A., J. Shalhoub, C. S. Lim, M. S. Gohel, and A. H. Davies. 2012. 'The effect of pressure-induced mechanical stretch on vascular wall differential gene expression', *J Vasc Res*, 49: 463-78.

Aranguren, X. L., A. Luttun, C. Clavel, C. Moreno, G. Abizanda, M. A. Barajas, B. Pelacho, M. Uriz, M. Arana, A. Echavarri, M. Soriano, E. J. Andreu, J. Merino, J. M. Garcia-Verdugo, C. M. Verfaillie, and F. Prosper. 2007. 'In vitro and in vivo arterial differentiation of human multipotent adult progenitor cells', *Blood*, 109: 2634-42.

Ariyaratne, T. V., Z. Ademi, C. H. Yap, B. Billah, F. Rosenfeldt, B. P. Yan, and C. M. Reid. 2014. 'Prolonged effectiveness of coronary artery bypass surgery versus drug-eluting stents in diabetics with multi-vessel disease: an updated systematic review and meta-analysis', *Int J Cardiol*, 176: 346-53.

Asada, H., J. Paszkowiak, D. Teso, K. Alvi, A. Thorisson, J. C. Frattini, F. A. Kudo, B. E. Sumpio, and A. Dardik. 2005. 'Sustained orbital shear stress stimulates smooth muscle cell proliferation via the extracellular signal-regulated protein kinase 1/2 pathway', *J Vasc Surg*, 42: 772-80.

Asahara, T., A. Kawamoto, and H. Masuda. 2011. 'Concise review: Circulating endothelial progenitor cells for vascular medicine', *Stem Cells*, 29: 1650-5.

Atala, A., and R. P. Lanza. 2002. *Methods of tissue engineering* (Academic Press).

Azhim, A., K. Yamagami, K. Muramatsu, Y. Morimoto, and M. Tanaka. 2011. "The use of sonication treatment to completely decellularize blood arteries: A pilot study." In *Engineering in Medicine and Biology Society,EMBC, 2011 Annual International Conference of the IEEE*, 2468-71.

Badylak, S. F. 2014. 'Decellularized allogeneic and xenogeneic tissue as a bioscaffold for regenerative medicine: factors that influence the host response', *Ann Biomed Eng*, 42: 1517-27.

Badylak, S. F., and T. W. Gilbert. 2008. 'Immune response to biologic scaffold materials', *Semin Immunol*, 20: 109-16.

Badylak, S. F., J. E. Valentin, A. K. Ravindra, G. P. McCabe, and A. M. Stewart-Akers. 2008. 'Macrophage phenotype as a determinant of biologic scaffold remodeling', *Tissue Eng Part A*, 14: 1835-42.

Barner, H. B. 2013. 'Conduits for Coronary Bypass: Arteries Other Than the Internal Thoracic Artery's', *Korean J Thorac Cardiovasc Surg*, 46: 165-77.

Barner, H. B., and E. A. Farkas. 2012. 'Conduits for coronary bypass: vein grafts', *Korean J Thorac Cardiovasc Surg*, 45: 275-86.

Beamish, J. A., P. He, K. Kottke-Marchant, and R. E. Marchant. 2010. 'Molecular regulation of contractile smooth muscle cell phenotype: implications for vascular tissue engineering', *Tissue Eng Part B Rev*, 16: 467-91.

Becker, R. C., T. W. Meade, P. B. Berger, M. Ezekowitz, C. M. O'Connor, D. A. Vorchheimer, G. H. Guyatt, D. B. Mark, and R. A. Harrington. 2008. 'The primary and secondary prevention of coronary artery disease: American College of Chest Physicians Evidence-Based Clinical Practice Guidelines (8th Edition)', *Chest*, 133: 776S-814S.

Bedi, U., M. Singh, P. Singh, J. Molnar, S. Khosla, and R. Arora. 2011. 'Effects of statins on progression of coronary artery disease as measured by intravascular ultrasound', *J Clin Hypertens (Greenwich)*, 13: 492-6.

Bello, YsabelM, AnnaF Falabella, and WilliamH Eaglstein. 2001. 'Tissue-Engineered Skin', *American Journal of Clinical Dermatology*, 2: 305-13.

Berard, X., S. Deglise, F. Alonso, F. Saucy, P. Meda, L. Bordenave, J. M. Corpataux, and J. A. Haefliger. 2013. 'Role of hemodynamic forces in the ex vivo arterialization of human saphenous veins', *J Vasc Surg*, 57: 1371-82.

Bhatia, V, R Bhatia, and M Dhindsa. 2004. 'Drug-eluting stents: new era and new concerns', *Postgraduate Medical Journal*, 80: 13-18.

Bhatnagar, Prachi, Kremlin Wickramasinghe, Julianne Williams, Mike Rayner, and Nick Townsend. 2015. 'The epidemiology of cardiovascular disease in the UK 2014', *Heart*.

Birukov, K. G. 2009. 'Cyclic stretch, reactive oxygen species, and vascular remodeling', *Antioxid Redox Signal*, 11: 1651-67.

Bobryshev, Y. V., S. M. Cherian, S. J. Inder, and R. S. Lord. 1999. 'Neovascular expression of VE-cadherin in human atherosclerotic arteries and its relation to intimal inflammation', *Cardiovasc Res*, 43: 1003-17.

Böer, Ulrike, LuisG Hurtado-Aguilar, Melanie Klingenberg, Skadi Lau, Stefan Jockenhoevel, Axel Haverich, and Mathias Wilhelmi. 2015. 'Effect of Intensified Decellularization of Equine Carotid Arteries on Scaffold Biomechanics and Cytotoxicity', *Annals of Biomedical Engineering*: 1-12.

Boron, W.F., and E.L. Boulpaep. 2008. *Medical Physiology* (Elsevier Health Sciences).

Bowen, Patrick K., Emily R. Shearier, Shan Zhao, Roger J. Guillory, Feng Zhao, Jeremy Goldman, and Jaroslaw W. Drelich. 2016. 'Biodegradable Metals for Cardiovascular Stents: from Clinical Concerns to Recent Zn-Alloys', *Advanced Healthcare Materials*, 5: 1121-40.

Bowers, Stephanie L. K., Indroneal Banerjee, and Troy A. Baudino. 2010. 'The Extracellular Matrix: At the Center of it All', *Journal of molecular and cellular cardiology*, 48: 474-82.

Braun, U., and J. Fohn. 2005. 'Duplex ultrasonography of the common carotid artery and external jugular vein of cows', *Am J Vet Res*, 66: 962-5.

Bruyneel, A. A. N., and C. A. Carr. 2017. 'Ambiguity in the Presentation of Decellularized Tissue Composition: The Need for Standardized Approaches', *Artif Organs*, 41: 778-84.

Buccheri, D., D. Piraino, G. Andolina, and B. Cortese. 2016. 'Understanding and managing in-stent restenosis: a review of clinical data, from pathogenesis to treatment', *J Thorac Dis*, 8: E1150-E62.

Campioni, D., G. Zauli, S. Gambetti, G. Campo, A. Cuneo, R. Ferrari, and P. Secchiero. 2013. 'In vitro characterization of circulating endothelial progenitor cells isolated from patients with acute coronary syndrome', *PLoS One*, 8: e56377.

Castillo, M., and H. Alvarez. 2011. 'Artery or Vein: To Be or Not To Be?', *American Journal of Neuroradiology*, 32: 791-93.

Castronuovo Jr, John J., Thomas J. Smith, and Ray M. Price. 2002. 'Validation of an in vitro model of human saphenous vein hyperplasia', *Journal of Vascular Surgery*, 35: 152-57.

Catto, Valentina, Far, #xe8, Silvia , Giuliano Freddi, and Maria Cristina Tanzi. 2014. 'Vascular Tissue Engineering: Recent Advances in Small Diameter Blood Vessel Regeneration', *ISRN Vascular Medicine*, 2014: 27.

Chelladurai, Prakash, Werner Seeger, and Soni Savai Pullamsetti. 2012. 'Matrix metalloproteinases and their inhibitors in pulmonary hypertension', *European Respiratory Journal*, 40: 766-82.

Chen, Chih-Wei, and Chin-Lon Lin. 2009. 'The Current Status of Coronary Drug-Eluting Stents', *Tzu Chi Medical Journal*, 21: 18-27.

Chi, J. T., H. Y. Chang, G. Haraldsen, F. L. Jahnsen, O. G. Troyanskaya, D. S. Chang, Z. Wang, S. G. Rockson, M. van de Rijn, D. Botstein, and P. O. Brown. 2003. 'Endothelial cell diversity revealed by global expression profiling', *Proc Natl Acad Sci U S A*, 100: 10623-8.

Chlupac, J., E. Filova, and L. Bacakova. 2009. 'Blood vessel replacement: 50 years of development and tissue engineering paradigms in vascular surgery', *Physiol Res*, 58 Suppl 2: S119-39.

Choi, D. S., D. K. Kim, Y. K. Kim, and Y. S. Gho. 2015. 'Proteomics of extracellular vesicles: Exosomes and ectosomes', *Mass Spectrom Rev*, 34: 474-90.

Cirino, G., S. Fiorucci, and W. C. Sessa. 2003. 'Endothelial nitric oxide synthase: the Cinderella of inflammation?', *Trends Pharmacol Sci*, 24: 91-5.

Clarke, D. R., R. M. Lust, Y. S. Sun, K. S. Black, and J. D. Ollerenshaw. 2001. 'Transformation of nonvascular acellular tissue matrices into durable vascular conduits', *Annals of Thoracic Surgery*, 71: S433-S36.

Comenzo, R. L., and E. M. Berkman. 1995. 'Hematopoietic stem and progenitor cells from blood: emerging uses for new components for transfusion', *Transfusion*, 35: 335-45.

Connelly, L., A. T. Jacobs, M. Palacios-Callender, S. Moncada, and A. J. Hobbs. 2003. 'Macrophage endothelial nitric-oxide synthase autoregulates cellular activation and pro-inflammatory protein expression', *J Biol Chem*, 278: 26480-7.

Cooperberg, E. 1992. 'Ultrasound Doppler spectral analysis in the diagnosis of occlusive lesions of the carotid arteries', *Ultrasound Med Biol*, 18: 421-5.

Corada, Monica, Massimo Mariotti, Gavin Thurston, Kelly Smith, Robin Kunkel, Manfred Brockhaus, Maria Grazia Lampugnani, Ines Martin-Padura, Antonella Stoppacciaro, Luigi Ruco, Donald M. McDonald, Peter A. Ward, and Elisabetta Dejana. 1999. 'Vascular endothelial–cadherin is an important determinant of microvascular integrity in vivo', *Proceedings of the National Academy of Sciences*, 96: 9815-20.

Cosgrove, D. M., F. D. Loop, B. W. Lytle, C. C. Gill, L. A. Golding, C. Gibson, R. W. Stewart, P. C. Taylor, and M. Goormastic. 1986. 'Predictors of reoperation after myocardial revascularization', *J Thorac Cardiovasc Surg*, 92: 811-21.

Crapo, P. M., T. W. Gilbert, and S. F. Badylak. 2011. 'An overview of tissue and whole organ decellularization processes', *Biomaterials*, 32: 3233-43.

Crawford, F., K. Welch, A. Andras, and F. M. Chappell. 2016. 'Ankle brachial index for the diagnosis of lower limb peripheral arterial disease', *Cochrane Database Syst Rev*, 9: CD010680.

Creager, Mark A., Joshua A. Beckman, and Joseph Loscalzo. 2012. *Vascular medicine : a companion to Braunwald's heart disease*.

D'Amore, P. A. 1992. 'Mechanisms of endothelial growth control', *Am J Respir Cell Mol Biol*, 6: 1-8.

Daly, K. A., S. Liu, V. Agrawal, B. N. Brown, S. A. Johnson, C. J. Medberry, and S. F. Badylak. 2012. 'Damage associated molecular patterns within xenogeneic biologic scaffolds and their effects on host remodeling', *Biomaterials*, 33: 91-101.

Darr, D., K. M. McCormack, T. Manning, S. Dunston, D. C. Winston, B. A. Schulte, T. Buller, and S. R. Pinnell. 1990. 'Comparison of Dolichos biflorus lectin and other lectin-horseradish peroxidase conjugates in staining of cutaneous blood vessels in the hairless mini-pig', *J Cutan Pathol*, 17: 9-15.

Davies, J. H., J. Richards, K. Conway, J. E. Kenkre, J. E. Lewis, and E. Mark Williams. 2017. 'Primary care screening for peripheral arterial disease: a cross-sectional observational study', *Br J Gen Pract*, 67: e103-e10.

Davies, M. J. 2000. 'Glagovian remodelling, plaque composition, and stenosis generation', *Heart*, 84: 461-2.

de Castro Bras, L. E., T. A. Ramirez, K. Y. DeLeon-Pennell, Y. A. Chiao, Y. Ma, Q. Dai, G. V. Halade, K. Hakala, S. T. Weintraub, and M. L. Lindsey. 2013. 'Texas 3-step decellularization protocol: looking at the cardiac extracellular matrix', *J Proteomics*, 86: 43-52.

de Vries, M. R., and P. H. A. Quax. 2018. 'Inflammation in Vein Graft Disease', *Front Cardiovasc Med*, 5: 3.

de Vries, M. R., K. H. Simons, J. W. Jukema, J. Braun, and P. H. Quax. 2016. 'Vein graft failure: from pathophysiology to clinical outcomes', *Nat Rev Cardiol*, 13: 451-70.

dela Paz, N. G., and P. A. D'Amore. 2009. 'Arterial versus venous endothelial cells', *Cell Tissue Res*, 335: 5-16.

Desai, M., A. M. Seifalian, and G. Hamilton. 2011. 'Role of prosthetic conduits in coronary artery bypass grafting', *Eur J Cardiothorac Surg*, 40: 394-8.

Destefani, A. C., G. M. Sirtoli, and B. V. Nogueira. 2017. 'Advances in the Knowledge about Kidney Decellularization and Repopulation', *Front Bioeng Biotechnol*, 5: 34.

E. Niklason, Laura, and Robert S. Langer. 1997. 'Advances in tissue engineering of blood vessels and other tissues', *Transplant Immunology*, 5: 303-06.

Edelman, E. R. 1999. 'Vascular tissue engineering : designer arteries', *Circ Res*, 85: 1115-7.

Egorova, A. D., M. C. DeRuiter, H. C. de Boer, S. van de Pas, A. C. Gittenberger-de Groot, A. J. van Zonneveld, R. E. Poelmann, and B. P. Hierck. 2012. 'Endothelial colony-forming cells show a mature transcriptional response to shear stress', *In Vitro Cell Dev Biol Anim*, 48: 21-9.

El-Menyar, A., M. Zubaid, A. Shehab, B. Bulbanat, N. Albustani, F. Alenezi, A. Al-Motarreb, R. Singh, N. Asaad, and J. Al Suwaidi. 2011. 'Prevalence and impact of cardiovascular risk factors among patients presenting with acute coronary syndrome in the middle East', *Clin Cardiol*, 34: 51-8.

Endo, M. 2000. '[The history and evolution of coronary artery bypass grafting]', *Nihon Geka Gakkai Zasshi*, 101: 827-32.

Fairbairn, L., R. Kapetanovic, D. Beraldi, D. P. Sester, C. K. Tuggle, A. L. Archibald, and D. A. Hume. 2013. 'Comparative analysis of monocyte subsets in the pig', *J Immunol*, 190: 6389-96.

Fasciano, S., R. C. Patel, I. Handy, and C. V. Patel. 2005. 'Regulation of vascular smooth muscle proliferation by heparin: inhibition of cyclin-dependent kinase 2 activity by p27(kip1)', *J Biol Chem*, 280: 15682-9.

Fitzpatrick, J. C., P. M. Clark, and F. M. Capaldi. 2010. 'Effect of decellularization protocol on the mechanical behavior of porcine descending aorta', *Int J Biomater*, 2010.

Flachskampf, Frank A., Michael Schmid, Christian Rost, Stephan Achenbach, Anthony N. DeMaria, and Werner G. Daniel. 2011. 'Cardiac imaging after myocardial infarction', *European Heart Journal*, 32: 272-83.

Flemming, S., N. Burkard, M. Renschler, F. Vielmuth, M. Meir, M. A. Schick, C. Wunder, C. T. Germer, V. Spindler, J. Waschke, and N. Schlegel. 2015. 'Soluble VE-cadherin is involved in endothelial barrier breakdown in systemic inflammation and sepsis', *Cardiovasc Res*, 107: 32-44.

Fowkes, F. G., D. Rudan, I. Rudan, V. Aboyans, J. O. Denenberg, M. M. McDermott, P. E. Norman, U. K. Sampson, L. J. Williams, G. A. Mensah, and M. H. Criqui. 2013. 'Comparison of global estimates of prevalence and risk factors for peripheral artery disease in 2000 and 2010: a systematic review and analysis', *Lancet*, 382: 1329-40.

Franzoni, G., P. Bonelli, S. P. Graham, A. G. Anfossi, S. Dei Giudici, G. Pilo, M. Pittau, P. Nicolussi, and A. Oggiano. 2017. 'Comparative phenotypic and functional analyses of the effects of autologous plasma and recombinant human macrophage-colony stimulating factor (M-CSF) on porcine monocyte to macrophage differentiation', *Vet Immunol Immunopathol*, 187: 80-88.

Fu, R. H., Y. C. Wang, S. P. Liu, T. R. Shih, H. L. Lin, Y. M. Chen, J. H. Sung, C. H. Lu, J. R. Wei, Z. W. Wang, S. J. Huang, C. H. Tsai, W. C. Shyu, and S. Z. Lin. 2014. 'Decellularization and recellularization technologies in tissue engineering', *Cell Transplant*, 23: 621-30.

Gang, E. J., J. A. Jeong, S. Han, Q. Yan, C. J. Jeon, and H. Kim. 2006. 'In vitro endothelial potential of human UC blood-derived mesenchymal stem cells', *Cytotherapy*, 8: 215-27.

Gensini, G. F., M. Comeglio, and A. Colella. 1998. 'Classical risk factors and emerging elements in the risk profile for coronary artery disease', *Eur Heart J*, 19 Suppl A: A53-61.

George, S. J., and A. Dwivedi. 2004. 'MMPs, cadherins, and cell proliferation', *Trends Cardiovasc Med*, 14: 100-5.

George, Sarah Jane, and Jason Dr Johnson. 2010. *Atherosclerosis : molecular and cellular mechanisms*.

Gerli, M. F. M., J. P. Guyette, D. Evangelista-Leite, B. B. Ghoshhajra, and H. C. Ott. 2018. 'Perfusion decellularization of a human limb: A novel platform for composite tissue engineering and reconstructive surgery', *PLoS One*, 13: e0191497.

Gilpin, A., and Y. Yang. 2017. 'Decellularization Strategies for Regenerative Medicine: From Processing Techniques to Applications', *Biomed Res Int*, 2017: 9831534.

Gilpin, S. E., J. P. Guyette, G. Gonzalez, X. Ren, J. M. Asara, D. J. Mathisen, J. P. Vacanti, and H. C. Ott. 2014. 'Perfusion decellularization of human and porcine lungs: bringing the matrix to clinical scale', *J Heart Lung Transplant*, 33: 298-308.

Glagov, S., E. Weisenberg, C. K. Zarins, R. Stankunavicius, and G. J. Kolettis. 1987. 'Compensatory enlargement of human atherosclerotic coronary arteries', *N Engl J Med*, 316: 1371-5.

Glagov, S., C. Zarins, D. P. Giddens, and D. N. Ku. 1988. 'Hemodynamics and atherosclerosis. Insights and perspectives gained from studies of human arteries', *Arch Pathol Lab Med*, 112: 1018-31.

Goldman, S., J. Copeland, T. Moritz, W. Henderson, K. Zadina, T. Ovitt, J. Doherty, R. Read, E. Chesler, Y. Sako, and et al. 1988. 'Improvement in early saphenous vein graft patency after coronary artery bypass surgery with antiplatelet therapy: results of a Veterans Administration Cooperative Study', *Circulation*, 77: 1324-32.

Goodman, J. W., and G. S. Hodgson. 1962. 'Evidence for stem cells in the peripheral blood of mice', *Blood*, 19: 702-14.

Grant, E. G., C. B. Benson, G. L. Moneta, A. V. Alexandrov, J. D. Baker, E. I. Bluth, B. A. Carroll, M. Eliasziw, J. Gocke, B. S. Hertzberg, S. Katarick, L. Needleman, J. Pellerito, J. F. Polak, K. S. Rholl, D. L. Wooster, E. Zierler, and Ultrasound Society of Radiologists in. 2003. 'Carotid artery stenosis: grayscale and Doppler ultrasound diagnosis--Society of Radiologists in Ultrasound consensus conference', *Ultrasound Q*, 19: 190-8.

Grech, E. D. 2003. 'Pathophysiology and investigation of coronary artery disease', *BMJ*, 326: 1027-30.

Griendling, K. K., M. Ushio-Fukai, B. Lassegue, and R. W. Alexander. 1997. 'Angiotensin II signaling in vascular smooth muscle. New concepts', *Hypertension*, 29: 366-73.

Gui, L., A. Muto, S. A. Chan, C. K. Breuer, and L. E. Niklason. 2009. 'Development of decellularized human umbilical arteries as small-diameter vascular grafts', *Tissue Eng Part A*, 15: 2665-76.

Guo, X., and S. Y. Chen. 2012. 'Transforming growth factor-beta and smooth muscle differentiation', *World J Biol Chem*, 3: 41-52.

Guyette, J. P., S. E. Gilpin, J. M. Charest, L. F. Tapias, X. Ren, and H. C. Ott. 2014. 'Perfusion decellularization of whole organs', *Nat Protoc*, 9: 1451-68.

Habib, R. H., K. R. Dimitrova, S. A. Badour, M. B. Yammine, A. K. El-Hage-Sleiman, D. M. Hoffman, C. M. Geller, T. A. Schwann, and R. F. Tranbaugh. 2015. 'CABG Versus PCI: Greater Benefit in Long-Term Outcomes With Multiple Arterial Bypass Grafting', *J Am Coll Cardiol*, 66: 1417-27.

Hafner, J., A. Kuhne, and R. M. Trueb. 2006. 'Successful grafting with EpiDex in pyoderma gangrenosum', *Dermatology*, 212: 258-9.

Hagensen, M. K., P. M. Vanhoutte, and J. F. Bentzon. 2012. 'Arterial endothelial cells: still the craftsmen of regenerated endothelium', *Cardiovasc Res*, 95: 281-9.

Hammond, J. S., T. W. Gilbert, D. Howard, A. Zaitoun, G. Michalopoulos, K. M. Shakesheff, I. J. Beckingham, and S. F. Badylak. 2011. 'Scaffolds containing growth factors and extracellular matrix induce hepatocyte proliferation and cell migration in normal and regenerating rat liver', *J Hepatol*, 54: 279-87.

Han, S. H., W. J. Chung, W. C. Kang, K. Lee, Y. M. Park, M. S. Shin, T. H. Ahn, I. S. Choi, and E. K. Shin. 2012. 'Rosuvastatin combined with ramipril significantly reduced atheroma volume by anti-inflammatory mechanism: comparative analysis with rosuvastatin alone by intravascular ultrasound', *Int J Cardiol*, 158: 217-24.

Hankey, G. J., P. E. Norman, and J. W. Eikelboom. 2006. 'Medical treatment of peripheral arterial disease', *JAMA*, 295: 547-53.

Harskamp, R. E., R. D. Lopes, C. E. Baisden, R. J. de Winter, and J. H. Alexander. 2013. 'Saphenous vein graft failure after coronary artery bypass surgery: pathophysiology, management, and future directions', *Ann Surg*, 257: 824-33.

Hayashi, K. 1975. 'A rapid determination of sodium dodecyl sulfate with methylene blue', *Anal Biochem*, 67: 503-6.

Henriques, J. P. S., and J. Elias. 2017. 'The first generation ABSORB BVS scaffold; to be or not to be?', *Neth Heart J*, 25: 416-18.

Hess, C. N., R. D. Lopes, C. M. Gibson, R. Hager, D. M. Wojdyla, B. R. Englum, M. J. Mack, R. M. Califf, N. T. Kouchoukos, E. D. Peterson, and J. H. Alexander. 2014. 'Saphenous vein graft failure after coronary artery bypass surgery: insights from PREVENT IV', *Circulation*, 130: 1445-51.

Hilenski, Lula L., and Kathy K. Griendling. 2013. 'Chapter 3 - Vascular Smooth Muscle A2 - Creager, Mark A.' in Joshua A. Beckman and Joseph Loscalzo (eds.), *Vascular Medicine: A Companion to Braunwald's Heart Disease (Second Edition)* (W.B. Saunders: Philadelphia).

Hirashima, M., and T. Suda. 2006. 'Differentiation of arterial and venous endothelial cells and vascular morphogenesis', *Endothelium*, 13: 137-45.

Hirsch, A. T., and S. Duval. 2013. 'The global pandemic of peripheral artery disease', *Lancet*, 382: 1312-4.

Hodges, Steve J., and Anthony Atala. 2007. 'Chapter Eighty-Three - Tissue-Engineered Organs.' in Robert LanzaRobert LangerJoseph Vacanti (ed.), *Principles of Tissue Engineering (Third Edition)* (Academic Press: Burlington).

Hong, Y. M. 2010. 'Atherosclerotic cardiovascular disease beginning in childhood', *Korean Circ J*, 40: 1-9.

Huang, A. H., and L. E. Niklason. 2014. 'Engineering of arteries in vitro', *Cell Mol Life Sci*, 71: 2103-18.

Huang, N. F., E. S. Lai, A. J. Ribeiro, S. Pan, B. L. Pruitt, G. G. Fuller, and J. P. Cooke. 2013. 'Spatial patterning of endothelium modulates cell morphology, adhesiveness and transcriptional signature', *Biomaterials*, 34: 2928-37.

Huleihel, L., G. S. Hussey, J. D. Naranjo, L. Zhang, J. L. Dziki, N. J. Turner, D. B. Stolz, and S. F. Badylak. 2016. 'Matrix-bound nanovesicles within ECM bioscaffolds', *Sci Adv*, 2: e1600502.

Huynh, Thanh N., and Robert T. Tranquillo. 2010. 'Fusion of Concentrically Layered Tubular Tissue Constructs Increases Burst Strength', *Annals of Biomedical Engineering*, 38: 2226-36.

Iakovou, I., T. Schmidt, E. Bonizzoni, and et al. 2005. 'INcidence, predictors, and outcome of thrombosis after successful implantation of drug-eluting stents', *JAMA*, 293: 2126-30.

Ielasi, A., A. Latib, and A. Colombo. 2014. 'The diabetic dilemma: which drug-eluting stent works best?', *Minerva Cardioangiol*, 62: 39-57.

Inacio, A. S., K. A. Mesquita, M. Baptista, J. Ramalho-Santos, W. L. Vaz, and O. V. Vieira. 2011. 'In vitro surfactant structure-toxicity relationships: implications for surfactant use in sexually transmitted infection prophylaxis and contraception', *PLoS One*, 6: e19850.

Iqbal, J., J. Gunn, and P. W. Serruys. 2013. 'Coronary stents: historical development, current status and future directions', *British Medical Bulletin*, 106: 193-211.

ISO. 2009. "ISO 10993-5 " In *Biological evaluation of medical devices — Part 5: Tests for in vitro cytotoxicity*. Switzerland, Geneva: International Organization for Standardization (ISO).

Ives, C. L., S. G. Eskin, and L. V. McIntire. 1986. 'Mechanical effects on endothelial cell morphology: in vitro assessment', *In Vitro Cell Dev Biol*, 22: 500-7.

Jacobsen, M. J., C. M. Mentzel, A. S. Olesen, T. Huby, C. B. Jorgensen, R. Barres, M. Fredholm, and D. Simar. 2016. 'Altered Methylation Profile of Lymphocytes Is Concordant with Perturbation of Lipids Metabolism and Inflammatory Response in Obesity', *J Diabetes Res*, 2016: 8539057.

Jahromi, A. S., C. S. Cina, Y. Liu, and C. M. Clase. 2005. 'Sensitivity and specificity of color duplex ultrasound measurement in the estimation of internal carotid artery stenosis: a systematic review and meta-analysis', *J Vasc Surg*, 41: 962-72.

Johnson, Jed. 2015. *Development of Novel, Bioresorbable, Small-Diameter Electrospun Vascular Grafts*.

Jufri, N. F., A. Mohamedali, A. Avolio, and M. S. Baker. 2015. 'Mechanical stretch: physiological and pathological implications for human vascular endothelial cells', *Vasc Cell*, 7: 8.

Jung, J., J. Chang, S. Oh, and M. Choi. 2010. 'Spectral Doppler ultrasound in the major arteries of normal conscious immature micropigs', *J Vet Sci*, 11: 155-9.

Kakos, G. S., H. N. Oldham, Jr., S. H. Dixon, Jr., R. W. Davis, P. O. Hagen, and D. C. Sabiston, Jr. 1972. 'Coronary artery hemodynamics after aorto-coronary artery vein bypass. An experimental evaluation', *J Thorac Cardiovasc Surg*, 63: 849-53.

Kanda, K., T. Matsuda, and T. Oka. 1993. 'Mechanical stress induced cellular orientation and phenotypic modulation of 3-D cultured smooth muscle cells', *Asaio j*, 39: M686-90.

Kannel, W. B. 1976. 'Prospects for prevention of atherosclerosis in the young', *Aust N Z J Med*, 6: 410-9.

Kanz, D., M. Konantz, E. Alghisi, T. E. North, and C. Lengerke. 2016. 'Endothelial-to-hematopoietic transition: Notch-ing vessels into blood', *Ann N Y Acad Sci*, 1370: 97-108.

Karakiulakis, G., E. Papakonstantinou, and M. Roth. 2001. 'Assay for cell migration and invasion of vascular smooth muscle cells', *Methods Mol Med*, 52: 163-9.

Kargar-Abarghouei, E., Z. Vojdani, A. Hassanpour, S. Alaee, and T. Talaei-Khozani. 2018. 'Characterization, recellularization, and transplantation of rat decellularized testis scaffold with bone marrow-derived mesenchymal stem cells', *Stem Cell Res Ther*, 9: 324.

Kastrati, A., J. Mehilli, N. von Beckerath, A. Dibra, J. Hausleiter, J. Pache, H. Schuhlen, C. Schmitt, J. Dirschinger, A. Schomig, and Isar-Desire Study Investigators. 2005. 'Sirolimus-eluting stent or paclitaxel-eluting stent vs balloon angioplasty for prevention of recurrences in patients with coronary in-stent restenosis: a randomized controlled trial', *JAMA*, 293: 165-71.

Kaushal, S., G. E. Amiel, K. J. Guleserian, O. M. Shapira, T. Perry, F. W. Sutherland, E. Rabkin, A. M. Moran, F. J. Schoen, A. Atala, S. Soker, J. Bischoff, and J. E. Mayer, Jr. 2001. 'Functional small-diameter neovessels created using endothelial progenitor cells expanded ex vivo', *Nat Med*, 7: 1035-40.

Kay, John F. 2007. 'Chapter Eighty-One - Tissue-Engineered Bone Products.' in Robert LanzaRobert LangerJoseph Vacanti (ed.), *Principles of Tissue Engineering (Third Edition)* (Academic Press: Burlington).

Keane, T. J., R. Londono, N. J. Turner, and S. F. Badylak. 2012. 'Consequences of ineffective decellularization of biologic scaffolds on the host response', *Biomaterials*, 33: 1771-81.

Kellogg, E. H., N. M. A. Hejab, S. Howes, P. Northcote, J. H. Miller, J. F. Diaz, K. H. Downing, and E. Nogales. 2017. 'Insights into the Distinct Mechanisms of Action of Taxane and Non-Taxane Microtubule Stabilizers from Cryo-EM Structures', *J Mol Biol*, 429: 633-46.

Ketchedjian, A., A. L. Jones, P. Krueger, E. Robinson, K. Crouch, L. Wolfinbarger, Jr., and R. Hopkins. 2005. 'Recellularization of decellularized allograft scaffolds in ovine great vessel reconstructions', *Ann Thorac Surg*, 79: 888-96; discussion 96.

Kim, S. J., J. S. Kim, J. Papadopoulos, S. Wook Kim, M. Maya, F. Zhang, J. He, D. Fan, R. Langley, and I. J. Fidler. 2009. 'Circulating monocytes expressing CD31: implications for acute and chronic angiogenesis', *Am J Pathol*, 174: 1972-80.

Kim, S. J., T. Masaki, J. K. Leypoldt, C. D. Kamerath, S. F. Mohammad, and A. K. Cheung. 2004. 'Arterial and venous smooth-muscle cells differ in their responses to antiproliferative drugs', *J Lab Clin Med*, 144: 156-62.

Kim, S., P. A. Thiessen, E. E. Bolton, J. Chen, G. Fu, A. Gindulyte, L. Han, J. He, S. He, B. A. Shoemaker, J. Wang, B. Yu, J. Zhang, and S. H. Bryant. 2016. 'PubChem Substance and Compound databases', *Nucleic Acids Res*, 44: D1202-13.

Kim, Sang-Hoon, Cho Hay Mun, Youngmee Jung, Sang-Heon Kim, Dong-Ik Kim, and Soo Hyun Kim. 2013. 'Mechanical properties of compliant double layered poly(L-lactide-co-ε-caprolactone) vascular graft', *Macromolecular Research*, 21: 886-91.

Kovacic, J. C., N. Mercader, M. Torres, M. Boehm, and V. Fuster. 2012. 'Epithelial-to-mesenchymal and endothelial-to-mesenchymal transition: from cardiovascular development to disease', *Circulation*, 125: 1795-808.

Kudo, F. A., A. Muto, S. P. Maloney, J. M. Pimiento, S. Bergaya, T. N. Fitzgerald, T. S. Westvik, J. C. Frattini, C. K. Breuer, C. H. Cha, T. Nishibe, G. Tellides, W. C. Sessa, and A. Dardik. 2007. 'Venous identity is lost but arterial identity is not gained during vein graft adaptation', *Arterioscler Thromb Vasc Biol*, 27: 1562-71.

Kumar, Vinay, Stanley L. Robbins, Vinay Kumar, and Ramzi S. Cotran. 2010. *Robbins and Cotran pathologic basis of disease*.

Kuntz, R. E., and D. S. Baim. 1993. 'Defining coronary restenosis. Newer clinical and angiographic paradigms', *Circulation*, 88: 1310-23.

L'Heureux, N., L. Germain, R. Labbe, and F. A. Auger. 1993. 'In vitro construction of a human blood vessel from cultured vascular cells: a morphologic study', *J Vasc Surg*, 17: 499-509.

L'Heureux, N., J. C. Stoclet, F. A. Auger, G. J. Lagaud, L. Germain, and R. Andriantsitohaina. 2001. 'A human tissue-engineered vascular media: a new model for pharmacological studies of contractile responses', *Faseb j*, 15: 515-24.

La, Anh, and Robert T. Tranquillo. 2018. 'Hemocompatible tissue-engineered vascular grafts using adult mesenchymal stem cells', *Current Opinion in Biomedical Engineering*, 5: 66-73.

Lamont, R. E., and S. Childs. 2006. 'MAPping out arteries and veins', *Sci STKE*, 2006: pe39.

Lampugnani, M. G., and E. Dejana. 1997. 'Interendothelial junctions: structure, signalling and functional roles', *Curr Opin Cell Biol*, 9: 674-82.

Lanner, F., M. Sohl, and F. Farnebo. 2007. 'Functional arterial and venous fate is determined by graded VEGF signaling and notch status during embryonic stem cell differentiation', *Arterioscler Thromb Vasc Biol*, 27: 487-93.

Lanza, R. P., R. S. Langer, and W. L. Chick. 1997. *Principles of tissue engineering* (Academic Press).

Lassance, L., H. Miedl, V. Konya, A. Heinemann, B. Ebner, H. Hackl, G. Desoye, and U. Hiden. 2012. 'Differential response of arterial and venous endothelial cells to extracellular matrix is modulated by oxygen', *Histochem Cell Biol*.

Lech, M., and H. J. Anders. 2013. 'Macrophages and fibrosis: How resident and infiltrating mononuclear phagocytes orchestrate all phases of tissue injury and repair', *Biochim Biophys Acta*, 1832: 989-97.

Lee, Kee-Won, Donna B. Stolz, and Yadong Wang. 2011. 'Substantial expression of mature elastin in arterial constructs', *Proceedings of the National Academy of Sciences*, 108: 2705-10.

Leta, Graziela C., Paulo A. S. Mourão, and Ana M. F. Tovar. 2002. 'Human venous and arterial glycosaminoglycans have similar affinity for plasma low-density lipoproteins', *Biochimica et Biophysica Acta (BBA) - Molecular Basis of Disease*, 1586: 243-53.

Levine, David W. 2007. 'Chapter Eighty - Tissue-Engineered Cartilage Products.' in Robert LanzaRobert LangerJoseph Vacanti (ed.), *Principles of Tissue Engineering (Third Edition)* (Academic Press: Burlington).

Li, Y. S., J. H. Haga, and S. Chien. 2005. 'Molecular basis of the effects of shear stress on vascular endothelial cells', *J Biomech*, 38: 1949-71.

Liang, M., Y. Wang, A. Liang, W. E. Mitch, P. Roy-Chaudhury, G. Han, and J. Cheng. 2015. 'Migration of smooth muscle cells from the arterial anastomosis of arteriovenous fistulas requires Notch activation to form neointima', *Kidney Int*, 88: 490-502.

Libby, P., and K. V. O'Brien. 1983. 'Culture of quiescent arterial smooth muscle cells in a defined serum-free medium', *J Cell Physiol*, 115: 217-23.

Lin, C. H., K. Hsia, H. Ma, H. Lee, and J. H. Lu. 2018. 'In Vivo Performance of Decellularized Vascular Grafts: A Review Article', *Int J Mol Sci*, 19.

Liu, Z. J., T. Shirakawa, Y. Li, A. Soma, M. Oka, G. P. Dotto, R. M. Fairman, O. C. Velazquez, and M. Herlyn. 2003. 'Regulation of Notch1 and Dll4 by vascular endothelial growth factor in arterial endothelial cells: implications for modulating arteriogenesis and angiogenesis', *Mol Cell Biol*, 23: 14-25.

Locker, C., H. V. Schaff, R. C. Daly, J. A. Dearani, M. R. Bell, R. L. Frye, K. L. Greason, J. M. Stulak, L. D. Joyce, A. Pochettino, Z. Li, R. J. Lennon, and A. Lerman. 2016. 'Multiple arterial grafts improve survival with coronary artery bypass graft surgery versus conventional coronary artery bypass grafting compared with percutaneous coronary interventions', *J Thorac Cardiovasc Surg*, 152: 369-79 e4.

Loesch, A., P. Milner, S. C. Anglin, R. Crowe, S. Miah, J. R. McEwan, and G. Burnstock. 1997. 'Ultrastructural localisation of nitric oxide synthase, endothelin and binding sites of lectin (from Bandeirea simplicifolia) in the rat carotid artery after balloon catheter injury', *J Anat*, 190 (Pt 1): 93-104.

Loop, F. D., B. W. Lytle, D. M. Cosgrove, R. W. Stewart, M. Goormastic, G. W. Williams, L. A. Golding, C. C. Gill, P. C. Taylor, W. C. Sheldon, and et al. 1986. 'Influence of the internal-mammary-artery graft on 10-year survival and other cardiac events', *N Engl J Med*, 314: 1-6.

Lopez-Soler, R. I., M. P. Brennan, A. Goyal, Y. Wang, P. Fong, G. Tellides, A. Sinusas, A. Dardik, and C. Breuer. 2007. 'Development of a mouse model for evaluation of small diameter vascular grafts', *J Surg Res*, 139: 1-6.

Lu, J. T., and M. A. Creager. 2004. 'The relationship of cigarette smoking to peripheral arterial disease', *Rev Cardiovasc Med*, 5: 189-93.

Lu, L., D. F. Mackay, and J. P. Pell. 2014. 'Meta-analysis of the association between cigarette smoking and peripheral arterial disease', *Heart*, 100: 414-23.

Lü, Wei-Dong, Ming Zhang, Zhong-Shi Wu, and Tie-Hui Hu. 2009. 'Decellularized and photooxidatively crosslinked bovine jugular veins as potential tissue engineering scaffolds', *Interactive CardioVascular and Thoracic Surgery*, 8: 301-05.

Lüscher, Thomas F., Jan Steffel, Franz R. Eberli, Michael Joner, Gaku Nakazawa, Felix C. Tanner, and Renu Virmani. 2007. 'Drug-Eluting Stent and Coronary Thrombosis: Biological Mechanisms and Clinical Implications', *Circulation*, 115: 1051-58.

Maas, S. L. N., X. O. Breakefield, and A. M. Weaver. 2017. 'Extracellular Vesicles: Unique Intercellular Delivery Vehicles', *Trends Cell Biol*, 27: 172-88.

Majesky, Mark W., Xiu Rong Dong, Jenna N. Regan, and Virginia J. Hoglund. 2011. 'Vascular Smooth Muscle Progenitor Cells: Building and Repairing Blood Vessels', *Circulation Research*, 108: 365-77.

Mangano, D. T. 2002. 'Aspirin and mortality from coronary bypass surgery ', *N Engl J Med*, 347: 1309-17.

Mann, Douglas L., Douglas P. Zipes, Peter Libby, Robert O. Bonow, and Eugene Braunwald. 2015. *Braunwald's heart disease : a textbook of cardiovascular medicine* (Elsevier/Saunders: Philadelphia, PA).

Mansbridge, Jonathan. 2007. 'Chapter Seventy-Nine - Tissue-Engineered Skin Products.' in Robert LanzaRobert LangerJoseph Vacanti (ed.), *Principles of Tissue Engineering (Third Edition)* (Academic Press: Burlington).

Marieb, E.N., and K.N. Hoehn. 2015. *Human Anatomy & Physiology* (Pearson Education).

Marin, A. C., T. Grossi, E. Bianchi, G. Dubini, and D. Lacroix. 2017. 'micro-Particle tracking velocimetry and computational fluid dynamics study of cell seeding within a 3D porous scaffold', *J Mech Behav Biomed Mater*, 75: 463-69.

Martin-Ramirez, J., M. Hofman, M. van den Biggelaar, R. P. Hebbel, and J. Voorberg. 2012. 'Establishment of outgrowth endothelial cells from peripheral blood', *Nat Protoc*, 7: 1709-15.

Martin, N. D., P. J. Schaner, T. N. Tulenko, I. M. Shapiro, C. A. Dimatteo, T. K. Williams, E. S. Hager, and P. J. DiMuzio. 2005. 'In vivo behavior of decellularized vein allograft', *J Surg Res*, 129: 17-23.

Masugi, Y., T. Abe, H. Tsujikawa, K. Effendi, A. Hashiguchi, M. Abe, Y. Imai, K. Hino, S. Hige, M. Kawanaka, G. Yamada, M. Kage, M. Korenaga, Y. Hiasa, M. Mizokami, and M. Sakamoto. 2018. 'Quantitative assessment of liver fibrosis reveals a nonlinear association with fibrosis stage in nonalcoholic fatty liver disease', *Hepatol Commun*, 2: 58-68.

Mathapati, Santosh, Satish Galla, Kavitha Sankaranarayanan, Rama Shanker Verma, Kotturathu Mammen Cherian, and Soma Guhathakurta. 2010. 'Qualitative and quantitative detection of sodium deoxycholic acid in decellularized tissue', *Indian Journal of Thoracic and Cardiovascular Surgery*, 26: 129-31.

McCredie, K. B., E. M. Hersh, and E. J. Freireich. 1971. 'Cells capable of colony formation in the peripheral blood of man', *Science*, 171: 293-4.

McFadden, Eugène P., Eugenio Stabile, Evelyn Regar, Edouard Cheneau, Andrew T. L. Ong, Timothy Kinnaird, William O. Suddath, Neil J. Weissman, Rebecca Torguson, Kenneth M. Kent, August D. Pichard, Lowell F. Satler, Ron Waksman, and Patrick W. Serruys. 'Late thrombosis in drug-eluting coronary stents after discontinuation of antiplatelet therapy', *The Lancet*, 364: 1519-21.

Medina, R. J., C. L. Barber, F. Sabatier, F. Dignat-George, J. M. Melero-Martin, K. Khosrotehrani, O. Ohneda, A. M. Randi, J. K. Y. Chan, T. Yamaguchi, V. W. M. Van Hinsbergh, M. C. Yoder, and A. W. Stitt. 2017. 'Endothelial Progenitors: A Consensus Statement on Nomenclature', *Stem Cells Transl Med*, 6: 1316-20.

Mehran, R., G. Dangas, A. S. Abizaid, G. S. Mintz, A. J. Lansky, L. F. Satler, A. D. Pichard, K. M. Kent, G. W. Stone, and M. B. Leon. 1999. 'Angiographic patterns of in-stent restenosis: classification and implications for long-term outcome', *Circulation*, 100: 1872-8.

Mendis, S., P. Puska, and B. Norrving. 2011. *Global atlas on cardiovascular disease prevention and control* (World Health Organization: Geneva).

Meyer, S. R., B. Chiu, T. A. Churchill, L. Zhu, J. R. Lakey, and D. B. Ross. 2006. 'Comparison of aortic valve allograft decellularization techniques in the rat', *J Biomed Mater Res A*, 79: 254-62.

Mikawa, T., and R. G. Gourdie. 1996. 'Pericardial mesoderm generates a population of coronary smooth muscle cells migrating into the heart along with ingrowth of the epicardial organ', *Dev Biol*, 174: 221-32.

Miller, S. A., D. D. Dykes, and H. F. Polesky. 1988. 'A simple salting out procedure for extracting DNA from human nucleated cells', *Nucleic Acids Res*, 16: 1215.

Mirensky, T. L., N. Hibino, R. F. Sawh-Martinez, T. Yi, G. Villalona, T. Shinoka, and C. K. Breuer. 2010. 'Tissue-engineered vascular grafts: does cell seeding matter?', *J Pediatr Surg*, 45: 1299-305.

Misra, A. 2000. 'Risk factors for atherosclerosis in young individuals', *J Cardiovasc Risk*, 7: 215-29.

Mohr, F. W., M. C. Morice, A. P. Kappetein, T. E. Feldman, E. Stahle, A. Colombo, M. J. Mack, D. R. Holmes, Jr., M. A. Morel, N. Van Dyck, V. M. Houle, K. D. Dawkins, and P. W. Serruys. 2013. 'Coronary artery bypass graft surgery versus percutaneous coronary intervention in patients with three-vessel disease and left main coronary disease: 5-year follow-up of the randomised, clinical SYNTAX trial', *Lancet*, 381: 629-38.

Montalescot, G., U. Sechtem, S. Achenbach, F. Andreotti, C. Arden, A. Budaj, R. Bugiardini, F. Crea, T. Cuisset, C. Di Mario, J. Rafael Ferreira, B. J. Gersh, A. K. Gitt, J. S. Hulot, N. Marx, L. H. Opie, M. Pfisterer, E. Prescott, F. Ruschitzka, M. Sabate, R. Senior, D. P. Taggart, E. E. van der Wall, and

C. J. M. Vrints. 2013. '2013 ESC guidelines on the management of stable coronary artery disease', *European Heart Journal*, 34: 2949-3003.

———. 2014. 'Corrigendum to: '2013 ESC guidelines on the management of stable coronary artery disease'', *European Heart Journal*, 35: 2260-61.

Morley, R. L., A. Sharma, A. D. Horsch, and R. J. Hinchliffe. 2018. 'Peripheral artery disease', *BMJ*, 360: j5842.

Moroni, F., and T. Mirabella. 2014. 'Decellularized matrices for cardiovascular tissue engineering', *American Journal of Stem Cells* 3: 1-20.

Motwani, J. G., and E. J. Topol. 1998. 'Aortocoronary saphenous vein graft disease: pathogenesis, predisposition, and prevention', *Circulation*, 97: 916-31.

Muller-Marschhausen, K., J. Waschke, and D. Drenckhahn. 2008. 'Physiological hydrostatic pressure protects endothelial monolayer integrity', *Am J Physiol Cell Physiol*, 294: C324-32.

Murphy, CM, FJ O'Brien, DG Little, and A Schindeler. 2013. 'Cell-scaffold interactions in the bone tissue engineering triad', *European cells and materials*, 26: 120-32.

Murphy, G. J., and G. D. Angelini. 2004. 'Insights into the pathogenesis of vein graft disease: lessons from intravascular ultrasound', *Cardiovasc Ultrasound*, 2: 8.

Negishi, J., S. Funamoto, T. Kimura, K. Nam, T. Higami, and A. Kishida. 2015. 'Porcine radial artery decellularization by high hydrostatic pressure', *J Tissue Eng Regen Med*, 9: E144-51.

Nemeno-Guanzon, Judee Grace, Soojung Lee, Johan Robert Berg, Yong Hwa Jo, Jee Eun Yeo, Bo Mi Nam, Yong-Gon Koh, and Jeong Ik Lee. 2012. 'Trends in Tissue Engineering for Blood Vessels', *Journal of Biomedicine and Biotechnology*, 2012: 14.

Nezarati, Roya M., Michelle B. Eifert, David K. Dempsey, and Elizabeth Cosgriff-Hernandez. 2015. 'Electrospun vascular grafts with improved compliance matching to native vessels', *Journal of Biomedical Materials Research Part B: Applied Biomaterials*, 103: 313-23.

Nichols, M., N. Townsend, P. Scarborough, and M. Rayner. 2014. 'Cardiovascular disease in Europe 2014: epidemiological update', *Eur Heart J*, 35: 2950-9.

Nieponice, A., L. Soletti, J. Guan, B. M. Deasy, J. Huard, W. R. Wagner, and D. A. Vorp. 2008. 'Development of a tissue-engineered vascular graft combining a biodegradable scaffold, muscle-derived stem cells and a rotational vacuum seeding technique', *Biomaterials*, 29: 825-33.

Niklason, L. E., J. Gao, W. M. Abbott, K. K. Hirschi, S. Houser, R. Marini, and R. Langer. 1999. 'Functional Arteries Grown in Vitro', *Science*, 284: 489-93.

Novak, M. L., and T. J. Koh. 2013. 'Phenotypic transitions of macrophages orchestrate tissue repair', *Am J Pathol*, 183: 1352-63.

O'Brien, Fergal J. 2011. 'Biomaterials & scaffolds for tissue engineering', *Materials Today*, 14: 88-95.

O'Neill, J. D., R. Anfang, A. Anandappa, J. Costa, J. Javidfar, H. M. Wobma, G. Singh, D. O. Freytes, M. D. Bacchetta, J. R. Sonett, and G. Vunjak-Novakovic. 2013. 'Decellularization of human and porcine lung tissues for pulmonary tissue engineering', *Ann Thorac Surg*, 96: 1046-55; discussion 55-6.

Obi, S., H. Masuda, T. Shizuno, A. Sato, K. Yamamoto, J. Ando, Y. Abe, and T. Asahara. 2012. 'Fluid shear stress induces differentiation of circulating phenotype endothelial progenitor cells', *Am J Physiol Cell Physiol*, 303: C595-606.

Obi, S., K. Yamamoto, N. Shimizu, S. Kumagaya, T. Masumura, T. Sokabe, T. Asahara, and J. Ando. 2009. 'Fluid shear stress induces arterial differentiation of endothelial progenitor cells', *J Appl Physiol (1985)*, 106: 203-11.

Oktar, S.O., C. Yücel, D. Karaosmanoglu, K. Akkan, H. Ozdemir, N. Tokgoz, and T. Tali. 2006. 'Blood-Flow Volume Quantification in Internal Carotid and Vertebral Arteries: Comparison of 3 Different Ultrasound Techniques with Phase-Contrast MR Imaging', *American Journal of Neuroradiology*, 27: 363-69.

Olausson, M., V. K. Kuna, G. Travnikova, H. Backdahl, P. B. Patil, R. Saalman, H. Borg, A. Jeppsson, and S. Sumitran-Holgersson. 2014. 'In Vivo Application of Tissue-Engineered Veins Using Autologous Peripheral Whole Blood: A Proof of Concept Study', *EBioMedicine*, 1: 72-9.

Olausson, M., P. B. Patil, V. K. Kuna, P. Chougule, N. Hernandez, K. Methe, C. Kullberg-Lindh, H. Borg, H. Ejnell, and S. Sumitran-Holgersson. 2012. 'Transplantation of an allogeneic vein bioengineered with autologous stem cells: a proof-of-concept study', *Lancet*, 380: 230-7.

Olyslaegers, D. A., L. M. Desmarets, A. Dedeurwaerder, H. L. Dewerchin, and H. J. Nauwynck. 2013. 'Generation and characterization of feline arterial and venous endothelial cell lines for the study of the vascular endothelium', *BMC Vet Res*, 9: 170.

Ong, Chin Siang, Xun Zhou, Chen Yu Huang, Takuma Fukunishi, Huaitao Zhang, and Narutoshi Hibino. 2017. 'Tissue engineered vascular grafts: current state of the field', *Expert Review of Medical Devices*, 14: 383-92.

Opitz, F., K. Schenke-Layland, W. Richter, D. P. Martin, I. Degenkolbe, T. Wahlers, and U. A. Stock. 2004. 'Tissue engineering of ovine aortic blood vessel substitutes using applied shear stress and enzymatically derived vascular smooth muscle cells', *Ann Biomed Eng*, 32: 212-22.

Ormiston, M. L., M. R. Toshner, F. N. Kiskin, C. J. Huang, E. Groves, N. W. Morrell, and A. A. Rana. 2015. 'Generation and Culture of Blood Outgrowth Endothelial Cells from Human Peripheral Blood', *J Vis Exp*: e53384.

Orr, A. W., N. E. Hastings, B. R. Blackman, and B. R. Wamhoff. 2010. 'Complex regulation and function of the inflammatory smooth muscle cell phenotype in atherosclerosis', *J Vasc Res*, 47: 168-80.

Ortega-Zilic, N., T. Hunziker, S. Lauchli, D. O. Mayer, C. Huber, K. Baumann Conzett, K. Sippel, L. Borradori, L. E. French, and J. Hafner. 2010. 'EpiDex(R) Swiss field trial 2004-2008', *Dermatology*, 221: 365-72.

Otsuka, Fumiyuki, Kazuyuki Yahagi, Kenichi Sakakura, and Renu Virmani. 2013. 'Why is the mammary artery so special and what protects it from atherosclerosis?', *Annals of Cardiothoracic Surgery*, 2: 519-26.

Pape, S. A., and P. O. Byrne. 2000. 'Safety and efficacy of TransCyte for the treatment of partial-thickness burns', *J Burn Care Rehabil*, 21: 390.

Parang, P., and R. Arora. 2009. 'Coronary vein graft disease: pathogenesis and prevention', *Can J Cardiol*, 25: e57-62.

Parker, W., and P. S. Song. 1992. 'Protein structures in SDS micelle-protein complexes', *Biophys J*, 61: 1435-9.

Pashneh-Tala, S., S. MacNeil, and F. Claeyssens. 2015. 'The Tissue-Engineered Vascular Graft-Past, Present, and Future', *Tissue Eng Part B Rev*.

Patel, J., P. Donovan, and K. Khosrotehrani. 2016. 'Concise Review: Functional Definition of Endothelial Progenitor Cells: A Molecular Perspective', *Stem Cells Transl Med*, 5: 1302-06.

Pearson, T. A., S. N. Blair, S. R. Daniels, R. H. Eckel, J. M. Fair, S. P. Fortmann, B. A. Franklin, L. B. Goldstein, P. Greenland, S. M. Grundy, Y. Hong, N. H. Miller, R. M. Lauer, I. S. Ockene, R. L. Sacco, J. F. Sallis, Jr., S. C. Smith, Jr., N. J. Stone, and K. A. Taubert. 2002. "AHA Guidelines for Primary Prevention of Cardiovascular Disease and Stroke: 2002 Update: Consensus Panel Guide to Comprehensive Risk Reduction for Adult Patients Without Coronary or Other Atherosclerotic Vascular Diseases. American Heart Association Science Advisory and Coordinating Committee." In *Circulation*, 388-91.

Peck, M., D. Gebhart, N. Dusserre, T. N. McAllister, and N. L'Heureux. 2012. 'The evolution of vascular tissue engineering and current state of the art', *Cells Tissues Organs*, 195: 144-58.

Pelissier, A., P. Boyer, Y. Boussetta, G. Bierry, W. Van Hille, P. Hamon, J. H. Jaeger, and P. Massin. 2014. 'Satisfactory long-term MRI after autologous chondrocyte implantation at the knee', *Knee Surg Sports Traumatol Arthrosc*, 22: 2007-12.

Perez, V. A., Z. Ali, T. P. Alastalo, F. Ikeno, H. Sawada, Y. J. Lai, T. Kleisli, E. Spiekerkoetter, X. Qu, L. H. Rubinos, E. Ashley, M. Amieva, S. Dedhar, and M. Rabinovitch. 2011. 'BMP promotes motility and represses growth of smooth muscle cells by activation of tandem Wnt pathways', *J Cell Biol*, 192: 171-88.

Porth, Carol, Glenn Matfin, and Carol Porth. 2009. *Pathophysiology : concepts of altered health states* (Wolters Kluwer Health/Lippincott Williams & Wilkins: Philadelphia, PA).

Poston, R. S., J. Gu, J. M. Brown, J. S. Gammie, C. White, L. Nie, R. N. Pierson, 3rd, and B. P. Griffith. 2006. 'Endothelial injury and acquired aspirin resistance as promoters of regional thrombin formation and early vein graft failure after coronary artery bypass grafting', *J Thorac Cardiovasc Surg*, 131: 122-30.

Powell, T. M., J. D. Paul, J. M. Hill, M. Thompson, M. Benjamin, M. Rodrigo, J. P. McCoy, E. J. Read, H. M. Khuu, S. F. Leitman, T. Finkel, and R. O. Cannon, 3rd. 2005. 'Granulocyte colony-stimulating factor mobilizes functional endothelial progenitor cells in patients with coronary artery disease', *Arterioscler Thromb Vasc Biol*, 25: 296-301.

Privratsky, J. R., D. K. Newman, and P. J. Newman. 2010. 'PECAM-1: conflicts of interest in inflammation', *Life Sci*, 87: 69-82.

Proudfoot, D., and C. Shanahan. 2012. 'Human vascular smooth muscle cell culture', *Methods Mol Biol*, 806: 251-63.

Punshon, G., K. M. Sales, D. S. Vara, G. Hamilton, and A. M. Seifalian. 2008. 'Assessment of the potential of progenitor stem cells extracted from human peripheral blood for seeding a novel vascular graft material', *Cell Prolif*, 41: 321-35.

Quint, C., M. Arief, A. Muto, A. Dardik, and L. E. Niklason. 2012. 'Allogeneic human tissue-engineered blood vessel', *J Vasc Surg*, 55: 790-8.

Quint, C., Y. Kondo, R. J. Manson, J. H. Lawson, A. Dardik, and L. E. Niklason. 2011. 'Decellularized tissue-engineered blood vessel as an arterial conduit', *Proc Natl Acad Sci U S A*, 108: 9214-9.

Raja, S. G., U. Benedetto, C. D. Ilsley, M. Amrani, and Group Harefield Cardiac Outcomes Research. 2015. 'Multiple arterial grafting confers survival advantage compared to percutaneous intervention with drug-eluting stents in multivessel coronary artery disease: A propensity score adjusted analysis', *Int J Cardiol*, 189: 153-8.

Ramanathan, Tamilselvi, and Henry Skinner. 2005. 'Coronary blood flow', *Continuing Education in Anaesthesia Critical Care & Pain*, 5: 61-64.

Rambol, M. H., J. Hisdal, J. O. Sundhagen, J. E. Brinchmann, and A. Rosales. 2018. 'Recellularization of Decellularized Venous Grafts Using Peripheral Blood: A Critical Evaluation', *EBioMedicine*, 32: 215-22.

Ratcliffe, Anthony. 2011. 'The translation of product concept to bone products: a partnership of therapeutic effectiveness and commercialization', *Tissue Engineering Part B: Reviews*, 17: 443-47.

Ravi, Swathi, and Elliot L. Chaikof. 2010. 'Biomaterials for vascular tissue engineering', *Regenerative medicine*, 5: 107.

Reing, J. E., L. Zhang, J. Myers-Irvin, K. E. Cordero, D. O. Freytes, E. Heber-Katz, K. Bedelbaeva, D. McIntosh, A. Dewilde, S. J. Braunhut, and S. F. Badylak. 2009. 'Degradation products of extracellular matrix affect cell migration and proliferation', *Tissue Eng Part A*, 15: 605-14.

Rensen, S. S., P. A. Doevendans, and G. J. van Eys. 2007. 'Regulation and characteristics of vascular smooth muscle cell phenotypic diversity', *Neth Heart J*, 15: 100-8.

Robbins, P. D., and A. E. Morelli. 2014. 'Regulation of immune responses by extracellular vesicles', *Nat Rev Immunol*, 14: 195-208.

Robinson, K. A., J. Li, M. Mathison, A. Redkar, J. Cui, N. A. Chronos, R. G. Matheny, and S. F. Badylak. 2005. 'Extracellular matrix scaffold for cardiac repair', *Circulation*, 112: I135-43.

Rodgerson, D. H., J. K. Belknap, G. L. Fontaine, and D. L. Kroll. 2000. 'Characterization of cultured smooth muscle cells obtained from the palmar digital arteries of horses', *Am J Vet Res*, 61: 1602-8.

Roffi, M., C. Patrono, J. P. Collet, C. Mueller, M. Valgimigli, F. Andreotti, J. J. Bax, M. A. Borger, C. Brotons, D. P. Chew, B. Gencer, G. Hasenfuss, K. Kjeldsen, P. Lancellotti, U. Landmesser, J. Mehilli, D. Mukherjee, R. F. Storey, S. Windecker, and E. S. C. Scientific Document Group. 2016. '2015 ESC Guidelines for the management of acute coronary syndromes in patients presenting without persistent ST-segment elevation: Task Force for the Management of Acute Coronary Syndromes in Patients Presenting without Persistent ST-Segment Elevation of the European Society of Cardiology (ESC)', *Eur Heart J*, 37: 267-315.

Rooke, T. W., A. T. Hirsch, S. Misra, A. N. Sidawy, J. A. Beckman, L. Findeiss, J. Golzarian, H. L. Gornik, M. R. Jaff, G. L. Moneta, J. W. Olin, J. C. Stanley, C. J. White, J. V. White, R. E. Zierler, Force American College of Cardiology Foundation Task, and Force American Heart Association Task. 2013. 'Management of patients with peripheral artery disease (compilation of 2005 and 2011 ACCF/AHA Guideline Recommendations): a report of the American College of Cardiology Foundation/American Heart Association Task Force on Practice Guidelines', *J Am Coll Cardiol*, 61: 1555-70.

Ross, R. 1999. 'Atherosclerosis--an inflammatory disease', *N Engl J Med*, 340: 115-26.

Roubos, N., F. L. Rosenfeldt, S. M. Richards, R. A. Conyers, and B. B. Davis. 1995. 'Improved preservation of saphenous vein grafts by the use of glyceryl trinitrate-verapamil solution during harvesting', *Circulation*, 92: II31-6.

Rzucidlo, E. M., K. A. Martin, and R. J. Powell. 2007. 'Regulation of vascular smooth muscle cell differentiation', *J Vasc Surg*, 45 Suppl A: A25-32.

Sambanis, Athanassios. 2007. 'Chapter Forty-Two - Bioartificial Pancreas.' in Robert LanzaRobert LangerJoseph Vacanti (ed.), *Principles of Tissue Engineering (Third Edition)* (Academic Press: Burlington).

Sanders, B., A. Driessen-Mol, C. V. C. Bouten, and F. P. T. Baaijens. 2017. 'The Effects of Scaffold Remnants in Decellularized Tissue-Engineered Cardiovascular Constructs on the Recruitment of Blood Cells<sup/>', *Tissue Eng Part A*, 23: 1142-51.

Sauvage, L. R., J. C. Smith, C. C. Davis, E. A. Rittenhouse, D. G. Hall, and P. B. Mansfield. 1986. 'Dacron® Arterial Grafts: Comparative Structures and Basis for Successful Use of Current Prostheses': 16-16-9.

Schaner, P. J., N. D. Martin, T. N. Tulenko, I. M. Shapiro, N. A. Tarola, R. F. Leichter, R. A. Carabasi, and P. J. Dimuzio. 2004. 'Decellularized vein as a potential scaffold for vascular tissue engineering', *J Vasc Surg*, 40: 146-53.

Schror, K. 1997. 'Aspirin and platelets: the antiplatelet action of aspirin and its role in thrombosis treatment and prophylaxis', *Semin Thromb Hemost*, 23: 349-56.

Schulte, Julia, Anja Friedrich, Trixi Hollweck, Fabian König, Markus Eblenkamp, Andres Beiras-Fernandez, Cornelia Fano, Christian Hagl, and Bassil Akra. 2014. 'A Novel Seeding and Conditioning Bioreactor for Vascular Tissue Engineering', *Processes*, 2: 526.

Sclavo, M. 2001. '[Cardiovascular risk factors and prevention in women: similarities and differences]', *Ital Heart J Suppl*, 2: 125-41.

Scott, D. W., and R. P. Patel. 2013. 'Endothelial heterogeneity and adhesion molecules N-glycosylation: implications in leukocyte trafficking in inflammation', *Glycobiology*, 23: 622-33.

Scruggs, A. K., E. A. Cioffi, D. L. Cioffi, J. A. King, and N. N. Bauer. 2015. 'Lectin-Based Characterization of Vascular Cell Microparticle Glycocalyx', *PLoS One*, 10: e0135533.

Seddon, A. M., P. Curnow, and P. J. Booth. 2004. 'Membrane proteins, lipids and detergents: not just a soap opera', *Biochim Biophys Acta*, 1666: 105-17.

Serruys, P. W., B. Chevalier, Y. Sotomi, A. Cequier, D. Carrie, J. J. Piek, A. J. Van Boven, M. Dominici, D. Dudek, D. McClean, S. Helqvist, M. Haude, S. Reith, M. de Sousa Almeida, G. Campo, A. Iniguez, M. Sabate, S. Windecker, and Y. Onuma. 2016. 'Comparison of an everolimus-eluting bioresorbable scaffold with an everolimus-eluting metallic stent for the treatment of coronary artery stenosis (ABSORB II): a 3 year, randomised, controlled, single-blind, multicentre clinical trial', *Lancet*, 388: 2479-91.

Serruys, Patrick W., Marie-Claude Morice, A. Pieter Kappetein, Antonio Colombo, David R. Holmes, Michael J. Mack, Elisabeth Ståhle, Ted E. Feldman, Marcel van den Brand, Eric J. Bass, Nic Van Dyck, Katrin Leadley, Keith D. Dawkins, and Friedrich W. Mohr. 2009. 'Percutaneous Coronary Intervention versus Coronary-Artery Bypass Grafting for Severe Coronary Artery Disease', *New England Journal of Medicine*, 360: 961-72.

Setton, Lori A., Lawrence J. Bonassar, and Koichi Masuda. 2007. 'Chapter Fifty-Eight - Regeneration and Replacement of the Intervertebral Disc.' in Robert LanzaRobert LangerJoseph Vacanti (ed.), *Principles of Tissue Engineering (Third Edition)* (Academic Press: Burlington).

Shai, I., J. D. Spence, D. Schwarzfuchs, Y. Henkin, G. Parraga, A. Rudich, A. Fenster, C. Mallett, N. Liel-Cohen, A. Tirosh, A. Bolotin, J. Thiery, G. M. Fiedler, M. Bluher, M. Stumvoll, M. J. Stampfer, and Direct Group. 2010. 'Dietary intervention to reverse carotid atherosclerosis', *Circulation*, 121: 1200-8.

Shanahan, C. M., P. L. Weissberg, and J. C. Metcalfe. 1993. 'Isolation of gene markers of differentiated and proliferating vascular smooth muscle cells', *Circ Res*, 73: 193-204.

Shin, Young Min, Hyeok Jun Shin, Yunhoe Heo, Indong Jun, Yong-Woo Chung, Kyeongsoo Kim, Youn Mook Lim, Hojeong Jeon, and Heungsoo Shin. 2016. *Engineering an aligned endothelial*

monolayer on a topologically modified nanofibrous platform with a micropatterned structure produced by femtosecond laser ablation.

Silvestre, J. S., and Z. Mallat. 2006. 'Arteries or veins?: VEGF helps EPCs choose their cAMP', *Arterioscler Thromb Vasc Biol*, 26: 1934-5.

Singh, R. B., S. A. Mengi, Y. J. Xu, A. S. Arneja, and N. S. Dhalla. 2002. 'Pathogenesis of atherosclerosis: A multifactorial process', *Exp Clin Cardiol*, 7: 40-53.

Singleton, H., S. P. Graham, K. B. Bodman-Smith, J. P. Frossard, and F. Steinbach. 2016. 'Establishing Porcine Monocyte-Derived Macrophage and Dendritic Cell Systems for Studying the Interaction with PRRSV-1', *Front Microbiol*, 7: 832.

Sipahi, I., E. M. Tuzcu, P. Schoenhagen, S. J. Nicholls, V. Ozduran, S. Kapadia, and S. E. Nissen. 2006. 'Compensatory enlargement of human coronary arteries during progression of atherosclerosis is unrelated to atheroma burden: serial intravascular ultrasound observations from the REVERSAL trial', *Eur Heart J*, 27: 1664-70.

Sisto, T., S. Yla-Herttuala, J. Luoma, H. Riekkinen, and T. Nikkari. 1990. 'Biochemical composition of human internal mammary artery and saphenous vein', *J Vasc Surg*, 11: 418-22.

Skalak, Richard, and C Fred Fox. 1988. *Tissue engineering: proceedings of a workshop, held at Granlibakken, Lake Tahoe, California, February 26-29, 1988* (Alan R. Liss).

Smith, Anthony J., and Paul T. Sharpe. 2007. 'Chapter Seventy - Biological Tooth Replacement and Repair.' in Robert LanzaRobert LangerJoseph Vacanti (ed.), *Principles of Tissue Engineering (Third Edition)* (Academic Press: Burlington).

Snider, F., and C. Vincenzoni. 2001. 'Carotid endarterectomy. Which diagnostic imaging technique is suitable for the indication and planning of surgery?', *Rays*, 26: 231-6.

Soletti, L., Y. Hong, J. Guan, J. J. Stankus, M. S. El-Kurdi, W. R. Wagner, and D. A. Vorp. 2010. 'A bilayered elastomeric scaffold for tissue engineering of small diameter vascular grafts', *Acta Biomater*, 6: 110-22.

Sotoda, Y., S. Hirooka, H. Orita, and I. Wakabayashi. 2015. '[Recent Knowledge of Smoking and Peripheral Arterial Disease in Lower Extremities]', *Nihon Eiseigaku Zasshi*, 70: 211-9.

Stegemann, H., and K. Stalder. 1967. 'Determination of hydroxyproline', *Clin Chim Acta*, 18: 267-73.

Stein, P. D., H. J. Schunemann, J. E. Dalen, and D. Gutterman. 2004. 'Antithrombotic therapy in patients with saphenous vein and internal mammary artery bypass grafts: the Seventh ACCP Conference on Antithrombotic and Thrombolytic Therapy', *Chest*, 126: 600S-08S.

Sun, L., K. Niwa, J. Z. Lin, and T. Karino. 2005. 'Cellular growth under hydrostatic pressure using bovine aortic EC-SMC co-cultured ePTFE vascular graft', *J Zhejiang Univ Sci B*, 6: 79-82.

Sun, Y., P. L. Filho, J. C. Bozelli, Jr., J. Carvalho, S. Schreier, and C. L. Oliveira. 2015. 'Unfolding and folding pathway of lysozyme induced by sodium dodecyl sulfate', *Soft Matter*, 11: 7769-77.

Sur, S., J. T. Sugimoto, and D. K. Agrawal. 2014. 'Coronary artery bypass graft: why is the saphenous vein prone to intimal hyperplasia?', *Can J Physiol Pharmacol*, 92: 531-45.

Suwanabol, P. A., S. M. Seedial, X. Shi, F. Zhang, D. Yamanouchi, D. Roenneburg, B. Liu, and K. C. Kent. 2012. 'Transforming growth factor-beta increases vascular smooth muscle cell proliferation through the Smad3 and extracellular signal-regulated kinase mitogen-activated protein kinases pathways', *J Vasc Surg*, 56: 446-54.

Suzuki, E., D. Nagata, M. Yoshizumi, M. Kakoki, A. Goto, M. Omata, and Y. Hirata. 2000. 'Reentry into the cell cycle of contact-inhibited vascular endothelial cells by a phosphatase inhibitor -

Possible involvement of extracellular signal-regulated kinase and phosphatidylinositol 3-kinase', *Journal of Biological Chemistry*, 275: 3637-44.

Svicero, D. J., D. P. Doiche, M. J. Mamprim, M. C. Heckler, and R. M. Amorim. 2013. 'Ultrasound evaluation of common carotid artery blood flow in the Labrador retriever', *BMC Vet Res*, 9: 195.

Swartz, D. D., J. A. Russell, and S. T. Andreadis. 2005. 'Engineering of fibrin-based functional and implantable small-diameter blood vessels', *Am J Physiol Heart Circ Physiol*, 288: H1451-60.

Syed, O., N. J. Walters, R. M. Day, H. W. Kim, and J. C. Knowles. 2014. 'Evaluation of decellularization protocols for production of tubular small intestine submucosa scaffolds for use in oesophageal tissue engineering', *Acta Biomater*, 10: 5043-54.

Syedain, Z. H., L. A. Meier, M. T. Lahti, S. L. Johnson, and R. T. Tranquillo. 2014. 'Implantation of completely biological engineered grafts following decellularization into the sheep femoral artery', *Tissue Eng Part A*, 20: 1726-34.

Tagawa, S., C. Nakanishi, M. Mori, T. Yoshimuta, S. Yoshida, M. Shimojima, J. Yokawa, M. A. Kawashiri, M. Yamagishi, and K. Hayashi. 2015. 'Determination of Early and Late Endothelial Progenitor Cells in Peripheral Circulation and Their Clinical Association with Coronary Artery Disease', *Int J Vasc Med*, 2015: 674213.

Taggart, D. P. 2013. 'Current status of arterial grafts for coronary artery bypass grafting', *Ann Cardiothorac Surg*, 2: 427-30.

Takayama, T., T. Hiro, M. Yamagishi, H. Daida, A. Hirayama, S. Saito, T. Yamaguchi, M. Matsuzaki, and Cosmos Investigators. 2009. 'Effect of rosuvastatin on coronary atheroma in stable coronary artery disease: multicenter coronary atherosclerosis study measuring effects of rosuvastatin using intravascular ultrasound in Japanese subjects (COSMOS)', *Circ J*, 73: 2110-7.

Teebken, Omke E., and Axel Haverich. 2002. 'Tissue Engineering of Small Diameter Vascular Grafts', *European Journal of Vascular and Endovascular Surgery*, 23: 475-85.

Theisen, G. J., and B. L. Grundy. 1987. 'Anesthesia and monitoring for carotid endarterectomy', *Bull N Y Acad Med*, 63: 803-19.

Thyberg, J. 1996. 'Differentiated properties and proliferation of arterial smooth muscle cells in culture', *Int Rev Cytol*, 169: 183-265.

Thygesen, K., J. S. Alpert, A. S. Jaffe, M. L. Simoons, B. R. Chaitman, H. D. White, E. S. C. Accf A. H. A. W. H. F. Task Force for the Universal Definition of Myocardial Infarction Joint, H. A. Katus, B. Lindahl, D. A. Morrow, P. M. Clemmensen, P. Johanson, H. Hod, R. Underwood, J. J. Bax, R. O. Bonow, F. Pinto, R. J. Gibbons, K. A. Fox, D. Atar, L. K. Newby, M. Galvani, C. W. Hamm, B. F. Uretsky, P. G. Steg, W. Wijns, J. P. Bassand, P. Menasche, J. Ravkilde, E. M. Ohman, E. M. Antman, L. C. Wallentin, P. W. Armstrong, M. L. Simoons, J. L. Januzzi, M. S. Nieminen, M. Gheorghiade, G. Filippatos, R. V. Luepker, S. P. Fortmann, W. D. Rosamond, D. Levy, D. Wood, S. C. Smith, D. Hu, J. L. Lopez-Sendon, R. M. Robertson, D. Weaver, M. Tendera, A. A. Bove, A. N. Parkhomenko, E. J. Vasilieva, and S. Mendis. 2012. 'Third universal definition of myocardial infarction', *Circulation*, 126: 2020-35.

Torpy, J. M., C. Lynm, and R. M. Glass. 2004. 'JAMA patient page. Percutaneous coronary intervention', *JAMA*, 291: 778.

Torrado, Juan, Leo Buckley, Ariel Durán, Pedro Trujillo, Stefano Toldo, Juan Valle Raleigh, Antonio Abbate, Giuseppe Biondi-Zoccai, and Luis A. Guzmán. 2018. 'Restenosis, Stent Thrombosis, and Bleeding Complications', *Navigating Between Scylla and Charybdis*, 71: 1676-95.

Touyz, R. M., and C. Berry. 2002. 'Recent advances in angiotensin II signaling', *Braz J Med Biol Res*, 35: 1001-15.

Tripura, C., and G. Pande. 2013. 'Applications of human hematopoietic stem cells isolated and expanded from different tissues in regenerative medicine', *Regen Med*, 8: 783-95.

Tsai, S., S. T. Hollenbeck, E. J. Ryer, R. Edlin, D. Yamanouchi, R. Kundi, C. Wang, B. Liu, and K. C. Kent. 2009. 'TGF-beta through Smad3 signaling stimulates vascular smooth muscle cell proliferation and neointimal formation', *Am J Physiol Heart Circ Physiol*, 297: H540-9.

Tukmachev, V. A., L. V. Nedospasova, BIu Zaslavskii, and S. V. Rogozhin. 1979. '[Effect of sodium dodecyl sulfate on biological membranes]', *Biofizika*, 24: 55-60.

Turner, Neil A., Selina Ho, Philip Warburton, David J. O'Regan, and Karen E. Porter. 2007. 'Smooth muscle cells cultured from human saphenous vein exhibit increased proliferation, invasion, and mitogen-activated protein kinase activation in vitro compared with paired internal mammary artery cells', *Journal of Vascular Surgery*, 45: 1022-28.

Vallely, Michael P., J. James B. Edelman, and Michael K. Wilson. 2013. 'Bilateral internal mammary arteries: evidence and technical considerations', *Annals of Cardiothoracic Surgery*, 2: 570-77.

van Niel, Guillaume, Gisela D'Angelo, and Graça Raposo. 2018. 'Shedding light on the cell biology of extracellular vesicles', *Nature Reviews Molecular Cell Biology*, 19: 213.

Vavken, Patrick, Shilpa Joshi, and Martha M. Murray. 2009. 'TRITON-X Is Most Effective among Three Decellularization Agents for ACL Tissue Engineering', *Journal of orthopaedic research : official publication of the Orthopaedic Research Society*, 27: 1612-18.

Veith, F. J., E. Ascer, and S. K. Gupta. 1986. 'Expanded Polytetrafluoroethylene (PTFE) Arterial Grafts: An Eight-Year Experience': 25-25-8.

Villalona, G. A., B. Udelsman, D. R. Duncan, E. McGillicuddy, R. F. Sawh-Martinez, N. Hibino, C. Painter, T. Mirensky, B. Erickson, T. Shinoka, and C. K. Breuer. 2010. 'Cell-seeding techniques in vascular tissue engineering', *Tissue Eng Part B Rev*, 16: 341-50.

Vorotnikova, E., D. McIntosh, A. Dewilde, J. Zhang, J. E. Reing, L. Zhang, K. Cordero, K. Bedelbaeva, D. Gourevitch, E. Heber-Katz, S. F. Badylak, and S. J. Braunhut. 2010. 'Extracellular matrix-derived products modulate endothelial and progenitor cell migration and proliferation in vitro and stimulate regenerative healing in vivo', *Matrix Biol*, 29: 690-700.

Voytik-Harbin, S. L., A. O. Brightman, M. R. Kraine, B. Waisner, and S. F. Badylak. 1997. 'Identification of extractable growth factors from small intestinal submucosa', *J Cell Biochem*, 67: 478-91.

Vriens, E. M., G. H. Wieneke, B. Hillen, B. C. Eikelboom, A. C. Van Huffelen, and G. H. Visser. 2001. 'Flow redistribution in the major cerebral arteries after carotid endarterectomy: A study with transcranial Doppler scan', *Journal of Vascular Surgery*, 33: 139-47.

Wagenseil, J. E., and R. P. Mecham. 2009. 'Vascular extracellular matrix and arterial mechanics', *Physiol Rev*, 89: 957-89.

Walker, C. M., F. T. Bunch, N. G. Cavros, and E. J. Dippel. 2015. 'Multidisciplinary approach to the diagnosis and management of patients with peripheral arterial disease', *Clin Interv Aging*, 10: 1147-53.

Wang, J. H., P. Goldschmidt-Clermont, J. Wille, and F. C. Yin. 2001. 'Specificity of endothelial cell reorientation in response to cyclic mechanical stretching', *J Biomech*, 34: 1563-72.

Ward, M. R., G. Pasterkamp, A. C. Yeung, and C. Borst. 2000. 'Arterial remodeling. Mechanisms and clinical implications', *Circulation*, 102: 1186-91.

Warner, T. D., S. Nylander, and C. Whatling. 2011. 'Anti-platelet therapy: cyclo-oxygenase inhibition and the use of aspirin with particular regard to dual anti-platelet therapy', *Br J Clin Pharmacol*, 72: 619-33.

Waybill, P. N., V. M. Chinchilli, and B. J. Ballermann. 1997. 'Smooth muscle cell proliferation in response to co-culture with venous and arterial endothelial cells', *J Vasc Interv Radiol*, 8: 375-81.

Waybill, P. N., and L. J. Hopkins. 1999. 'Arterial and venous smooth muscle cell proliferation in response to co-culture with arterial and venous endothelial cells', *J Vasc Interv Radiol*, 10: 1051-7.

Wessely, R., and V. Andres. 2012. 'Limus is not limus--a proposal to adjust terminology in the context of drug-eluting stents', *J Cardiovasc Pharmacol*, 59: 485-6.

Willette, R. N., J. L. Gu, P. G. Lysko, K. M. Anderson, H. Minehart, and T. Yue. 1999. 'BMP-2 gene expression and effects on human vascular smooth muscle cells', *J Vasc Res*, 36: 120-5.

Wilson, S. L., L. E. Sidney, S. E. Dunphy, J. B. Rose, and A. Hopkinson. 2013. 'Keeping an eye on decellularized corneas: a review of methods, characterization and applications', *J Funct Biomater*, 4: 114-61.

Wojciak-Stothard, B., and A. J. Ridley. 2003. 'Shear stress-induced endothelial cell polarization is mediated by Rho and Rac but not Cdc42 or PI 3-kinases', *J Cell Biol*, 161: 429-39.

Woldringh, C. L., and W. van Iterson. 1972. 'Effects of treatment with sodium dodecyl sulfate on the ultrastructure of Escherichia coli', *J Bacteriol*, 111: 801-13.

Wong, A. P., N. Nili, Z. S. Jackson, B. Qiang, H. Leong-Poi, R. Jaffe, E. Raanani, P. W. Connelly, J. D. Sparkes, and B. H. Strauss. 2008. 'Expansive remodeling in venous bypass grafts: novel implications for vein graft disease', *Atherosclerosis*, 196: 580-9.

Wong, A. P., N. Nili, and B. H. Strauss. 2005. 'In vitro differences between venous and arterial-derived smooth muscle cells: potential modulatory role of decorin', *Cardiovasc Res*, 65: 702-10.

Woodfin, A., M. B. Voisin, and S. Nourshargh. 2007. 'PECAM-1: a multi-functional molecule in inflammation and vascular biology', *Arterioscler Thromb Vasc Biol*, 27: 2514-23.

Worth, N. F., B. E. Rolfe, J. Song, and G. R. Campbell. 2001. 'Vascular smooth muscle cell phenotypic modulation in culture is associated with reorganisation of contractile and cytoskeletal proteins', *Cell Motil Cytoskeleton*, 49: 130-45.

Wu, Q., J. Bao, Y. J. Zhou, Y. J. Wang, Z. G. Du, Y. J. Shi, L. Li, and H. Bu. 2015. 'Optimizing perfusion-decellularization methods of porcine livers for clinical-scale whole-organ bioengineering', *Biomed Res Int*, 2015: 785474.

Wynn, T. A., and K. M. Vannella. 2016. 'Macrophages in Tissue Repair, Regeneration, and Fibrosis', *Immunity*, 44: 450-62.

Xiong, Y., W. Y. Chan, A. W. Chua, J. Feng, P. Gopal, Y. S. Ong, and C. Song. 2013. 'Decellularized porcine saphenous artery for small-diameter tissue-engineered conduit graft', *Artif Organs*, 37: E74-87.

Xu, Q., and T. A. Keiderling. 2004. 'Effect of sodium dodecyl sulfate on folding and thermal stability of acid-denatured cytochrome c: a spectroscopic approach', *Protein Sci*, 13: 2949-59.

Yamamoto, K., T. Takahashi, T. Asahara, N. Ohura, T. Sokabe, A. Kamiya, and J. Ando. 2003. 'Proliferation, differentiation, and tube formation by endothelial progenitor cells in response to shear stress', *J Appl Physiol (1985)*, 95: 2081-8.

Yang, D., T. Guo, C. Nie, and S. F. Morris. 2009. 'Tissue-engineered blood vessel graft produced by self-derived cells and allogenic acellular matrix: a functional performance and histologic study', *Ann Plast Surg*, 62: 297-303.

Yang, Zhihong, Barry S. Oemar, Thiery Carrel, Beat Kipfer, Friedgard Julmy, and Thomas F. Lüscher. 1998. 'Different Proliferative Properties of Smooth Muscle Cells of Human Arterial and Venous Bypass Vessels: Role of PDGF Receptors, Mitogen-Activated Protein Kinase, and Cyclin-Dependent Kinase Inhibitors', *Circulation*, 97: 181-87.

Yin, R. X., D. Z. Yang, and J. Z. Wu. 2014. 'Nanoparticle drug- and gene-eluting stents for the prevention and treatment of coronary restenosis', *Theranostics*, 4: 175-200.

Yurugi-Kobayashi, T., H. Itoh, T. Schroeder, A. Nakano, G. Narazaki, F. Kita, K. Yanagi, M. Hiraoka-Kanie, E. Inoue, T. Ara, T. Nagasawa, U. Just, K. Nakao, S. Nishikawa, and J. K. Yamashita. 2006. 'Adrenomedullin/cyclic AMP pathway induces Notch activation and differentiation of arterial endothelial cells from vascular progenitors', *Arterioscler Thromb Vasc Biol*, 26: 1977-84.

Zaman, A., N. Ali, M. Sajid, and T. Hayat. 2015. 'Effects of unsteadiness and non-Newtonian rheology on blood flow through a tapered time-variant stenotic artery', *AIP Advances*, 5.

Zhang, E. G., S. K. Smith, and D. S. Charnock-Jones. 2002. 'Expression of CD105 (endoglin) in arteriolar endothelial cells of human endometrium throughout the menstrual cycle', *Reproduction*, 124: 703-11.

Zhang, G., J. Zhou, Q. Fan, Z. Zheng, F. Zhang, X. Liu, and S. Hu. 2008. 'Arterial-venous endothelial cell fate is related to vascular endothelial growth factor and Notch status during human bone mesenchymal stem cell differentiation', *FEBS Lett*, 582: 2957-64.

Zhang, L., Q. Ao, A. Wang, G. Lu, L. Kong, Y. Gong, N. Zhao, and X. Zhang. 2006. 'A sandwich tubular scaffold derived from chitosan for blood vessel tissue engineering', *J Biomed Mater Res A*, 77: 277-84.

Zhang, M., M. Yang, L. P. Liu, W. B. Lau, H. Gao, M. K. Xin, L. X. Su, J. Wang, S. J. Cheng, Q. Fan, and J. H. Liu. 2014. 'BMP-2 overexpression augments vascular smooth muscle cell motility by upregulating myosin Va via Erk signaling', *Oxid Med Cell Longev*, 2014: 294150.

Zhou, J., O. Fritze, M. Schleicher, H. P. Wendel, K. Schenke-Layland, C. Harasztosi, S. Hu, and U. A. Stock. 2010. 'Impact of heart valve decellularization on 3-D ultrastructure, immunogenicity and thrombogenicity', *Biomaterials*, 31: 2549-54.

Zhou, W., C. Dasgupta, S. Negash, and J. U. Raj. 2007. 'Modulation of pulmonary vascular smooth muscle cell phenotype in hypoxia: role of cGMP-dependent protein kinase', *Am J Physiol Lung Cell Mol Physiol*, 292: L1459-66.

Zvarova, B., F. E. Uhl, J. J. Uriarte, Z. D. Borg, A. L. Coffey, N. R. Bonenfant, D. J. Weiss, and D. E. Wagner. 2016. 'Residual Detergent Detection Method for Nondestructive Cytocompatibility Evaluation of Decellularized Whole Lung Scaffolds', *Tissue Eng Part C Methods*, 22: 418-28.